# Design and Modelling of Variability Tolerant on-Chip Communication Structures for Future High Performance System on Chip Designs

by

## Faiz-ul-Hassan

Thesis submitted in fulfilment of the requirements for the degree of

Doctor of Philosophy

in

Electronics and Electrical Engineering

at

# University *of* Glasgow

May 2011

# Abstract

The incessant technology scaling has enabled the integration of functionally complex System-on-Chip (SoC) designs with a large number of heterogeneous systems on a single chip. The processing elements on these chips are integrated through on-chip communication structures which provide the infrastructure necessary for the exchange of data and control signals, while meeting the strenuous physical and design constraints. The use of vast amounts of on chip communications will be central to future designs where variability is an inherent characteristic. For this reason, in this thesis we investigate the performance and variability tolerance of typical on-chip communication structures. Understanding of the relationship between variability and communication is paramount for the designers; i.e. to devise new methods and techniques for designing performance and power efficient communication circuits in the forefront of challenges presented by deep sub-micron (DSM) technologies.

The initial part of this work investigates the impact of device variability due to Random Dopant Fluctuations (RDF) on the timing characteristics of basic communication elements. The characterization data so obtained can be used to estimate the performance and failure probability of simple links through the methodology proposed in this work. For the Statistical Static Timing Analysis (SSTA) of larger circuits, a method for accurate estimation of the probability density functions of different circuit parameters is proposed. Moreover, its significance on pipelined circuits is highlighted. Power and area are one of the most important design metrics for any integrated circuit (IC) design. This thesis emphasises the consideration of communication reliability while optimizing for power and area. A methodology has been proposed for the simultaneous optimization of performance, area, power and delay variability for a repeater inserted interconnect. Similarly for multi-bit parallel links, bandwidth driven optimizations have also been performed. Power and area efficient semi-serial links, less vulnerable to delay variations than the corresponding fully parallel links are introduced. Furthermore, due to technology scaling, the coupling noise between the link lines has become an important issue. With ever decreasing supply voltages, and the corresponding reduction in noise margins, severe challenges are introduced for performing timing verification in the presence of variability. For this reason an accurate model for crosstalk noise in an interconnection as a function of time and skew is introduced in this work. This model can be used for the identification of skew condition that gives maximum delay noise, and also for efficient design verification.

Dedicated

to

My Family

# Acknowledgements

# List of Publications

The following list details publications that have been produced while undertaking this research project.

## Journal Papers

1. Faiz-ul-Hassan, Wim Vanderbauwhede, Fernando Rodriguez-Salazar, "Impact of Random Dopant Fluctuations on the Timing Characteristics of Flip-Flops," *IEEE Transactions on Very Large Scale Integration (VLSI) Systems*, Princeton, USA, 2011.

2. Faiz-ul-Hassan, Wim Vanderbauwhede, Fernando Rodriguez-Salazar, "Performance Analysis of on-chip Communication Structures under Device variability," INVITED PAPER *in International Journal of Embedded and Real-Time Communication Systems (IJERTCS)*, vol. 1(4), 2010, pp. 40-62.

## Conference Papers

1. Faiz-ul-Hassan, Wim A. Vanderbauwhede, Fernando Rodriguez-Salazar, "Optimization of on-chip link performance under area, power and variability constraints," *in Proceedings of IEEE International Conference on Microelectronics (ICM 2010)*, pp. 48-51, 19-22 Dec. 2010, Cairo, Egypt.

2. Faiz-ul-Hassan, Wim Vanderbauwhede, Fernando Rodriguez-Salazar, "Power dissipation in NoC repeaters under random dopant fluctuations," in *Proceedings of IEEE PrimeAsia 2009,* pp. 388-391, 19-21 Jan. 2009, Shanghai, China.

3. Faiz-ul-Hassan, Binjie Cheng, Wim Vanderbauwhede, Fernando Rodriguez-Salazar, "Impact of Device Variability in the Communication Structures for Future Synchronous SoC Designs," *in Proceedings of IEEE International Symposium on System-on-Chip (SoC 2009)*, pp. 68-72, Tamepre, Finland.

4. Faiz-ul-Hassan, Wim Vanderbauwhede, Fernando Rodriguez-Salazar, "Timing Yield of Pipelined Circuits under Statistical Device variability," in *Proceedings (on cd) of 2$^{nd}$ IEEE Latin American Symposium on Circuits and \Systems (LASCAS 2011)*, 23-25 Feb. 2011, Bogota, Colombia.

5. Faiz-ul-Hassan, Wim Vanderbauwhede, Fernando Rodriguez-Salazar, "Maximizing Bandwidth Over Faulty Links," 21$^{st}$ International Conference on Field Programmable Logic and Applications (FPL 2011), Sep. 5-7, 2011, Chania, Crete, Greece (ACCEPTED).

# Table of Contents

# List of Figures

# List of Tables

# List of Abbreviations

| | |
|---|---|
| ADC | Analog to Digital Converter |
| AMBA | Advanced Microcontroller Bus Architecture |
| CDF | Cumulative Density Function |
| CDN | Clock Distribution Network |
| CMOS | Complementary Metal Oxide |
| CMP | Chemical Mechanical Polishing |
| DAC | Digital to Analog Converter |
| DCs | Data Channels |
| DFF | Data Flip-Flop |
| DSM | Deep Sub-micron |
| DSPs | Digital Signal Processors |
| FFs | Flip-Flops |
| FPGA | Field Programmable Gate Array Logic |
| FUs | Functional Units |
| IC | Integrated Circuit |
| ILD | Inter layer Dielectric |
| IP | Intellectual Property |
| ITRS | International Technology Roadmap for Semiconductors |
| LER | Line edge roughness |
| LFP | Link Failure Probability |
| MC | Mont Carlo |
| MPU | Microprocessor Unit |
| MSI | Minimum Size Inverter |
| NAs | Network Adapters |
| NoC | Network-on-a Chip |

| | |
|---|---|
| OTV | Oxide thickness variation |
| PDF | Probability Density Function |
| RAM | Random Access Memory |
| RO | Ring Oscillator |
| ROM | Read only Memory |
| RV | Random Variable |
| SerDes | Serializer Deserializer |
| SoC | System-on a Chip |
| SSTA | Statistical Static Timing Analysis |
| STA | Static Timing Analysis |
| VC | Video Converter |
| $\mu$P | Microprocessor |

# Author's Declaration

This thesis presents the work that was carried out at the Department of Electronics and Electrical Engineering, University of Glasgow under the supervision of Dr. Fernando Rodríguez-Salazar, during the period from June 2007 to January 2011. I declare that the work is entirely my own, except where reference is made to the work of others, and it has not been previously submitted for any other degree or qualification in any university.

*Faiz-ul-Hassan*

*Glasgow, UK*

*May 2011*

# Chapter 1

# Introduction

As transistor gate lengths continue to shrink according to Moore's law [1], designers are able to integrate increasingly complex systems in a single microchip. Although in principle it is possible to construct a multi-billion transistor chip in today's technology, the practical problems faced while designing and testing such designs have proven to be too arduous, as evidenced by the increasing designer's productivity gap [50]. Techniques, such as SoC design, where the design complexity is managed by the use of a hierarchy of interconnected modules, have been introduced to overcome this limitation. A typical SoC may include different functional units (FUs) like Microprocessors (μPs), Digital Signal Processors (DSPs), Random Access Memory (RAM), Read only Memory (ROM), Digital to Analog Converters (DACs), Analog to Digital Converters (ADCs), Video Controllers (VCs) and several other Intellectual Property (IP) elements, which typically have already been designed and validated independently (perhaps by third parties). The current state-of-the-art SoCs allow the design and integration of highly diversified and complex systems using adaptive circuits and increased parallelism [2]. Figure 1.1 shows the example of a SoC with diversified functionalities. For such systems, the designer still faces a number of challenging problems in the design, project management, simulation and verification of these devices. For instance, as the number of FUs integrated into a SoC increases, the role played by the on-chip communication structures becomes progressively important. However the semiconductor industry predicts that future generation of SoCs may possibly

contain several thousands of cores. According to the International Technology Roadmap for Semiconductors (ITRS), on-chip communication is becoming the limiting factor in designing high performance and power efficient SoCs.
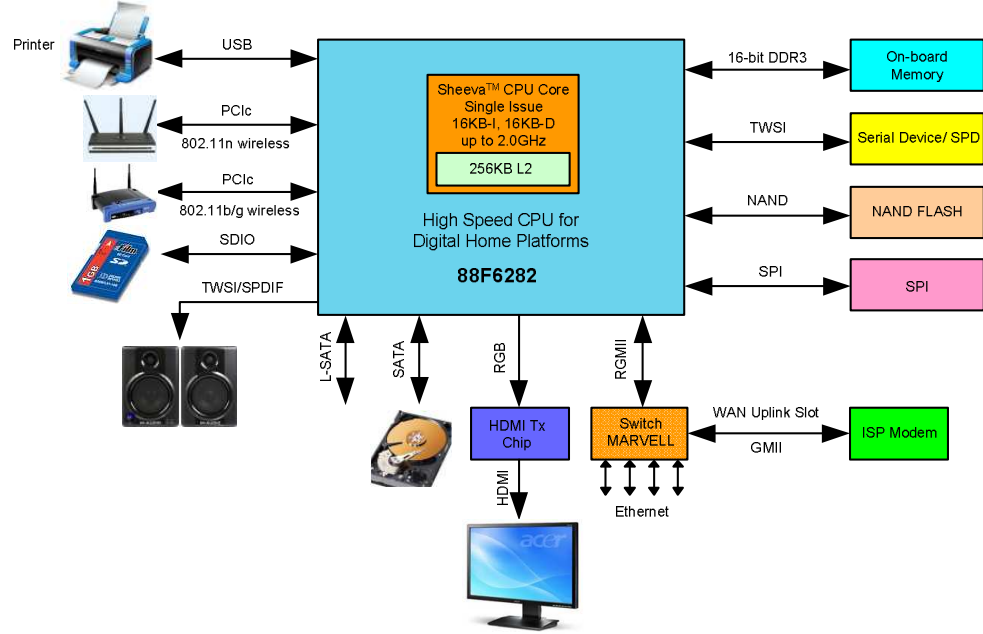


Figure 1.1: Typical system implementation of Marvell 88F6282 SoC [3].

## 1.1   Interconnect-Centric Design Paradigm

Historically, the performance of designs was limited by that of the individual functional units, as communication (through wires) was substantially faster than computation (via transistors). However, the effect of technology scaling is not equally favourable for transistors and wires. With technology scaling, the performance of the devices is continuously improving, whereas the wires are becoming relatively slower, as highlighted by the ITRS [4] and shown in Figure 1.2. Several clock cycles are required for the signals to travel across newer chips. Therefore modern SoC designs, which are abundant with interconnects, are faced with the difficult task of orchestrating the computation of a large number of fast local islands, across the whole chip, by using (relatively) progressively slower interconnects. In order to mitigate this problem, the design paradigm has shifted from computation-centric to interconnect centric, in-line with the SoC methodology as we have seen. In DSM region, the interconnect has become the main bottleneck in the designing of high performance and complex SoCs [5], [6]. The design of efficient interconnects is affected by many issues, as detailed in the following subsections.
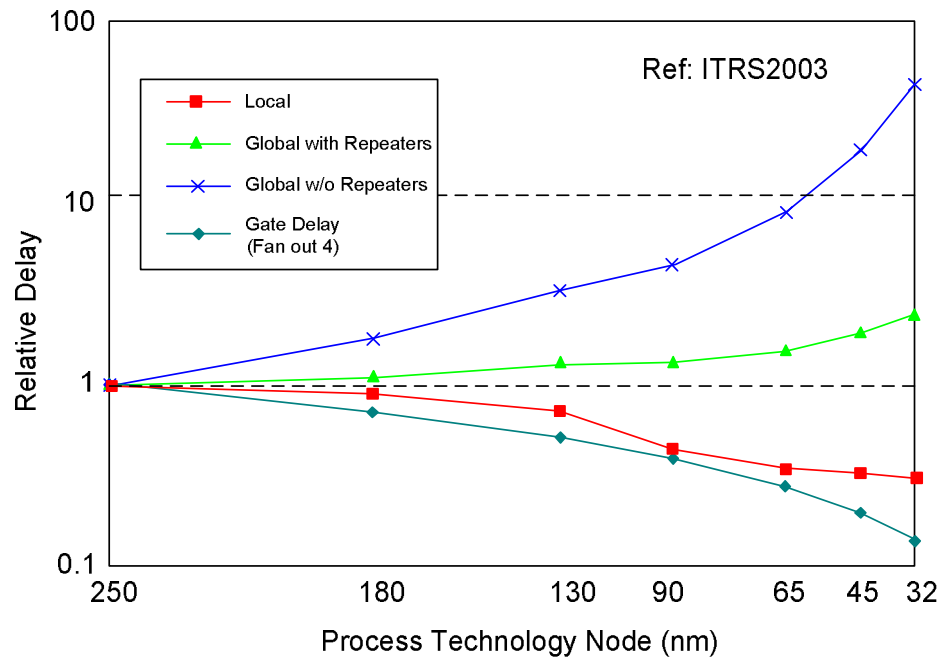
Figure 1.2: Projected relative delay of devices and interconnects (local and global) for different technology generations. The relative performance of the global interconnect is decreasing with technology scaling.

### 1.1.1 Scaling

The objective of the technology scaling is to produce faster devices, increase on-chip component density and reduce energy per storing [7]. The impact of technology scaling on the computational units is that they can now be constructed in smaller sizes (due to device scaling) with same or even with much more functionalities. Therefore the local wires in the cores reduce. However, the global wires which are used to connect cores do not reduce. This allows the cores to operate at a higher frequency, whereas the communication between the cores do not speeds up in the same proportion [8]. Again according to ITRS the interconnect width and pitch decreases with technology scaling, while chip size increases. The result is that the devices and local wires scales with the process technology, whereas the global interconnect do not improve much [9].

### 1.1.2 Power Dissipation

The circuits are designed to operate at higher and higher frequencies in the interest of improved performance. However very dense interconnects switching at high frequencies becomes a major source of power consumption in the circuits and this trend is continuously growing with technology scaling. It has been reported that in a 130nm microprocessor, about 50% of the total power is consumed in the interconnect [10]. In circuit designing, power consumption is taken as a design constraint [11] and designers are always struggling

to reduce it. However, in DSM technologies, reducing power consumption is quite challenging. The supply voltages are decreasing with technology scaling, requiring threshold voltages to decrease to prevent junction breakdown due to higher fields. However, there is an exponential dependence of the leakage current on the threshold voltage so it is expected to become the prevailing part of the total power [12]. Thus the dynamic power which was the dominant component of the power dissipation may not account for the maximum share of the total power in DSM technologies.

### 1.1.3 Crosstalk

In order to incorporate more and more functionality, the number of transistors on a chip is continuously increasing for every new generation of SoCs [13]. Reduction in the gate delay of devices has made it possible to switch the circuits at higher frequencies to obtain higher performance. But this has introduced an important issue of Crosstalk, which can introduce functional noise and delay variation. The main reason behind the emergence of crosstalk in DSM region is the increase of capacitive and inductive coupling due to the shrinkage of geometries. The functional noise can cause a glitch on the victim line which can travel to the dynamic node causing circuit state to change and resulting in functional failures. Each victim line in a bus may experience different coupling capacitance due to which their propagation delay may vary significantly under different switching patterns of the neighbouring lines. Therefore, this introduces uncertainty in the timing of the signals, thus affecting the communication reliability. As we will demonstrate, crosstalk failures are particularly sensitive to skew variations, which are of course a prevailing characteristic of future designs.

### 1.1.4 Variability

In the semiconductor industry, variability is often defined as the deviation of the process parameters from their intended or designed values. It has always been an important aspect of semiconductor manufacturing, process control and circuit design. As the semiconductor feature sizes continue to shrink with every new technology generation, the importance of the underlying variability is increasing; so much in fact that in DSM region, variability has become one of the major design challenges and is considered as the hindrance in the way of technology scaling [14]-[16]. The variability affects devices as well as interconnects causing significant unpredictability in the performance and power characteristics of the integrated circuits (ICs). This can lead to certain undesirable effects such as malfunctioning of circuits or performance degradation.

Amongst various sources of device variability, intrinsic parametric fluctuations play an increasingly important role in contemporary and future CMOS devices [17]. These variations are introduced due to the discreteness of charge and matter and cannot be controlled or diminished by tightening the process tolerances. Some of the sources of intrinsic device variability are

- Random dopant fluctuation (RDF)
- Local oxide thickness variation (OTV)
- Gate line edge roughness (LER)
- Strain variations

For state-of-the-art nano-scale circuits and systems, intrinsic parametric fluctuations have significantly affected the signal system timing [18] and behaviour of the circuits at higher frequencies [19]-[20]. In the circuits, it results in component mismatch and thus can reduce the yield and performance.
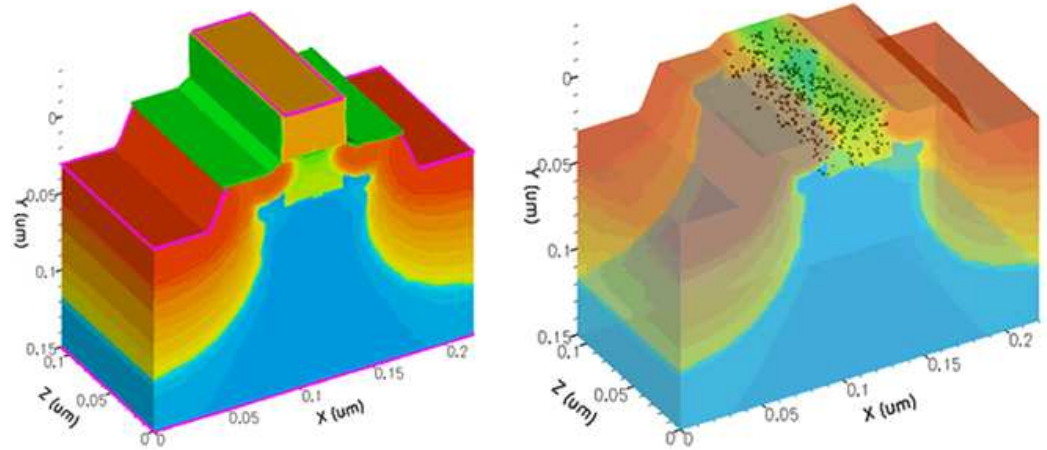


Figure 1.3: Random discrete dopant effects in deep sub-micrometer CMOS devices [21]. The figure on the left hand side is a solid model of a CMOS transistor and that on the right side is its transparent version showing the discreteness due to dopants in the channel region.

One of the most important sources of intrinsic parameter fluctuations is random dopant fluctuation (RDF) [17] which is caused by the randomness of the dopant position and number in the devices, thus making every device microscopically different from its counterparts. Therefore, the devices which are macroscopically identical will have different performance characteristics, mainly due to the variation in the threshold voltage (Vt). Figure 1.3 shows the significance of RDF in deep sub-micrometer CMOS technologies. The normalized magnitude of the variations due to random dopant

fluctuations increases steadily with technology scaling; as fewer number of dopant atoms are now left in smaller devices (see Figure 1.4 and [21]).
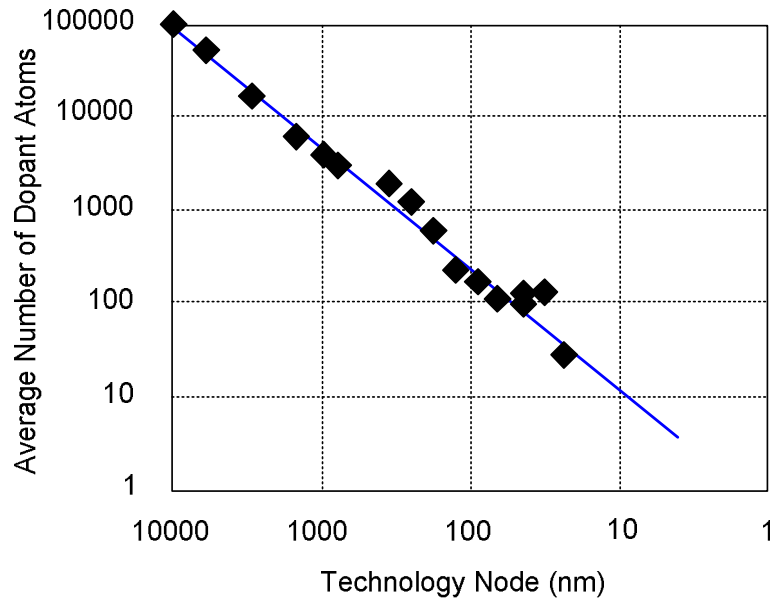


Figure 1.4: Impact of technology scaling on the average number of dopant atoms in the channel.

Variability is also affecting interconnects in deep submicron technologies causing variation in their width, spacing, thickness and inter-layer dielectric thickness. However, there could exist strong spatial pattern dependencies, especially when interconnect variability in chemical mechanical polishing (CMP) is considered. Therefore, total variability can be classified into systematic and random components. A significant portion of the systematic component of variations can be modelled by analyzing the layout characteristic; whereas random variations cannot be modelled.

## 1.2    Research Overview

The challenges imposed by interconnects in the development of high performance SoCs, and ways to overcome them are an active field of academic research. The aim of this thesis is to advance this effort, in particular on understanding how variability intrinsically affects communication performance, fault tolerance, signal integrity, area and power consumption of the interconnect. To achieve this goal the following objectives are defined.

### 1.2.1 Research Objective 1

On-chip communication involves the use of different circuit elements and interconnects to move data from one location of the circuit to another. The communication performance entirely depends on these elements. The intrinsic device variability cannot be eliminated in nanometer CMOS devices as it is process independent. This defines a minimum amount of

variations in the circuit parameters for a particular size of the devices. In order to design communication structures for DSM technologies, an accurate and realistic estimation of the delay performance of all related circuit elements is required. Unfortunately, there is insufficient data available in this regard. Therefore the objective is:

*Accurate characterization of the delay performance of on-chip communication circuit elements for future CMOS technologies in the presence of variability due to RDF.*

This data is required to estimate the performance of a complete channel. Based on this information, it is possible to explore and design circuit level fault tolerant communication (sub) systems.

### 1.2.2 Research Objective 2

In the presence of characterization data of circuit elements, it is more convenient to use computationally efficient analysis techniques like Static Timing Analysis (STA) or Statistical Static Timing Analysis (SSTA). Presently, SSTA is preferred over STA, being computationally efficient and more accurate than STA. The SSTA technique can be used to evaluate the performance of a communication link. However, its accuracy strongly depends on accurate representation of the characterization data of the associated circuit elements. So far, underlying timing distributions are assumed to be Normal, but its validity needs to be investigated in DSM technologies. Therefore objective 2 of this thesis is:

*Study the nature of the timing distributions of communication elements and try to find their accurate probability density function. Once this is done, apply these distributions for the SSTA of a large communication channel.*

### 1.2.3 Research Objective 3

As pointed out in [10], as much as 50% of the chip power is consumed by the global interconnects. This power is mainly dissipated in the drivers and repeaters used to improve the delay performance of interconnects. Different coding techniques are used at software level for efficient data transmission [22], [23]. A power optimal repeater insertion technique proposed in [24] is commonly used along with data coding. This technique gives excellent results in terms of power and area savings at the cost of nominal performance degradation. However, the implications of this technique are yet to be investigated for DSM technologies where variability and leakage power effects become quite prominent. Therefore objectives 3 of this thesis is:

*To measure different components of power dissipation in repeaters of future technology generations. This data can be useful by the designers to make a choice between low activity parallel links or high activity serial links (as low activity parallel links will dissipate a large amount of the leakage power as compared to the serial links, for particular data requirements). Similarly, a power-optimal repeater insertion technique which accounts for delay variability is required to be developed.*

### 1.2.4 Research Objective 4

Quite significant amount of academic work has been undertaken in finding the optimum configuration of a multi-bit communication channel for best possible performance under power and area constraints [25]-[27]. Again very little work is found in this area considering variability in the figure of merit. So objective 4 is:

*Find the optimum configuration of the channel link which gives best bandwidth under power, area and variability constraints. Moreover, a comparison of serial and parallel links is also required to be made in this perspective.*

### 1.2.5 Research Objective 5

In order to ascertain signal integrity in the channel bus, accurate modelling of the crosstalk in aggressor and victim lines is required. In the past, many researchers have published crosstalk analysis models and algorithms [28]-[30] but all of them either require numerical techniques to solve them or do not give sufficient insight into the underlying crosstalk effects on signal responses. In order to reduce this difficulty, this thesis aims:

*To find closed form expressions that give accurate voltages for the aggressor and victim lines in time domain, as a function of wire length, due to switching transitions on them. Also study the effect of variability on the delay performance of interconnects in the presence of crosstalk.*

## 2.1    Thesis Organization

The rest of the thesis is organized as follows:

**Chapter 2-** In the beginning of the chapter, different structures used for on-chip communication are briefly discussed. Subsequently, different performance metrics that have been used throughout the thesis to evaluate the performance of on-chip communications are defined.

**Chapter 3-** In this chapter, the performance of on-chip communication structures under device variability has been characterized through HSPICE simulations. The

characterization results of all the basic elements have been included and discussed. At the end of the chapter, a methodology is given that can be used to estimate the performance of a complete channel link using the characterization data. Moreover, link failure probability has been estimated using this approach.

**Chapter 4-** If we talk about core-to-core or router-to-router (for NoCs) communication links, flip-flops are normally used at the input and output of the functional units. Therefore, the output of a router or functional unit is emitted from the flip-flops and is then amplified through the tapered buffer drivers before transmitting through the link. Similarly, at the receiving end, flip-flops are used at the input of the functional unit or router. Again, flip-flops are also used in pipelined interconnects. Therefore, in order to estimate the performance of a link using Statistical Static Timing Analysis (SSTA), accurate representation of the characterization data of the timing parameters of the flip-flops (in the form of PDFs) is required. Furthermore, accurate approximation of the probability distribution functions is also required. In this chapter, this aspect has been described in detail and its application in pipelined communication circuits has been discussed.

**Chapter 5-** In the start of this chapter, the measurement results for the power dissipation in repeaters for the given three technology generations have been presented. The impact of device variability on the leakage power has also been studied and its implication on NoC links has been discussed. In the next part of this chapter, the optimization of the performance of a single wire link under area, power and variability constraints has been described. The impact of repeater size and inter-repeater segment length on the delay, power, area and variability has been discussed and an optimization scheme has also been proposed.

**Chapter 6-** This chapter describes the performance of a multi-bit parallel link under area and power constraints. The optimization of bandwidth under area, power and variability constraints has been discussed. Moreover, a comparison of parallel vs. serial links has also been described.

**Chapter 7-** In this chapter analytical model for the voltages at aggressor and victim lines under crosstalk effects have been presented. The validity of the data through comparison with the simulation results has been demonstrated. Moreover, the effect of crosstalk on input skew variability has been studied.

**Chapter 8-** This chapter makes a conclusion of the study and also mentions some future work.

# Chapter 2

# On-Chip Communication Structures

A SoC design typically consists of many functional units (FUs) that work together to perform desired functions. The FUs always need to communicate with each other during the execution of the application and it is the responsibility of the on-chip communication structure/ architecture to provide a mechanism for the correct and reliable transfer of information from the source units to the destination units [31]. In addition to this, the on-chip communication structure must satisfy certain metrics like latency, bandwidth, area and power dissipation. The performance of SoC designs largely depends on the choice and design of the underlying communication architecture. Therefore, depending upon the performance requirements, a suitable communication architecture is designed or selected for the SoC design.

## 2.1 Communication Architectures for SoCs

### 2.1.1 Buses

The simplest on-chip communication architecture which is widely used in SoCs is the bus interconnection network [8]. In its simplest form, a bus is a group of wires which provides

a communication media for the exchange of data between different functional units connected to it. Figure 2.1 [31] shows the example of a simple system with many functional units connected through on-chip buses.
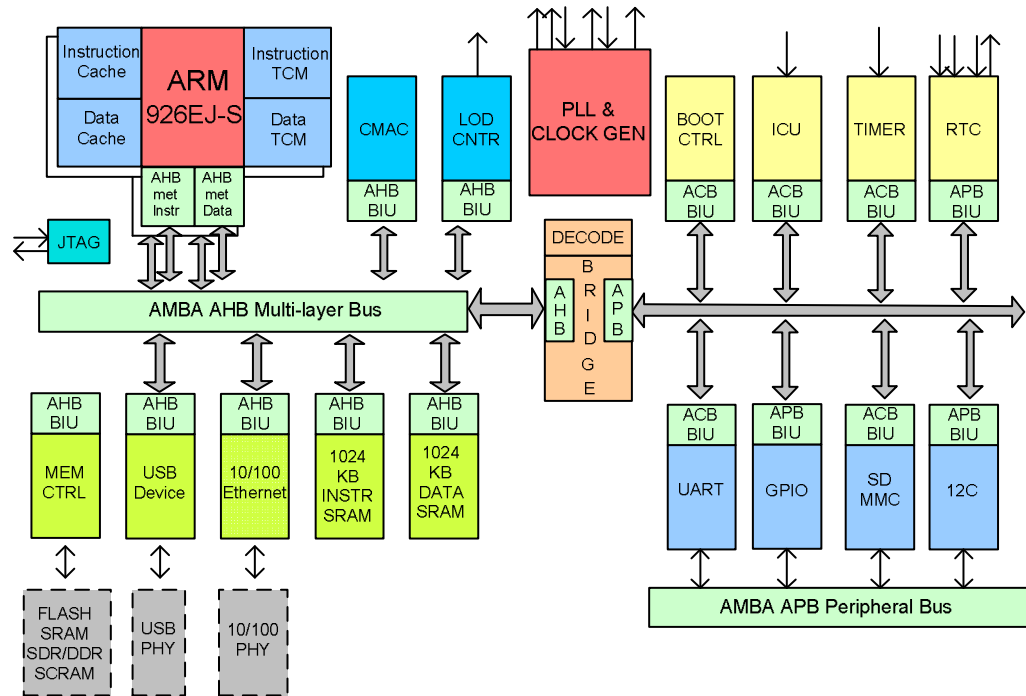


Figure 2.1: A SoC in which different components are integrated through the bus communication architecture.

There are several types of bus configurations used in SoCs and the simplest one is called simple shared bus, as shown in Figure 2.2. In this case only one FU at a time has a control over the bus and transfers data. If some other unit also tries to use the bus at the same time in order to transfer data, this will cause bus contention. Arbitrators are used to resolve the conflict who gives the control to one of the units on the basis of the assigned priorities. In bus based systems, this is one of the major problems and efforts have been made to reduce this problem.
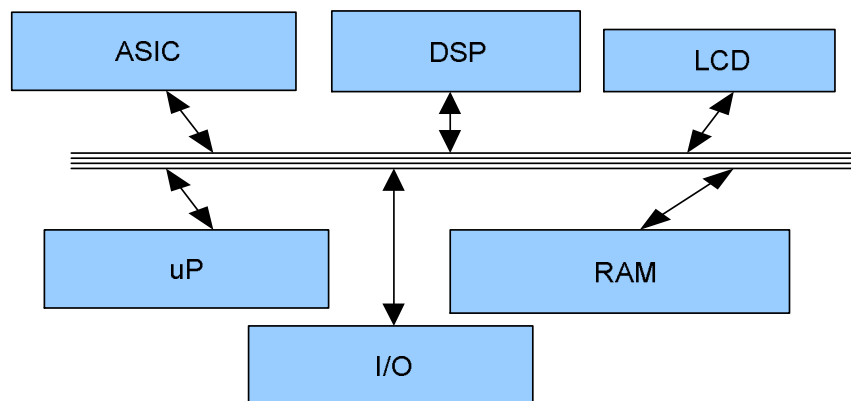


Figure 2.2: A simple shared bus, allowing different FUs to share the same communication channel.

In such systems, every unit attached to the bus adds capacitance which results in large delays and large power consumption. This allows only a limited number of components to be attached with the bus in order to keep the delay and power consumption within permissible limits. Due to this reason, the simple bus architecture is not *scalable*.
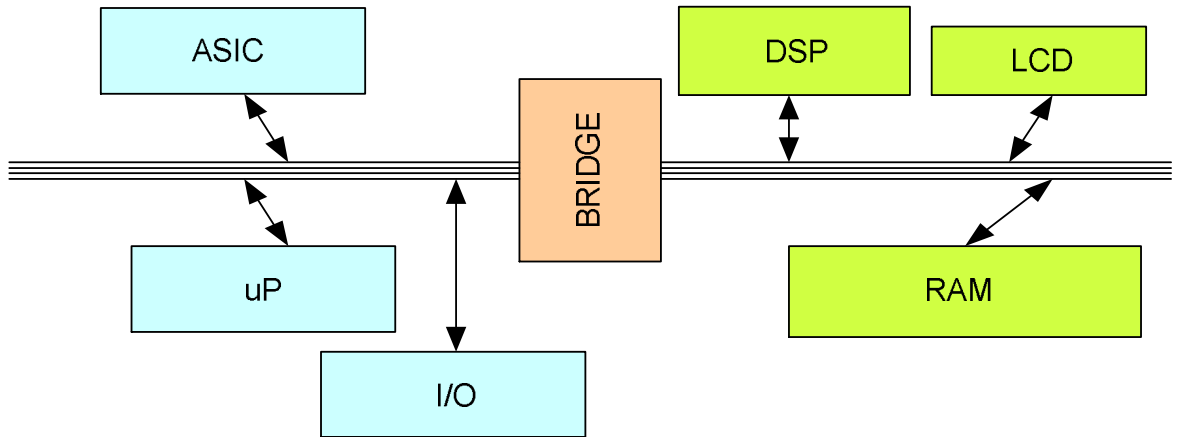


Figure 2.3: A bus divided into two sub-buses using a bridge.

This difficulty is typically reduced by dividing a common bus into several buses using bridges [32]. Figure 2.3 shows a bus split up into two sub-buses using a bridge. The implementation of bridges is fairly simple if it connects buses with same protocols and operating frequencies. There are also other types of bus configurations used in SoCs. Amongst them, Advanced Microcontroller Bus Architecture (AMBA) from ARM [33] defines several bus types which are widely used in SoCs. AMBA proposes various bus solutions for SoCs ranging from simple bus architectures to multi-master high performance bus structures. An example of an AMBA bus is shown in Figure 2.4.
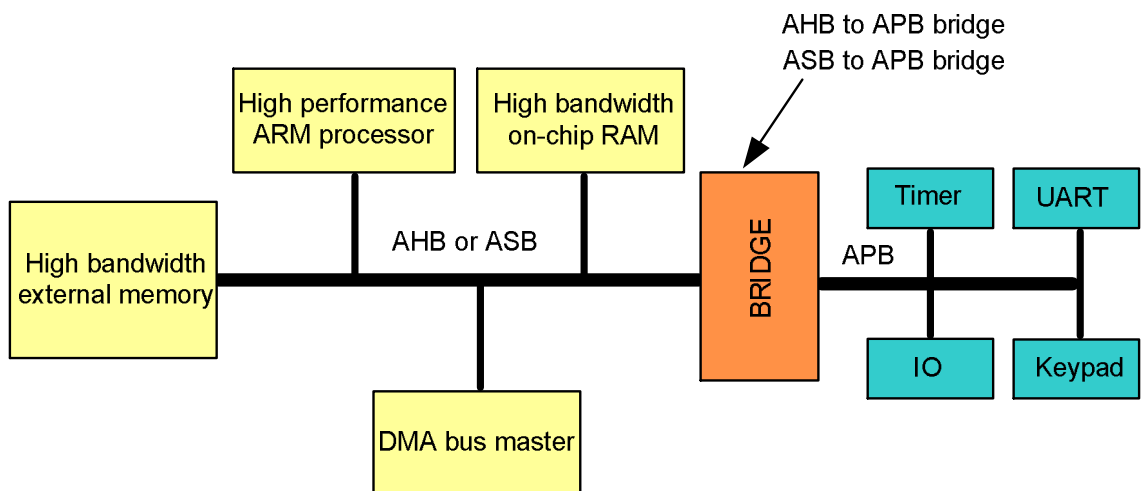


Figure 2.4: An example of AMBA bus. The bridge provides an interface to connect two different types of buses.

### 2.1.2 Point-to-Point Direct Links

In this architecture, each functional unit is directly connected with a subset of other functional units on the chip, as shown in Figure 2.5. The point-to-point communication architecture eliminates the contention problem of shared medium (buses). Each functional unit, in this architecture, has a network interface block, usually called a router and is directly connected with the neighbouring functional units through the communication links. These links can either be of *input*, *output* or *bidirectional* type. Unlike buses, as the number of routers (nodes) in this architecture increases, the total bandwidth increases. This property makes point-to-point links suitable to make large scale systems [34]. Unfortunately the number of links (and hence the power and area) grows with the square of the number of functional units. Hence this architecture is not promising for very large systems.
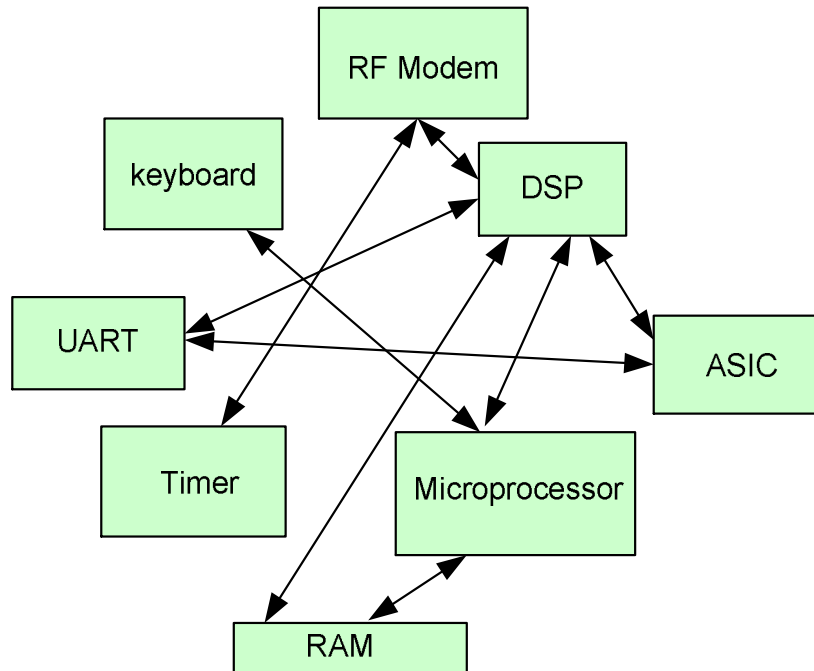


Figure 2.5: A point-to-point communication architecture.

### 2.1.3 Network Architecture

Network-on-Chip (NoC) has been proposed as a promising solution for on-chip communication in large SoC designs, where the complexity of the design is managed by the use of a number of networked, but self contained blocks [35], [36]. NoC provides a generalized scheme for on-chip global communication. Routing nodes (R) are spread over the chip and connected by point-to-point communication links. The resources or IP blocks are connected to NoC through network adapters (NAs), as shown in Figure 2.6. In a

Network-on-Chip, data is exchanged amongst computing elements (IP blocks) by transmitting and relaying data packets through the interconnection network. There are similarities between the conventional computer networks and NoC, like layered communication models and decoupling of computation and communication. However, there are also some differences which are mainly due to the difference in the cost ratio of wiring and processing resources [37].
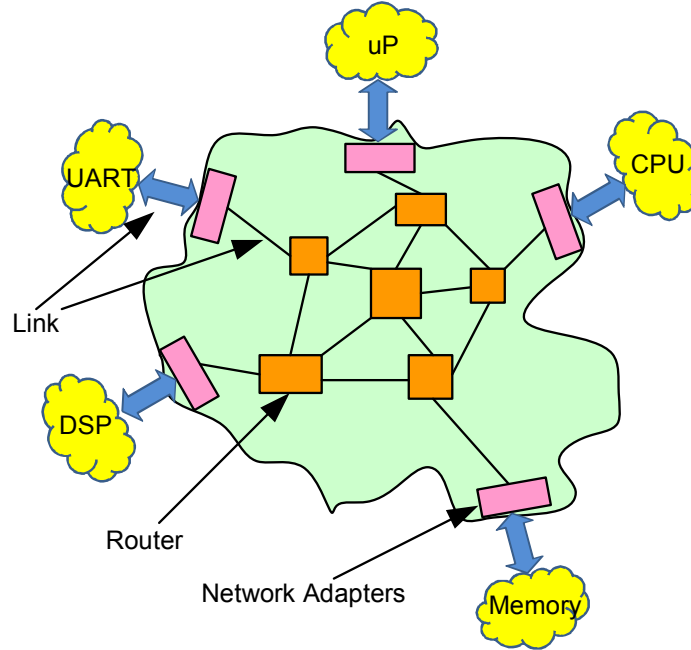


Figure 2.6: A conceptual realization of a NoC [34].

In NoC the whole chip can be partitioned into several regions, each of which contains one (or several) IP block(s). These IP blocks can operate with their own clocks and exchange data with other IPs through the switches and communication links. In this way the requirement of a global synchronization is relaxed. Computations are undertaken within locally synchronous IP blocks, and global synchronization is obtained by the execution of semantics embedded within the global communications network. Similarly, in addition to communication infrastructure, NoC can also provide standard IP interfaces which will facilitate the reuse of already verified IP resources [37]. This can simplify the design process and also reduce verification efforts. Due to a layered structure, the signal integrity issues can be addressed at physical, data-link or any higher layer [38].

NoC can be constructed in different types of topologies such as 2D mesh, Star, Torus, Octagon, Hypercube [37], [39]. The topology defines the connectivity and layout of the nodes and links on the chip. A $4 \times 4$ grid topology is shown in Figure 2.7 which presents a regular structure. The topology can be application specific having an irregular structure.

Depending upon the specific requirements of, say bandwidth, the protocol dictates how the nodes and links of NoC will be utilized in the operation.
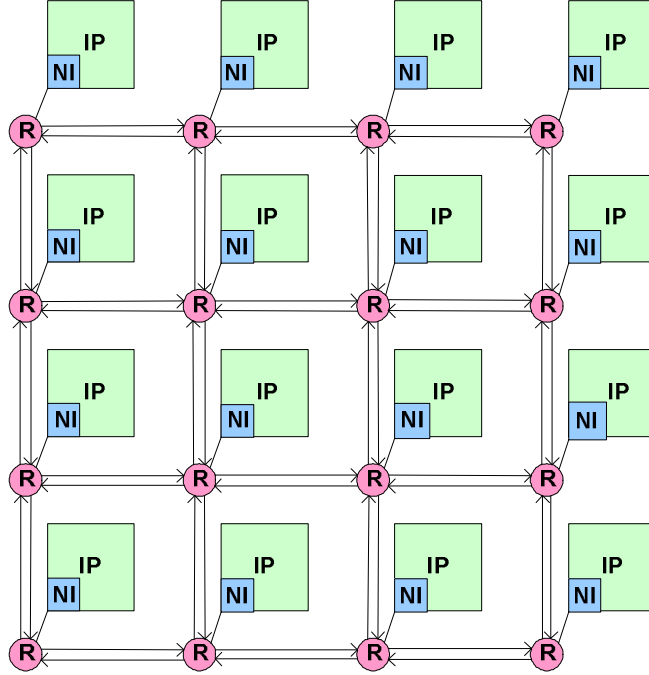
Figure 2.7: A 4×4 grid structured NoC. Each intellectual property (IP) block is connected to a router through a network interface (NI) adapter. The routers are connected with each other through communication links in a certain topology.

## 2.2 Link as an important Communication Media

In all communication architectures, the underlying communication links between the functional units or between the functional units and routers are always used. These links form the backbone of any communication architecture. These links can be synchronous, asynchronous or self-timed. However, in this thesis we have chosen to focus on synchronous links due to their prevalence in the industry. Ideally these links should consist of a certain number of parallel wires running between the source and destination. However, in practical circuits (especially in DSM technologies), their construction is not so simple in order to meet certain design requirements. Therefore, it is of great importance to study these links in detail to design high efficiency links.

A link can be bidirectional or unidirectional as shown in Figure 2.8 and 2.9 respectively [40]. A bidirectional link allows the signals to travel in either direction. This provides a flexibility in the routing of interconnects and makes it possible to effectively use available metal tracks on the chip. The implementation of this approach requires the use of tristate buffers on transmitter and receiver sides, as shown in Figure 2.8.
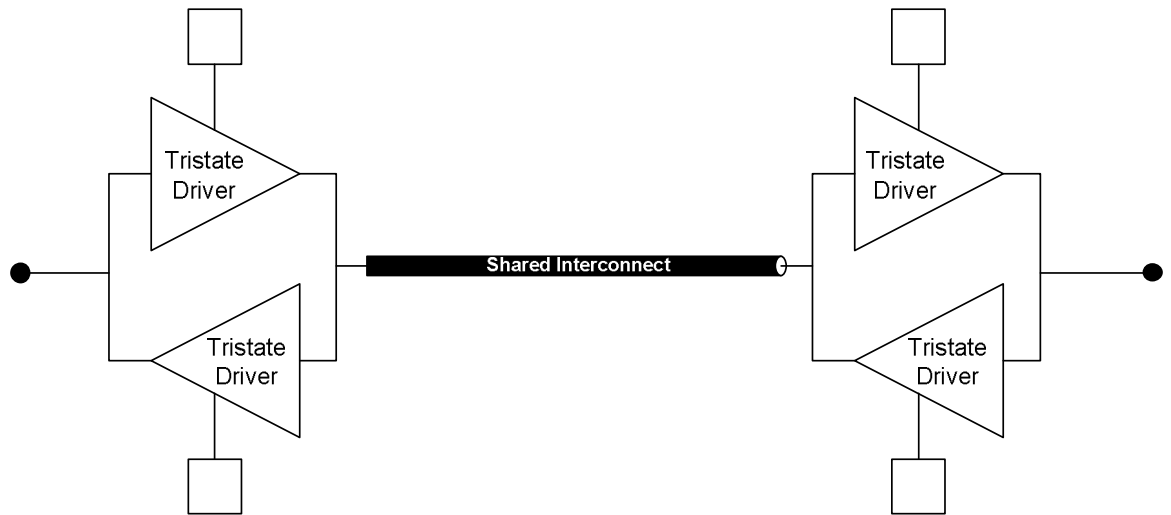
Figure 2.8: A bidirectional link. There is a shared interconnect between the transmitter and receiver.

A unidirectional channel allows the signals to travel only in one direction and thus suggest that a pair of wires should be used in each channel. This approach is less flexible than the bidirectional approach for routing the tracks on the chip, however it provides less contention and more bandwidth.
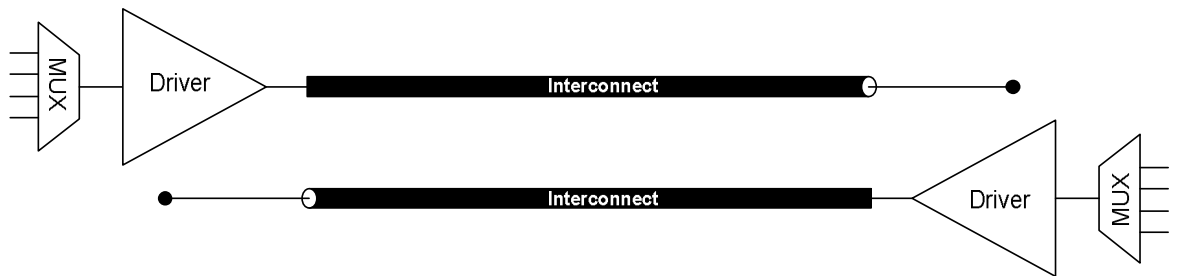
Figure 2.9: A unidirectional link.

Furthermore, in each interconnect line, different circuit elements like tapered buffer drivers, repeaters and flip-flops are used and there are two basic designs for the interconnect-repeater inserted interconnects and flip-flop (or latch) inserted pipelined interconnects, as shown in Figure 2.10 and 2.11 respectively.
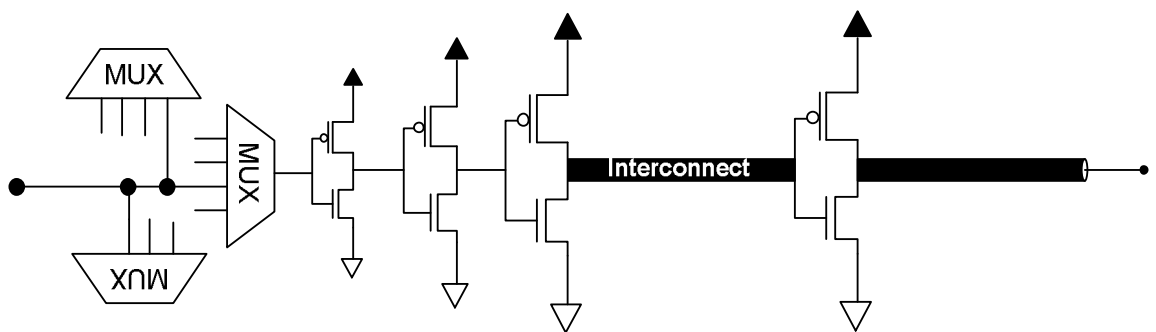
Figure 2.10: Repeater inserted interconnect.

16
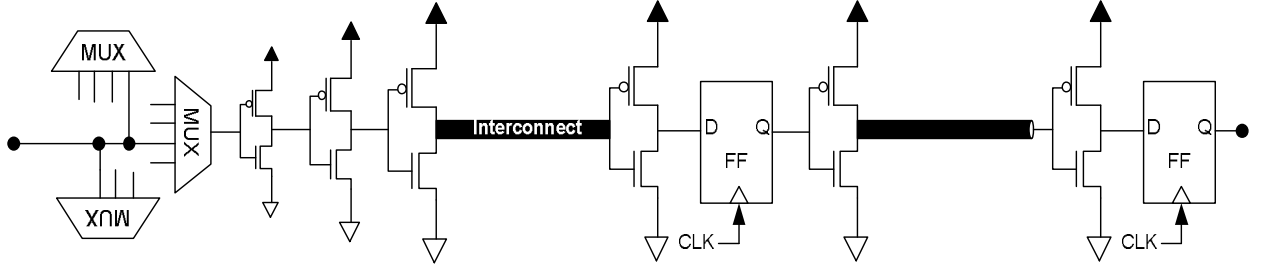
Figure 2.11: Flip-flop inserted pipelined interconnect.

## 2.3 Performance of On-Chip Communication

The performance of on-chip communication in the physical layer can be evaluated from several aspects. In this thesis, however, we consider the metrics exposed in this chapter as important for interconnect centric circuits. We start with a short review on interconnect design. Subsequently, some basic concepts and the mathematical equations describing these metrics are provided. We will make use of these metrics in subsequent chapters for evaluating the merits of different interconnects and for quantifying the effects that variability introduces in the design.

## 2.4 Interconnect Modelling in DSM Technologies

In early days of VLSI design, the clock speeds and integration densities on the chip were low and so the signal integrity effects were minimal. However, with rapid evolution of the semiconductor technology, several important issues associated with interconnects in deep sub-micron technologies have emerged that are effecting the performance of high speed circuits. The problems such as interconnect delay, device and interconnect variability, power dissipation, crosstalk, substrate coupling, inductive coupling and IR drop are among the many emergent challenges which the circuit designers are facing [5], [6].

The fundamental parameters influencing the interconnect delay are on-resistance of the driver, output capacitance of the driver and wire parasitics. The interconnect parasitics of interest are the wire resistance and the wire capacitance (and inductance for very high frequency signalling). These parasitics are a function of the physical properties of the construction and layout of the wires, and will act as an RC load increasing the propagation delay.

A simple lumped element model is not sufficiently accurate to model state of the art interconnects, which of course are formed by continuously distributed RC (or RLC) elements in space. For simulation purposes, an approximation to a distributed element

17

model can be formed by breaking the interconnect into a large number (N) of smaller identical lumped sections (RLC cells). Some possible models are shown in Figure 2.12 [41]. The accuracy of the simulation results depends on the number of RLC cells (segments) used (i-e the resolution of the lumped RLC model). However, this number is limited in practice by the correspondingly large simulation time of the model.
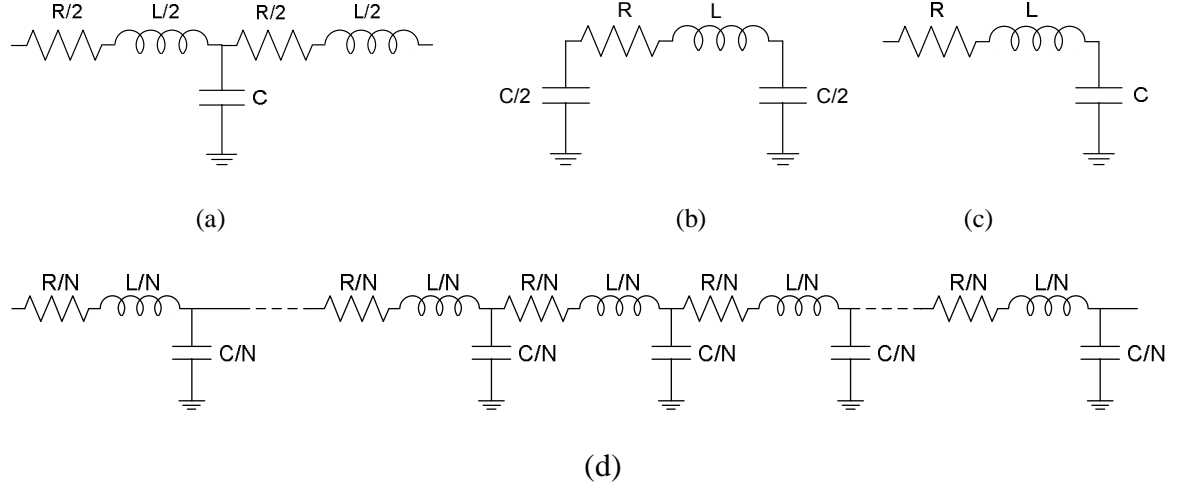


Figure 2.12: Different interconnect models, (a) the 'T', (b) the 'pi' and (c) the 'ladder'. A long wire is divided into N segments using ladder model and is shown in (d).

## 2.4.1 Parasitic Resistance

The signal speed through a wire depends, to a first order approximation, to the distributed RC constants in it, and hence to the parasitic resistance. The resistance depends on the wire dimensions and the type of the material used (gold, aluminium, copper or polysilicon). For an interconnect having thickness $T$ and width $W$, the resistance can be calculated as [41]

$$R = \rho \frac{l}{TW} \tag{2.1}$$

where $\rho$ is the resistivity and $l$ is the length of the interconnect. Using this formula, the parasitic resistance of a wire of given dimensions can be estimated.

With technology scaling, the wires are becoming thinner and so the parasitic resistance per unit length is increasing for minimum wire widths (according to ITRS).

## 2.4.2 Parasitic Capacitance

The accurate estimation of the parasitic capacitances of the interconnects in DSM technologies is a complex task. This is due to the fact that each interconnect is a three dimensional metal structure surrounded by a number of other interconnects with significant variations of shape, width, thickness and spacing with respect to other conductors and

ground planes [42]. Unlike the simplest way of calculating the capacitance of a parallel plate capacitor, the capacitance measurement in integrated circuits require the consideration of other factors like coupling capacitance and fringe capacitance in addition to ground capacitance, as shown in Figure 2.13. It has been observed that the contribution of the coupling capacitance in the total interconnect capacitance is increasing rapidly with technology scaling due to the reduction of interconnect spacing and an increased aspect ratio of wires.
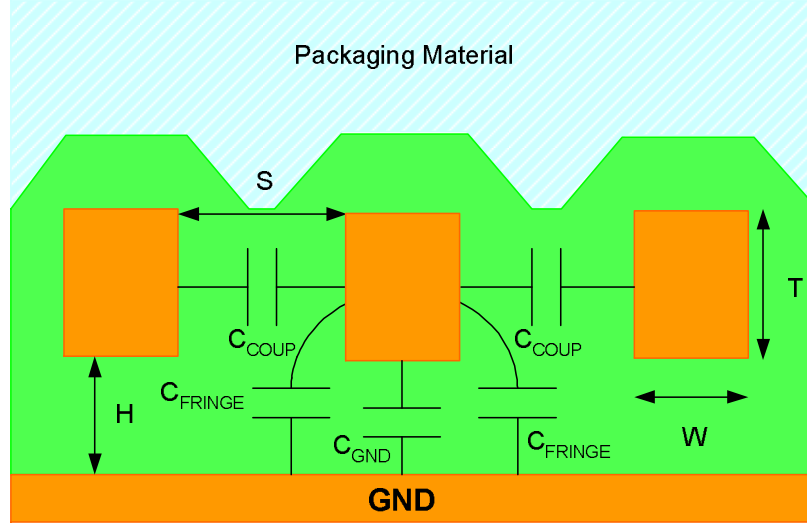


Figure 2.13: The cross-sectional view of an interconnect surrounded by two parallel similar interconnects over a ground plane (in the top global layer) showing different components of capacitance.

An accurate estimation of the parasitic capacitance can be made by solving Maxwell's equations in three dimensions, provided all material and geometrical details are available. Presently, computer aided software tools like Raphael [43] and FASTCAP [44] are available which are based on 2D or 3D field solvers which can calculate the parasitic capacitance with reasonable accuracy. However, some important aspects of interconnect parasitic capacitance can also be calculated using closed form models such as [45] as follows- The ground capacitance per unit length (considering the fringe flux) to the underlying plane is given by

$$C_g = \varepsilon \left[ \frac{W}{H} + 3.28 \left( \frac{T}{T + 2H} \right)^{0.023} \left( \frac{S}{S + 2H} \right)^{1.16} \right] \tag{2.2}$$

Where $\varepsilon$ is the dielectric constant of the insulating material and $W, H, S$ and $T$ are the geometrical dimensions shown in Figure 2.13. Similarly the coupling capacitance per unit length is given by

$$C_c = \varepsilon \left[ 1.064 \left( \frac{T}{S} \right) \left( \frac{T + 2H}{T + 2H + 0.5S} \right)^{0.695} + \left( \frac{W}{W + 0.8S} \right)^{1.4148} \left( \frac{T + 2H}{T + 2H + 0.5S} \right)^{0.804} \right.$$

$$\left. + 0.831 \left( \frac{W}{W + 0.8S} \right)^{0.055} \left( \frac{2H}{2H + 0.5S} \right)^{3.542} \right] \tag{2.3}$$

The total capacitance of the wire can be calculated as

$$C_{Tot} = C_g + 2C_c \tag{2.4}$$

Typically such derivations are limited to particular domains. In this case the valid range for using the approximation is

$$0.3 \leq \frac{W}{H} \leq 10, \qquad 0.3 \leq \frac{S}{H} \leq 10, \qquad \frac{T}{H} \leq 10$$

Other closed form capacitance models with different interconnect configurations are also given in [46], [47], [134].

### 2.4.3 Inductance

Inductance is another important parasitic. It can be described by the magnetic flux generated due to the flow of current in a loop. In integrated circuits several electrical loops can exist which produce inductive parasitic effects. At high enough operational frequencies of the circuits, the inductive impedance associated with interconnects become comparable or prevail over the resistive part [48]. The inductive interference caused due to the interaction of the magnetic fields can affect the signal integrity in the form of signal distortion, delay variation, crosstalk noise and glitches.

In this research we have ignored the effects of inductance due to the following reasons:

(a) The interconnect delay is not significantly effected by the inductive effects. For scaled global interconnects, the line resistance per unit length increases (according to the ITRS) and so the effects of inductance on the performance of global interconnects actually diminishes [49]. This is true, especially for the technologies and interconnect geometries we have considered in this thesis. Using the delay models of [143] for RC and RLC interconnects, it has been found that the percent increase in the propagation delay caused by neglecting inductance and considering an RLC line as an RC line, is nominal. For instance, for the global interconnects of 25, 18 and 13 nm technology generations at $S = 1S_{min}$ and $W = 1W_{min}$, this increase is 1.74%, 1.25% and 1.16% respectively. Similarly for the fastest interconnects with

S=10S$_{min}$, W=10W$_{min}$ (we used in this thesis), the maximum increase in delay is 14.2%, 10.92% and 10.01% for the corresponding technologies.

(b) The inductive effects have much longer spatial range in contrast to the capacitive effects which primarily depends on features in close proximity. The inductance matrix generally becomes very dense and is difficult to specify in a straightforward way. Therefore, accurately simulating inductive effects might not be practical [48].

(c) The effective interconnect inductance in a chip environment is very difficult to predict accurately. For the estimation of the inductance associated with a wire, the return current path should be defined. However, the return current path can be dynamic in a real chip environment, as it depends strongly on the signal condition and the overall layout and configuration of the integrated circuit.

### 2.4.4 Impact of Technology Scaling on Interconnect Parasitics

In order to study the impact of technology scaling on interconnect resistance and capacitance parasitics, particular interconnect parameters have been taken from the International Technology Roadmap for Semiconductors (ITRS) [50] for the technology generations of 25, 18, 13 and 10 nm. These are given in Table 2.1. It is important to mention that these lengths (technologies) correspond to the MPU physical gate length. The data shows that interconnect pitch is reducing and height is increasing with technology scaling for all three wiring tiers. The parasitics have been calculated using equations (2.1)-(2.4) for minimum wire width and pitch and are plotted in Figure 2.14 as a function of the technology generation.

Table 2.1: Interconnect Technology Parameters for the Three Wiring Tiers

| Parameter/ Technology Generation | 25nm | 18nm | 13nm | 10nm |
|---|---|---|---|---|
| Local wiring pitch (nm) | 136 | 90 | 64 | 50 |
| Local wiring aspect ratio | 1.7 | 1.8 | 1.9 | 1.9 |
| Intermediate wiring pitch (nm) | 136 | 90 | 64 | 50 |
| Intermediate wiring aspect ratio | 1.8 | 1.8 | 1.9 | 1.9 |
| Global wiring pitch (nm) | 210 | 135 | 96 | 75 |
| Global wiring aspect ratio | 2.3 | 2.4 | 2.5 | 2.6 |
| Metal Resistivity (μΩ-cm) | 2.2 | 2.2 | 2.2 | 2.2 |
| Dielectric Constant | 2.5-2.9 | 2.3-2.7 | 2.1-2.5 | 1.9-2.3 |
| On-chip local clock frequency (MHz) | 4,700 | 5,875 | 7,344 | 8,522 |
| Chip Size at production (mm$^2$) | 310 | 310 | 310 | 195 |

The curves show that the interconnect resistance is increasing more rapidly as compared to the capacitance which is decreasing (as wire widths are decreasing) with technology scaling. This indicates that RC delay increases with technology scaling and will contribute a larger portion of the path delay.



(a)                                                                        (b)
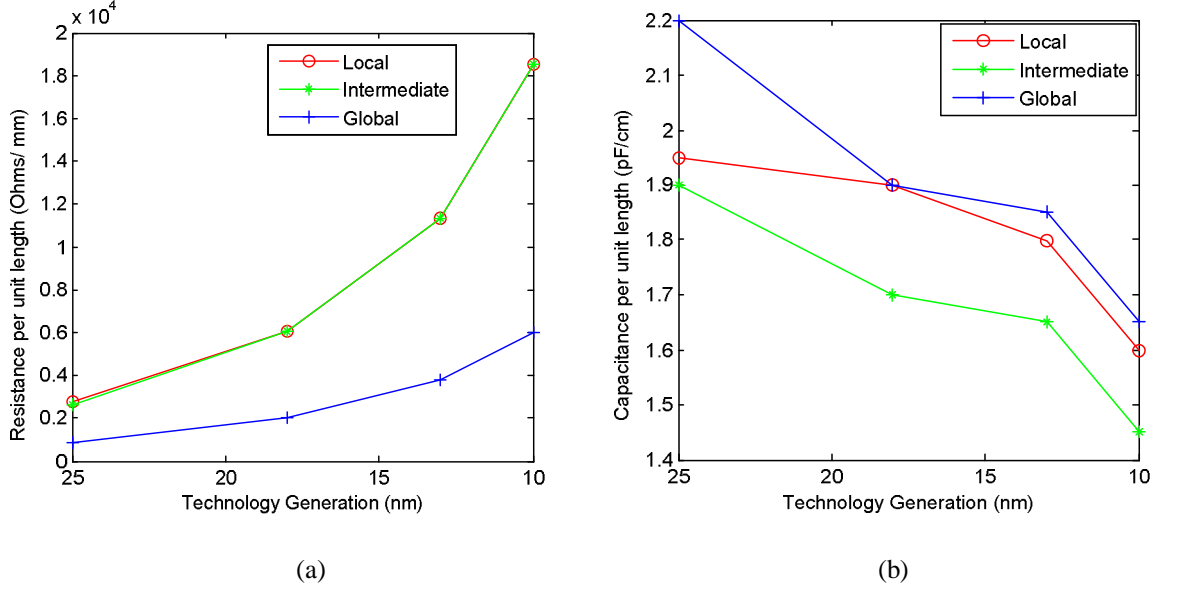
Figure 2.14: Impact of technology scaling on interconnect resistance and capacitance per unit length (Fig. (a) and (b) respectively) for local, intermediate and global interconnects with minimum width and pitch.

## 2.5 Performance Metrics

### 2.5.1 Signal Delay

Signal delay is the most important parameter describing the performance of on-chip communication, as it determines the maximum possible speed at which communication can be made. For reliable communication, it is required that the signals reach their destinations within the specified timing constraints. Consider the simple circuit of Figure 2.15 where a signal propagates through two buffers via the interconnect. The signal delay depends on the interconnect RC, the driver resistance and load capacitance.

If $t_{delay}$ is the time between the step input voltage excitation $V_{in}$ and output voltage $V_{out}$ reaching 90 percent (0-90%) of the final value then according to Bakoglu [51], the signal delay to the first order is given by

$$t_{delay} = 0.7R_{int}C_L + 0.4R_{int}C_{int} + 0.7R_{tr}C_L + 0.7R_{tr}C_{int} \qquad (2.5)$$

Where different interconnect parameters have been shown in the equivalent circuit in Figure 2.15 and are defined as follows:

22

$R_{int}$ = total interconnect resistance,

$R_{tr}$ = on-resistance of the transistors in the buffer,

$C_{int}$ = total interconnect capacitance,

$C_L$ = load capacitance (capacitance of the output buffer).
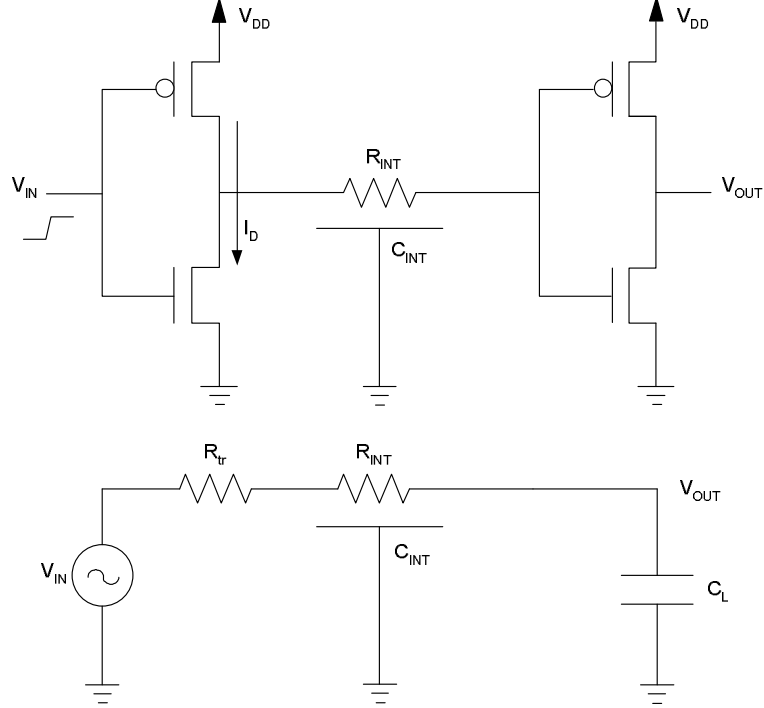


Figure 2.15: The circuit used for the derivation of the delay expression, where an interconnect is driven by an input buffer and at the output another buffer is connected.

It is assumed that when nMOS transistor in the buffer turns ON, the pMOS transistor immediately turns OFF and vice versa (so no cross-bar current occurs). The on-resistance of nMOS and pMOS transistors can be approximated as

$$R_{trn} = \frac{l_{eff}}{\mu_n C_{ox}(V_{DD} - V_{Tn})W} \tag{2.6}$$

and

$$R_{trp} = \frac{l_{eff}}{\mu_p C_{ox}(V_{DD} - V_{Tp})W} \tag{2.7}$$

where,

$l_{eff}$ = transistor gate length,

$W$ = transistor width,

$\mu$ = mobility of carriers in the transistor,

$C_{ox}$ = gate capacitance per unit area.

If the interconnect is long such that $C_{int} \gg C_L$, then equation (2.5) reduces to

23

$$t_{delay} = 0.4R_{int}C_{int} + 0.7R_{tr}C_{int} \qquad (2.8)$$

The expressions given above can provide a qualitative idea of the effects of different parameters on the delay. Moreover, they help to understand how variations in these parameters can affect the delay characteristics.

It may be noted that the delay given by the expressions (2.5) and (2.8) is the Elmore delay [52]. Elmore delay is the most common and fastest approach for computing the signal delay of a wire. However, it accounts for only the first order moment and thus gives an approximation of the actual RC delay. When better accuracy in delay estimation is required, higher moments will have to be included using SPICE simulation.

## 2.5.2 Skew

The difference in the arrival times amongst a group of signals (at a specific location) is defined as the skew in the group. The skew is a critical parameter for high speed circuits, as it can limit their performance. Therefore its minimization is emerging as a difficult engineering challenge to afford proper circuit operation under the tight design margins left by the increasingly short clock period. Traditionally, skew has always been a point of concern for the clock distribution network in synchronous circuits. However, it is also becoming an important parameter to control in high speed data transmission between different functional blocks on the chip.

### 2.5.2.1 Clock Skew

There is a fundamental difference between clock distribution and data distribution because clock signal is periodic and predictable and every sequential element in a synchronous circuit needs it. Generally, the delay of the clock signals does not matter, as long as the clock signal reaches all circuit locations simultaneously [53]. However, in all practical systems (especially large synchronous systems), the clock signals do not exactly arrive at the same time at different spatial locations, and hence are skewed. Figure 2.16 gives an illustration of clock skew in a simple H-tree clock distribution network (CDN).

The possible causes of skew in the clock signals may be the mismatch of the signal path length in the clock tree, imbalance of loads at different nodes of CDN, or process variations in the devices and interconnects. Clock drivers (buffers) of different sizes are used in the CDN which can be a potential source for introducing skew (due to device variability) along with the interconnect variability.

(a)



(b)
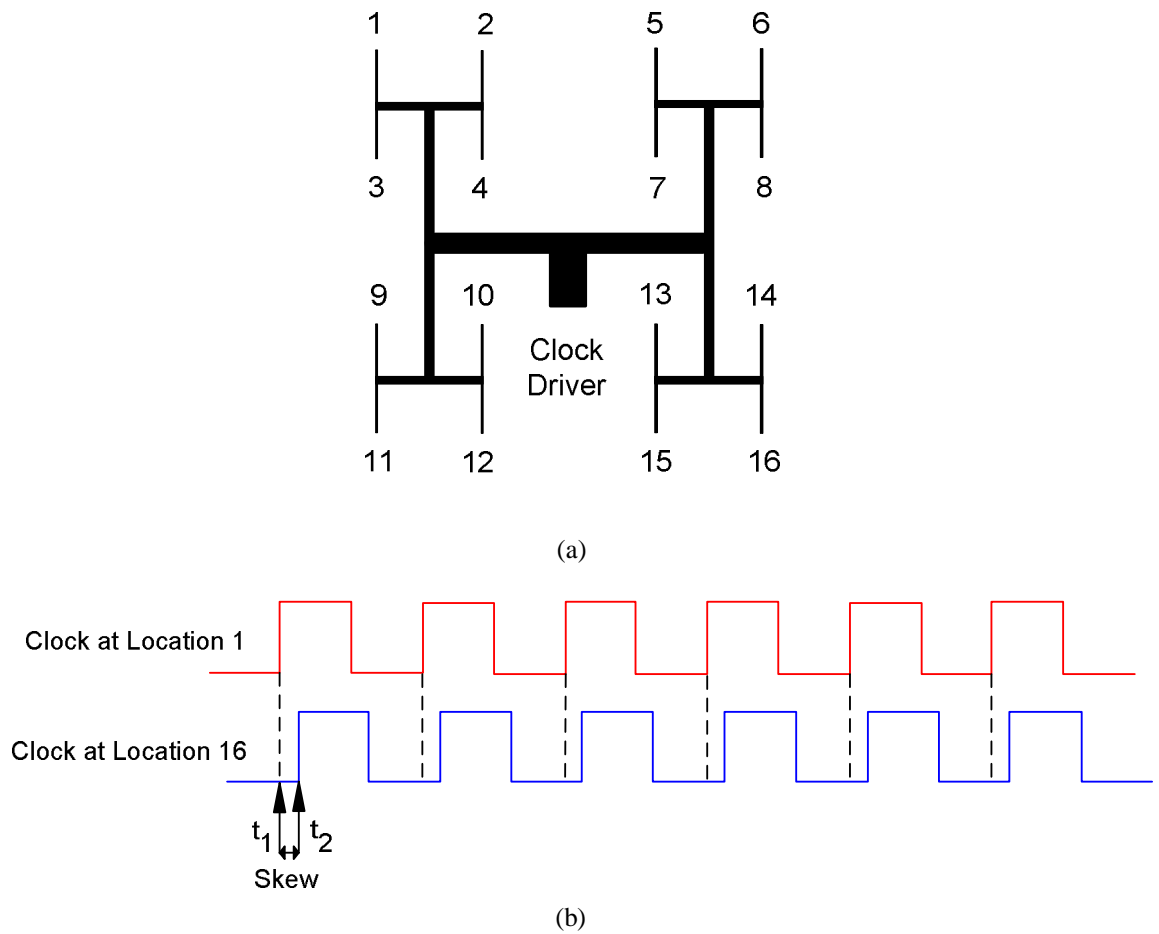
Figure 2.16: (a) A simple H-tree with 16 nodes, and (b) an illustration of skew in the clock signals due to difference in their arrival times at location 1 and location 16 of the H-tree.

### 2.5.2.2 Skew in Data Links

With the speed increase of digital systems, the demand for high speed links used for the exchange of data between different functional blocks on the chip has also increased. The link can consist of a single wire, a group of wires forming a parallel link or a more complex serial link. However, all these links have to perform the difficult task of orchestrating fast computation and data transfers through the functional units connected to them.

The serial links use a small number of wires and usually operate at high frequency to meet bandwidth requirements. The overall bandwidth of serial links depend on the characteristics of the interconnect and the abilities (complexity) of the receiver (and transmitter).

A high speed differential serial link is shown in Figure 2.17. Ideally, the differential signals travelling on two separate lines should remain synchronous at any time until they reach the receiver. However, in reality there are certain factors such as mismatching of wire lengths

due to routing constraints, variability in interconnects and/ or devices, due to which the signals arrive at slightly different times. This effect causes skew in differential pairs as shown in the figure. Skew beyond a certain value may not be tolerable for proper functioning of the receiver. Thus the skew beyond permissible limits can either limit the speed of these links or can cause functional errors.
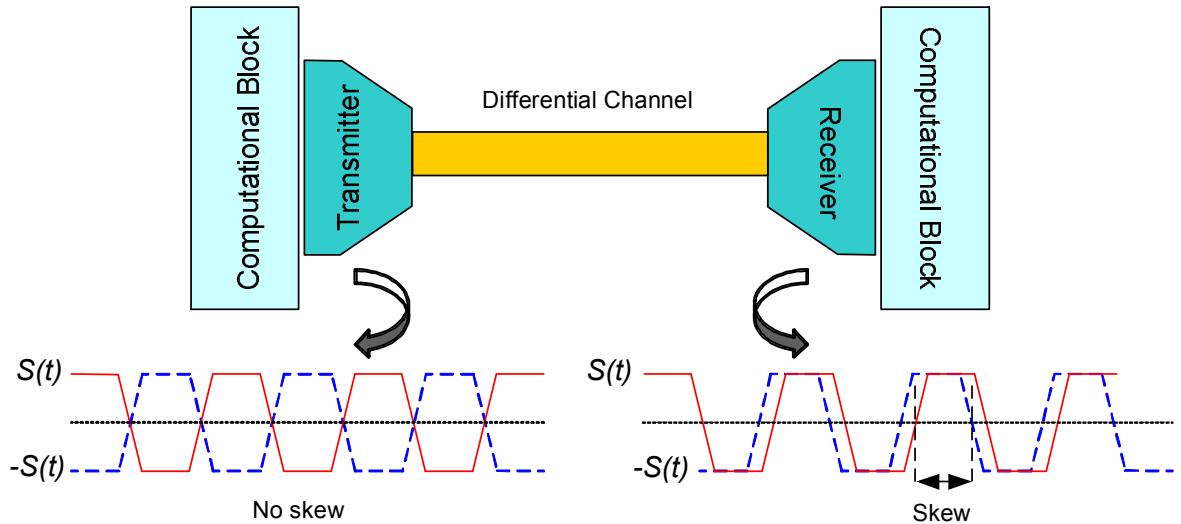


Figure 2.17: A high speed differential serial link. The skew beyond a limit can also effect its functioning.

Alternatively, parallel links can also be used for data communication. Here a group of bits is simultaneously transferred through a number of wires (typically the number of bits is equal to the word size). Ideally, all the bits arrive simultaneously and are sampled with the arrival of a clock edge. Again, in reality this is an idealization and in reality signals travelling through different wires of a parallel link arrive at the destination at slightly different time instant as shown in Figure 2.18.
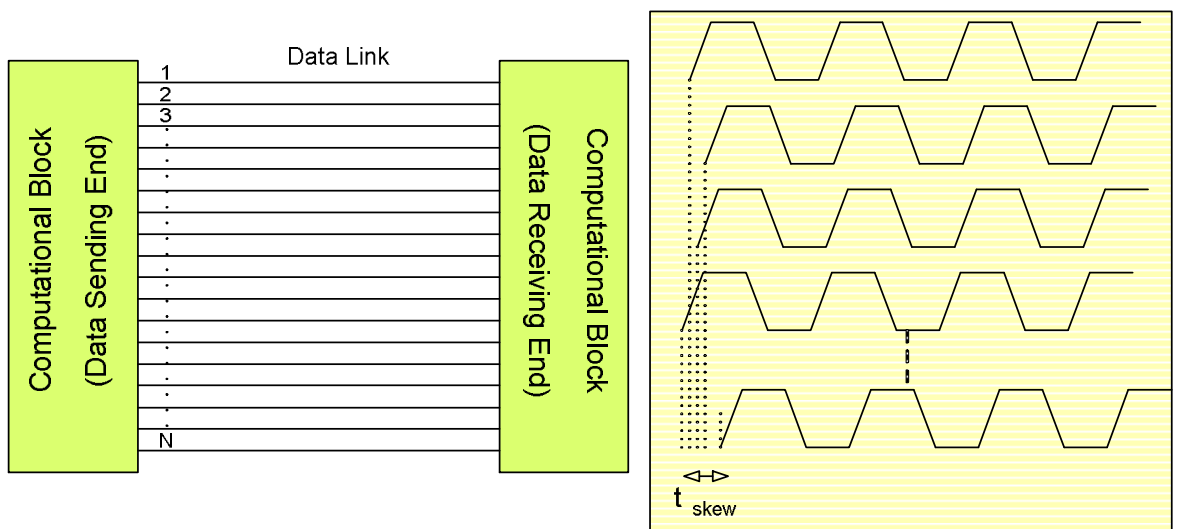


Figure 2.18: An N-bit parallel link. The skew reduces the amount of the bit overlap.

Due to the presence of the skew in the signals, the amount of overlap at the destination reduces, thereby increasing the probability of data sampling error. The skew can either reduce the operational distance or the throughput of a parallel link. If left unbounded, data corruption and functional errors will ensue.

### 2.5.3 Delay Variability

The variability in the devices and/ or interconnect has a direct impact on the performance of circuits. In the presence of variability, the signal delay no longer remains a deterministic fixed quantity and so the arrival times of signals can vary significantly. Thus the signal paths which are not critical in a circuit design may become critical under the impact of variability and can result in the malfunctioning of the circuit; in other words, there ceases to exist a unique critical path. On-chip communication circuits may also suffer from such variability issues and can affect the performance of circuits. The delay variability is, therefore, an important design metric and should be considered in the design process for making accurate signal timing plans.

Under the impact of variability, the signal delay becomes a random variable (RV). The characteristics of this RV can be determined by computing its probability distribution function (PDF) or cumulative distribution function (CDF). The moments of the probability distribution function represents their different characteristics. For instance, the first moment represents the mean value ($\mu$) and the second moment gives the dispersion of the distribution about the mean (in terms of the standard deviation, $\sigma$). Similarly, other aspects of the distribution such as whether the distribution is skewed or peaked are described by higher moments.

The delay variability is defined as ($3\sigma/\mu$) where $\sigma$ is the standard deviation and $\mu$ is the mean value of a set of delay data. It provides a measure of the dispersion of delay values about the mean value. This metric should be as small as possible for the circuits. Depending upon the shape of the distribution, other higher moments are also required for accurate timing analysis.

### 2.5.4 Crosstalk

Crosstalk arises when a neighbouring wire (aggressor) unintentionally affects (couples energy into) another wire (victim). It occurs due to the coupling between the neighbouring wires and can be classified into *functional noise and delay variation*. Functional noise refers to a fluctuation in the signal state of a quiet wire (non-switching) due to switching in

the neighbouring wire. This noise produces a glitch that may propagate through the interconnect to the dynamic node or a latch and may tend to change the signal state. This is illustrated in Figure 2.19, where the effect is shown on a quiet victim line due to the switching in a neighbouring aggressor line.



(a)



(b)
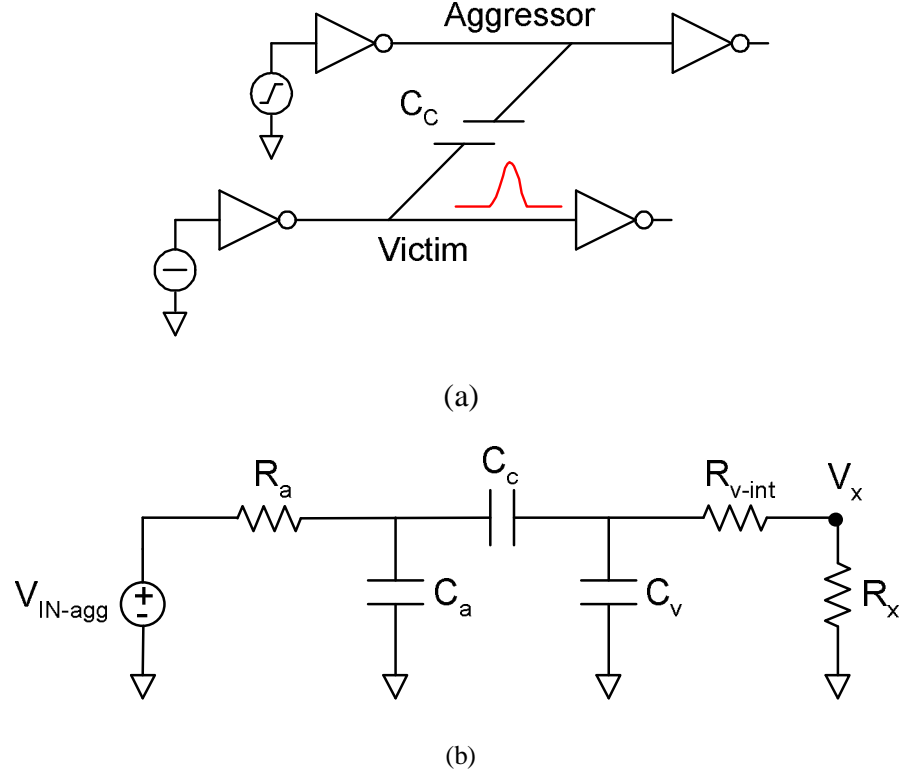
Figure 2.19: Two RC coupled interconnects. Due to switching of the aggressor line, a voltage is induced in the victim line as shown in (a). The equivalent circuit of the crosstalk model is given in (b).

Crosstalk can also cause variation in the delay of signals depending on the phases of the aggressor and victim line signals. If the aggressor and victim lines switch in the same phase, the signal speed on the victim line will increase and this is called in-phase crosstalk. On the other hand, if the two signals switch in the opposite phase, the crosstalk will reduce the signal speed in the victim line and this is called out-of-phase crosstalk [54]. On a chip, an interconnect may have multiple couplings with neighbouring wires and simultaneous switching on these wires will increase the magnitude of the crosstalk, thereby affecting the propagation delay and introducing delay variations [55]. These delay variations may result in timing failures. Therefore, crosstalk effects are very critical in the designing of high performance circuits.

There are several publications [30], [56], [57] which have discussed crosstalk in interconnects and have derived analytical expressions. A relatively simple expression used

to calculate the induced voltage due to a rising step of amplitude $V_{dd}$ and rise time $T_r$ at aggressor driver output, in an RC coupled interconnect is given by [58] and is

$$V_x = \frac{R_v C_c V_{dd}}{\tau_0 T_r} \left\{ \tau_1 \left[ e^{-t/\tau_1} - e^{-(t-T_r)/\tau_1} \right] - \tau_2 \left[ e^{-t/\tau_2} - e^{-(t-T_r)/\tau_2} \right] \right\}, \quad t \geq T_r \quad (2.9)$$

The equivalent circuit of the crosstalk model is shown in Figure 2.19(b), where $R_a, C_a, C_v$ and $C_c$ are respectively the aggressor line resistance, total capacitance of the aggressor line, total capacitance of the victim line and coupling capacitance between the two lines. $R_{v-int}$ is the victim line resistance and $R_x$ is the driver resistance of the victim line. The victim resistance $R_v$ is $R_{v-int} + R_x$. The time constants $\tau_0, \tau_1$, and $\tau_2$ are given by

$$\tau_0 = \sqrt{\alpha^2 - 4\beta} \qquad (2.10)$$

$$\tau_1 = \frac{2\beta}{\alpha + \tau_0} \qquad (2.11)$$

$$\tau_2 = \frac{2\beta}{\alpha - \tau_0} \qquad (2.12)$$

where,

$$\alpha = R_v(C_v + C_c) + R_a(C_a + C_c) \qquad (2.13)$$

$$\beta = R_v R_a(C_a C_c + C_a C_v + C_c C_v) \qquad (2.14)$$

The above expressions clearly show the dependence of crosstalk noise on interconnect and device parameters.

With technology scaling, signal speeds are increasing, interconnect aspect ratios are increasing and also interconnects are coming closer. Moreover, the supply voltages and also the design margins are reducing. More importantly, variability is also influencing crosstalk effects. Therefore, it is important to analyse the performance of on-chip communication networks in crosstalk environment under the impact of variability.

### 2.5.5 Power Dissipation

Buffer (repeater) insertion is a common technique to optimize the performance of global interconnects for on-chip communication networks. With technology scaling, more and more functionality is being integrated and thus on-chip communication networks are also growing rapidly. Moreover, the number of optimal buffers per unit interconnect length are also increasing (due to progressively resistive interconnect) and therefore very large number of these buffers are used in high performance designs [59]-[60]. Optimal repeaters

are used to construct delay optimal interconnections and are of a significant size. Thus they consume a proportionally large portion of the silicon and power [61]. The power dissipation has been pointed out as the main limiting factor in the scaling of the future CMOS circuits [62]. Therefore, power estimation for on-chip communication (and the whole chip) is an important metric to consider during the design process.

The power dissipation in CMOS circuits comprises: (1) the dynamic (switching) power ($P_{SW}$), (2) the short circuit power ($P_{SC}$) and (3) the leakage power ($P_{leak}$). The average power can be expressed as the sum of these three components

$$P_{Total} = P_{SW} + P_{SC} + P_{leak} \tag{2.15}$$

A brief description of these power components is given below [24], [42]:

### 2.5.5.1 Switching Power

Switching power is the power dissipation whenever there is a state transition, from low-to-high or from high-to-low, in the circuit. The energy during this transition is actually consumed in charging or discharging (low-high or high-low) the load capacitance connected at the output of the driver (a buffer). In deep sub-micron on-chip communication networks, the load capacitance consists primarily of the interconnect and gate capacitance.

The switching power dissipation in a buffer driving an interconnect of length $l$ having resistance $r$ and capacitance $c$ per unit length is given by [24]

$$P_{SW} = \alpha\big[s(c_0 + c_p) + lc\big]V_{dd}^2 f_{CLK} \tag{2.16}$$

where

$c_0 =$ input capacitance of a minimum sized buffer,

$c_p =$ output parasitic capacitance of the minimum sized buffer,

$f_{CLK} =$ clock frequency,

$V_{dd} =$ power supply voltage,

$s =$ buffer size,

$\alpha =$ switching or activity factor and gives the fraction of buffers switching during an average clock cycle.

The switching power is independent of the rise or fall time of the input waveform. The expression of $P_{SW}$ (Eq. 2.16) shows that the switching power can be reduced by reducing the supply voltage $V_{dd}$. However, this is at the cost of increased delay.

**2.5.5.2 Short Circuit Power**

The buffers or repeaters which are used to drive interconnects consist of inverters constructed with nMOS and pMOS devices. If the input to a buffer has a finite rise time and fall time, then during the switching process both nMOS and pMOS transistors may conduct simultaneously for a short interval of time, forming a direct path between the supply and ground for the flow of the current. The short circuit power is that dissipated during this eventuality. Unlike the switching power, the rise time and fall time play an important role in the determination of the magnitude of the short circuit power. If $V_{Tn}$ and $V_{Tp}$ are the threshold voltages of the nMOS and pMOS transistors respectively, then following condition holds during the short circuit phase

$$V_{Tn} < V_{IN} < V_{dd} - |V_{Tp}|$$

Approximating the short circuit current by a triangular waveform, the total short circuit power is given by [24]

$$P_{SC} = \alpha t_r V_{dd} W_{n_{min}} s I_{SC} f_{CLK} \qquad (2.17)$$

where

$W_{n_{min}}$ =minimum width of the nMOS transistor,

$s$ = transistor size

$I_{SC} \approx 65 \mu A/\mu m$  across all technologies.

$t_r$ is given by

$$t_r = \left[ r_s(c_0 + c_p) + \frac{r_s}{s} cl + rlsc_0 + \frac{1}{2} rcl^2 \right] \ln 3 \qquad (2.18)$$

If the input rise and fall times are much larger than the output rise and fall times, the transistors will conduct for longer time and therefore short circuit current will increase. It is proposed in [63] that the short circuit current can be eliminated if the power supply voltage is adjusted such that

$$V_{dd} < V_{Tn} + |V_{Tp}|$$

Under this condition, both nMOS and pMOS transistors will not be ON simultaneously for any input voltage. However, this technique will make the circuit more vulnerable to noise effects due to reduced signal to noise ratio.

Figure 2.20 shows a rough sketch of the voltage and current waveforms of a simple buffer (inverter) circuit during its switching. Figure 2.20(b) shows the short circuit current and Figure 2.20(c) shows the switching current. Note that short circuit current is much smaller as compared to the switching current.

### 2.5.5.3 Leakage (static) Power

Ideally, the power dissipation in CMOS circuits is thought to occur only during their state transitions and once the circuits are in a stable state, there should not be any power dissipation. However, a leakage current flows through the CMOS circuits during any of the states. This constitutes an increasingly important component of the total power dissipation-called leakage power.
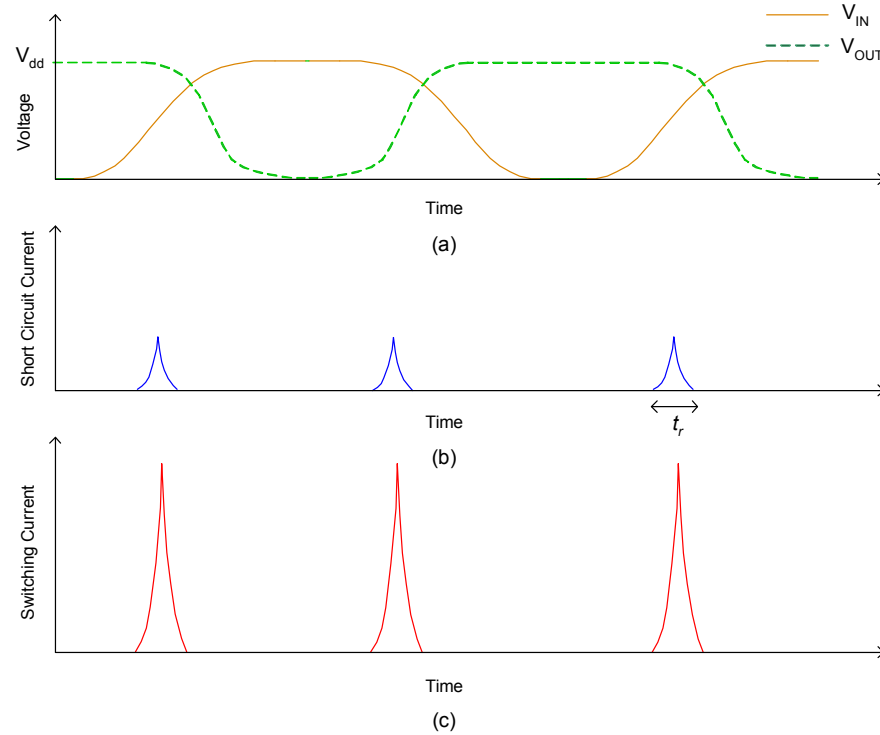


Figure 2.20: (a) A rough sketch of voltage and current waveforms of a simple buffer circuit, (a) input and output voltage waveforms, (b) the short circuit current peaks appear when both nMOS and pMOS conduct, and (c) the switching current used for the charging and discharging of the capacitive load.

Five major sources of leakage power in CMOS devices are [64]

(i)     Sub-threshold leakage, $(ISUB)$

(ii)    Gate oxide tunneling leakage, $(I_G)$

(iii)   Reverse bias junction leakages, $(IREV)$

(iv)    Gate induced drain leakage, $(IGIDL)$

(v)     Gate current due to hot carrier injection, $(I_H)$

These effects are becoming more important as the devices are miniaturized with technology scaling and so leakage power is rapidly increasing and dominating in the CMOS circuits [65].

The buffers used in on-chip communication also exhibit this mode of power dissipation. According to [24], the average amount of leakage power in the buffers inserted in the interconnect is given by

$$P_{leak} = V_{dd} I_{leak} \tag{2.19}$$

$$= V_{dd} \frac{1}{2} \left( I_{off_n} W_{n_{min}} + I_{off_p} W_{p_{min}} \right) s \tag{2.20}$$

where, $I_{leak}$ = leakage current through the buffer,

$I_{off_n} \left( I_{off_p} \right)$ = leakage current per unit width of nMOS (pMOS) transistor,

$W_{n_{min}} \left( W_{p_{min}} \right)$ = width of the nMOS(pMOS) transistor in a minimum size buffer(inverter). Like delay, statistical device variability has also introduced variability in the leakage power and has become a point of serious concern in deep sub-micron technologies. Both delay and leakage power variability, are seriously effecting the performance, yield and reliability of the circuits and seems to be an obstacle in the progression of designing power-constrained high performance circuits using miniaturized devices [65]-[67].

### 2.5.6 On-Chip Area

On-chip communication networks are deeply spread over the whole chip to provide communication media to the functional units. However, as previously stated, they consume a larger portion of the chip area due to large number of buffers. In future technology generations, unconstrained optimal buffering of interconnects might require up to 80% of the total on-chip area [68].

The area of the on-chip communication network is simply the area occupied by the wires and the area of CMOS circuitry used to drive these wires (line drivers, buffers, switches, etc.). The total area of the repeaters of size $s$ placed at regular intervals of length $l$ in an interconnect of length $L$ can be estimated as

$$A_{repeaters} = \frac{L l_{eff} s}{l} \tag{2.21}$$

where, $l_{eff}$ is the effective transistor gate length. (This is actually a lower bound; routing might add more area).

Limited area resources available on the chip have made this metric very important for the present and future system designs.

### 2.5.7 Throughput

Throughput is one of the important parameters of interest and is defined as the average rate of error free delivery of data over a communication channel. It is generally measured in bits per second (bps) or data packets per second.

### 2.5.8 Bandwidth

Bandwidth refers to the maximum capacity of error free data transmission over a communication channel. The higher the bandwidth, better will be system performance and so there are always been design efforts to maximize it.

### 2.5.9 Parametric Yield

Due to process variations, the uncertainty in the performance and power characteristics of the designs is increasing [69]. This can lead to a significant deviation of the manufactured products from their actual designs.

Parametric yield is defined as the percentage of the manufactured dies which meet the specified frequency and power consumption requirements [70]. It can be calculated as

$$P\left(\chi \le \chi_{Target}\right) = \int_{0}^{\chi_{Target}} p(\theta)d\theta \qquad (2.22)$$

where, $\chi$ is the observed delay or power dissipation and $\chi_{Target}$ is the corresponding constraint.

The yield measurement could result in discarding a large number of dies which do not meet the performance or power criteria, even if they are otherwise functional. This results in parametric yield loss. Since power dissipation and delay are negatively correlated, fast designs may consume more power, causing an increased yield loss. Similarly, power efficient designs may not fulfill the performance requirements and again result in yield loss. Therefore, careful consideration of this metric is required in the designs.

## 2.6   Performance Characterization Methodology

In some recent studies, the effect of intrinsic parameter fluctuations introduced due to RDF and other sources, on the performance of CMOS circuits has been studied for the future technology generations [71]-[73]. The 3-D atomistic simulation method [74], [75] is used

to study the effect of different sources of variability at device level. However, this method is not feasible for circuit level analysis, being computationally expensive.

In this research, the performance of on-chip communication circuits for the future technology generations of 25, 18 and 13 nm physical gate length bulk MOSFETs has been accurately characterized using Monte Carlo (MC) method and HSPICE simulations of a large number of distinct realizations of the circuit under investigation. The industry standard BSIM4 model card libraries have been used for the given technology generations [76]. These model card libraries are developed through parameter extraction strategy [77] in which the comprehensive Glasgow 3D statistical physical device simulations are performed and fluctuation information due to random dopant fluctuation (RDF) is transferred into the model card libraries.

The devices in each library are macroscopically similar but are microscopically different due to the difference in the number and position of the dopant atoms in the channel. So all the devices in each library have different characteristics due to statistical variations in the device parameters and the distribution of these variations represents the distribution of variations found in the general population. For the statistical analysis, a Monte Carlo simulation method has been used (as previously stated) with random selection of the devices from the given model card libraries, while constructing different circuit realizations. The circuits are biased with a supply voltage of 1.1V, 1.0V and 0.9V for the technology generations of 25, 18, and 13 nm, respectively [78]. Different delay measurements taken during this study correspond to 50% of the signal levels during the transitions. Power measurements for the circuits have also been made through this methodology. Several sets of HSPICE simulations have been performed for the transient analysis of the circuits.

## 2.6.1 Extraction of I-V Characteristics of MOSFETs

The dependence of the device drain current on the gate voltage is given by the I-V characteristic curves. In order to validate the test methodology, the IV characteristics of the devices in the library has been measured. These curves have been plotted for the nMOS and pMOS devices of the given three technology generations and are shown in Figure 2.21. Each set of the curves is plotted for 200 devices taken from the model card libraries. The blue curve (with symbols) over the red curves and red curve (with symbols) over the blue curves is for the uniformly doped devices. These curves match the data in [145] and show that I-V characteristics of the devices in the model card libraries differ from each other

under the impact of RDF and lie on both sides of the uniformly doped device curves. It may also be noted that the spread of these curves increases with technology scaling. This hints that the delay characteristics of the devices (and circuits) will certainly be affected due to the variability in the I-V performance.
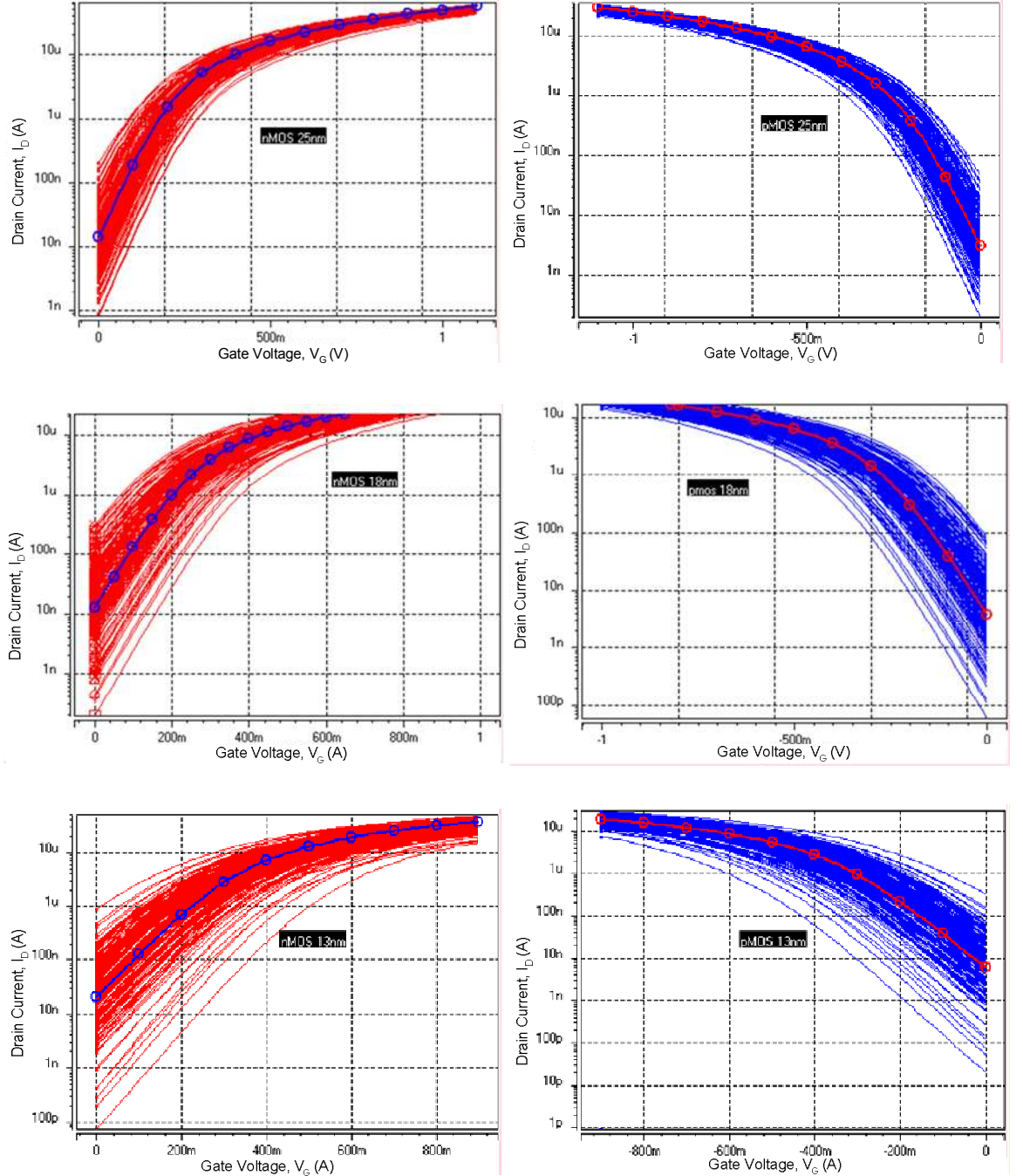


Figure 2.21: I-V characteristic curves of 200 devices for each of nMOS (left) and pMOS (right) for the technology generations of 25, 18 and 13nm. Along with each set of curves, the characteristic curve for the uniformly doped device is also plotted and the dispersion of other curves around this curve shows the effect of variability due to RDF.

## 2.7 Summary

This chapter gives an introduction to the on-chip communication structures used in SoCs. In all the structures, the underlying communication links play an important role in their design. Therefore, modeling of interconnects used in these links is first presented. Subsequently, different performance metrics used to evaluate the performance of the communication structures in DSM regions have been discussed. Finally, the methodology used in this thesis to characterize the performance of different circuits is outlined.

# Chapter 3

# Communication Structures under Device Variability

A clock distribution network (CDN) and a data channel (DC) consists of basic circuit elements like tapered buffer drivers, buffers (repeaters), flip-flops (or latches) and interconnects, as shown in Figure 3.1. Hence the performance of CDN and DC (and consequently the synchronous system) depends on the performance of these circuit elements.

The performance of on-chip communication circuits (CDN or DCs) can be estimated either through modelling or simulation. However, it is very difficult (if possible) to accurately model these circuits while considering variability effects due to different parameters. In this situation, simulation can provide accurate results. The performance can be characterized by simulating the complete communication network or from the known performance of the individual communication elements. Again, evaluating the performance of a complete communication network through simulation is computationally very expensive and might not be feasible for large systems. Therefore, the performance of such large systems can be estimated with reasonable accuracy using the performance of the individual communication structures in some statistical framework.

Courtesy of IBM Austin Research Laboratory

◩ Clock Driver          ◩ Repeaters          ▨ Flip-flop or Latch

(a)



(b)



(c)
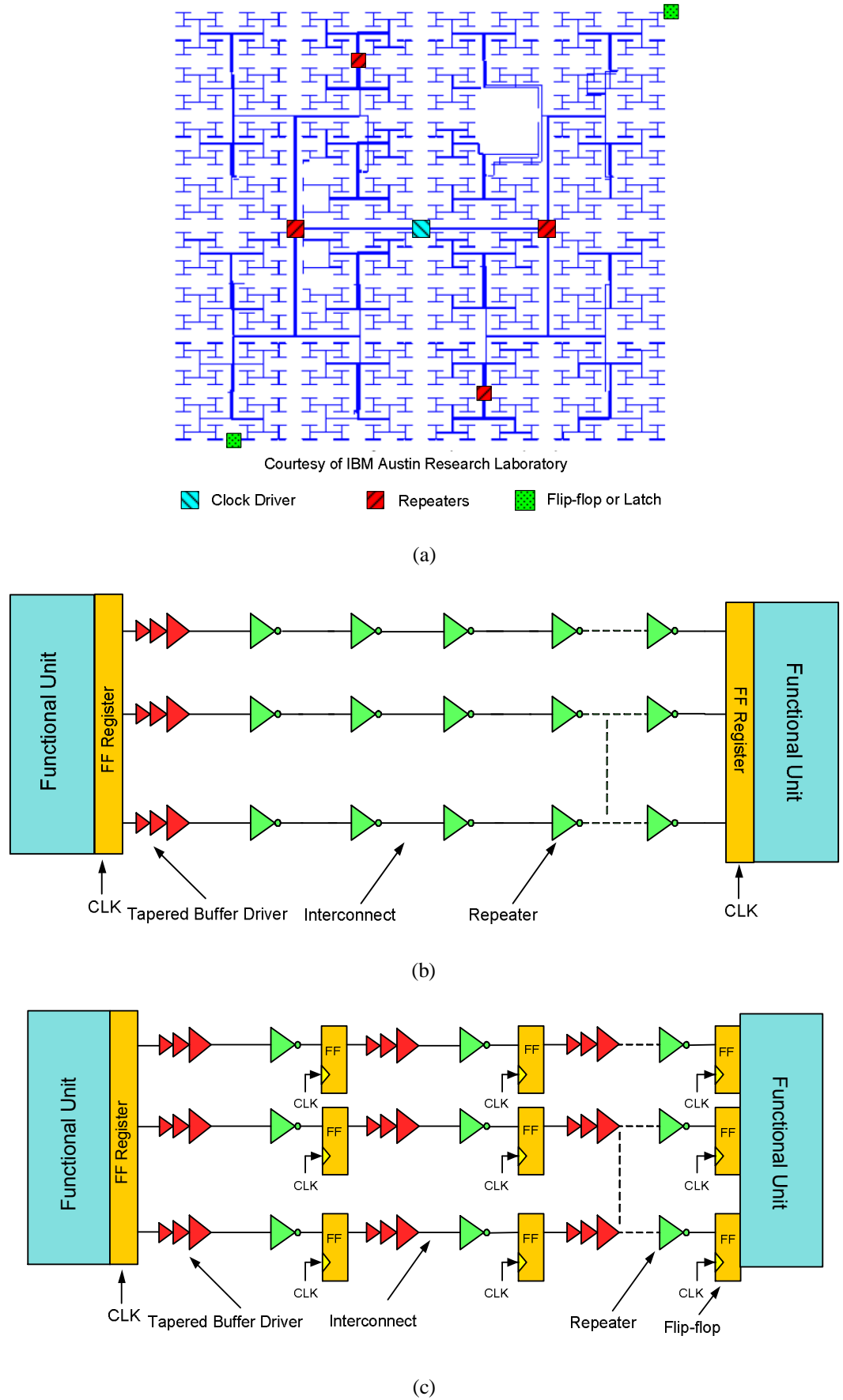
Figure 3.1: Communication structures in CDN and data channels: (a) an H-type CDN, (b) a repeater inserted synchronous data channel, (c) a flip-flop based pipelined data channel.

In this chapter we present a systematic study to investigate the effect that variability will introduce in the communication structures for future technology generations. Such a study becomes important for designers and academia so that they can formulate efficient design methodologies for the coming technology generations under tight design margins and other technology challenges.

## 3.1    Technology Scaling and Gate Delay

In a particular technology generation, the maximum clock speed and the speed at which computation can be performed, is determined by the gate delay. On-chip communication will need to be designed to support these speeds in order to preclude data starvation. Due to statistical variation in the devices, gate delay is no longer a fixed quantity, but a random variable (RV) which follows a given distribution. For better estimation of the maximum clock speed, statistically accurate description of the delay is required to be derived with consideration of the effects introduced due to variability. In this section, we study the impact of device variability in the gate delay of an inverter in a given technology, as representative of delay in more complex combinational circuits and gates. This delay has been measured in terms of FO4 delay and is used as a reference or benchmark to which we can compare the results of the communication structures. The metric FO4 delay or "fan-out-of-four inverter delay" has been used elsewhere [6] and is a quite reasonable metric, as four is the typical average gate connectivity in a digital circuit [79]. This is defined as the delay through an inverter driving four copies of itself. Since the effect of variability is more pronounced in smaller geometries, FO4 delay has been measured corresponding to
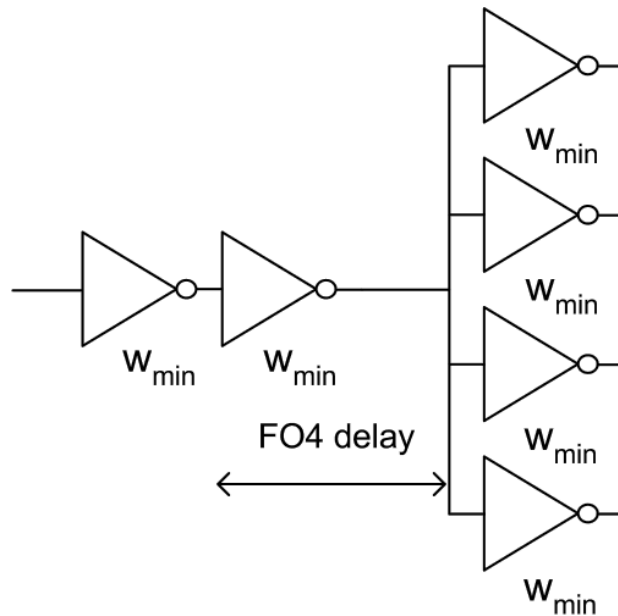


Figure 3.2: The definition of FO4 delay.

40

the delay of minimum sized inverters, as shown in Figure 3.2. Here we have used minimum sized inverters of size $w_{min}$=25, 18 and 13 nm for the given three technology generations of 25, 18 and 13 nm, respectively.

HSPICE simulations were performed (using the Monte Carlo method, described in section 2.6) and FO4 delay measurements were taken for the given technology generations. The mean value of the FO4 delay is plotted for the three technologies and results are shown in Figure 3.3. The standard deviation of the FO4 delay is also represented in the form of error bars. It can be seen that the mean value of the FO4 delay decreases, whereas the delay variability increases, with the decrease of the gate length. This is to be expected. However, we are interested in determining the nature of the delay distributions. For this reason, histograms are plotted from the measurement data and shown in Figure 3.4. It becomes evident that the dispersion of the distributions increases with gate length scaling. Moreover, the distributions are asymmetric about the mean delay and the degree of asymmetry increases with the decrease of the gate length. The positively skewed nature of the distributions has a detrimental impact on the performance of the circuits as a significant number of samples beyond the nominal value imply a long tail which will certainly limit the speed of the circuits and also introduces reliability issues.
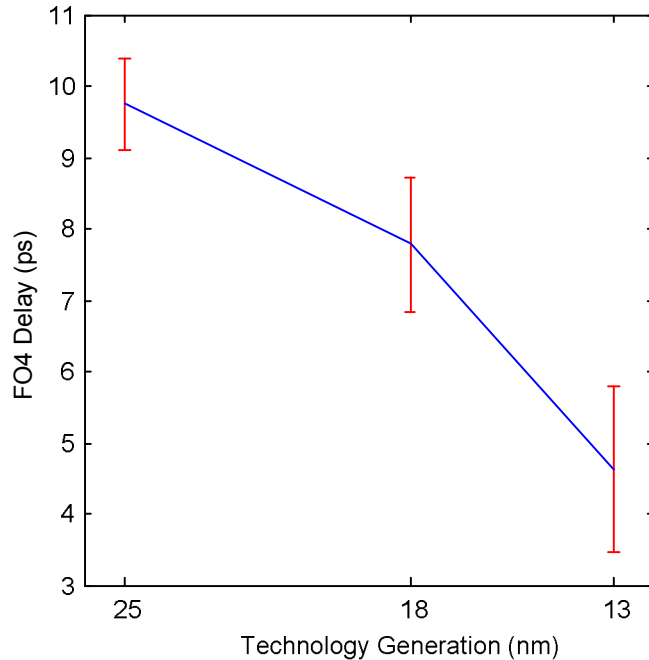


Figure 3.3: FO4 delay for different technology generations. The error bars represent the uncertainty in delay($\pm 1\sigma$).

More importantly, it becomes obvious that the dispersion and the worst case of FO4 delay grow hyper-linearly as the technology scales down. Due to this fact, the performance of

circuits will certainly be affected unless some corrective measures are not incorporated in their design. The effect becomes more important in the design of synchronous systems under the tight design margins typical of high performance circuits. It is obvious then, that variability in the devices warrants a careful consideration during the design of high performance circuits.
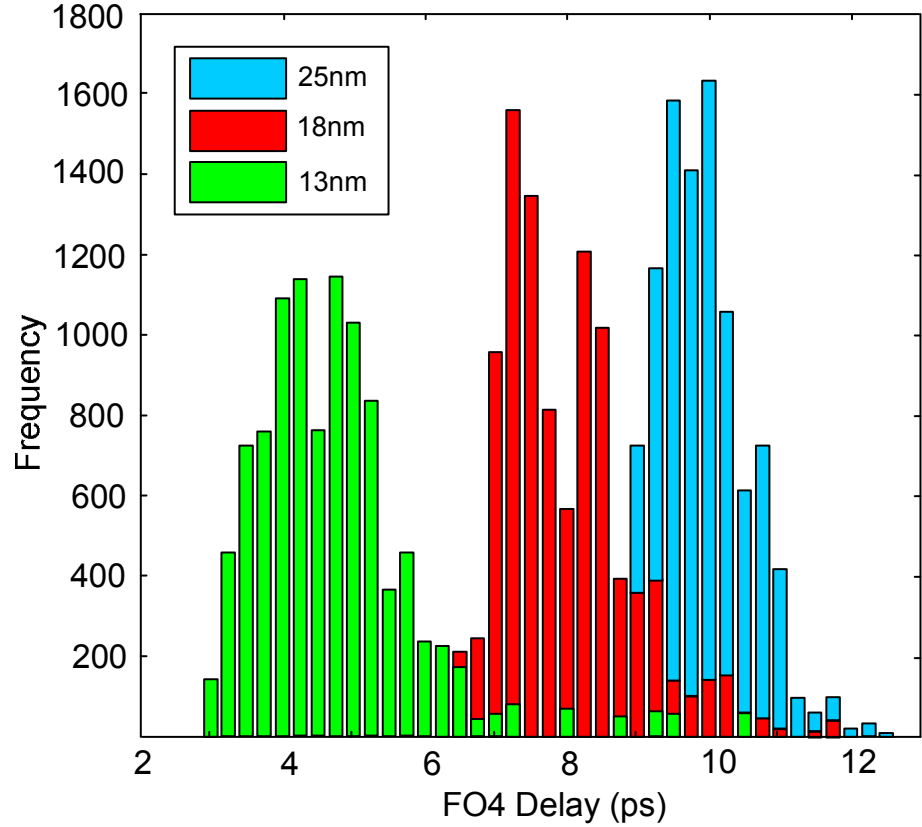


Figure 3.4: Delay distribution of minimum sized inverters with a fan-out of four for the technology generations of 25, 18, and 13 nm.

## 3.2   Delay Uncertainty in Buffers

The efficiency of high performance circuits not only depends on the performance of computational elements but also depends greatly on the communication network responsible for the exchange of data between the computational elements. Delay uncertainty in the clock signal can produce setup and hold time violations at the data registers. Similar violations can also occur in the data signals. A large number of buffers are used in these communication networks that can introduce delay uncertainty in the signals. For designing high performance circuits (with correspondingly tight timing constraints), the delay uncertainty will have to be reduced. Therefore, design methodologies that reduce delay uncertainty should be explored.

The delay of a CMOS buffer (inverter) to the first order, as given by Bakoglu [51] is

$$t_d = 0.7R_{drv}C_L \tag{3.1}$$

where $R_{drv}$ is the on-resistance and $C_L$ is the capacitive load at the output of the inverter. The inverter resistance $R_{drv}$, which is approximated by averaging the drain currents at the extreme points (0 and $V_{DD}$) of the high-to-low and low-to-high transitions, is given by

$$R_{drv} = \frac{L}{W\mu C_{ox}(V_{DD} - V_T)} \tag{3.2}$$

where,

$L$ = transistor gate length,

$W$ = transistor gate width,

$C_{ox}$ = gate capacitance per unit area,

$\mu$ = mobility of the transistor,

$V_{DD}$ = supply voltage.

A variation in these factors will cause the inverter resistance (and consequently the drain current) to change and eventually will result in variability of the gate delay. In deep sub-micron (DSM) region, it is impossible to precisely control all transistor parameters during the fabrication process. Therefore in a batch of similar transistors, different parameters can have a complete distribution with some nominal value and a wide spread about this nominal value. For instance, due to variations (in particular to random dopant fluctuations), the threshold voltage $V_T$ of the transistors will have some distribution (wider or narrower). Hence, the on-resistance of the transistors can no longer be treated as a fixed quantity; rather it will follow a distribution, resulting in the distribution of the inverter delay. Let $\chi_{dev}$ represents the effect of RDF on $V_T$, then the on-resistance of the inverter will be given by

$$R_{drv} = \frac{L}{W\mu C_{ox}(V_{DD} - V_T\chi_{dev})} \tag{3.3}$$

Therefore,

$$t_d = \frac{0.7LC_L}{W\mu C_{ox}(V_{DD} - V_T\chi_{dev})} \tag{3.4}$$

In order to evaluate the effect of variations in $V_T$ on the delay of the inverter, we differentiate $t_d$ with respect to $\chi_{dev}$, yielding

$$\frac{\partial t_d}{\partial \chi_{dev}} = \frac{0.7LV_TC_L}{W\mu C_{ox}(V_{DD} - V_T\chi_{dev})^2} \tag{3.5}$$

This shows that the sensitivity of the inverter delay is inversely proportional to the size (width) of the inverter. In the same way, the delay sensitivity to other transistor parameters

can be determined. Therefore, we can deduce that the simple technique of circuit scaling can be used to minimize the effect of RDF on delay variability.

We proceed to quantify the effect of RDF on the delay performance of individual buffers of different sizes. To this end SPICE models are developed for the buffers of sizes 1, 2, 3, 5, 7, 10, 15, 20, and 25 times $w_{min}$, with a load of a $25w_{min}$ buffer connected at their output (where $w_{min}$ = size of the minimum sized buffer = 25, 18 and 13 nm for the given three technology generations). The results of Monte Carlo simulations are shown in Figure 3.5, where mean delay and delay variability are plotted for the given buffer sizes. It can be seen that the buffer delay and dispersion in delay is inversely proportional to the buffer size, as expected from equation (3.4) and (3.5). More importantly, the relation is not linear and a small increase in the size of the buffer can give us significant advantage towards the improvement in delay and delay variability, especially at smaller buffer sizes.

It has also been found that there is a difference in the amount of delay variability for low-to-high and high-to-low transitions, as shown by the dashed lines in Figure 3.6. For instance, it is larger during high-to-low transitions and the effect is more prominent at smaller buffer sizes. This is due to the inherent nMOS and pMOS asymmetries i-e the size of the pMOS transistor is normally taken as twice the size of the nMOS transistor to make identical delay in both swings. Therefore, while considering delay variability, its magnitude in both swings is required to be considered.



(a)                                         (b)
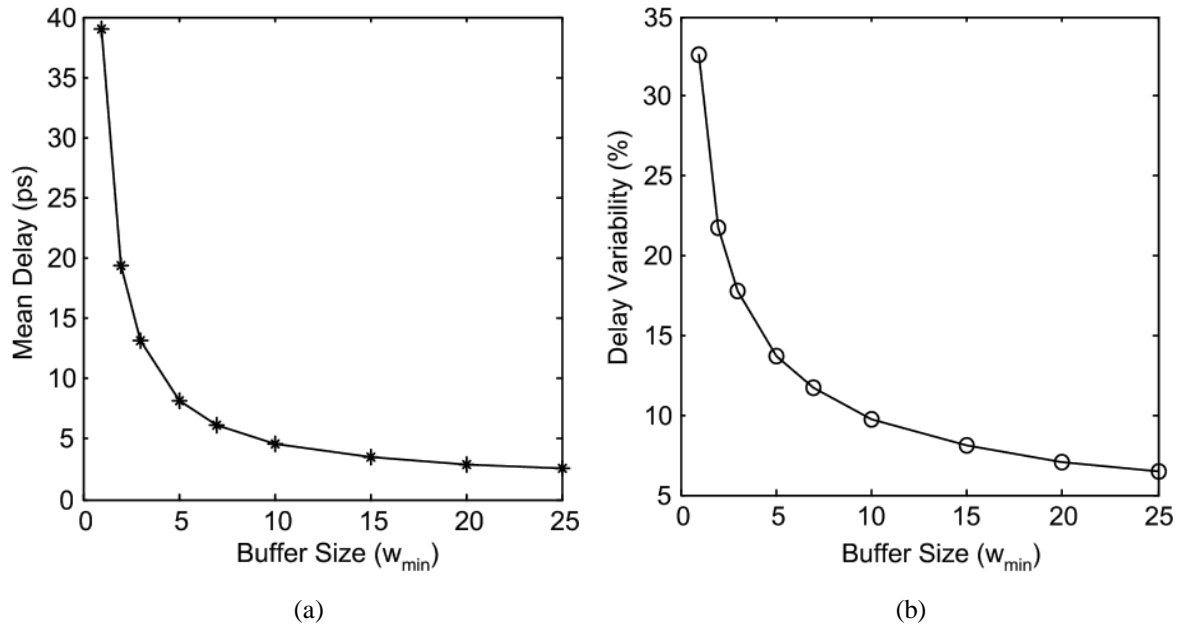
Figure 3.5: Mean buffer delay (a), Delay variability (b), plotted as a function of buffer size for 18 nm technology generation. The curves have been plotted for the average response in low-to-high and high-to-low transitions.

If we assume that delay variations in buffers of different sizes are independent of each other and if $V_d(1w_{min}) = 3\sigma(1w_{min})/\mu(1w_{min})$ is the delay variability of a minimum sized inverter in a given technology generation, then the delay variability of an inverter of size $mw_{min}$ can be approximated as

$$V_d(mw_{min}) = \frac{3\sigma(mw_{min})}{\mu(mw_{min})} \approx \frac{3\sigma(1w_{min})/\mu(1w_{min})}{\sqrt{m}} \tag{3.6}$$

(due to properties of the normal distribution). This relation can be used to make an estimate of the delay variability in a buffer of given size. It is, however, important to mention that equation (3.6) gives only an approximate result, especially in deep sub-micron technologies because this relation is valid for the distributions which are close to the normal distribution. However, we have seen that the delay distributions under RDF are skewed and the degree of skewness increases with scaling down of the technology.
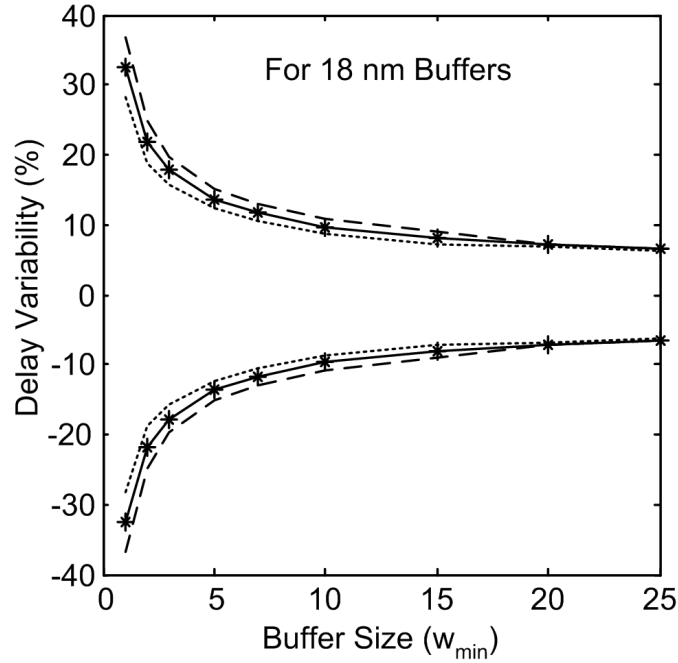


Figure 3.6: Delay variability plotted against buffer size for 18 nm buffers. The smaller dashed lines represent delay variability for low-to-high transition and bigger dashed lines for high-to-low transition. Similarly, the solid lines are for the average response.

### 3.2.1  Skewness of Delay Distributions

Skewness is a measure of the degree of asymmetry (lack of symmetry) of a probability distribution of a real valued random variable. The skewness of a distribution can be positive or negative or zero. If the tail on the right side of the probability density function is more pronounced than the left tail, the distribution is said to have positive skewness. In this case, the bulk of the values lie to the left of the mean. If the reverse is true, it is said to

have negative skewness. Zero skewness indicates that the values are relatively evenly distributed on both sides of the mean. The skewness of a distribution is defined as

$$\gamma_1 = \frac{\mu_3}{\mu_2^{3/2}}$$

where $\mu_i$ is the $i^{th}$ central moment.

As we have mentioned earlier, delay distributions of the buffers under RDF are positively skewed. The degree of skewness, however, depends on the size of the buffers. Figure 3.7 shows the dependence of the skewness on the size of the buffers for 13 nm technology generation. The curve shows that the delay distributions corresponding to small buffers are significantly skewed and the degree of skewness decreases as the size of the buffers increases. Thus for larger buffers, the delay distributions tend to approximate Gaussian distribution.

We will discuss skewness in more detail in Chapter 4.
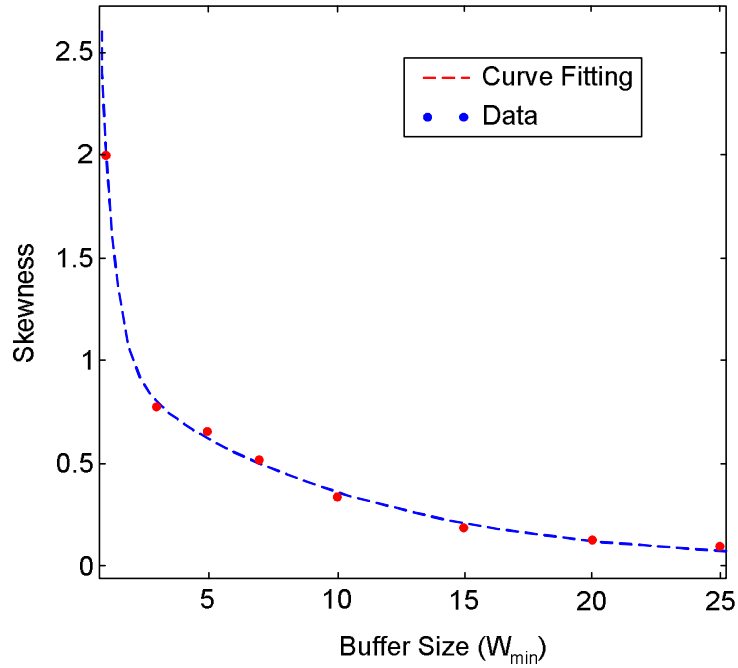


Figure 3.7: Skewness of delay distributions as a function of the buffer size for 13 nm technology.

## 3.3 Ring Oscillator (RO)

A ring oscillator is a type of test structure which is commonly used [80]-[81] for timing tests. It requires only one input start up signal (or no signal in case of self oscillating) and gives output in the form of frequency. This circuit can be used to assess the performance of buffers under the impact of RDF for a certain input signal and load conditions. A five stage

ring oscillator is shown in Figure 3.8 where the inverters have been constructed of minimum sized square devices and interconnect capacitance have been assumed to be negligible.
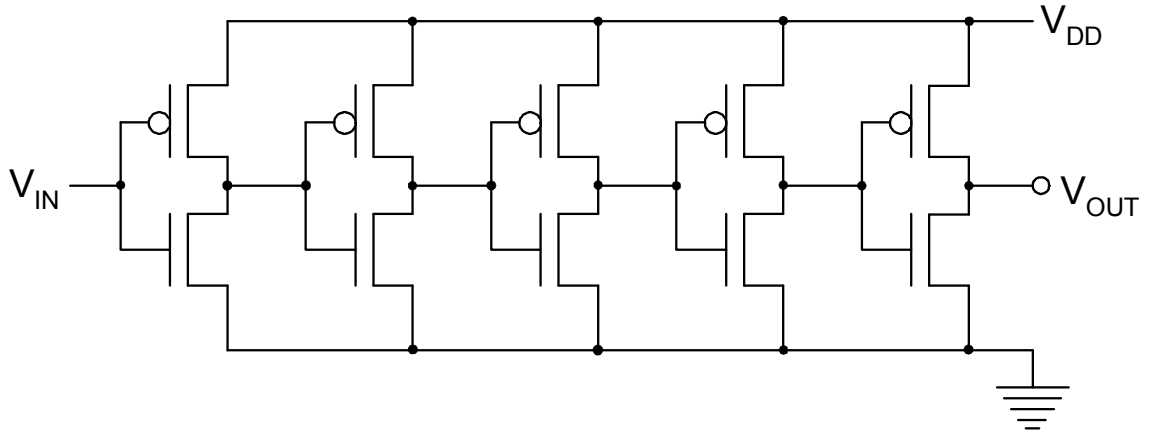


Figure 3.8: A five-stage ring oscillator circuit constructed of minimum sized devices.

The netlists for the ring oscillator were generated with random selection of the devices from the model card libraries and HSPICE simulations were performed. The results show that the average delay of a five-stage ring oscillator for 25 and 18 nm technology generation is 20.4 ps and 16.6 ps, which corresponds to a frequency of 24.5GHz and 30.1GHz respectively. However, due to RDF, the frequency has a spread with standard deviation of 0.8GHz and 1.67GHz (corresponding to a five-stage delay variation of $\sigma=0.67ps$ and $\sigma=0.925ps$), respectively for 25 and 18nm technology generations. This shows that the uncertainty in the timing signals increases with technology scaling.

## 3.4 Tapered Buffer Drivers

In CMOS integrated circuits, large capacitances are common in large fan-out circuits and/ or in long range interconnects. Therefore, in order to source and sink a relatively large amount of current, a tapered buffer system is used to drive such circuitry, especially where the load is predominantly capacitive. For instance, in a clock distribution network, such drivers are used to power up the clock source signal. As in any element, device variability will introduce delay uncertainty in these drivers resulting in the introduction of skew in clock distribution networks and in on-chip communication networks, thus limiting the performance and yield.

Such drivers are composed of a chain of cascaded inverters with increasing buffer sizes as shown in Figure 3.9. The drivers are sized according to [82] with total number of inverters

in the system equal to $N$ such that the last inverter in the chain can drive the load connected at its output. For the optimal delay performance of tapered buffers, a logarithmic tapering factor ($\beta = e = 2.72$) has been proposed [83], though in practice this value is seldom used.
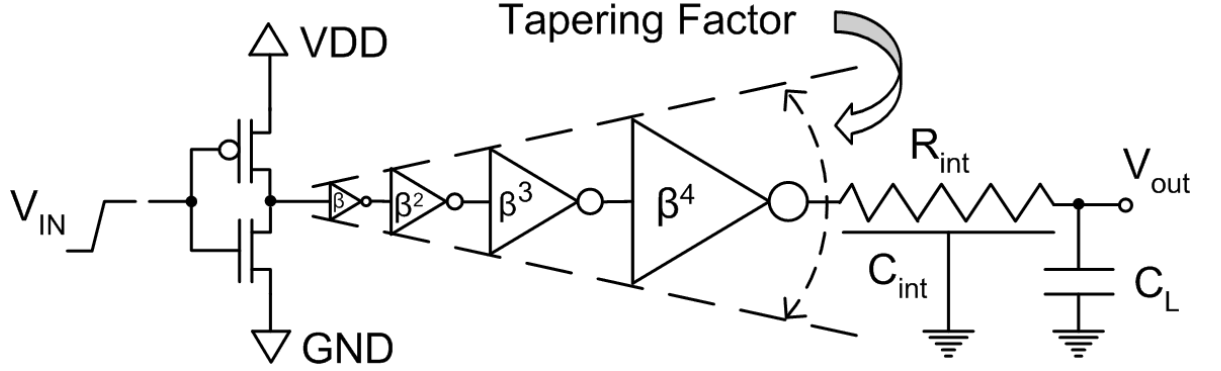


Figure 3.9: Tapered buffer driver system.

While using such buffers in the circuits, their delay performance under device variability needs to be known. Therefore, in this work we have investigated their delay performance when implemented in the given three technologies. A chain of five inverters (the first stage being of minimum size) has been used for this study and adjacent inverters in the driver chain are sized with a tapering factor β equal to 3. The delay performance of the drivers has been studied during low-to-high and high-to-low input transitions.
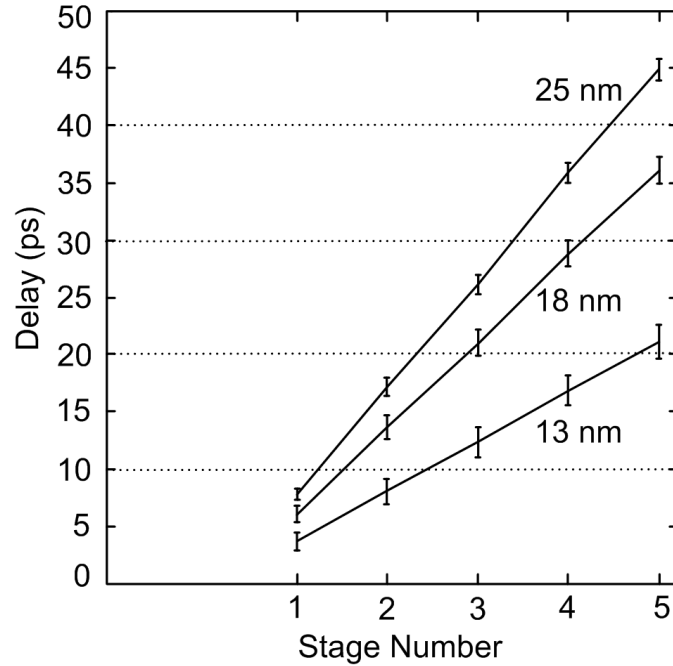


Figure 3.10: Cumulative mean delay in tapered buffer drivers of the given three technology generations along with the delay uncertainty shown as error bars (corresponding to 1σ).

The results show that as we proceed along the chain of inverters, the cumulative mean delay increases at each next stage, in a linear manner, as shown by the straight lines in Figure 3.10. However, the slope of these lines decreases with technology scaling, which means that tapered buffers can be constructed with relatively lesser delay penalty for smaller technologies. However due to device variability, the inverters used in the tapered buffer drivers introduce delay uncertainty at each stage which accumulates statistically and appears at the output of the driver. The amount of this delay variability increases in a non linear fashion with the number of stages and is shown in the form of error bars in Figure 3.10. This delay variability will have a detrimental effect in the designing of high speed circuits. The tapered buffer drivers from all the given technology generations show the same response and maximum delay variability has been observed in 13 nm drivers.
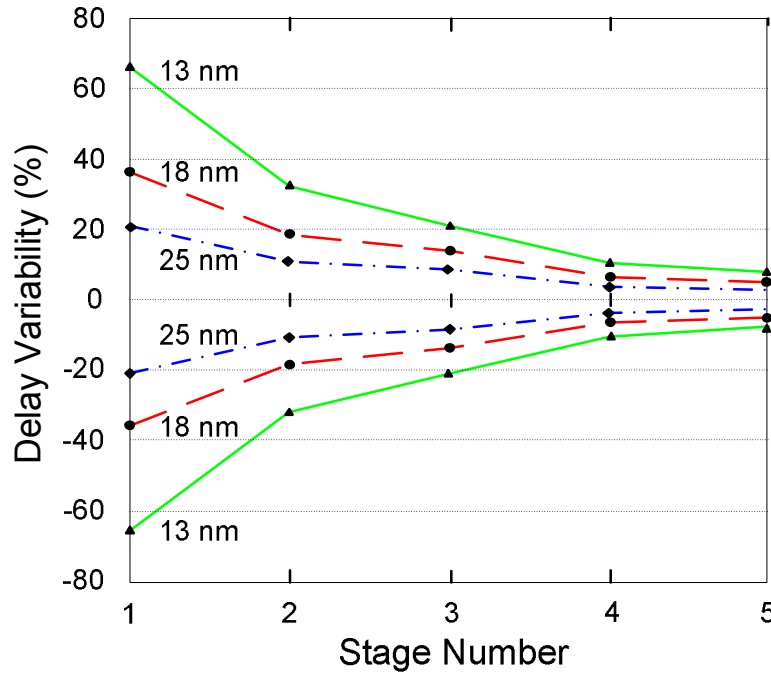


Figure 3.11: Delay variability introduced by different stages of the tapered buffer driver for low-to-high input transition.

Since inverters of different sizes are used in the driver chain, the share of each stage towards delay variability cannot be the same. The results show that earlier stages of the tapered buffer drivers contribute a major portion of the delay variability (as shown in Figure 3.11), because they are constructed with relatively smaller transistors. Again, it has also been found that the delay uncertainty introduced by each stage is different during low-to-high and high-to-low transitions due to the reason mentioned before. However, this difference reduces as we move along the chain towards larger sizes. This fact is shown in Figure 3.12 where the gap between the two solid lines gradually decreases with stage

number and finally the lines almost coincide after the fifth stage. The difference developed in all the stages travels through the chain and accumulates accordingly, thus making a difference in the delay variability at the output of the $n^{th}$ stage, depending upon the type of the input transition. For instance, the difference in the delay variability for low-to-high and high-to-low input transitions at the output of the 3$^{rd}$ and 5$^{th}$ stages is about 9% and 5%, respectively, for 13 nm drivers. It is also observed that maximum delay variability appears in the cumulative and stage delays for low-to-high input transitions, as shown in Figure 3.12.
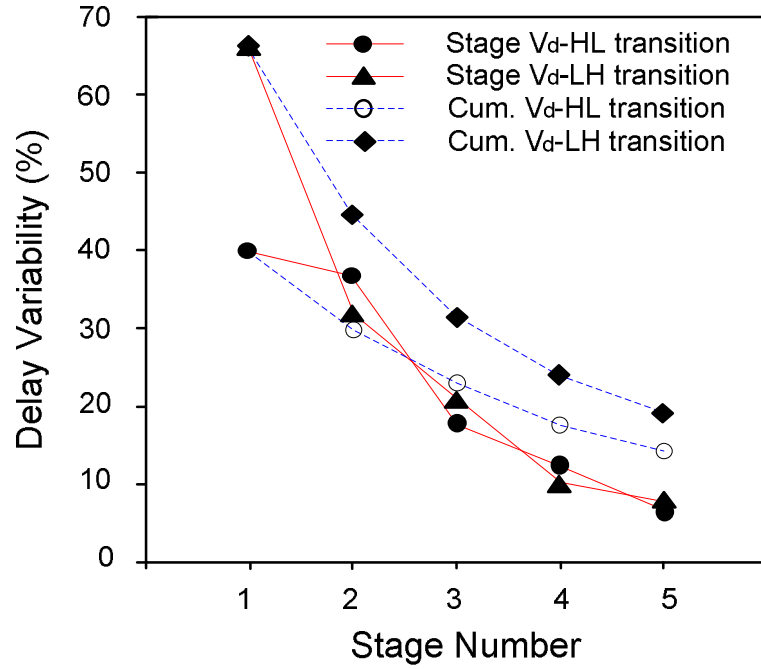


Figure 3.12: Cumulative and stage delay variability during low-to-high and high-to-low transitions for 13 nm tapered buffer driver.

As previously stated, during the circuit design, a tapering factor $\beta = e$ is not always the best choice and so tapered buffers with different tapering factor are used. Therefore, we have extended the study on tapered buffers to see the effect of $\beta$ on their delay characteristics. The results are shown in Figure 3.13, where delay variability has been plotted for the tapered buffers having tapering factors of two, three and four for the given three technology generations. In all these cases, tapered buffers are so constructed that their first stage is a minimum sized inverter ($w_{min}$ = 25, 18 and 13 nm for the technology generation of 25, 18 and 13 nm, respectively) with number of stages equal to 6, 4 and 3 corresponding to the tapering factor of 2, 3, and 4, respectively. All these tapered buffers are driving a load equivalent to a $64w_{min}$ inverter in the corresponding technology.

An interesting observation has been made on the results that delay variability increases with the increase of tapering factor and this effect becomes more prominent for smaller technology generations. This is to be expected since the majority of variability is introduced by the smaller inverters. As discussed before, the delay variability is different for low-to-high and high-to-low transitions for even properly T-sized devices in the inverters (for identical performance in both swings). However, it has been observed that this difference in performance also increases with the increase of the tapering factor and becomes worse for smaller technologies at larger tapering factors.
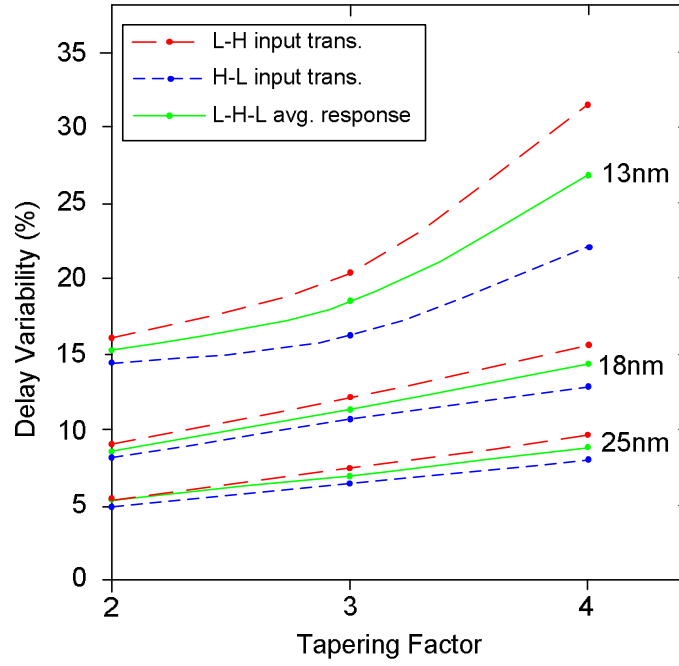


Figure 3.13: Delay variability of tapered buffer drivers for different tapering factors during high-to-low and low-to-high input transitions.

Larger tapering factors are sometimes attractive for power and area efficient designs. However, in the presence of device variability, the designers will have to make a trade-off between these parameters and the amount of tolerable delay variability (larger β means lesser power and area requirement as compared to smaller β, but greater delay variability).

If $n$ is the stage number in the tapered buffer driver, then its size will be given by

$$w(n) = \beta^{n-1} \tag{3.7}$$

Due to random dopant fluctuations, the delay uncertainty introduced by each stage of the tapered buffer driver is independent of each other (independent RVs). Therefore, the delay uncertainty introduced by the $n^{th}$ stage can be approximated by

$$\sigma_d(n) \approx \frac{\sigma(1w_{min})}{\sqrt{w(n)}} \tag{3.8}$$

For optimally sized chain of buffers (according to $\beta$) in the tapered buffer driver, the mean value of the delay at $n^{th}$ stage is

$$t_{d_{mean}}(n) \approx n \cdot t_{d_{mean}}(1w_{min}) \tag{3.9}$$

By using equation (3.8) and (3.9), the delay variability at the $n^{th}$ stage of the tapered buffer driver can be approximated in first order as

$$V_d(n) \approx \left[ \frac{3\sqrt{\sigma_d^2(1) + \sigma_d^2(2) + \sigma_d^2(3) \dots \sigma_d^2(n)}}{t_{d_{mean}}(n)} \right]$$

$$V_d(n) \approx \left[ \frac{3\sqrt{\sum_{i=1}^{n} \sigma_d^2(i)}}{t_{d_{mean}}(n)} \right] \tag{3.10}$$

The denominator of equation (3.10) increases linearly whereas the numerator increases as a square root with the increase of the number of stages in a tapered buffer driver. This means that the delay variability decreases with the increase of buffer stages; however at the cost of a relatively slower driver.

## 3.5   Repeaters

Owing to the technology scaling, the interconnect is becoming slower relative to the devices. Therefore, the use of repeaters is very common in long interconnects for reducing the dependence of the interconnect delay on length from quadratic to linear. Although, the insertion of repeaters in the interconnect lines reduces the overall delay, it introduces delay uncertainty in the lines. In the individual interconnect lines, the effect of the delay uncertainty introduced by the repeaters is that the bandwidth will have to be reduced in order to obtain a particular yield. In clock distribution networks, the delay variation due to these repeaters can produce skew across various branches and will limit its performance. This delay variation is particularly unfavourable in wider communication channels because in synchronous links, the speed of the link is limited by the slowest line in the complete channel. Due to statistical variations in the devices, the cumulative delay at the receiving end of the communication channel will become a random variable. Moreover, the delay characteristics of the same communication channel on different chips produced in the same

batch will not be the same but randomly distributed. Therefore, while designing such communication links, the delay characteristics of the repeaters should be known to explore different design options for better performance.

In this study, we have quantified the amount of delay variability in a chain of repeaters of various sizes. Figure 3.14 shows the results for the repeaters constructed with minimum sized inverters (MSI). It is evident that the mean cumulative delay increases linearly with the increase of the number of repeater stages in the chain. The dispersion (standard deviation) of delay also increases as square root of the number of repeater stages. This is because statistical variations in each repeater stage are independent of each other and can be additive or subtractive towards the cumulative delay. The delay variability on the other hand decreases with the number of repeater stages but at the expense of reduced speed of the repeater line.
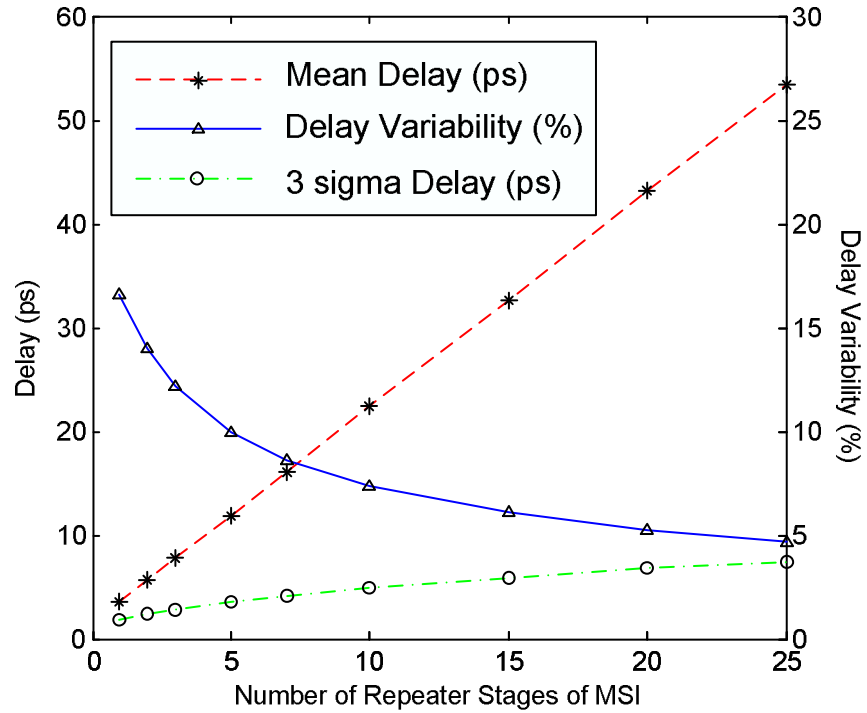


Figure 3.14: Delay variability in a chain of minimum sized repeaters of 13 nm plotted against the number of repeater stages.

If $t_{d_{sec}}$ is the mean delay and $\sigma_{d_{sec}}$ is the standard deviation in the delay for every section of repeated interconnect line, then the cumulative mean delay at the $n^{th}$ stage will be

$$t_{d_{cum}}(n) \approx n t_{d_{sec}} \tag{3.11}$$

and the standard deviation for cumulative delay at this stage will be

$$\sigma_{d_{cum}}(n) \approx \sqrt{n}\sigma_{d_{sec}} \tag{3.12}$$

Therefore, the normalized delay variability at the $n^{th}$ stage will be

$$V_{d_{cum}} = \frac{3\sigma_{d_{cum}}(n)}{t_{d_{cum}}(n)} \approx \frac{3\sqrt{n}\sigma_{d_{sec}}}{nt_{d_{sec}}} = \frac{3\sigma_{d_{sec}}}{\sqrt{n}t_{d_{sec}}} \qquad (3.13)$$

Since the magnitude of the delay uncertainty introduced by buffers (inverters) depends on their size, a repeater line having large sized repeaters will have less delay variability as compared to one constructed with small repeaters driving a particular interconnect load. The simulation results shown in Figure 3.15 endorse this fact. Here cumulative delay uncertainty has been plotted as a function of repeater size for a chain of 20 repeaters. The results demonstrate that a repeater interconnect with large repeaters offers less delay uncertainty as compared to the similar chain constructed with small repeaters. However, a trade-off will have to be made for getting this advantage, as large sized repeaters consume more power and chip area.
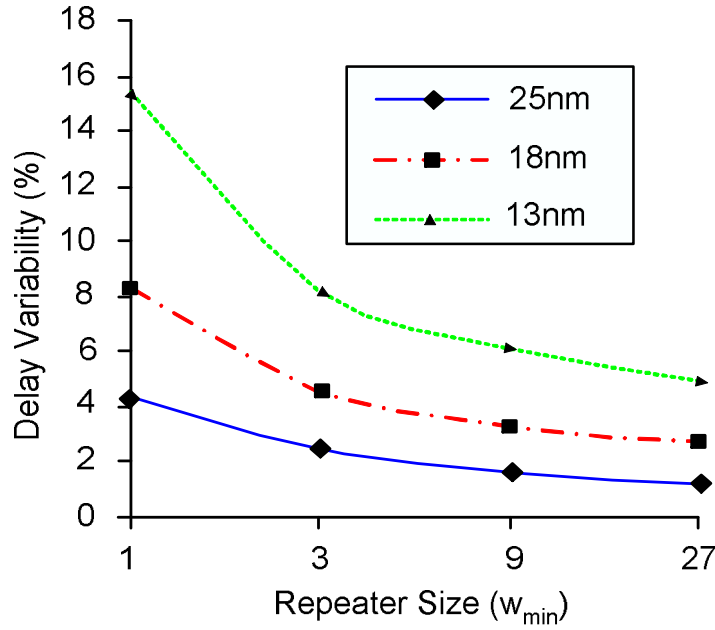


Figure 3.15: Cumulative delay variability plotted as a function of repeater size in a chain of 20 repeaters.

## 3.6   Data Storage Elements (Flip-flops)

A common technique to enhance the throughput in synchronous digital circuits is the use of Flip-Flops (FFs) to implement pipelined designs. Similarly, flip-flops are also used for the storage of different digital signals on the chip, for instance as the last stage of a communication channel. Thus clocked storage elements are essential for a digital circuit. As a result of this tendency, the number of flip-flops on a chip is growing and therefore FFs represent a significant area of the chip.

The performance of the circuits incorporating flip-flops as storage elements depends, to a great extent, on the timing characteristics of the flip-flops. However, as before, these become random variates due to variability. Consequently, the performance of the whole circuit is affected by this variability. Hence it becomes imperative to estimate the timing characteristics of the flip-flops under the impact of statistical variations in order to design high-performance circuits with high yield.
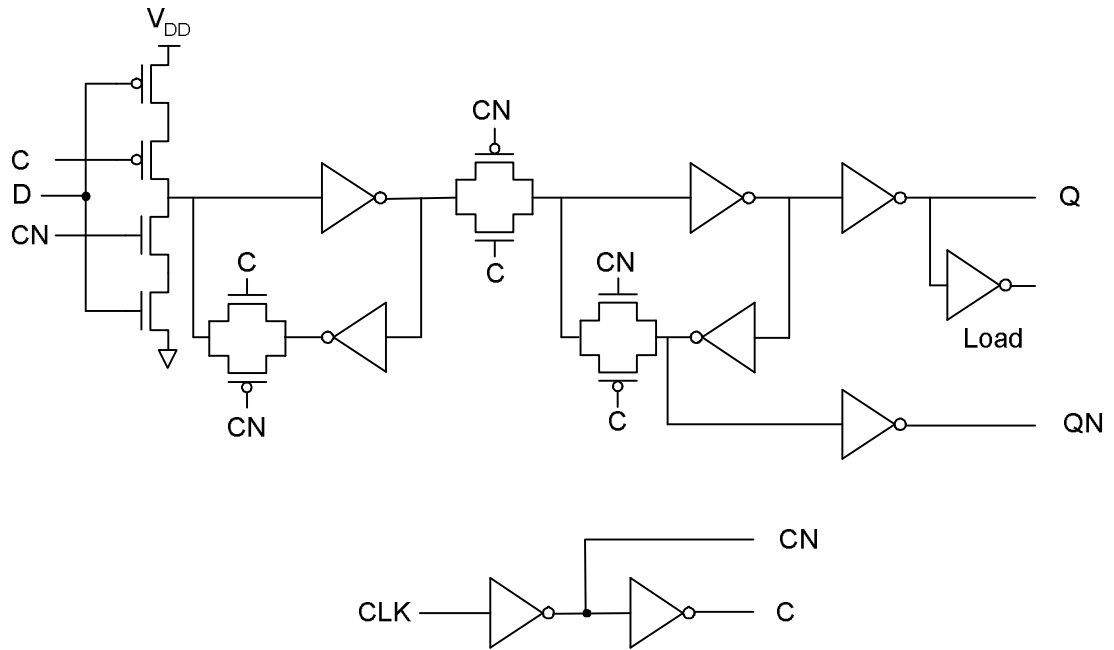


Figure 3.16: Schematic view of a standard CMOS D flip-flop circuit [84]-[85].
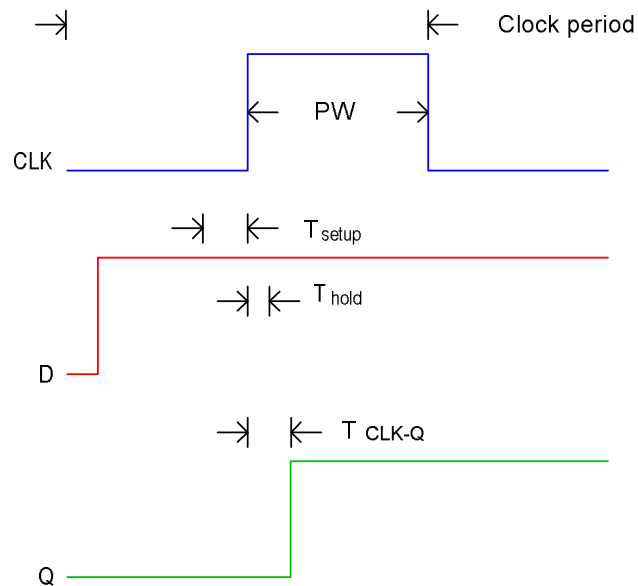


Figure 3.17: Basic timing parameters of a flip-flop.

In this work, the effect of device variability due to RDF on the timing characteristics of a standard CMOS D-flip-flop (DFF) [84]-[85], as shown in Figure 3.16, has been studied.

Flip-flops are typically characterized by different timing parameters which are pictorially represented in Figure 3.17. Since accurate analytical modelling of flip-flops with statistical variations in the devices is difficult, transient analysis of the timing parameters of the FFs has been performed through HSPICE simulations for accurate results. Although flip-flops of various sizes are available in the standard cell libraries used for modern designs, we chose to construct them with the minimum size (i-e minimum transistor dimensions).

## 3.6.1 Timing Measurement Procedure

The procedure adopted for the measurement of different timing parameters of the flip-flops is given below:

### 3.6.1.1 Setup time

The minimum data-to-clock rising edge time for which the flip-flop correctly latches the data is the setup time. In order to find the setup time for a large sample of flip-flops under RDF, a rough estimation of it is made first. For this purpose the flip-flop circuit is constructed using uniform devices (having uniform dopant fluctuations and is available in the device models). The clock pulse width is made sufficiently large and the data is also kept stable for sufficiently long time after the arrival of the clock signal. The data is made available at the data input D of the flip-flop quite earlier than the arrival of the clock edge. Thus the flip-flop safely latches the data at output Q. In the next step, the data at input port D is made available with some delay than the previous case and latching of the data at the output of the flip-flop is monitored. The process is repeated until the flip- flop is just able to hold the data. At this point, the time difference between the arrival of the data and the clock signal is the setup time for the uniform devices. This value gives a reference point and setup times of large number of devices under RDF are expected to lie around this value.

Now 5500 netlists of the flip-flop circuits were generated with random selection of devices from the model card libraries. For each of these netlists, several new netlists were generated by gradually delaying the arrival time of the data (with an increment of 0.2ps), starting from a large value with reference to the setup time we have already measured for the uniform devices. HSPICE simulations were carried out and setup time was measured for each of the flip-flops.

### 3.6.1.2 Hold Time

The hold times were measured in a similar way as that of the setup time. During the measurements, the setup time and the clock pulse width were made sufficiently large to

avoid setup time and other timing violations. The time for which the data remains stable after the clock pulse was gradually reduced (starting from a long time) and the hold time was measured as the minimum time between the rising edge of the clock and the falling edge of the data for which the data at output Q is correctly registered. Again the hold times were measured with an accuracy of 0.2ps for the flip-flop circuits used for the setup time measurement.

### 3.6.1.3 CLK-to-Q time

The CLK-to-Q time is measured as the time delay between the rising edge of the clock and the output Q. Since CLK-to-Q time depends on the arrival time of the data prior to the clock edge (D-to-CLK time) as shown in Figure 3.18, therefore in this study CLK-to-Q time has been measured for large value of D-to-CLK time. Similarly, the hold time and clock pulse width were also made quite large to avoid any of the timing violations due to these parameters. These measurements were made for several flip-flops (5500) constructed with random selection of devices and CLK-to-Q time is measured with an accuracy of 0.2ps.
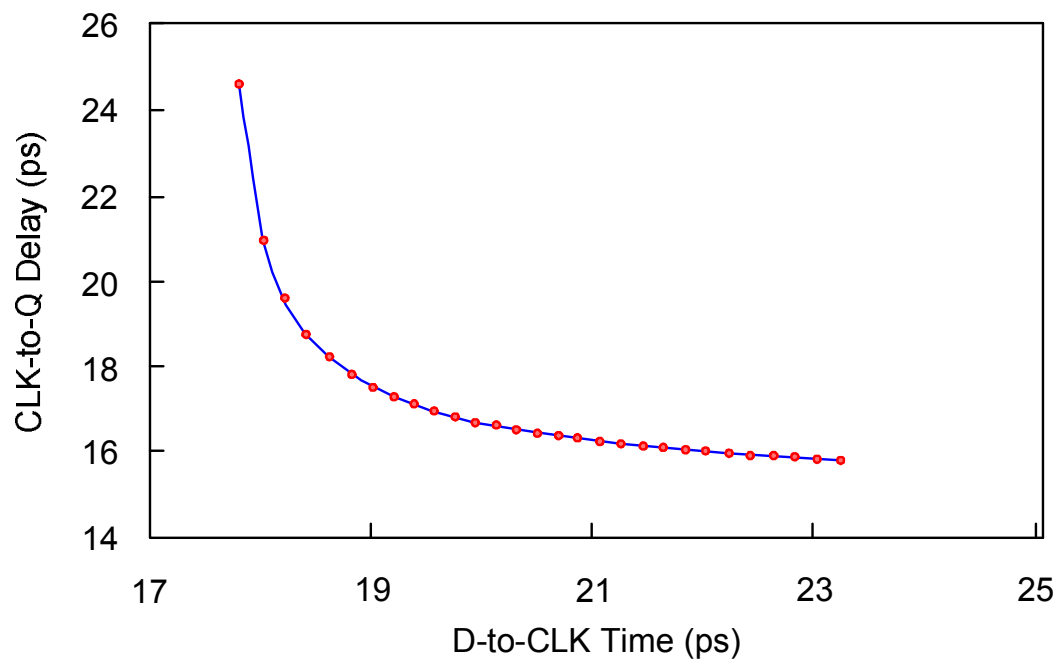


Figure 3.18: Dependence of CLK-to-Q delay on the D-to-CLK time.

### 3.6.1.4 Minimum Clock Pulse Width

Again for these measurements, the setup time and hold times were made sufficiently large. The clock pulse width was gradually reduced to measure minimum clock pulse width for which the flip-flop can hold data, similar to the technique used for setup time measurement.

57

### 3.6.2 Results and Discussion

From the Monte Carlo simulations, different timing parameters of the flip-flops have been characterized and are given in Table 3.1 in terms of the first four moments of their distribution. The results show that the timing parameters of the flip-flops are very sensitive to statistical variation in the devices. It has been observed that while the mean decreases, the dispersion of these timing parameters is increased with technology scaling. The increase in the standard deviation quantifies this dispersion and warns for careful consideration of timing variability analysis during the design of synchronous systems. For instance, for 13nm technology generation, the variability ($\sigma/\mu$) in the setup time increases up to 13%. Similarly, the variation in the hold time, the clock-to-Q time and minimum pulse width requirement reaches up to 15%, 19% and 22%, respectively. Due to the variability in the timing parameters of the flip-flops, extra safety margins will have to be assigned, thus slowing the pipeline. Although the hold time is negative for the Master-Slave flip-flops used, its spread also increases, which suggests transparent latches will be affected by this increase.

Table 3.1: Statistical Analysis of the Timing Parameters of a Standard Flip-flop

| Statistical attribute | Technology | Setup Time (ps) | Hold Time (ps) | CLK-Q Time (ps) | D-Q Time (ps) | Min. PW (ps) |
|---|---|---|---|---|---|---|
| Mean, μ (ps) | 25 nm | 17.5 | -12.7 | 13.9 | 43.7 | 12.8 |
| Standard deviation, σ (ps) | | 0.78 | 0.72 | 0.88 | 4.84 | 1.10 |
| Skewness | | 0.33 | -0.32 | 0.25 | 1.69 | 0.09 |
| Kurtosis | | 3.46 | 3.08 | 3.29 | 7.32 | 2.99 |
| Mean, μ (ps) | 18 nm | 14.5 | -10.2 | 11.1 | 36.2 | 10.4 |
| Standard deviation, σ (ps) | | 1.06 | 0.91 | 1.09 | 4.67 | 1.37 |
| Skewness | | 0.53 | -0.44 | 0.36 | 1.74 | -0.385 |
| Kurtosis | | 3.81 | 3.67 | 3.28 | 7.87 | 6.97 |
| Mean, μ (ps) | 13 nm | 9.5 | -6.38 | 6.9 | 23.9 | 7.54 |
| Standard deviation, σ (ps) | | 1.25 | 0.98 | 1.29 | 3.94 | 1.49 |
| Skewness | | 0.94 | -0.88 | 0.88 | 1.76 | -0.17 |
| Kurtosis | | 4.46 | 4.48 | 4.77 | 9.40 | 5.82 |

From Figure 3.19, we can see that setup time, hold time and CLK-to-Q time spans a large timing space (there appears to be no visible correlation between the parameters) and design

margins will have to be chosen while keeping in view this space in order to achieve a particular yield.
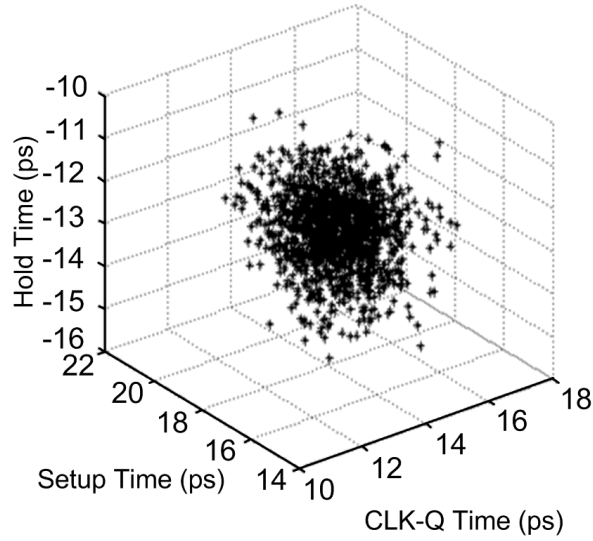


Figure 3.19: 3D-space occupied by the timing parameters of the DFF.

Circuits become increasingly faster with technology scaling, demanding a drastic reduction in the tolerances allowed to their clocks. However, the magnitude of the timing variability we have observed in the flip-flop circuits will certainly tend to reduce the performance of the circuits, unless some corrective measures are not taken.

## 3.7   Interconnect

The interconnect also exhibits variation in its characteristics due to the structural variation in the lateral and vertical dimensions. Besides material variations, the structural variation in the interconnect can appear in conductor thickness($T$), the width($W$), and interlayer dielectric thickness($H$). It is important to mention that interconnect spacing is not an independent parameter and is automatically effected with the variation in interconnect width. In addition, there are other sources of interconnect variability such as surface and edge roughness or sidewall thickness but all of these geometrical variations result in the deviation of the electrical properties of the interconnect like, the resistance $(R)$, the capacitance $(C)$ and the inductance $(L)$. Consequently, this will result in the delay variability of interconnects.

## 3.8 Performance of Communication Links

The variability in the delay characteristics of the individual communication circuits (discussed above) will cause uncertainty in the signal delay through the complete channel.

If the delay of a signal is larger than the nominal value plus the design margin, this will introduce a link failure. In order to get the best performance of the design, we need to quantify the effect and allow for the expected variation in the design margins. It is important that these margins are neither pessimistic (which waste resources) nor optimistic (which affect yield). Whatever these margins are, it is certain that under delay variability, the throughput of the channel will have to be certainly compromised (as compared to the deterministic case) in order to keep the probability of link failure below a certain acceptable limit. Conversely, additional resources (area and power) will be required to attain the same bandwidth. It is clear then that device variability will contribute significantly towards the performance/area/power compromise of clock distribution networks and the data links, which are basically composed of these structures.

### 3.8.1 Estimation of Link Performance

A simple communication link is shown in Figure 3.20 which consists of tapered buffer drivers, interconnect wires, repeaters and data storage elements. The output of the combinational logic is powered up using tapered buffer driver before transmitting it through the link. The repeaters are used to improve the delay characteristics, especially in predominantly resistive interconnects. Similarly, flip flops or latches are used to hold the data at the receiving end. The link operating frequency depends upon the cumulative delay introduced by each of these elements plus the setup time of the flip-flop. The nominal delay of such a data link from input to output can be calculated using the following equation

$$T_{d_{link}} = t_{d_{tap-buff}} + t_{d_{rep-inter}} + t_{CLK-Q_{FF}} \tag{3.14}$$

In the above expression, $T_{d_{link}}$ is the total delay of the link, $t_{d_{rep\_inter}}$ is the repeater-inserted interconnect delay and $t_{CLK-Q_{FF}}$ is the CLK-Q time of the flip-flop.
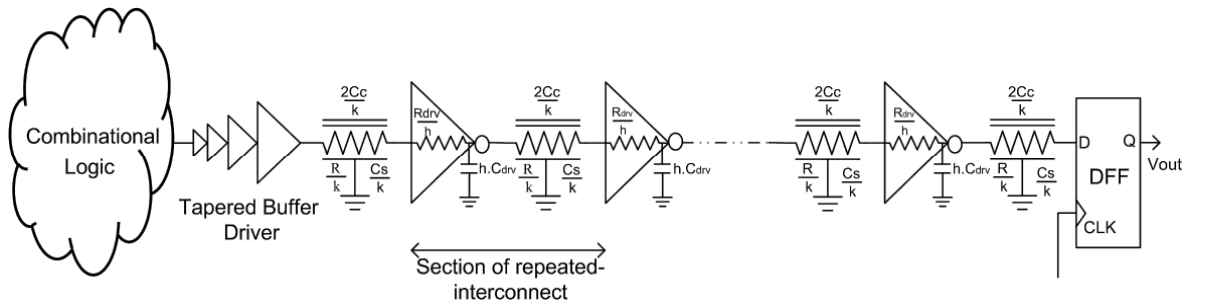


Figure 3.20: A simple data communication link. The signal coming out from the combinational logic is powered up through tapered buffer driver and then it passes through the repeater inserted interconnect to reach the input of the flip-flop.

Let $k$ be the number of repeaters (each of size $h$ times the size of the minimum sized repeater). In a particular technology, if the output impedance of a minimum sized inverter is $R_{drv}$ and output capacitance is $C_{drv}$, then the output impedance of a repeater of size $h$ becomes $R_{drv}/h$ and the output capacitance $h * C_{drv}$. In Figure 3.20, the symbol ⌁⌁⌁ represents a capacitively coupled interconnect. If we assume that $R$ is the interconnect resistance, $C_c$ is the coupling capacitance with the neighbouring interconnects and $C_s$ is the self capacitance of the interconnect, the propagation delay of one section of the repeated interconnect [86], which is taken to be the time difference of the input and output waveforms at 50% of the transition points, is given by

$$t_{0.5,sec} = 0.7R_{drv}(C_s + C_{drv} + 2.2 \times 2C_c) + R(0.4C_s + 0.58C_c + 0.7C_{drv}) \quad (3.15)$$

The total delay of the interconnect inserted with repeaters is given by

$$t_{0.5} = k\left[0.7\frac{R_{drv}}{h}\left(\frac{C_s}{k} + hC_{drv} + 2.2\frac{2C_c}{k}\right) + \frac{R}{k}\left(0.4\frac{C_s}{k} + 0.58\frac{C_c}{k} + 0.7hC_{drv}\right)\right] \quad (3.16)$$

Under the assumption of statistical independence, the time delay in the link can be calculated from its component's distributions as follows

$$T_{d_{link}} \approx \mu_{d_{tap-buff}} + \mu_{d_{rep-inter}} + \mu_{CLK-Q_{FF}}$$
$$+ \sqrt{\sigma^2_{d_{tap-buff}} + \sigma^2_{d_{rep-inter}} + \sigma^2_{CLK-Q_{FF}}} \quad (3.17)$$

This equation consists of two parts, the mean value and standard deviation of the delay distribution. The standard deviation has been added in the mean delay in order to estimate the maximum delay ($3\sigma$ or $6\sigma$ can also be used to estimate the worst cases of delay). Two parts of the equation (3.17) can be denoted as

$$\mu_{d_{link}} = \mu_{d_{tap-buff}} + \mu_{d_{rep-inter}} + \mu_{CLK-Q_{FF}} \quad (3.18)$$

$$\sigma_{d_{link}} = \sqrt{\sigma^2_{d_{tap-buff}} + \sigma^2_{d_{rep-inter}} + \sigma^2_{CLK-Q_{FF}}} \quad (3.19)$$

Similarly, $\mu_{d_{rep-inter}}$ and $\sigma^2_{d_{rep-inter}}$ are given by
$$\mu_{d_{rep-inter}} = \mu_{sec1} + \mu_{sec2} + \mu_{sec3} + \cdots \mu_{secN} \quad (3.20)$$

and
$$\sigma^2_{d_{rep-inter}} = \sigma^2_{sec1} + \sigma^2_{sec2} + \sigma^2_{sec3} + \cdots \sigma^2_N \quad (3.21)$$

where $\mu_{sec}$ and $\sigma^2_{sec}$ represents the mean and variance of the delay of each section of the repeater inserted interconnect.

Now if we have complete description of the delay characteristics of the individual communication structures under the impact of device and/ or interconnect variability due to any of their parameters, we can approximate the overall performance of the complete link

using equations (3.17)-(3.21). The results can also be used to estimate the probability of the link failure due to variability, as explained below.

### 3.8.2 Link Failure Probability

Let us assume that the link is operating at a clock frequency $f$ having clock period $T_{CLK}$. For the flip-flop (having setup time $T_{setup}$) to correctly latch the data, the delay of the interconnect must satisfy the following constraint

$$T_{CLK} - T_{setup} \geq t_{d_{tap-buff}} + t_{d_{rep-inter}}$$

Therefore, the probability that correct data is transmitted between the input and output is given by

$$q = P\left(T_{CLK} - T_{setup} \geq t_{d_{tap-buff}} + t_{d_{rep-inter}}\right) \tag{3.22}$$

A design margin is also used to cater for the delay variation due to different circuit parameters and let it be $\Delta_m$. Therefore, expression (3.22) can be written as

$$q = P\left(T_{CLK} - \Delta_m - T_{setup} \geq t_{d_{tap-buff}} + t_{d_{rep-inter}}\right) \tag{3.23}$$

We define the time delay between the input of the tapered buffer driver and the input D of the receiving flip-flop to be $T'_{d_{link}}$. Then the probability that the delay of the link will be greater than $T_{CLK} - \Delta_m - T_{setup}$ is given by

$$P\left[T'_{d_{link}} > T_{CLK} - \Delta_m - T_{setup}\right] = 1 - P\left[T'_{d_{link}} < T_{CLK} - \Delta_m - T_{setup}\right]$$

$$= 1 - F\left(\frac{T_{CLK} - \Delta_m - \mu_{setup} - \mu'_{d_{link}}}{\sqrt{(\sigma'_{d_{link}})^2 + (\sigma_{setup})^2}}\right) \tag{3.24}$$

$$= Q\left(\frac{T_{CLK} - \Delta_m - \mu_{setup} - \mu'_{d_{link}}}{\sqrt{(\sigma'_{d_{link}})^2 + (\sigma_{setup})^2}}\right) \tag{3.25}$$

In the above expressions,

$$\mu'_{d_{link}} = \mu_{d_{tap-buff}} + \mu_{d_{rep-inter}}$$

$$\text{and } \sigma'_{d_{link}} = \sqrt{\sigma^2{}_{d_{tap-buff}} + \sigma^2{}_{d_{rep-inter}}}$$

If we assume that the delay variability in the clock signal is $\sigma_{CLK}$ with some mean $\mu_{CLK}$, Eq. (3.25) will become

$$P\left[T'_{d_{link}} > T_{CLK} - \Delta_m - T_{setup}\right] = Q\left(\frac{\mu_{CLK} - \Delta_m - \mu_{setup} - \mu'_{d_{link}}}{\sqrt{(\sigma'_{d_{link}})^2 + (\sigma_{setup})^2 + (\sigma_{CLK})^2}}\right) \qquad (3.26)$$

Again in expressions (3.24)-(3.26), $F$ is the cumulative distribution function of the link delay and $Q$ is the classical error function, respectively. The Borjesson's approximation [87], as given below, can be used to evaluate $Q$.

$$Q(x) \approx \left[\frac{1}{(1-a)x + a\sqrt{x^2 + b}}\right] \frac{1}{\sqrt{2\pi}} e^{-x^2/2} \qquad \text{for } x \geq 0$$

with $a = \frac{1}{\pi}$ and $b = 2\pi$.

### 3.8.3 Case Study

Consider a typical interconnect of length 500 $\mu m$, width 0.675 $\mu m$, and thickness 0.324 $\mu m$ in 18 nm technology. The delay characteristics of this interconnect inserted with 10 repeaters of size $5w_{min}$ are given in Table 3.2 along with the performance characteristics of the tapered buffer driver and flip-flop used in the complete link.

Table 3.2: Statistical Delay Characteristics of Different Elements of the Link. These values have been taken from the characterization data of different elements.

|  | Tapered Buffer | Repeater Inserted Interconnect | Flip-Flop Setup Time | Flip-Flop CLK-Q Time |
|---|---|---|---|---|
| Mean, $\mu$ | 20.95 ps | 152.9 ps | 14.52 ps | 11.12 ps |
| Standard Deviation, $\sigma$ | 1.11 ps | 2.12 ps | 1.05 ps | 1.09 ps |

For a design margin $\Delta_m = 5$ ps and an uncertainty in the clock period $\sigma_{CLK} = 2$ ps, the probability of the link failure has been plotted as a function of the operating frequency and is shown in Figure 3.21. Both curves, one obtained using equation 3.26 and the other through Monte Carlo simulation of the complete channel, are shown for comparison. It has been observed that beyond a certain operating frequency, the link failure probability starts increasing from zero (observe the slope due to spread in the PDF). These particular curves correspond to delay variability due to only RDF in the devices. However in the real case, there are other sources of variability in the devices as well as in the interconnect, and therefore overall delay variability in the link will be even larger. Thus for a particular link failure probability, the operating frequency will have to be reduced, otherwise the yield will be reduced for high speed links under tight design margins.
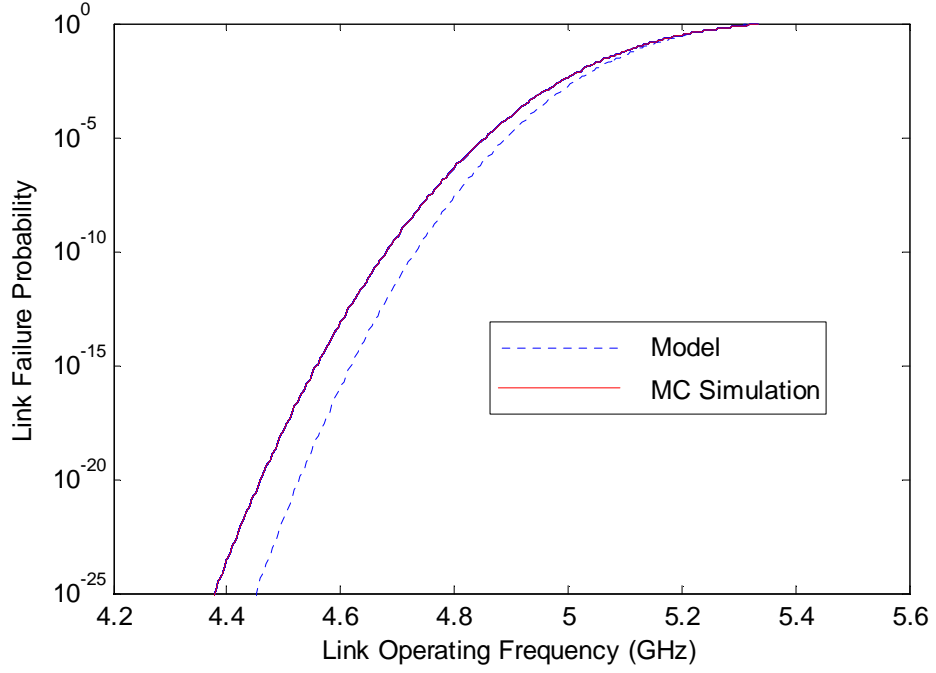
Figure 3.21: Link failure probability as a function of link operating frequency, as calculated using the analytical model and Monte Carlo simulation.

It may also be noted in Figure 3.21 that the results of the analytical model slightly deviate from the simulation results, especially in the beginning of the curves. This is due to the reason that the probability distribution function of the delay of different communication structures, for smaller devices, deviate from the normal distribution (as explained before). Therefore, the cumulative delay distribution of the complete channel may also be non-normal (skewed). Hence, in order to obtain accurate results, the delay distributions of all the communication structures should be accurately characterised and corresponding statistical operators may be used to obtain the cumulative delay distribution.

## 3.9   Summary

In this chapter, we have critically examined the effect of device variability due to RDF on the performance of the basic elements of on-chip communication, such as tapered buffer drivers with different tapering factor, repeaters of different sizes, and data storage registers (FFs). FO4 delay measurements have also been taken, as representative of the logic circuitry and results can be used as a performance benchmark. The study revealed that RDF has significant impact on the performance of communication structures and their performance deteriorates very significantly with technology scaling from 25 to 13 nm. As a design methodology, scaling up of circuits in the critical paths can be employed to minimize the effects of device variability, in particular, since we have shown that this trade-off is not linear and a small increase in the repeater size can give substantial benefit

towards the performance. For instance, we have corroborated that large sized repeaters can be used in the interconnect to reduce delay variability, however, the power and area penalties due to this passive technique of circuit scaling should be compared with active countermeasure techniques which can be used to mitigate the delay variability.

Although NoC is more robust against on-chip communication faults than simpler designs, we note that such occurrences have increased hyper-linearly (and will continue to do so) due to device variability. In order to evaluate the performance of a typical NoC link, we have derived analytical models to predict link failure probability (LFP) using the characterization data of the individual on-chip communication elements. The results show that link failure probability increases significantly with the increase of device variability and is a limiting factor in the maximum operating frequency of a synchronous link.

# Chapter 4

# SSTA of Pipelined Communication Circuits

The performance of circuits under variability can be evaluated accurately through simulation (as it has been done so far in this thesis). However, for large designs this method is not feasible; being computationally expensive. The solution to this problem is the use of Statistical Static Timing Analysis (SSTA) which is a powerful analysis tool and provides a convenient means of estimating the circuit performance under the impact of variability. In this chapter we describe the use of SSTA to examine the performance of large on-chip communication networks, formed by the components that have been analysed and characterized so far (FFs, Buffers and Tapered Buffers).

## 4.1    Introduction to STA

During the designing of the digital circuits, it is always necessary to ensure that timing constraints are met. This requires to find the maximum delay between the inputs and outputs along different paths. In the traditional design, this analysis is used to identify (and subsequently optimize) a critical path in the circuit. The delay along this path determines the maximum operating frequency. Figure 4.1 shows a simple circuit consisting of seven combinational blocks between two flip-flops. The critical path for such a circuit can be

determined using Static Timing Analysis (STA), in which individual circuit elements are pre-characterized through simulation and then delays (corresponding to the worst-case) are added up along different paths from input to output. The latest arrival time of the signals along different paths for which the data is correctly received at the output is calculated and is then compared with the required timing. The difference between these two values is signal slack. For the example of Figure 4.1, the latest arrival time of the signal is 4.4. If the slack is negative, the circuit will not meet the performance requirements. The minimum slack along any of the paths in a circuit is the critical path.
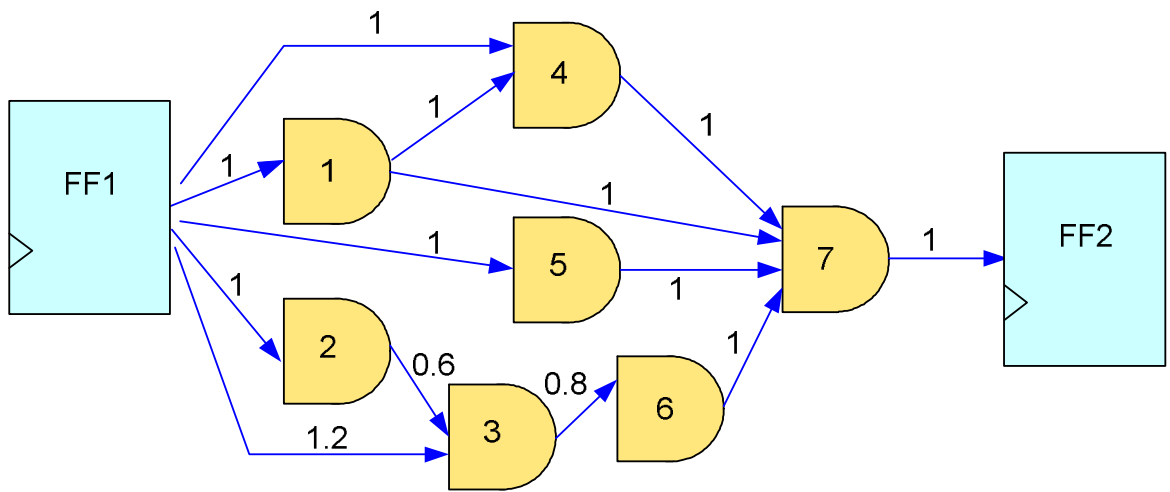


Figure 4.1: Demonstration of static timing analysis of a simple circuit.
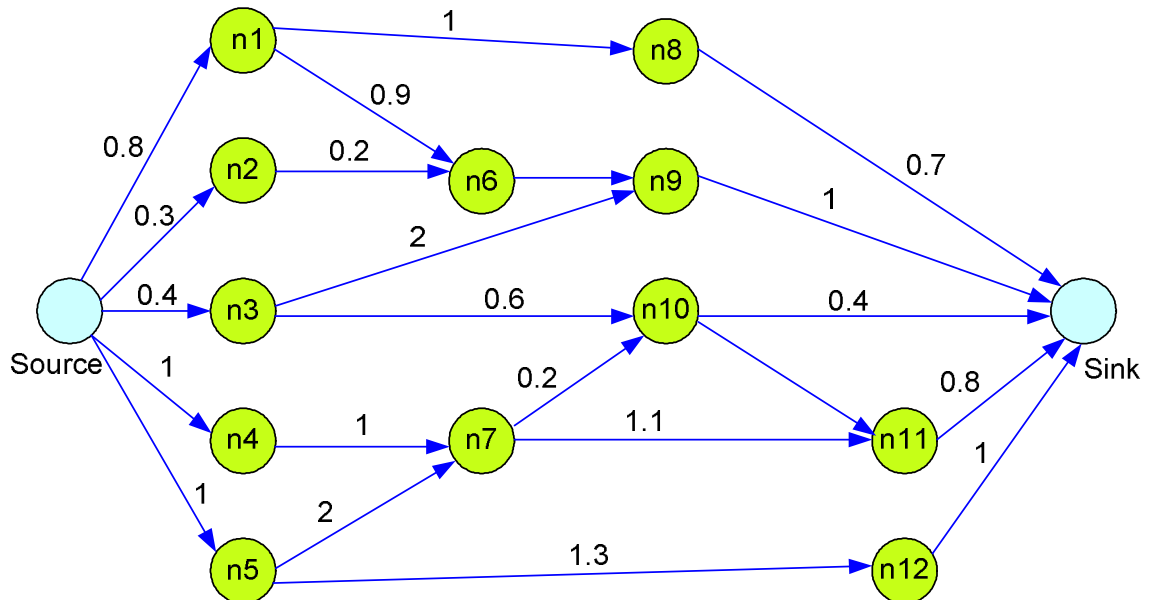


Figure 4.2: An example of the timing graph for delay traversal from source to sink.

A timing graph is very useful for the timing analysis of the circuits and describes the timings of the combinational logic between the source and the sink along different paths. It

is a Directed Acyclic Graph (DAG), as shown in Figure 4.2. In the timing graph, the signal lines are denoted as nodes and input-output transformation through every gate in the circuit is shown as an edge. The delay associated with every input-output is represented as the weight over the corresponding edge. For STA, the weight over every edge is usually corresponds to the worst-case delay.

## 4.2 Introduction to SSTA

In traditional circuit design, corner based approaches are used alongside STA in which the best-case or worst-case corner values are identified corresponding to different sources of variability. Thus for die-to-die variations, it is then assumed that 3σ deviation of circuit parameters for different manufactured circuits will not be beyond these corner values [88]. However, due to technology scaling, the magnitude of the variability due to different sources is increasing manifold and so guard-banding based on 3σ corners will significantly affect the performance due to excessive margins for delay variations. Moreover, in actual chips with many sources of variability, it is extremely unlikely of all the factors contributing towards delay variability, being at their corner values and so this approach produces pessimistic results and too much slack in the design [89].

Under the impact of statistical variability, the delay of each gate becomes a random variable. Therefore, statistical methods are required to accurately analyze the circuit delay. SSTA modifies STA such that the random variations of the delay are considered as random variables. During the SSTA of large digital circuits, the probability density function (PDF) and cumulative density function (CDF) of the timing parameters of different circuit elements are analytically processed to estimate the timing characteristics of the complete circuit. Notice then that the design paradigm is shifted from deterministic to stochastic. There is no single critical path in the circuit; any path can potentially become the critical path. Because of its statistical nature, the accuracy of the analysis depends on the characterization data of individual circuit elements, accurate representation of the characterization data in the form of PDFs and finally the correctness of different analytical operations, like MIN, MAX, or SUM which are applied during the analysis, and are usually computed with fast approximations.

The statistical SUM and MAX operations are used to calculate the PDF of the delay at each node of the timing graph. These operations take delay variations of the gates and interconnect as input and give that of the outputs. Thus by traversing the timing graph using the statistical operations, the overall PDF of different circuit parameters can be

calculated. The basic statistical operations (SUM and MAX) are pictorially shown in Figure 4.3. For the signal paths in series, the delay at the output is calculated using the SUM operation. If the two circuits in series have PDFs as 'g1' and 'g2' then the PDF of the circuit at the output can be calculated using the convolution integration. Similarly, if a gate has multiple inputs, the delay distribution at the output is calculated using the MAX operation.



(a)



(b)
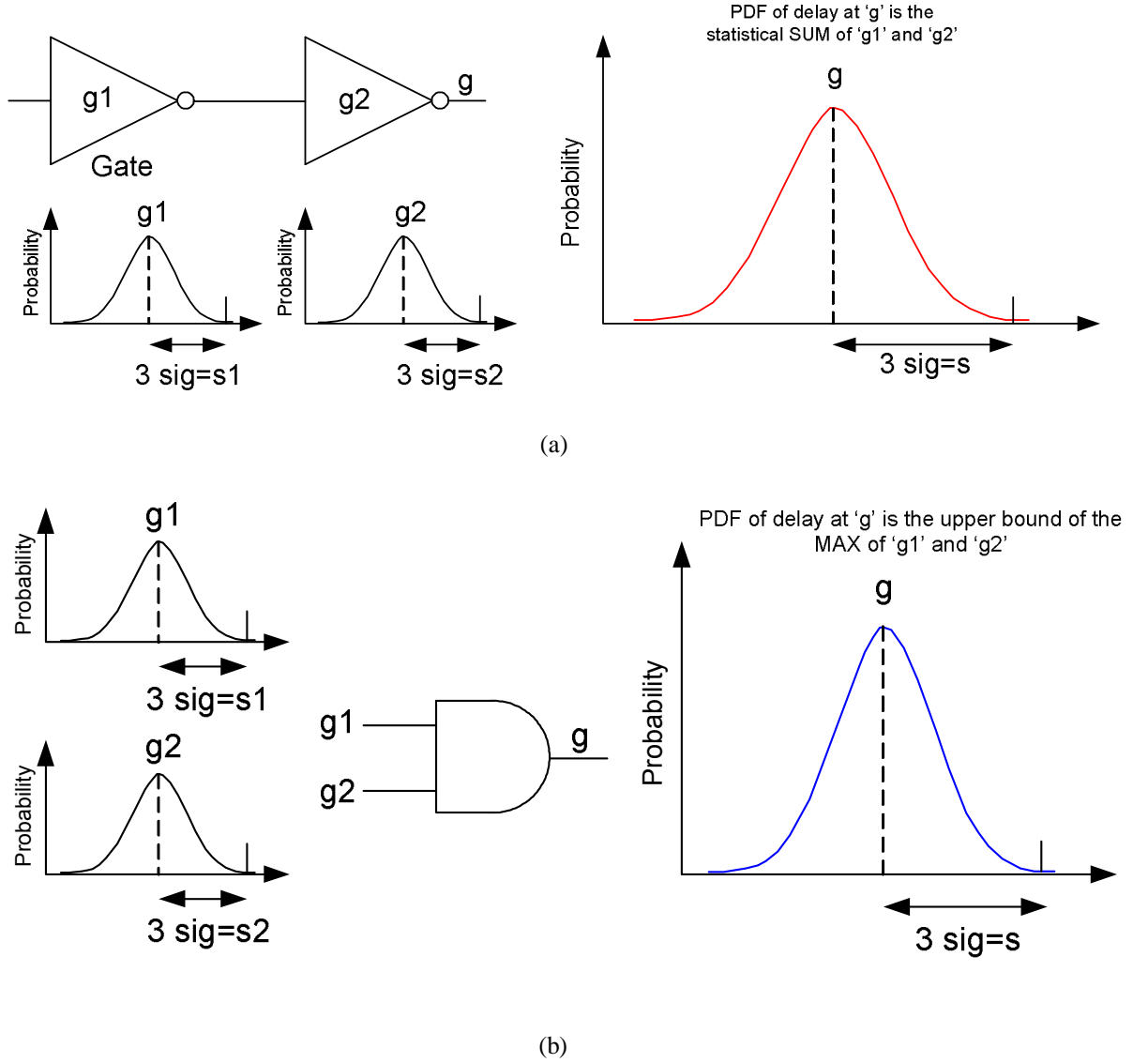
Figure 4.3: Basic statistical operations used in STA and SSTA. The SUM operation (a), and the MAX operation (b) [89].

## 4.3 Representation of Characterization Data

For the SSTA of circuits, accurate characterization of the timing parameters of the combinational logic, interconnect and sequential elements (flip-flops and latches) is vitally important [90]. This need becomes more crucial in the design of high speed circuits due to

the strict design margins required [91]. The task becomes more challenging when statistical device variability effects are also considered. While the maximum achievable performance and yield of a circuit depends on the magnitude of the variability in the timing parameters, a better estimate of these parameters can only be made by the transient analysis of the circuits through the SPICE simulation using detailed device models. In current state-of-the-art chips, the device count has already exceeded one billion, mandating the estimation of the distributions more precisely, especially in the tail regions, as events deep within the tails will most likely be realized.

Parametric analysis, in which a known parametric distribution (e.g. normal) is fitted on the experimental data, can be used to undertake this estimation. However, the limitation of this approach is that its accuracy depends on the choice of a particular a-priori density function [92]. Therefore, the distribution functions may be determined through non-parametric estimations. With correct approximation of the density functions, a better estimate of the circuit yield can be made which is neither optimistic nor pessimistic and thus helps in enhancing circuit performance with minimum yield loss.

In order to demonstrate the effectiveness of using non-parametric estimations, we use the simulation data obtained during the characterization of different timing parameters of the CMOS flip-flops (Chapter 3). The histograms of various timing parameters of FFs for 13 nm technology are shown in Figure 4.4. The histograms indicate that the timing distributions are asymmetric (positively skewed except hold time which is negatively skewed). The degree of asymmetry (around the mean) and the shape of distributions have been measured in terms of skewness and kurtosis and are given in Table 4.1 for all the timing parameters. As mentioned earlier, skewness is a measure of the degree of asymmetry; whereas kurtosis is a measure of whether the data is peaked or flat relative to a normal distribution (high kurtosis means peaked distribution). The non-zero value of skewness and kurtosis confirms that the distributions are not normal, supporting our conclusion drawn from the visual inspection of the distributions. Similar asymmetry has recently been reported for the distribution of $V_t$ in 65nm technology generation [93] and in 35nm channel length MOSFETs [94]. The increasing value of these parameters with technology scaling shows that the asymmetry increases as the technology scales.

The characterization of these timing parameters can be used alongside SSTA to determine analytically the impact that variability will impair in a more complex circuit. This is done by determining its probability distribution function (PDF). For instance, the timing analysis

of flip-flop based sequential circuits involve the timing characteristics of the sequential elements and circuit elements pertaining to a clock network, in addition to the combinational logic.
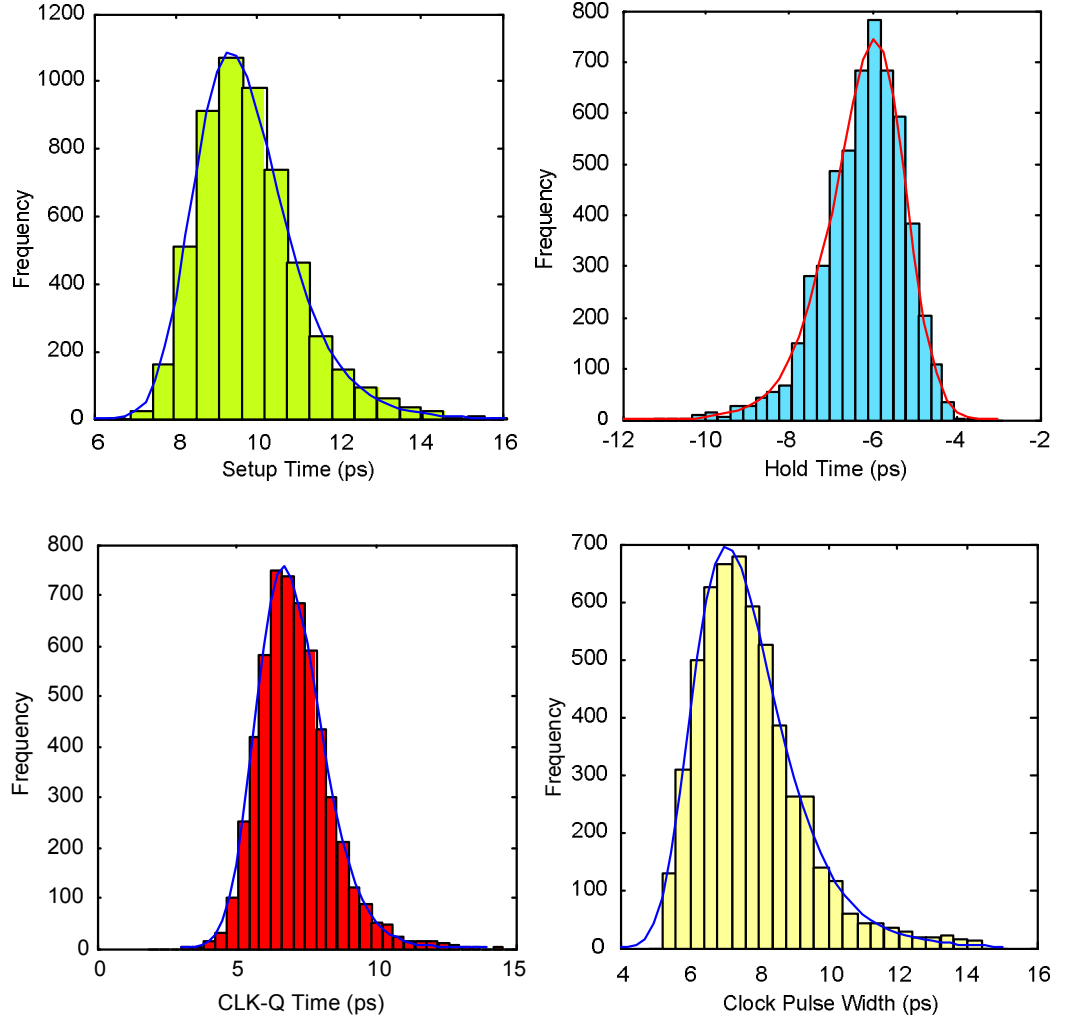


Figure 4.4: Histograms of observed data taken through Monte Carlo simulations for the timing parameters of the FFs of 13 nm.

Table 4.1: Statistical Analysis of the Timing Parameters of the Standard Flip-flop shown in Figure 3.16

| Statistical attribute | Technology | Setup Time (ps) | Hold Time (ps) | CLK-Q Time (ps) | D-Q Time (ps) | Min. PW (ps) |
|---|---|---|---|---|---|---|
| Skewness | 25 nm | 0.33 | -0.32 | 0.25 | 1.69 | 0.09 |
| Kurtosis | | 3.46 | 3.08 | 3.29 | 7.32 | 2.99 |
| Skewness | 18 nm | 0.53 | -0.44 | 0.36 | 1.74 | -0.385 |
| Kurtosis | | 3.81 | 3.67 | 3.28 | 7.87 | 6.97 |
| Skewness | 13 nm | 0.94 | -0.88 | 0.88 | 1.76 | -0.17 |
| Kurtosis | | 4.46 | 4.48 | 4.77 | 9.40 | 5.82 |

Most of the previous work on statistical static timing analysis (SSTA) is based on the

assumption that the underlying distributions are Gaussian (i.e. the distributions of various timing, physical and electrical parameters of the devices). Any deviation from normality (as for instance the skewness and kurtosis shown in Figure 4.4) in the timing parameters of the circuit elements will introduce inaccuracy in the analysis results. However, the use of non-Gaussian distributions is likely to pose several challenges for efficient SSTA, as analytical results for the combination of non-Gaussian PDFs would need to be determined. As a first step into this uncharted territory, it is required to determine an analytical distribution which provides a good match to the observed data.

## 4.4 Estimation of the Timing Distributions

Statistical methods can be used to estimate the distributions from the experimental data. As mentioned before, parametric estimation of the distributions does not give a satisfactory fit to the experimental data (for instance Normal or Gaussian), since higher moments (skewness and kurtosis) are not zero in our case. Therefore, in this work we chose to use non-parametric statistical methods and found that Pearson and Johnson systems fit the data much more precisely, as they have the ability to adapt themselves to the data and do not require *a priori* or *a posteriori* knowledge of the data-producing process. They have the property of being able to capture skew and kurtosis and so provide a good match to the data.

The PDF based on the simulation data has been compared with the normal distribution, Pearson and Johnson systems. It has been found that the normal distribution does not provide an accurate fit to the simulation data due to its asymmetric nature, whereas Pearson type IV from the Pearson system and the SU system from the Johnson family of systems closely matches the data. A good description of Pearson and Johnson systems is available in [144].

### 4.4.1 Pearson Distributions

The Pearson distribution is a family of continuous probability distributions to model skewed observations. The Pearson system defines a family of distributions parameterized on the mean, standard deviation, skewness, and kurtosis. There are seven basic types of distributions all available in a single parametric framework [95].

The Pearson type IV distribution is characterized by four parameters, $\theta = (m, \nu, a, \lambda)$ and these parameters uniquely determine the first four moments of the distribution. The probability density function of the Pearson type IV distribution can be expressed as [96], [97]

$$p(x) = k(m, v, a) \times \left[1 + \left(\frac{x - \lambda}{a}\right)^2\right]^{-m} \exp\left[-v\tan^{-1}\left(\frac{x - \lambda}{a}\right)\right] , \qquad \left(m > \frac{1}{2}\right) \qquad (4.1)$$

Here the parameters $a$ and $\lambda$ are for the scale and location, whereas the shape parameters $m$ and $v$ jointly determine the degree of skewness and kurtosis of the distribution. $k(m, v, a)$ is a normalization constant given as

$$k(m, v, a) = \frac{\Gamma(m)}{\sqrt{\pi}a\Gamma(m - \frac{1}{2})} \left|\frac{\Gamma(m + \frac{iv}{2})}{\Gamma(m)}\right|^2 \qquad (4.2)$$

where $\Gamma$ is the Gamma function.

The maximum likelihood fitting requires minimizing the negative log likelihood [96] given below and can be computed numerically.

$$-\ln L = m \sum_{i=1}^{N} \ln\left[1 + \left(\frac{x_i - \lambda}{a}\right)^2\right] + v \sum_{i=1}^{N} \tan^{-1}\left(\frac{x_i - \lambda}{a}\right) - N \ln k \qquad (4.3)$$

We have used this equation to fit a Pearson type IV distribution for the PDF of the setup time from the simulation data of 13 nm flip-flops. This is shown in Figure 4.5 along with the normal distribution fit. It can be seen that the Pearson type IV distribution closely matches the PDF of simulation data, as determined by the goodness of fit statistics given in Table 4.2. This clearly shows that the assumption that the timing distributions are normal is not correct and can produce incorrect conclusions. As an example (refer Figure 4.5), consider the probability of occurrence of a timing event at $t_{setup} = 12.76 \, ps$ (corresponding to 3σ of normal distribution). With the assumption of a normal distribution, this probability is given by $p = 0.0043$, whereas it is $p = 0.0243$ with the Pearson type IV estimation (5.6 times higher than the normal case).

The CDF of Pearson type IV is given by [96]

$$P(x) = \frac{ka}{2m - 1}\left[1 + (\frac{x - \lambda}{a})^2\right]^{-m} \exp\left[-v\tan^{-1}(\frac{x - \lambda}{a})\right]$$

$$\times \left(i - \frac{x - \lambda}{a}\right) F\left(1, m + \frac{iv}{2}; 2m; \frac{2}{1 - i\frac{x - \lambda}{a}}\right) \qquad (4.4)$$

where F is a hypergeometric function and can be calculated using the method given in [98]. The above function converges for $x < \lambda - a\sqrt{3}$. For $x > \lambda + a\sqrt{3}$, the symmetry identity

$P(x|m, v, a, \lambda) \equiv 1 - P(-x|m, -v, a, -\lambda)$ can be used and in the case $|x - \lambda| < a\sqrt{3}$, the linear transformation as given in [99] can be employed.
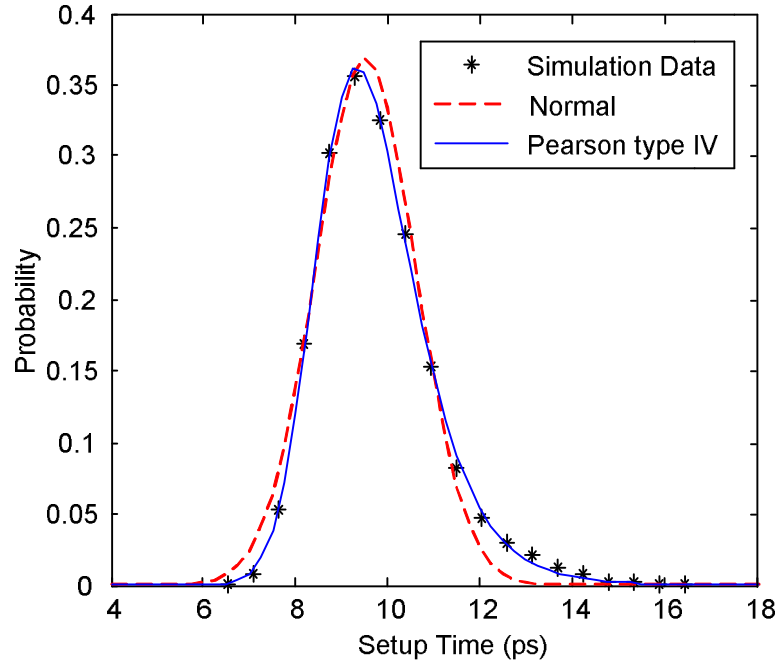


Figure 4.5: The probability density function of setup time for the 13 nm flip-flops plotted with different systems.

Table 4.2: Goodness of Fit Statistics (for Figure 4.5) in terms of R-Square, Sum of Squares due to Error (SSE), Adjusted R-Square, Root Mean Squared Error (RMSE)

| Distribution | R-square | SSE | Adjusted R-square | RMSE |
|---|---|---|---|---|
| Normal | 0.9845 | 0.004279 | 0.9826 | 0.01635 |
| Pearson type IV | 0.9989 | 0.0002925 | 0.9986 | 0.004571 |

## 4.4.2 Johnson Distribution

Statistician Norman Johnson formulated a system of distributions such that for every valid combination of mean, standard deviation, skewness and kurtosis, there is also a unique distribution. The Johnson system is based on exponential, logistic, and hyperbolic sine transformations, plus the identity transformation [95]. The systems of distributions corresponding to these transformations are known as SL, SU, SB and SN, respectively. The general form of the three normalizing transformations (exponential, logistic and hyperbolic sine) is given by [100]

$$Z = \gamma + \delta f \left[ \frac{X - \xi}{\lambda} \right] \tag{4.5}$$

Where $Z$ is a standard normal random variable, $f$ is the transformation, $\gamma$ and $\delta$ are shape parameters, $\lambda$ is a scale parameter and $\xi$ is a location parameter.

74

The lognormal system of distributions, SL, is given by

$$Z = \gamma + \delta \log\left[\frac{X - \xi}{\lambda}\right], \quad X > \xi \tag{4.6}$$

The unbounded system of distributions SU is defined by

$$Z = \gamma + \delta \log\left[\left[\frac{X - \xi}{\lambda}\right] + \left\{\left[\frac{X - \xi}{\lambda}\right]^2 + 1\right\}^{1/2}\right], \quad -\infty < X < +\infty \tag{4.7}$$

and the bounded system SB is given by

$$Z = \gamma + \delta \log\left[\frac{X - \xi}{\xi + \lambda - X}\right], \quad \xi < X < \xi + \lambda \tag{4.8}$$

In order to generate a sample from the Johnson distribution that matches the given data, first the sample quantiles of the data for the cumulative probabilities of 0.067, 0.309, 0.691, and 0.933 are computed. These probabilities correspond to four evenly spaced standard normal quantiles of -1.5, -0.5, 0.5 and 1.5 [95].

The cumulative distribution function of the experimental data for the setup time of the flip-flop and Johnson system which matches four evenly spaced standard normal quantiles of -1.5, -0.5, 0.5, and 1.5 corresponding to the cumulative probabilities of 0.067, 0.309, 0.691, and 0.933 are plotted in Figure 4.6. The normal CDF has also been plotted for comparison. Again, the type of the distribution within the Johnson family of systems which matches these quantiles is the SU system.
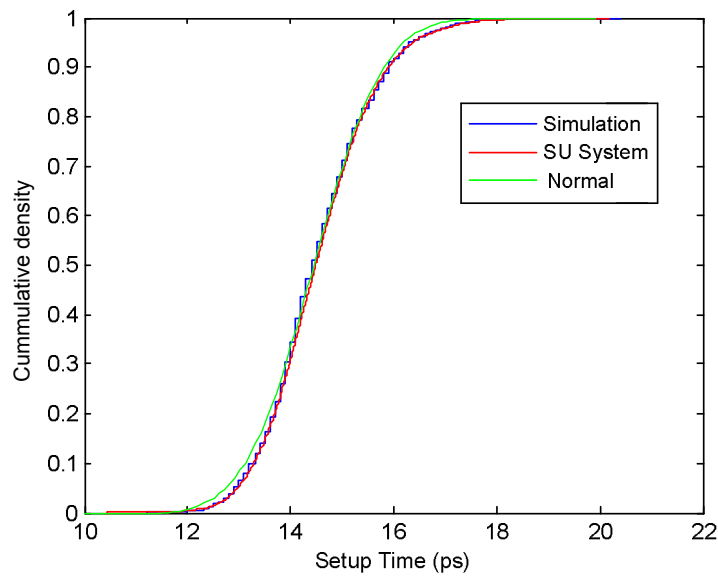


Figure 4.6: Cumulative delay distribution of setup time of 18 nm flip-flops. The SU system from Johnson family of distributions better fits the simulation data as compared to normal distribution.

## 4.5 Estimation of Timing Distributions and Yield

Accurate estimation of the yield depends significantly on the evaluation of the CDF at the tail of the distribution. With a better estimation of the probability distributions with Pearson or Johnson systems, the designer can predict the yield of a design more accurately. The use of a normal approximation will produce optimistic results, whereas fabricated chips will suffer from significant yield loss. For instance, the cumulative distribution function (CDF) for the setup time of 13 nm flip-flops is plotted in Figure 4.7. The performance yield for the target setup time of 11.5 ps is 96.69% with normal and 91.57% with a Pearson IV approximation. Since typical designs include a large number of flip-flops, and no failures are tolerable, the failure probability for the whole system behaves as a power function of the probability of failure of a single device. Therefore even small errors in the estimation of this probability are readily scaled up and will provide very different failure rates for the complete system.
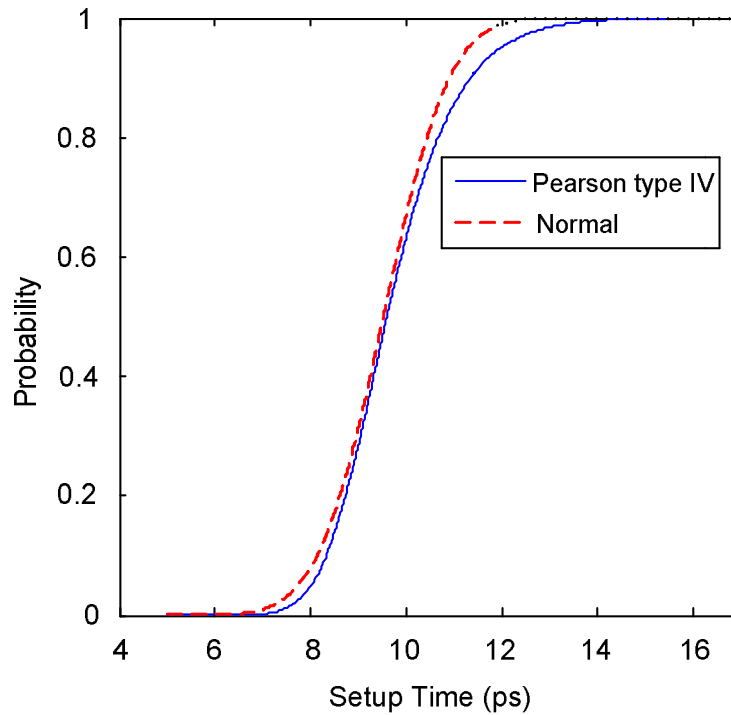


Figure 4.7: Cumulative distribution functions for the setup time of 13 nm flip-flops with Normal and Pearson type IV approximations.

## 4.6    Timing Distributions of Pipelined Circuits

In high performance designs, data and control paths are aggressively pipelined to enhance the throughput. The pipelining is realized by inserting sequential elements (flip-flops or latches) in the circuit at different locations, thus dividing it into several segments.

However, after a certain pipeline depth, the timing overheads of the pipeline become a significant bottleneck for the throughput of the circuits [101], so the number of segments for maximum throughput is bounded. In any case, a large number of sequential elements are used in heavily pipelined designs.

The effectiveness of high performance system design strongly depends on the timing yield of the fabricated chips. The timing yield is defined as the ratio of the chips who meet certain target delay (or the target frequency) to the total number of fabricated chips. Conventionally, high performance circuits are designed for particular target frequencies. In synchronous data transmission through the pipeline, the speed of the circuit is limited by the pipe segment which is slowest (having largest delay) amongst the other pipe segments [102] in the complete path, which becomes the critical path. However, due to variability any pipe segment can potentially be the critical one. Therefore, statistical approaches are required to determine the maximum pipeline delay so that an estimation of the maximum achievable speed of the circuit can be made under permissible yield loss. From the arrival time distributions of different pipeline segments, the maximum arrival time distribution of the complete pipeline is computed in SSTA through the use of SUM and MAX operations.

Most of the existing statistical static timing analysis (SSTA) approaches [103], [104] are invariably based on Clark's approximation [105] to compute the distribution of the maximum arrival time. The Clark's approximation for the MAX operation gives exact results for the operands having joint bivariate normal distributions. The MAX operation is intrinsically a nonlinear function as the maximum of two normally distributed arrival times is typically a positively skewed distribution [106]. Moreover, the variability in the devices and interconnect also results in asymmetric non-normal distributions [107], [108]. Therefore, performing Clark's MAX operation by approximating the non-normal distributions with normal distributions will produce inaccurate results.

There are some recent studies [109]-[111] which propose analytical evaluation of SUM and MAX operations by approximating the arrival times with skew-normal distributions. However, the accuracy of the proposed models strongly depends on how accurate the arrival times are represented by the skew-normal distributions.

## 4.7   Pipeline Delay

Consider an N-stage pipeline as shown in Figure 4.8. The flip-flops have been inserted at regular intervals to store the signal states. If we denote the delay of the combinational logic in the $i$-th segment by $T_{CL^i}$, the CLK-Q delay of the flip-flop by $T_{CLK-Q^i}$, and the

setup time of the $i + 1$-th flip-flop by $T_{setup^{i+1}}$, then the delay of the $i$-th pipeline segment, $T_{seg^i}$, will be given by

$$T_{seg^i} = T_{CL^i} + T_{CLK-Q^i} + T_{setup^{i+1}} \qquad (4.9)$$
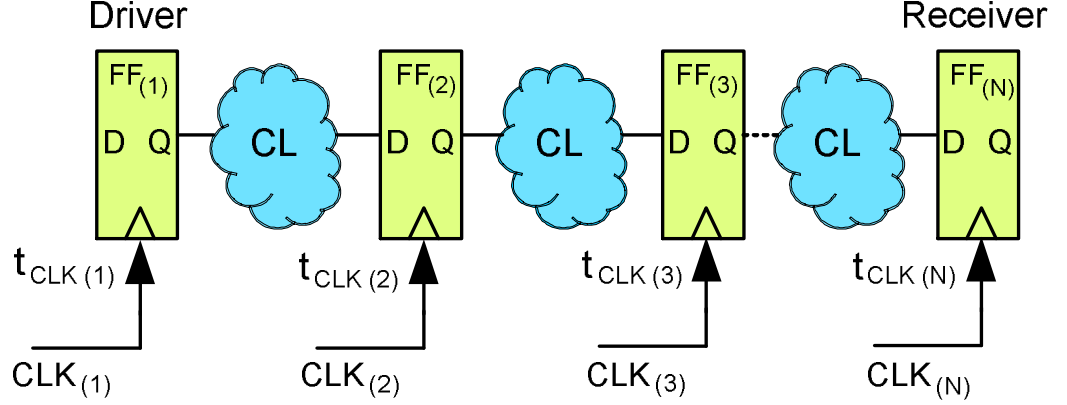


Figure 4.8: N-stage flip-flop based pipeline.

Under the impact of variability, the delay of each pipeline segment is a random variable (RV) with a certain distribution and the delay of the overall pipeline will depend upon the distributions of the individual segment delays.

In order to determine the overall delay of the pipeline, we will make use of the Jensen's inequality [105], [112]. It states that the expected value $E$ of the convex transformation $f$ of a random variable $x$ is at least the value of the convex function at the mean of the random variable

$$E[f(x)] \geq f(E[x])$$

Since "max" is inherently a convex function [112], therefore according to the Jensen's inequality, the overall delay of the pipeline, $T_{PL}$, will be the maximum of the individual pipeline segment delays and a relatively less tight lower bound on the expected maximum is given by

$$E\left[\max_{i=1,\dots,N} T_{seg^i}\right] \geq \max_{i=1,\dots,N}\left(E[T_{seg^i}]\right) \qquad (4.10)$$

$$E\left[\max_{i=1,\dots,N} T_{seg^i}\right] \geq \max_{i=1,\dots,N}\left(E[T_{CL^i} + T_{CLK-Q^i} + T_{setup^{i+1}}]\right) \qquad (4.11)$$

The statistical static timing analysis of the pipelined circuits can be performed using numerical integration method, Monte Carlo method, or probabilistic analysis method [106]. However, the first two approaches are quite expensive in runtime as compared to the third approach.

The overall pipeline delay can be approximated as [103]

$$T_{PL} = \max\left[T_{seg^1,}\, T_{seg^2}\,,T_{seg^3}\,,\ldots,T_{seg^{N-1}},T_{seg^N,}\right] \qquad (4.12)$$

$$= \max\left\{T_{seg^1}, T_{seg^2}, T_{seg^3}, \ldots, \max\left(T_{seg^{N-1}}, T_{seg^N}\right)\right\} \qquad (4.13)$$

$$= \max\left\{T_{seg^1}, T_{seg^2}, T_{seg^3}, \ldots, \max\left\{T_{seg^{N-2}}, \psi_{seg^{N-1,N}}\right\}\right\} \qquad (4.14)$$

where $\psi_{seg^{N-1,N}}$ represents a distribution which is obtained as a result of max operation on $T_{seg^{N-1}}$ and $T_{seg^N}$. Now, once $\psi_{seg^{N-1,N}}$ is determined, we can find $\psi_{seg^{N-2,N}} = \max\left(T_{seg^{N-2,}} \psi_{seg^{N-1,N}}\right)$ by iteratively applying the above procedure. Hence by repeating this procedure N-1 time, by taking two variables at a time, we can get the overall distribution of the pipeline delay in terms of its moments that can accurately represent the distribution.

The maximum of two normally distributed random variables typically produces non-normal positively skewed distributions [111]. The skewed arrival time distribution resulting from the MAX operation at a given node becomes input for the max operation at a downstream node. Moreover, due to device and interconnect variability, the timing distributions of the circuits themselves are asymmetric (non-normal) [93], [106], [107]. Hence, in the pipeline system described above, if Clark's approximation is used at each stage, the final distribution will deviate significantly from the actual distribution. Again, there are some recent works [109]-[111] which proposes the evaluation of max function by approximating the timing distributions with skew-normal distributions. However, the SSTA results entirely depend on how accurately the timing distributions are represented by the underlying approximation models.

## 4.8 Statistical Analysis of the Timing Yield

We now proceed to discuss the yield of a pipelined circuit. The timing yield of a pipeline depends on the timing constraints introduced due to the setup time and the hold time of the sequential elements. The pipeline should be so designed that the signal from one flip-flop to the next flip-flop reaches at least one setup time earlier than the next clock edge. Moreover, the signal should not be so fast that the second register can not latch the data correctly. Under statistical variations, both shortest and longest paths in the pipeline no more remain fixed and therefore both setup and hold time constraints need to be considered in the statistical analysis and for yield estimation.

Considering data transmission between flip-flop $FF_{(i)}$ and $FF_{(i+1)}$ such that $FF_{(i)}$ is the source and $FF_{(i+1)}$ is receiver, then the constraint introduced by the setup time for proper data latching by the $FF_{(i+1)}$ is

$$0 \leq T_{CLK-Q^i} + T_{CL^i} \leq T_{CLK} - T_{skew} - T_{setup^{i+1}} \qquad (4.15)$$

where $T_{CLK}$ is the clock period, $T_{skew}$ is the skew between the clock signals $CLK_i$ and $CLK_{i+1}$.

In order to avoid race-through condition, the constraint imposed by the hold time is

$$T_{CL-Q^i} + T_{CL^i} \geq T_{hold^{i+1}} - T_{skew} \qquad (4.16)$$

The above constraints dictate that, for successful data transmission, the longest path delay should be less than and the shortest path delay should be greater than some target values.

The time margin under setup time constraint for the pipe segment $i$ is given by

$$\delta tm_{setup^i} = T_{CLK} - T_{skew} - T_{setup^{i+1}} - T_{CLK-Q^i} - T_{CL^i} \qquad (4.17)$$

Similarly, the time margin under hold time constraint for the pipe segment $i$ is given by

$$\delta tm_{hold^i} = T_{CL-Q^i} + T_{CL^i} - T_{hold^{i+1}} + T_{skew} \qquad (4.18)$$

In order to minimize the yield loss, both these time margins should be greater than zero for all the pipeline segments. Therefore, we need to find the minimum of both the timing margins for the whole pipeline so as to check that these are greater than zero.

All the parameters in the expression of $\delta tm_{setup^i}$ and $\delta tm_{hold^i}$, except $t_{CLK}$, are circuit dependent and have certain timing distributions that can either be obtained through detailed device and circuit modeling or through simulation. From the distributions of timing margins of different pipeline segments, the timing margins of the complete pipeline under setup and hold time constraints ($\delta tm_{setup^c}, \delta tm_{hold^c}$) can be determined by applying the MIN operation over all pipeline segments, following the same procedure as laid down in the previous section. Finally, MIN operation is again applied over $\delta tm_{setup^c}, \delta tm_{hold^c}$ to find the combined time margin $\delta tm_{comb}$ of the pipeline. The MIN operation can be performed in the same way as that of MAX: MIN(x1,x2) = -MAX(-x1,-x2).

The timing yield of the pipeline at a clock period $T_{CLK}$ can then be determined as

$$\text{Yield}(T_{CLK}) = P(\delta tm_{comb}(T_{CLK}) > 0)$$

It can be seen that for SSTA, the accuracy of the timing yield depends on how accurately the timing distributions are represented and MIN/MAX operations are performed.

## 4.9    Experimental Setup and Results

We used Monte Carlo simulations in HSPICE for the pipeline structure of Figure 4.8 with six pipeline stages. The transistor level structure of the single segment of the pipeline is

shown in Figure 4.9. The study has been carried out for the technology generations of 18 and 13 nm. During the simulation of the pipeline, the variation in the clock signal is not considered and a common clock signal is applied at all the flip-flops. Large numbers of simulations (5000) were run to extract the timing parameters. All timing measurements were taken corresponding to 50% of the maximum swing level.
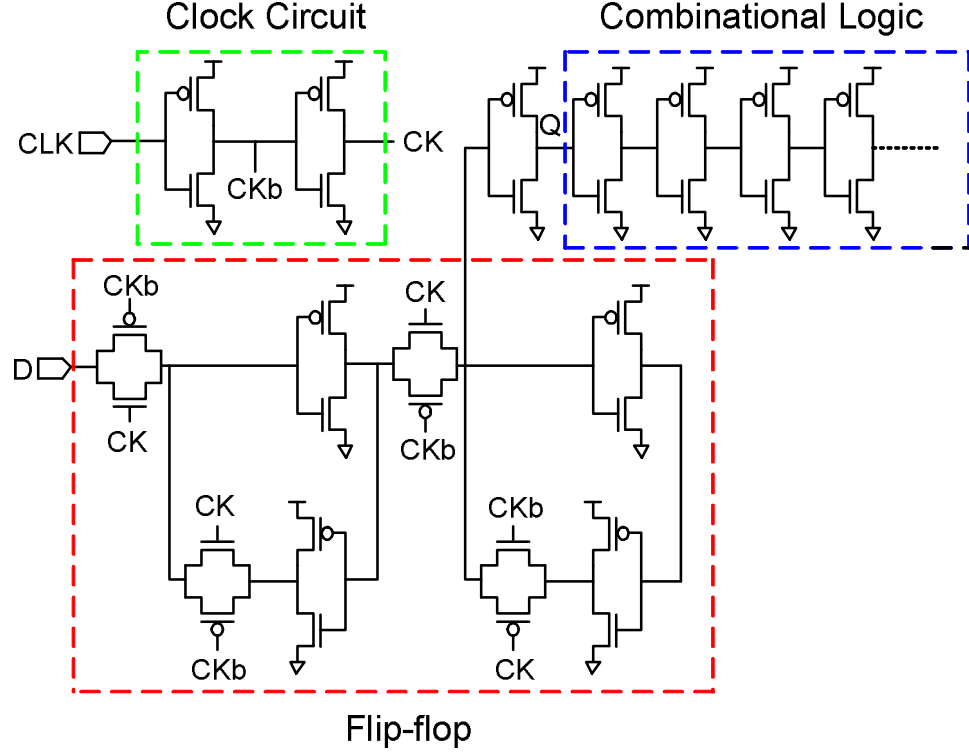


Figure 4.9: Transistor level model of the pipeline segments.

The CLK-Q delay of each flip-flop and the propagation delay of the combinational logic between the flip-flops has been measured. Based on these measurements, the delay distribution of the maximum of the complete pipeline, using Clark's approximation [105], has been determined and plotted in Figure 4.10 along with the delay distributions of the individual stage delays. It may be observed that the individual stage delays are not Gaussian and rather are having skewed distributions, under the impact of RDF. Therefore, the maximum delay distribution of the complete pipeline can no longer be Gaussian, as expected. However, the Clark's approximation always gives the results in terms of Normal distribution. The maximum delay distribution of the complete pipeline has also been obtained through Monte Carlo simulations and is also plotted in Figure 4.10. The visual inspection shows that the actual distribution has a long positive tail and significantly differs from the Normal distribution. The statistical parameters of the two distributions verify this fact.

In order to examine the impact of technology scaling on the evaluation of MAX distribution, the simulations were performed for the technology generations of 18 and 13 nm and the results are shown in Figure 4.11. The results show that the asymmetry in different timing parameters of the flip-flops and the combinational logic increases with technology scaling, resulting in increased asymmetry in the MAX distribution, as is also evident from the statistical parameters given in Table 4.3 (for 0-1 input transition).
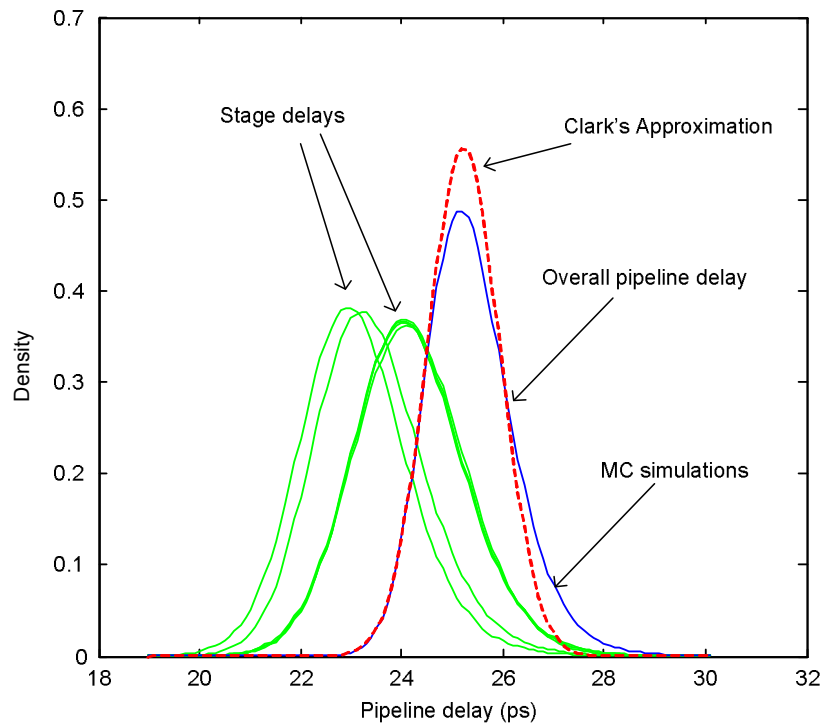


Figure 4.10: MAX delay distributions of individual pipeline stages and overall pipeline for 18nm technology generation.
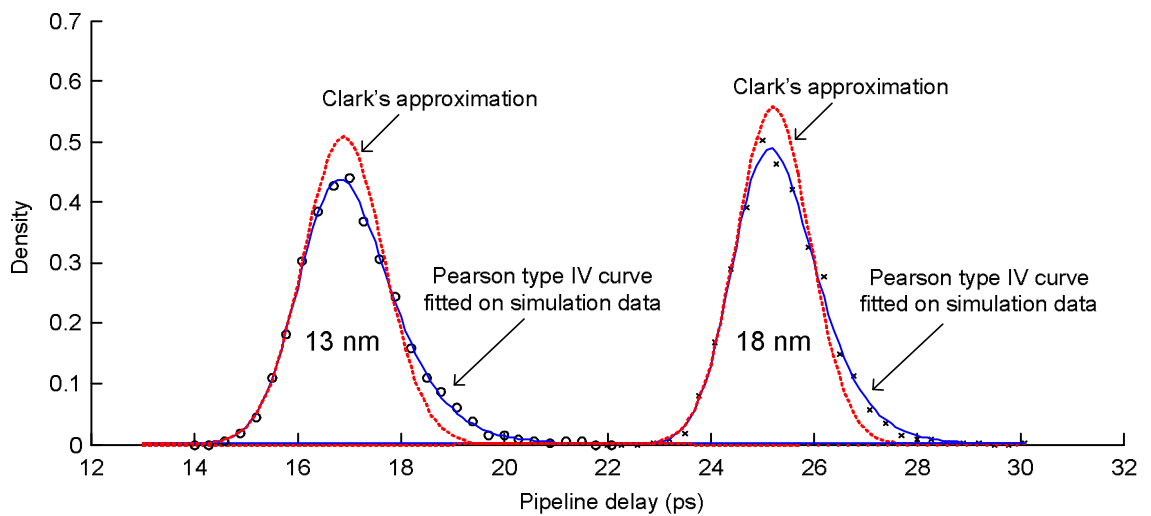


Figure 4.11: Overall pipeline delay distributions of a pipeline consisting of 6 stages simulated for the technology generations of 18 and 13 nm.

82

The increased asymmetry means greater deviation from the Gaussian distribution and more error in estimating MIN/MAX distribution using Clark's approximation, as is evident from Figure 4.11. Although the Clark's approximation provides a conveniently fast means of finding MAX distribution, but the inaccuracy of results, particularly in the tail section makes it not a good choice for the given purpose, as it will give very optimistic results for the pipeline delay. Therefore, it will result in yield loss due to difference in the PDFs at the tail section.

Table 4.3: Statistical Parameters of the MAX Delay Distribution of the Complete Pipeline

| Parameters | 18 nm | 13 nm |
|---|---|---|
| Mean Delay (ps) | 25.2 | 16.93 |
| Std. Dev. (ps) | 0.843 | 0.994 |
| Skewness | 0.464 | 0.676 |
| Kurtosis | 0.426 | 0.922 |

It has also been observed that stage delays are different in opposite transitions even if NMOS and PMOS transistors are properly T-sized. For instance, the stage delay distributions for low-high and high-low transitions are shown in Figure 4.12. Although the size of the PMOS transistors is chosen to be double the size of the NMOS transistors to keep the circuit delay close in the two swings. However, the delay variability is inversely
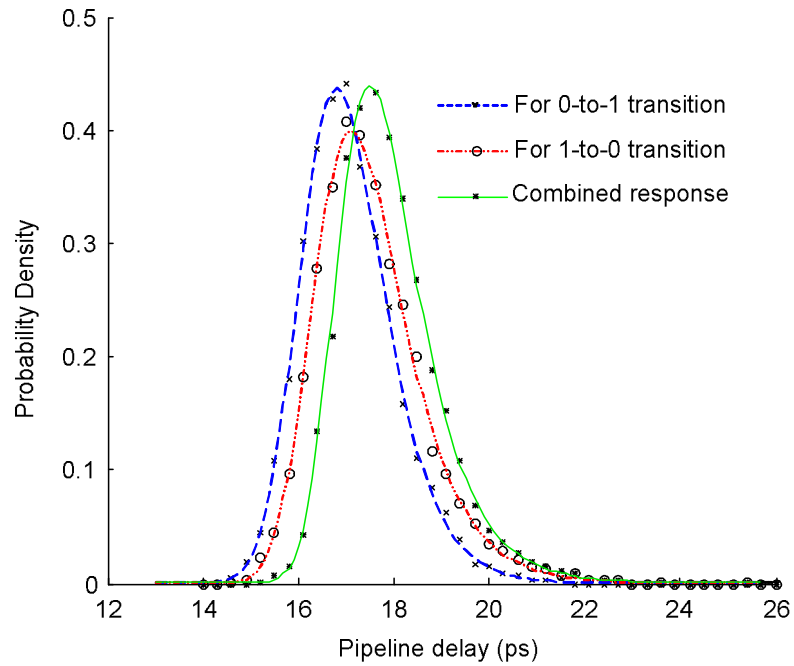


Figure 4.12: Maximum delay distributions plotted for low-high and high-low transitions for the 13 nm pipeline.

proportional to the size of the transistors [107] and therefore the statistical parameters (mean, standard deviation, skewness, and kurtosis) are also different for the two transitions. Therefore, while determining the MAX distribution, the delay distribution in both swings needs to be considered.

While measuring the timing parameters of the flip-flops, different interdependencies need to be considered. These interdependencies also have a negative impact on the shape of the distributions due to variability, thus pushing them away from the normal distribution. For example, Figure 4.13 shows two histograms for a timing random variable formed by the sum of D-CLK time, CLK-Q time and combinational logic delay. The narrow and high peak histogram is corresponding to the case when D-CLK time is very large. Similarly, the wider histogram is corresponding to the case when D-CLK time is short. The setting of D-CLK time depends on the clock period and combinational logic delay. However, its value greatly affects the shape of the timing distributions and then increased deviation from normality for small D-CLK time.
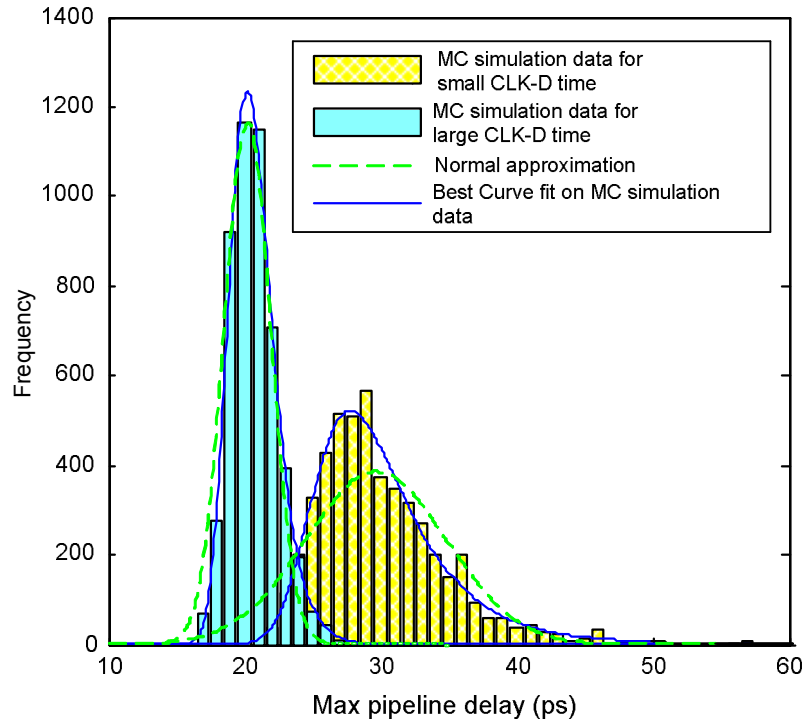


Figure 4.13: Histograms of timing variable comprising of D-CLK time, CLK-Q time and combinational delay for a 13 nm pipeline.

As mentioned before, some recently reported works [108], [111], [113] propose to approximate skewed arrival time distributions with skew-normal and also present analytical models for the computation of the MAX function. However, we have seen in this work that skew-normal is also not an appropriate choice for representing skewed timing

distributions of highly scaled devices as shown by the probability distributions in Figure 4.14. The solid curve corresponds to the actual simulation data and the other two curves are for the normal and skew-normal approximations. It can be seen that although skew-normal distribution better matches the actual data as compared to the normal approximation, but still it does not exactly approximate it. Similar discrepancy is also reported in the arrival time plots given in [108], [111], [113].
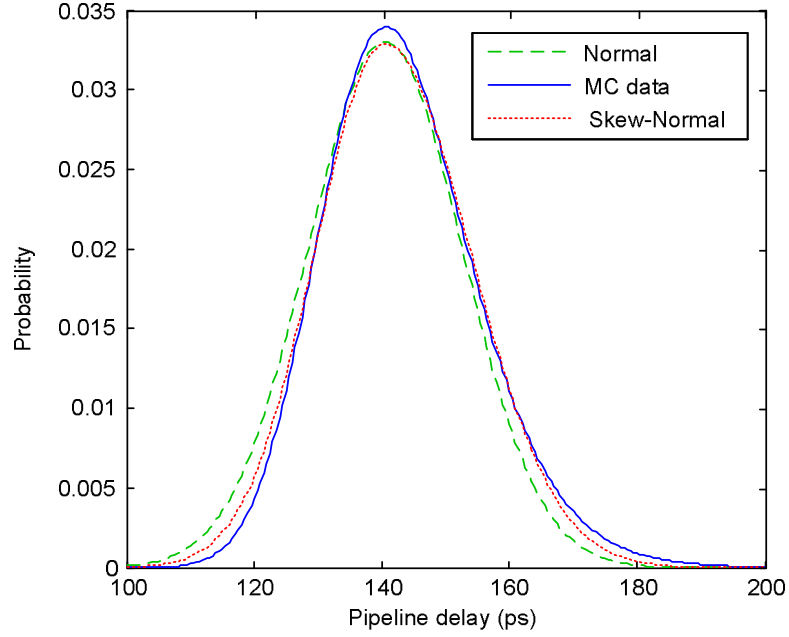


Figure 4.14: Probability density functions for the pipeline delay with a combinational logic of 60 inverters in series for 13 nm.
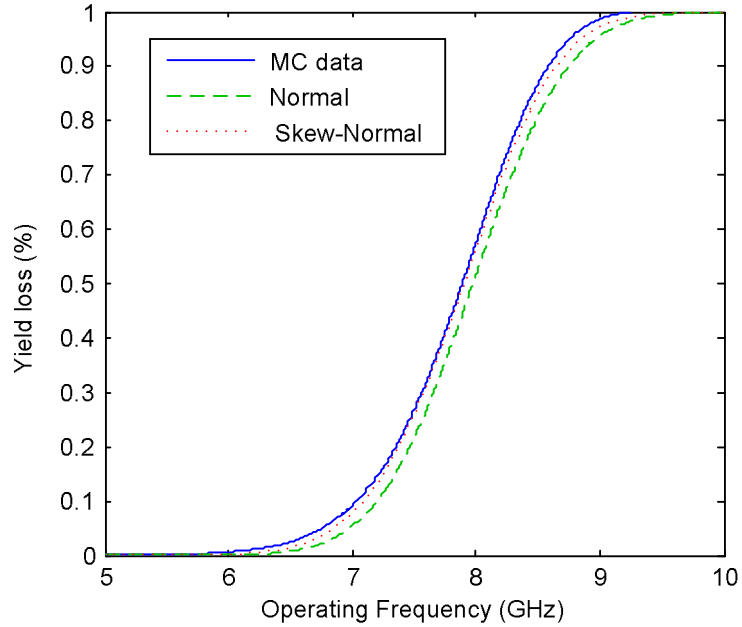


Figure 4.15: Difference in timing yield estimation with normal and skew-normal approximations.

85

The inaccuracy in approximating the arrival times for SSTA has a dreadful impact on yield estimation. In Figure 4.15, timing yield loss as a function of operating frequency has been plotted for normal and skew-normal distributions for their comparison with the MC simulation results. For this purpose, the model laid down in section 4.8 has been followed. Again it can be seen that normal approximation produces optimistic results but quite different from the MC results. The skew-normal approximation gives relatively better results but still with some error. For instance, the yield loss at a frequency of 7GHz is 9.3% with MC simulation data, 5.2% with normal and 7.8% with skew normal. This error increases to significant levels for deeply pipelined circuits with multiple MIN/MAX operations during SSTA. Therefore, in order to keep yield loss below permissible limits, operating frequency will have to reduce.

## 4.10  Summary

In this chapter accurate estimation of the shape of timing distributions of flip-flop parameters has been discussed. The study of the exact shape of these distributions, especially in the tail section, is of fundamental importance in the design and modeling of high-performance, reliable, economically feasible circuits. In this chapter, the distribution tails are estimated based on simulation data, with the aid of statistical nonparametric probability density functions, and it has been found that timing distributions can better be represented by certain nonparametric distributions, in particular Pearson and Johnson systems. The use of these representations during the statistical static timing analysis will provide more accurate results as compared with the normal approximation of distributions and will eventually reduce the probability of yield loss. The skew normal distribution provides an interesting alternative to represent the skewed data; however, it does not give better results than Pearson and Johnson systems. Since in current state-of-the-art systems the device count has already crossed several billion, accurate representation of data for SSTA is imperative to avoid yield loss. Therefore for such large systems also, Pearson and Johnson distributions provide very accurate results as compared to other distributions.

Under statistical device variations, the delay distributions of the pipeline stages follow a skewed distribution in highly scaled devices. Therefore, in order to determine the maximum operating frequency of the pipelined circuits, accurate estimation of the slowest pipeline stage will have to be determined. This study shows that identifying the slowest pipeline stage using Clark's approximation will produce quite optimistic results and will lead to significant yield loss. Moreover, it has been shown that while estimating the yield,

the stage delay distributions in both low-to-high and high-to-low transitions need to be considered and hold time distributions should also be considered along with setup time distributions.

# Chapter 5

# Optimal Scaling for Variability Tolerant Repeaters

## 5.1 Introduction

As technology scales, on-chip interconnections are becoming progressively slower when normalised by the logic delay. Techniques to manage this discrepancy, and avoid a possible bottleneck, are therefore required. The use of caching, and wide buses are all possible. However the most fundamental solution is the use of repeaters inserted in the communication links. The placement and size of repeaters can be tuned to construct delay optimal interconnections. Again due to technology scaling, the number of optimal repeaters per unit length is also increasing. Optimal repeaters are of significantly large size as compared to the minimum sized repeaters. Thus they require larger portions of the silicon and routing area [114] and a significantly larger portion of the chip power [61]. Due to their large number and size, their total power consumption can be as high as 60W [115]. For the future technology generations, unconstrained optimal buffering of interconnects might require up to 80% of the total on-chip area [68]. The impact of technology scaling on the number and size of delay optimal repeaters is shown in Figure 5.1.
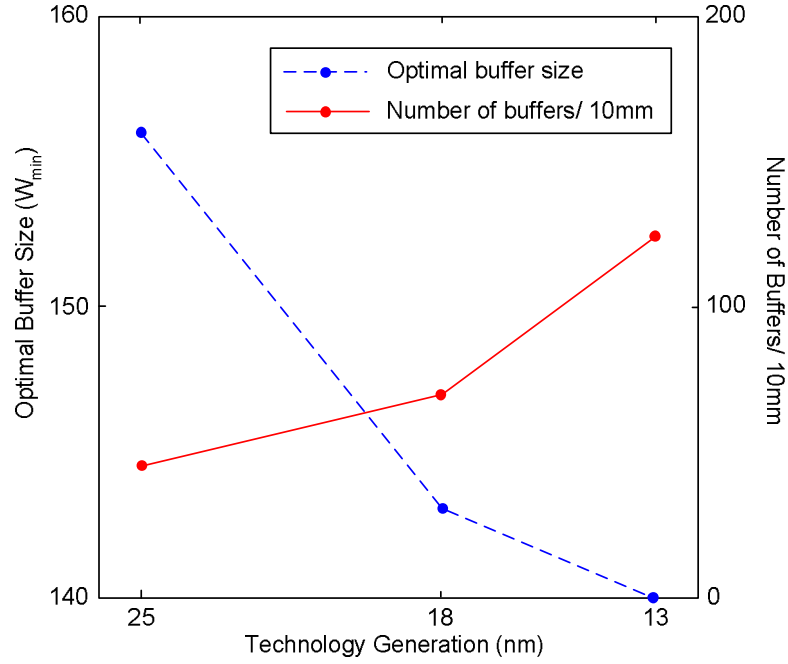
Figure 5.1: Optimal number and size ($\times W_{min}$) of uniformly inserted buffers in an interconnect of minimum width and spacing for the three technology generations.

Due to the increasing trend of the on-chip power dissipation, it has been pointed out as the main limiting factor in the scaling of CMOS circuits [62]. In previous technology generations, the switching power was the dominant component of power dissipation. However the relative contribution of different components of power dissipation (switching, short circuit, and leakage) is changing along scaling. Therefore, it becomes important to determine different components of power dissipation individually, as this approach may be helpful in designing more power efficient designs.

The increasing magnitude of the variability in deep sub-micron (DSM) technologies is not only affecting the delay characteristics of the devices but also their power dissipation. In this work we will show that RDF causes inherent variability in the power dissipation of the devices. Therefore, similar to the operating frequency and yield which are affected by the delay variability, the variability in the power dissipation may also affect yield.

In the first part of this chapter, we present the results for the power measurement in repeaters. We used Monte Carlo simulation method for the accurate characterization of power dissipation in repeaters of 25, 18 and 13 nm bulk MOSFETs, and to see the effect of RDF on all the components of power dissipation. Since repeaters of different sizes are used on the chip, therefore, the effect of repeater size on power dissipation has also been investigated under the impact of RDF. The results obtained through this study can be used

to develop accurate models for other sizes and configuration of devices. Moreover, the characterization data so obtained can be used to design more effective power optimal links.

In the second part of this chapter, we investigate the impact of variability on area and power optimal repeater insertion technique for on-chip links. In [116] it has been shown that absolute performance is expensive in terms of power dissipation and silicon area and we can make significant savings in these parameters at the cost of a little performance penalty. However, we argue that in addition to the delay performance, the predictability of the timing of the signals for all the wires in a multi-bit link is another important parameter for high performance designs. The timing variability not only degrades the system performance but can also produce timing violations and system faults, thus reducing system yield. With aggressive technology scaling, the variability in the devices and interconnect is continuously increasing, posing many challenges for high performance and yet reliable designs [117], [118]. The power optimal repeater insertion methodologies in [116], [24] suggest the use of smaller sized buffers (and increased inter-repeater segment length), whereas it has been shown in [107] that delay variability of the buffers is inversely proportional to their size and that this relation is not linear. Therefore, reducing the size of the buffers may be of little benefit if variability, reliability and yield are to be maintained within certain acceptable limits. Hence, robust designing of communication links require the need for studying any power and area efficient methodologies against the reliability of the system and any such methodology should also include this metric in the optimization process.

## 5.2 Methodology for Power Measurement

The arrangement for the measurement of different components of power dissipation is shown in Figure 5.2. Minimum sized inverters (MSI) of 25, 18 and 13 nm technology generations were used with a supply voltage of 1.1V, 1.0V and 0.9V, respectively. Based on the predictive model card libraries, Monte Carlo simulation method has been used and 10,000 HSPICE simulations were run for accurate measurements, for each of the given technology generations. The measurements were taken during both swings ($V_{HL}$ and $V_{LH}$) for the repeaters switching at a frequency of 2GHz for all the three technology generations. The typical value of activity factor 0.15 [119] is used in this study.

The leakage power of the inverter R is measured using the leakage current flowing through zero-volt voltage sources $V_P$ and $V_N$ in each of its possible states.

The short circuit power has been determined by measuring the energy dissipated across the supply voltage $V_{DD}$ by integrating the current over the period ($T$) of interest:

$$E = V_{DD} \int_0^T i(t)dt \tag{5.1}$$

where $i(t)$ is the short circuit current flowing through the inverter which can be sensed through the zero-volt voltage source $V_N$ for the LH transition and through the zero-volt voltage source $V_P$ for the HL transition. The transient analysis was carried out over the whole switching period, which was taken to be significantly long to cover the whole transition.

The switching power is determined by first measuring the total energy dissipated by the inverter over both transitions and then subtracting the short circuit and leakage components.
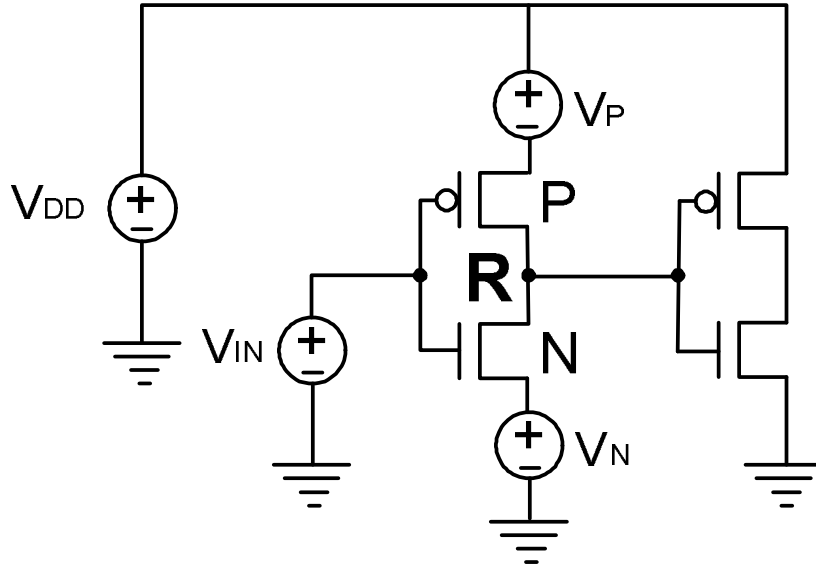


Figure 5.2: Arrangement for the measurement of power dissipation in the repeater.

$$E_{total} = V_{DD} \int_0^{2T} i_{V_P}(t)dt \tag{5.2}$$

$$= E_{sw_{LH}} + E_{sw_{HL}} + E_{sc_{LH}} + E_{sc_{HL}} + 2TP_{leak}$$

$$E_{sw\,LH} = E_{sw\,HL} = \frac{1}{2}\left(E_{total} - E_{sc_{LH}} - E_{sc_{HL}} - 2TP_{leak}\right) \tag{5.3}$$

where $E_{total}$, $E_{sw}$, $E_{sc}$ are the total, switching and short circuit energies, respectively. The subscripts LH and HL represent the transitions from low-high and high-low, respectively. $P_{leak}$ is the leakage power.

## 5.3    Results and Discussion

Different components of power dissipation along with the total power are shown in Figure 5.3 for the three technology generations. The curves show the trend of these components with technology scaling. It may be noted that leakage power increases; whereas the other two components decreases, as the technology scales from 25nm to 13nm. The pace at which leakage power and short circuit power changes is roughly the same, whereas the switching power decreases more rapidly.
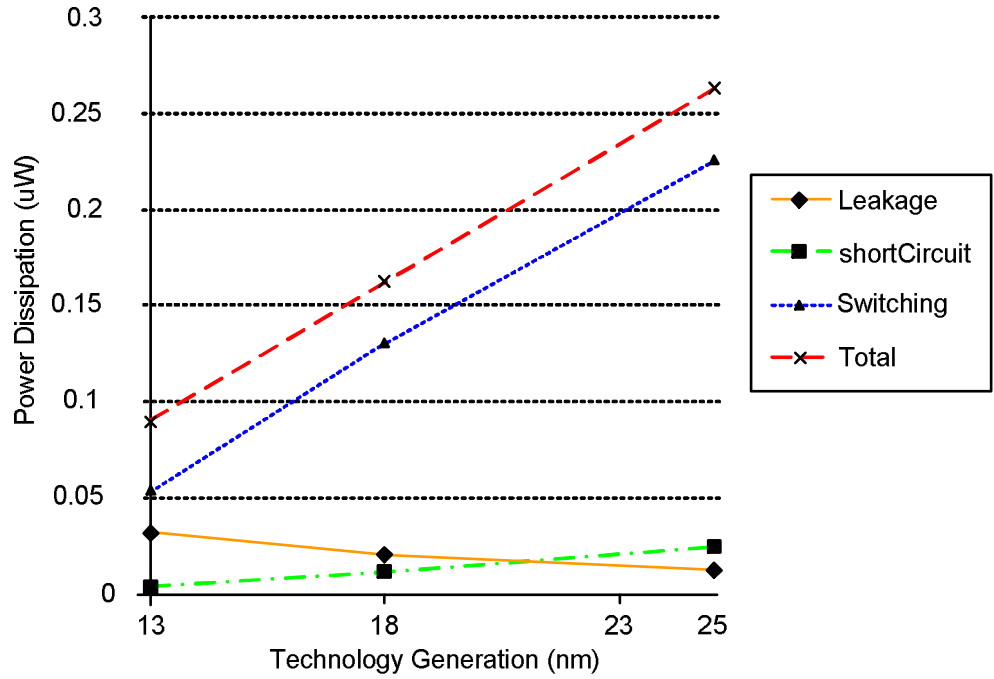


Figure 5.3: Different components of power dissipation along with the total power in a minimum sized inverter (MSI). The inverter under investigation refers '**R**' in Figure 5.2 operating at a frequency of 2GHz.

Technology scaling has made it possible to switch the circuits at higher speeds. As mentioned before, the FO4 delay metric can be used to compare the speed of the circuits in different technologies. In Figure 5.4, the FO4 delay in the given three technologies has been plotted along with the leakage power in MSI of the corresponding technologies. It can be seen that the devices become faster with technology scaling, as expected. However this gain in performance is associated with dramatic increase in the leakage power. Hence there is an inverse correlation between circuit speeds and leakage power.

The relative contribution of different components of power dissipation in the total power is graphically shown in Figure 5.5 and the corresponding data is given in Table 5.1. It has been found that leakage power is no more an insignificant quantity in comparison with other two components and can affect the performance of high performance designs. The

increase in the leakage power is mainly due to the increase of sub-threshold leakage current. The short circuit power is decreasing and is due to the reason that devices are becoming smaller with technology scaling, having relatively higher output resistance. Amongst all components of power dissipation, switching power is the most dominant mode of power dissipation.
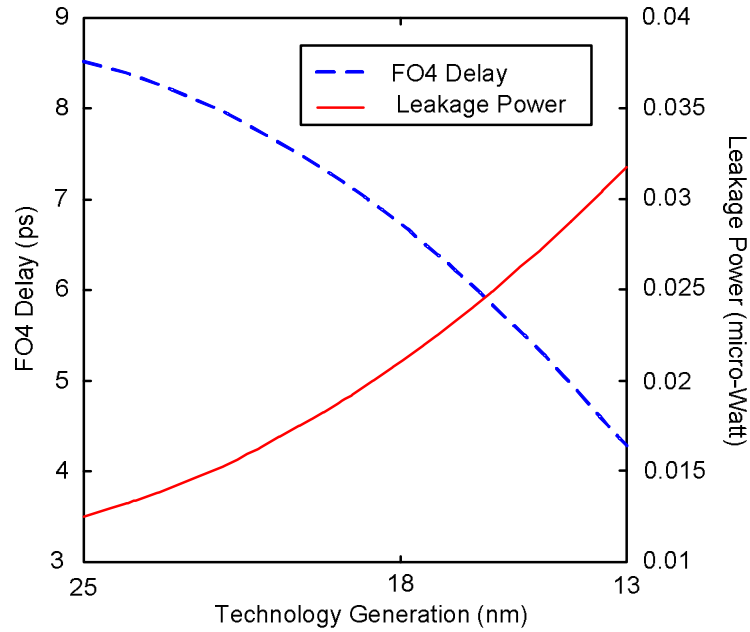


Figure 5.4: A plot of FO4 delay and the leakage power in MSI.
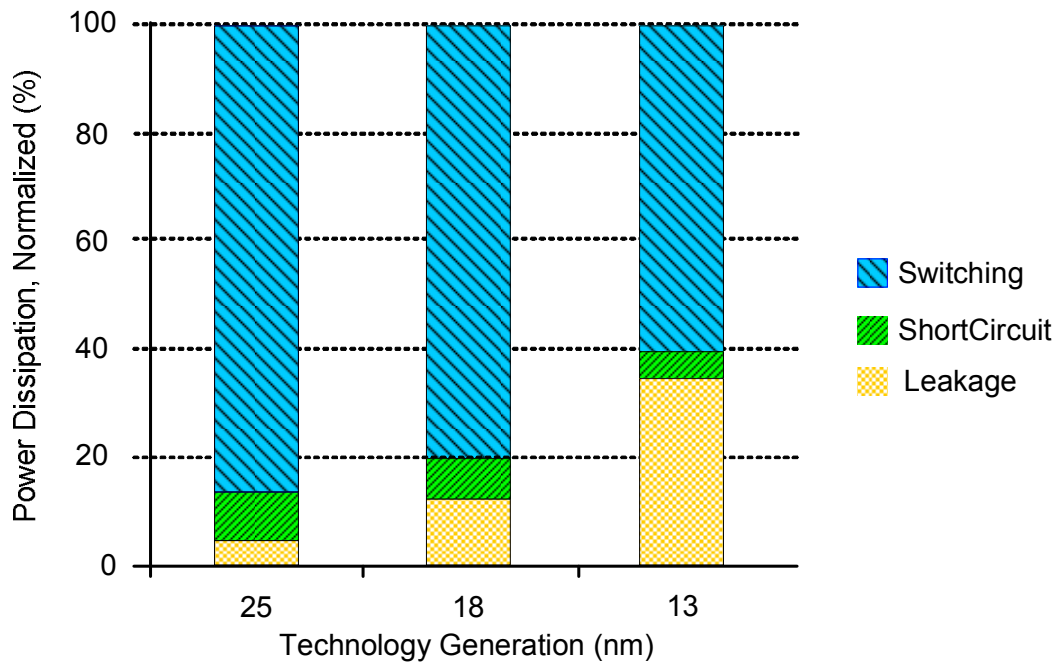


Figure 5.5: Normalized power distribution components in MSI operating at 2GHz.

From Table 5.1, we can see that the leakage power represents a very significant portion of the total power dissipation. It becomes even more prominent if the system is operating at lower frequencies because short circuit and switching power components are frequency dependent and become small as frequency decreases. Therefore power optimization methodologies should also consider individual power dissipation components along with total power dissipation.

Table 5.1: Statistics of Power Measurements for MSI

|  | Tech. | $P_{leak}$ | $P_{sc}$ | $P_{sw}$ | $P_{tot}$ |
|---|---|---|---|---|---|
| Mean (µW) |  | 0.0125 | 0.16 | 1.5 | 1.67 |
| St. Dev. (µW) | 25nm | 0.01 | 0.004 | 0.016 | 0.022 |
| 3σ/ Mean (%) |  | 259.1 | 7.0 | 3.3 | 4.0 |
| Mean (µW) |  | 0.021 | 0.0754 | 0.8701 | 0.966 |
| St. Dev. (µW) | 18nm | 0.021 | 0.0034 | 0.0095 | 0.0209 |
| 3σ/ Mean (%) |  | 303.1 | 13.7 | 3.3 | 6.5 |
| Mean (µW) |  | 0.0318 | 0.0285 | 0.364 | 0.425 |
| St. Dev.(µW) | 13nm | 0.0368 | 0.0066 | 0.0121 | 0.0341 |
| 3σ/ Mean (%) |  | 346.6 | 69.4 | 10.0 | 24.1 |

Due to variability in the devices, power dissipation becomes a random variable. For instance, due to the variation in the threshold voltage of devices, the leakage current is different for different devices on the chip. Similarly, due to the mismatching in the switching timing of the NMOS and PMOS devices in the inverter, the short circuit power varies for different inverters. However, there is little effect of device variability on the switching power. As a result of this behaviour, power dissipation follows a certain distribution, with statistical data given in Table 5.1. It may be noted that there is a significant variation in the power dissipation, especially in the leakage component. As can be seen (Table 5.1), the variability of leakage power in 13nm inverters reaches up to 346% with respect to the mean power.

Figure 5.6 shows the histogram of leakage power in 25nm minimum sized repeaters. The spread of the distribution is quite evident which means that the leakage power of a large number of repeaters is away from the mean value. Therefore, when considering power issues (for instance, in optimizing a circuit for power consumption), the complete distribution of power dissipation needs to be considered instead of just the mean value. More importantly, it is apparent that the distribution is not normal; rather it is quite

asymmetric about the mean value having positive skewness. This implies that some devices will dissipate a far larger amount of power than the mean.

### 5.3.1 Impact on Repeater Inserted Links

Due to the long tail in the distribution, a large number of on-chip repeaters will dissipate an excessively large amount of power. A similar asymmetry has already been observed in the delay distribution of the repeaters [107]. This is relevant, since an inverse correlation between the repeater delay and leakage power exists [120], and therefore the simultaneous optimization for delay and power becomes challenging. The variability in the devices, with asymmetric distributions of delay and power, has serious implications on the yield of the chips, as many of the chips would have to be discarded due to unacceptable delays and many more due to excessive power dissipation. If spatial correlations exist (due to process issues; not due to RDF), there may exist a cluttering of such highly leaky devices on the chip which can further create reliability issues. We have also observed that the skewness in the leakage power distribution greatly increases with technology scaling which further deteriorates the situation. This instigates the use of some preventive measures to control the leakage power in the circuits.
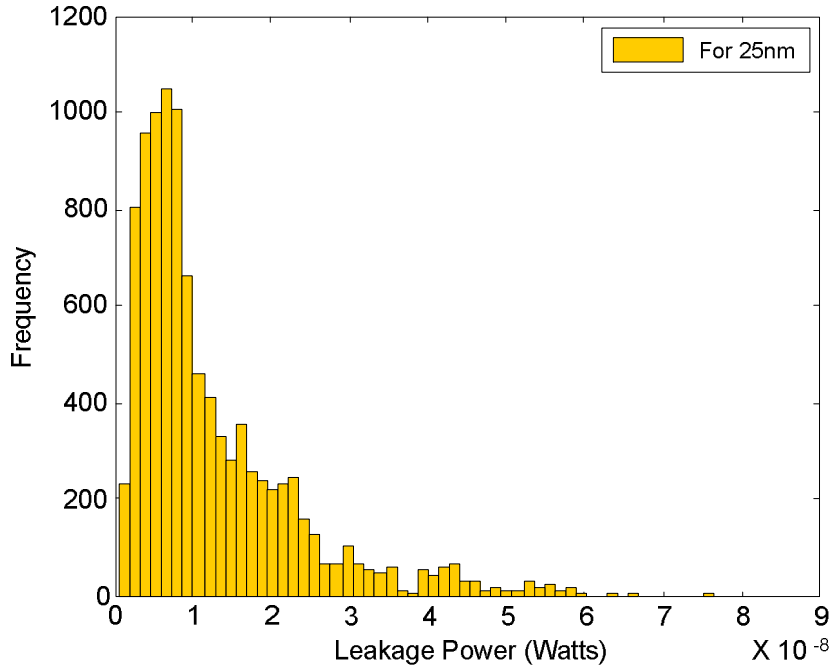


Figure 5.6: Histogram of leakage power in 25nm MSIs. The distribution is quite asymmetric about the mean.

### 5.3.2 Impact of Repeater Size on Power Dissipation

In the global interconnect, repeaters of different sizes are used. Therefore, the study has been extended to investigate the effect of repeater size on power variability. We have

chosen repeaters of sizes 1X, 2X, 4X, 8X and 16X with a similar repeater connected at their outputs to act as the load. HSPICE simulations were performed and results are shown in Figure 5.7 for 18nm technology. The error bars represent the uncertainty (corresponding to 1xsigma) in the leakage power. It can be seen that the leakage power increases linearly with repeater size. Similarly, the uncertainty in the leakage power also increases almost linearly with the increase in the repeater size. However, we have shown in [107] that increasing the size of the repeaters reduces the delay uncertainty but this advantage is not achieved in case of power. The normalized leakage power, on the other hand, decreases with the increase of repeater size.

### 5.3.3 Impact on NoC links

In Network-on-Chip (NoC), links of different width are designed to achieve a given throughput, and latency. The width of a communication link is usually defined in terms of the *phit size*, which determines the number of bits that can be simultaneously transferred through the link. In many cases the link utilization rates are not constant and can be very low, just a few percents [121]. Large *phit sizes* are preferred to meet latency requirements but such links also remain idle for most of the time. Thus in such links, leakage power will be the main contributor of power dissipation. Therefore, a stronger tradeoff will have to be made between the power and other performance metrics, in the presence of increased variability.
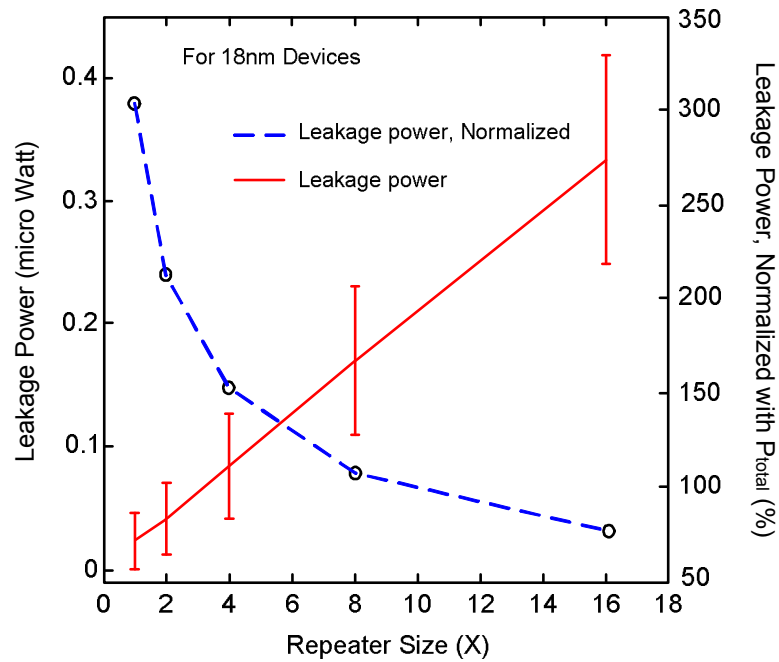


Figure 5.7: Effect of repeater size on leakage power. Leakage power and its variability increases with repeater size.

## 5.4 Power and Area Optimal Repeater Insertion

### 5.4.1 Unconstrained Repeater Insertion

We consider a global interconnect having resistance $r$ and capacitance $c$ per unit length, inserted with repeaters of equal size at equal distance as shown in Figure 5.8. The whole interconnect, therefore, consists of $K$ wire-segments each with repeater of size $s$ and interconnect length $l$ (which is the length of the interconnect between any two repeaters). We assume that the output resistance of a minimum sized repeater in a given technology generation is $r_s$, the input capacitance is $c_o$, and an output parasitic capacitance is $c_p$. These values are scaled accordingly for the repeaters of different sizes such that for a repeater of size $s$, the total output resistance becomes $R_{tr} = {r_s}/{s}$, the total input capacitance becomes $C_L = c_o s$ and the total output parasitic capacitance becomes $C_p = c_p s$. The delay per unit length corresponding to 50% of the full swing voltage is given by [24], [51].

$$T_l = \left( \frac{1}{l} r_s (c_o + c_p) + \frac{r_s}{s} c + rsc_o + \frac{1}{2} rcl \right) \log_e 2 \tag{5.4}$$
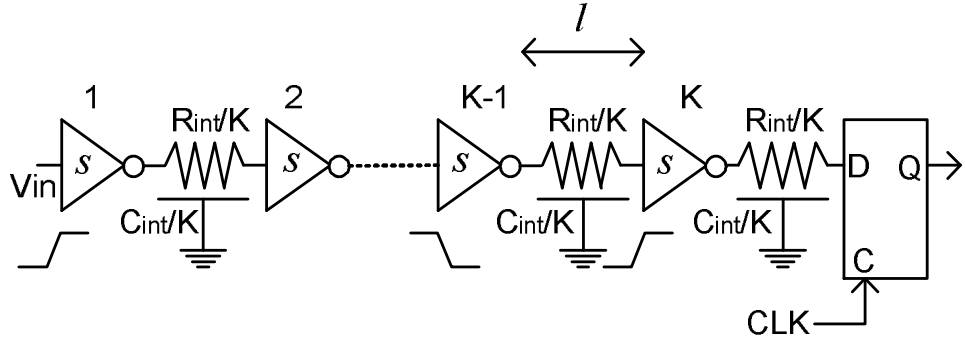


Figure 5.8: Buffer inserted interconnect.

The values of $l$ and $s$, which gives optimal delay per unit length, are given by [51]

$$l_{opt} = \sqrt{\frac{2r_s(c_o + c_p)}{rc}} \tag{5.5}$$

$$s_{opt} = \sqrt{\frac{r_s c}{rc_o}} \tag{5.6}$$

Using $l_{opt}$ and $s_{opt}$ in equation (5.4), the optimal delay per unit length is given by

$$T_{l-opt} = 2\sqrt{r_s c_o rc} \left( 1 + \sqrt{\frac{1}{2}\left(1 + \frac{c_p}{c_o}\right)} \right) \tag{5.7}$$

### 5.4.2 Repeater Insertion under Area Constraints

We consider again the interconnect of Figure 5.8. Let $s_{opt}$ and $l_{opt}$ be the optimal repeater size and inter-repeater segment length and let $s$ and $l$ be the corresponding values under some area constraint. Then $l = \alpha l_{opt}$ and $s = \beta s_{opt}$, where $\alpha$ and $\beta$ are taken to be $\alpha \geq 1$ and $0 < \beta \leq 1$. The area required for a repeater inserted interconnect of length $L$ is the sum of the area of all the repeaters inserted at a regular interval of length $l$. The area occupied by the interconnect itself is not included in the total area because it remains the same in the area constrained and area unconstrained case. Only the number and size of the repeaters will be reduced in the area constrained case as shown in Figure 5.9.
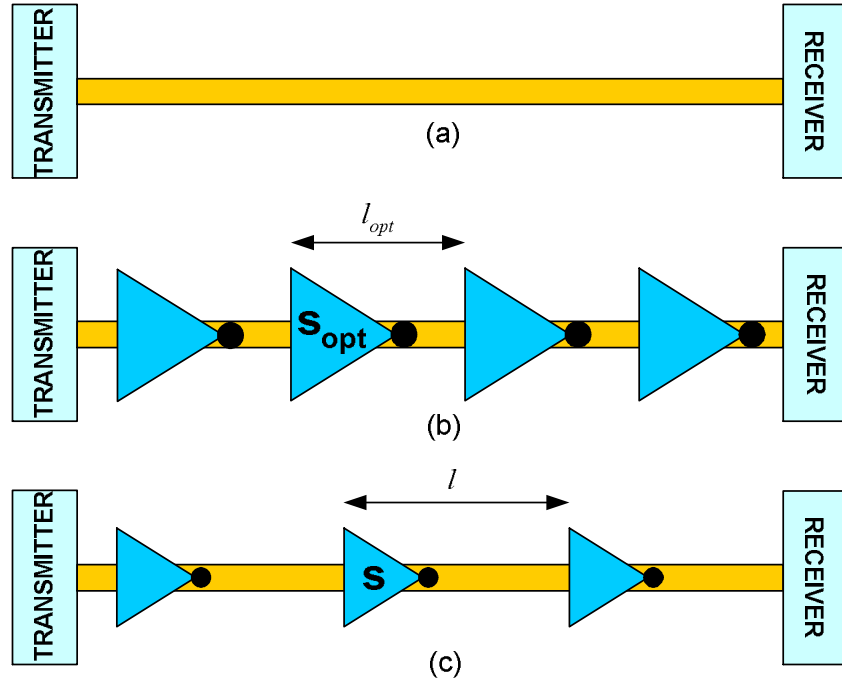


Figure 5.9: An interconnect between the transmitter and receiver (a), optimal buffer insertion (b), buffer insertion under area constraint (c).

If $A$ is the total buffer area for the area constrained case and $A_{opt}$ is the area for the area-unconstrained case, then we define the area ratio $\gamma = A/A_{opt}$, $0 < \gamma \leq 1$ [116].

$$\gamma = \frac{A}{A_{opt}} = \frac{L.l_{eff}.s/l}{L.l_{eff}.s_{opt}/l_{opt}} = \frac{s/s_{opt}}{l/l_{opt}} = \frac{\beta}{\alpha} \tag{5.8}$$

Using the value of $l_{opt}$ and $s_{opt}$ from equation (5.5) and (5.6) and performing some simple mathematical steps, we can find the optimal values of $\alpha$ under the area constraint as follows.

$$\alpha^2_{opt}(\gamma) = \frac{\sqrt{1 + {c_p}/{c_o} + \sqrt{2}\gamma^{-1}}}{\sqrt{1 + {c_p}/{c_o} + \sqrt{2}\,\gamma}} \tag{5.9}$$

The value of $\alpha_{opt}(\gamma)$ can be used in equation (5.8) to get the value of $\beta_{opt}(\gamma)$ such that

$$\beta_{opt}(\gamma) = \gamma\alpha_{opt}(\gamma) \tag{5.10}$$

The speed at which the signal travels through the interconnect of length $L$ in time $T$ is the signal velocity $v$. Under area constraint, the delay per unit length given by equation (5.7) can be used to derive the optimum value of reciprocal velocity, which can be written as

$$v^{-1}_{opt} = performance^{-1}$$

$$= 2\log(2)\,(r_s cr)^{1/4}$$

$$* \sqrt{\left(\frac{\sqrt{c_o + c_p}}{\sqrt{2}} + \frac{\sqrt{c_o}}{\gamma}\right)\left(\gamma\sqrt{r_s crc_o} + \frac{1}{\sqrt{2}}\sqrt{r_s cr(c_o + c_p)}\right)} \tag{5.11}$$

Now for any value of $\gamma$, there will be a combination of $\alpha_{opt}$ and $\beta_{opt}$ (equation (5.9) and (5.10)) that will give the best possible performance through equation (5.11), as shown in Figure 5.10.
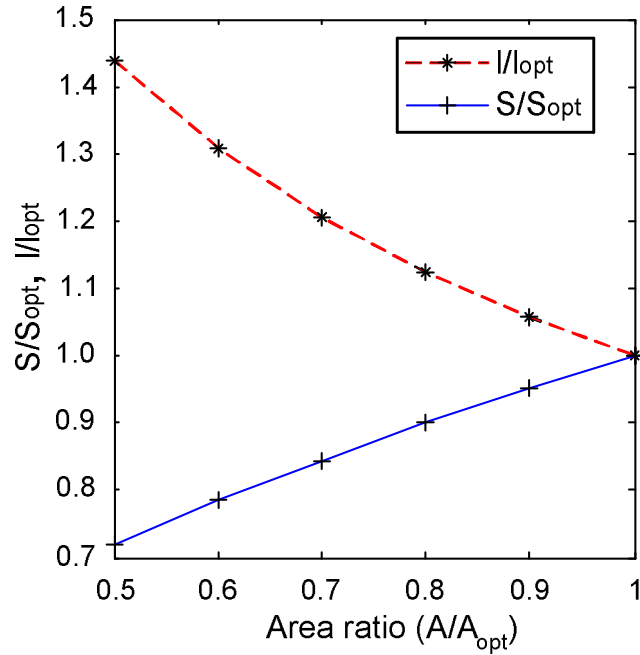


Figure 5.10: Optimal repeater size and inter-repeater segment length (both normalized) for different area ratios.

### 5.4.3 Repeater Insertion under Power Constraint

The power dissipation in repeaters ($P_{rep}$) consists of three components namely, short circuit power ($P_{sc}$), switching power ($P_{sw}$) and leakage power ($P_{leak}$) such that the total power is

$$P_{rep} = P_{sc} + P_{sw} + P_{leak} \tag{5.12}$$

In an interconnect of length $L$ having $K$ uniformly inserted repeaters, the power dissipation per unit length is given by [24]

$$P'_{rep} = \frac{K.P_{rep}}{L} = \left[ \alpha t_r V_{DD} W_{n_{min}} I_{sc} f_{CLK} + \alpha(c_o + c_p) V_{DD}^2 f_{CLK} + \frac{1}{2} V_{DD} (I_{off_n} W_{n_{min}} \right.$$

$$\left. + I_{off_p} W_{p_{min}}) \right] \frac{s}{l} + \alpha V_{DD}^2 f_{CLK} c \tag{5.13}$$

$$P'_{rep} = \frac{K P_{rep}}{L} = k_1 \frac{s}{l} + k_2 c, \tag{5.14}$$

where $k1$ and $k2$ are constants. But $l = \alpha l_{opt}$ and $s = \beta s_{opt}$, therefore,

$$P'_{rep} = \frac{K P_{rep}}{L} = k_1 \frac{\beta s_{opt}}{\alpha l_{opt}} + k_2 c \tag{5.15}$$

This expression shows that in order to reduce power dissipation per unit length (due to repeaters), the ratio $\frac{\beta}{\alpha}$ will have to be minimized. This will simultaneously reduce the area because $\frac{\beta}{\alpha} = \frac{A}{A_{opt}}$.

### 5.4.4 Communication Reliability

Reducing the repeater size seems attractive in terms of the silicon area and power savings. However in deep sub-micron region, reducing the size of the repeaters for area and/ or power savings will increase variability and produce reliability issues in data transmission. This is because the delay variability is inversely proportional to the size of the repeaters and spread in the delay distribution increases with technology scaling [107]. The variability in the devices and interconnect can produce uncertainty in the arrival times of the signals with respect to target values and thus can cause critical data loss. In this section we will determine the probability of such a failure in a single line interconnect.

We again consider Figure 5.8, where at the receiving end of the interconnect, a positive-edge triggered D-flip-flop (DFF) is used to register the data. For the DFF, let $\tau_{setup}$ be the setup time and $\tau_{prop}$ be the propagation delay from D to Q after the positive clock edge

and $\tau_{wire}$ be the propagation delay of the interconnect of length $L$. We assume that the link is operating at a clock frequency $f_{CLK}$ having period $T_{CLK}$.

For a data bit meeting the desired timing constraint to reach the output of the FF, the following delay constraint must be satisfied

$$0 \leq \tau_{wire} \leq T_{CLK} - \tau_{setup} - \tau_{prop} \tag{5.16}$$

The probability of correct data transmission can, therefore, be expressed as follows

$$q = \Pr\left(0 \leq \tau_{wire} \leq T_{CLK} - \tau_{setup} - \tau_{prop}\right) \tag{5.17}$$

where the clock period $T_{CLK}$, wire delay $\tau_{wire}$, propagation delay $\tau_{prop}$, and setup time of the DFF, $\tau_{setup}$ are random variables. Therefore, the total delay through the interconnect (from source to receiver output) will also be a random variable. This distribution can be determined analytically (by considering all possible sources of variability) or through simulation (as in this work). This relies on accurate characterization of the underlying distributions. Let $\mu_{ch}$ and $\sigma_{ch}$ be the mean and standard deviation of resultant *pdf* of $pdf(wire) + pdf(setup) + pdf(prop) - pdf(CLK)$, then the probability of correct data transmission is given by the error function [122]

$$q = \frac{1}{2} + \mathrm{erf}\left(\frac{\mu_{ch}}{\sigma_{ch}}\right) \tag{5.18}$$

where $\mathrm{erf}(x) = \frac{1}{\sqrt{2\pi}} \int_0^x \exp\left(-\frac{t^2}{2}\right) dt$

and the probability of failure for the data bit transmitted through the on-chip communication channel is then given by

$$PoF = 1 - q \tag{5.19}$$

## 5.5   Optimization Methodology

The design objective can either be the optimization of area, power or performance, under the permissible limits of delay variability. These metrics are coupled with each other so a trade-off will need to be established. For a particular communication link design, a unique cost function is established. For this function an optimum configuration is found, which will give the best results in terms of the given parameters. This optimum is determined though a standard optimization technique using the trade-off curves connecting these parameters.

## 5.5.1 Case Study

We used Monte Carlo simulation method to perform experiments for this optimization study under the impact of device variability due to RDF. The interconnect structure is such that the middle wire under consideration is surrounded by two similar wires. The width of each wire and interspacing between them was kept at 0.048 $\mu$m for 13 nm and 0.0675 $\mu$m for 18 nm technology generation. The interconnect parameters were taken from ITRS 2007 [50] and interconnect capacitances have been derived using the analytical models given in [45]. The wires are modelled as distributed RC interconnect with 100 ladder-segments. The variability in the interconnect wires is not considered in this study. The buffer size and inter-repeater segment length for optimal repeater insertion is $s_{opt}$=140 and $l_{opt}$= 80.67 $\mu$m for 13 nm and $s_{opt}$=137 and $l_{opt}$= 152.1 $\mu$m for 18 nm technology generation. A supply voltage of 0.9V for 13 nm and 1.0V for 18 nm circuits was used. A large number of HSPICE simulations (6000) were performed and delay-power measurements were taken during each run. The delay measurements were made corresponding to 50% of the maximum swing level. The total power measurement results are based on leakage, switching and short circuit power components at a frequency of 2GHz.

Based on the simulation data, the delay variability ($\sigma_{delay}/\mu_{delay}$) is determined and plotted in Figure 5.11(a) for the given technologies. It can be seen that the delay variability increases rapidly with the decrease of repeater size and also increases with technology scaling. In the presence of other sources of variability, the delay variability increases to



(a)                                                      (b)
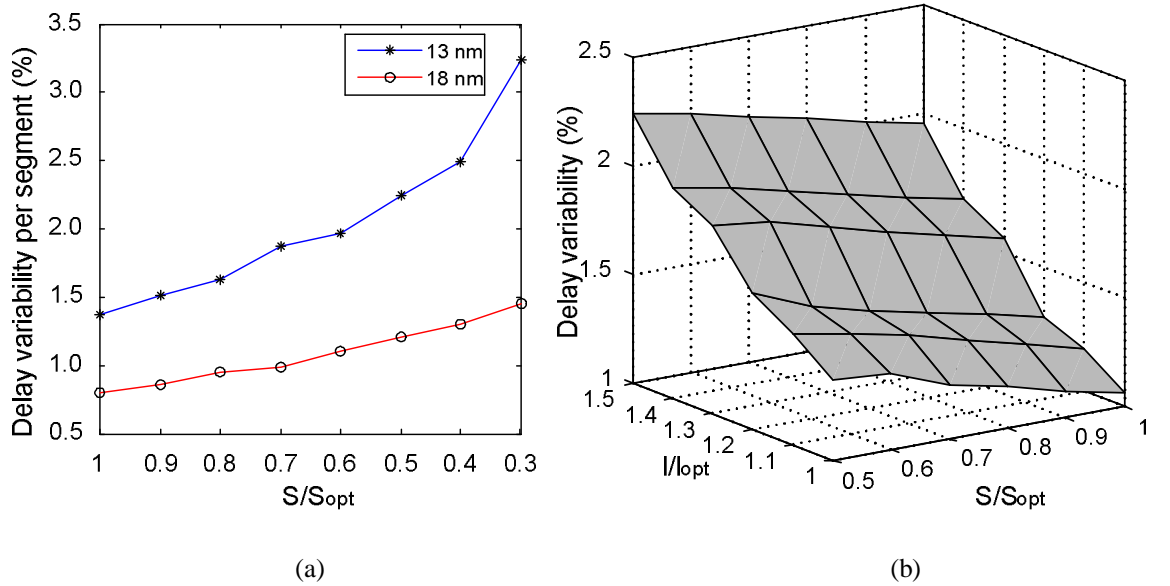
Figure 5.11: Delay variability as a function of different ratios of repeater size, in the absence of crosstalk (a), Dependence of delay variability on repeater size and inter-repeater segment length (b).

greater extent. The dependence of delay variability on $s$ and $l$ is also shown in Figure 5.11(b) for 13 nm technology. It may be noted that delay variability not only increases with the decrease of repeater size but also with the increase of interconnect segment length. For using this trade-off in the optimization process, the surface plot can be converted into an empirical expression using multiple regression techniques. This helps to understand how the typical value of the dependent variable (for instance, delay variability) changes when any one of the independent variables (l and S) is varied over a particular range.

As we have already seen, in order to reduce area, we need to increase $l/l_{opt}$ and decrease $S/S_{opt}$ ratios according to Figure 5.10 for getting the optimum performance for a particular configuration. The performance degradation due to different values of $S$ and $l$ with respect to $S_{opt}$ and $l_{opt}$ can be predicted using equation (5.11). In Figure 5.12, these predictions are compared with the simulation results which matches very well at most of the area ratios. The model, however, deviates slightly from the simulation results at smaller area ratios. This is because at smaller repeater sizes, the delay distributions deviate from normality due to RDF [93], [94] and show some asymmetry. Figure 5.12 also shows the effect of area scaling on delay uncertainty. It can be seen that the standard deviation of the delay increases almost 3 times with $A/A_{pt}$=0.2.
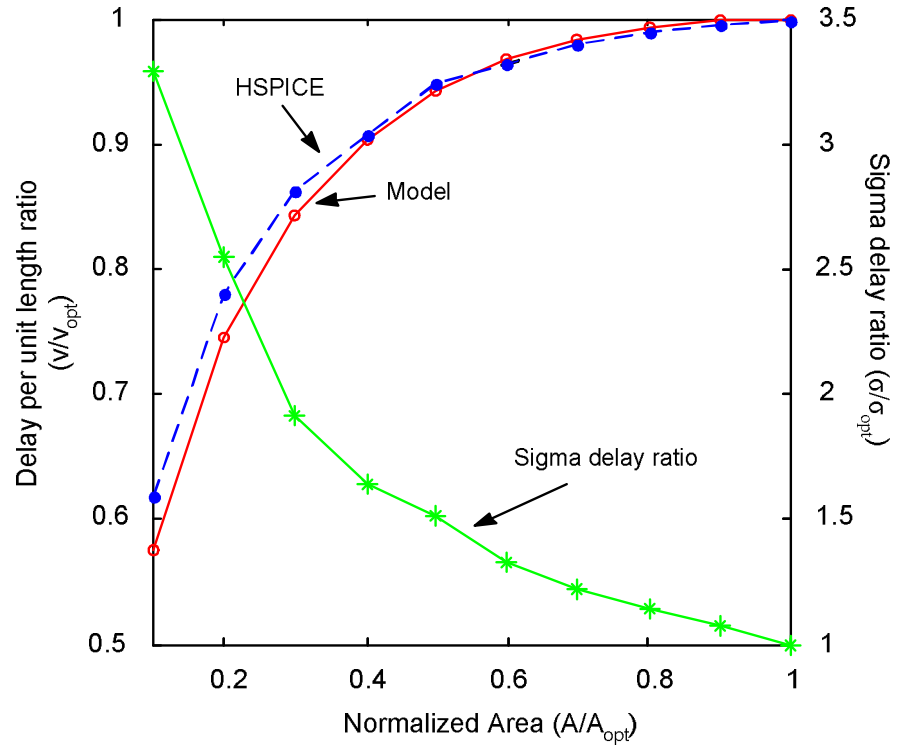


Figure 5.12: Comparison between analytical model and simulation results for performance degradation due to area scaling.

In Figure 5.13 different trade-off curves have been plotted together to explore different design choices. The area, power and performance curves show that in order to get ultimate performance, we will have to consume significant amount of power and area. However, with only 4% of performance degradation, we can reduce 30% power dissipation and 40% area. Whereas, in the presence of variability, an adverse effect of this trade-off is that delay certainty (defined as the reciprocal of delay variability) will reduce by 24% from the optimum level. This will increase the probability of failure of the link at a particular frequency, which can be estimated using equation (5.18)-(5.19). Therefore, the speed of the link will be limited in order to keep the probability of link failure below some acceptable limits. This problem will aggravate in high speed wider links where the skew amongst various wires in the link will play a detrimental role in determining its performance. This effect will be considered in Chapter 6. It becomes evident then that during the optimization process, the delay variability should also be considered in the figure of merit; otherwise the yield will be badly affected.
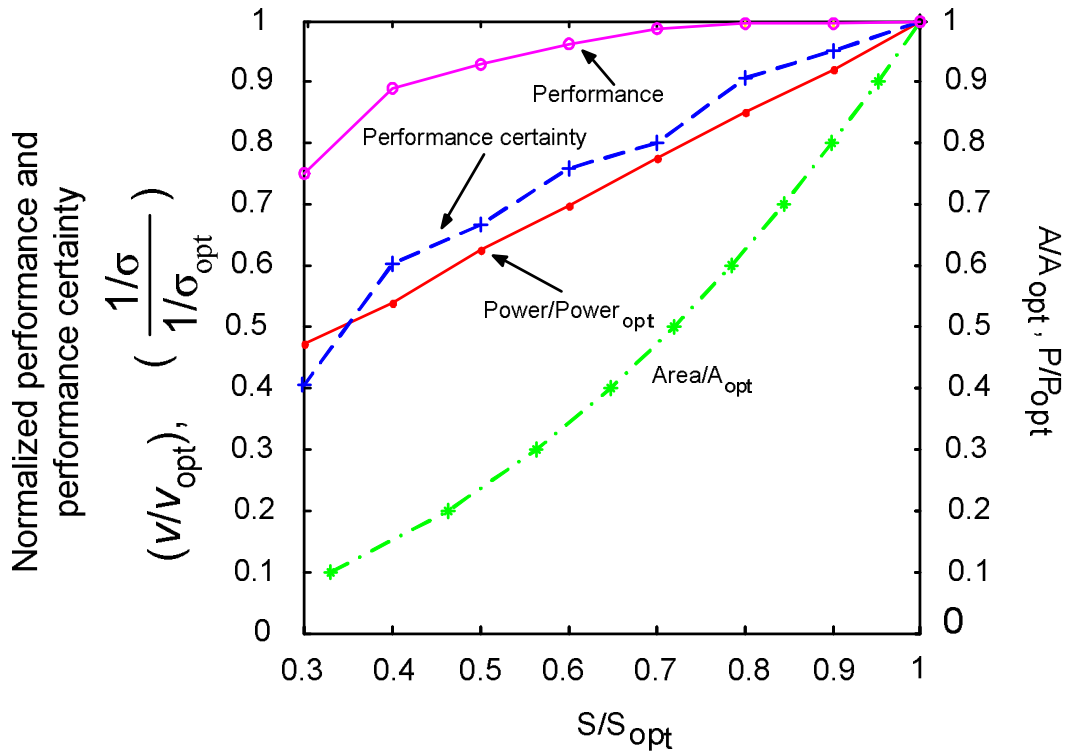


Figure 5.13: Performance, area, power and performance certainty trade-off curves.

## 5.6   Summary

In the first part of this chapter we have measured power dissipation in repeaters of given three technology generations under RDF. The results show that the relative proportion of different components of power dissipation is changing and leakage power is emerging as a

serious problem in the designing of high performance and power optimal chips. Therefore, design methodologies should consider individual components of power dissipation along with the total power. Wider links in NoCs, which are preferred for better latency, will consume more power due to higher leakage currents at low activity levels.

The variability in the devices which is affecting the delay characteristics is also effecting the distribution of power dissipation. A significant asymmetry has been observed in the distribution of leakage power and hence effectively, leakage is increasing more rapidly than anticipated. This in turn, is badly affecting the yield. It will be more advantageous to consider power variability along with delay variability while making different circuit optimizations. Active countermeasures, such as the use of sleep transistors, could be a possible solution against leakage power.

In the second part of this chapter, we have analysed the impact of device variability on the performance of on-chip single bit data links. We emphasize that due to increasing trend of the variability, power and area optimal repeater insertion methodologies should also consider performance variability. Analytic models for area, power, performance and probability of link failure have been presented in terms of the size of the repeaters and inter-repeater segment length. It has been found that beyond a certain reduction in the size of the repeaters, the delay variability may exceed acceptable limits while still satisfying other constraints. Therefore, while optimizing area, power and performance of on-chip communication links, delay (and power) variability should also be included in the figure of merit.

# Chapter 6

# Design of Variability Tolerant Data Channels

## 6.1 Inter-Resource Communication

Different functional units in SoCs communicate with each other through the communication infrastructure, consisting of several links. The inter-resource communication link usually consists of a large number of parallel interconnects, as shown in Figure 6.1(a), which are coupled with each other (RC/RLC) along the length of the channel. In a Network-on-Chip (NoC) platform, the functional units are connected to the routers through such communication links. Similarly, the routers are also connected with each other, in a certain topology, through another group of communication channels, as shown in Figure 6.1(b). The communication channels can be wider or narrower in terms of the number of lines they contain and this determines the *phit size*.

In order to reduce the resistance-capacitance (RC) delay of interconnects, low resistivity and low dielectric constant materials are used [124], [125]. A common technique to reduce the delay of the global interconnects is the use of repeaters and increasing the width of the wires [126]. However, increasing the width of the wires may reduce the channel capacity, as fewer wires can then be accommodated in the same channel width($W_C$). Similarly,

interconnect spacing also effects the delay and bandwidth (since the coupling capacitance changes with spacing). The literature is abundant with several works on the optimization of the performance of global interconnects considering different metrics [24], [25], [127]-[129]. However, most of the literature ignores variability and sources of noise (for instance, crosstalk), during their proposed optimization techniques.



(a)



(b)
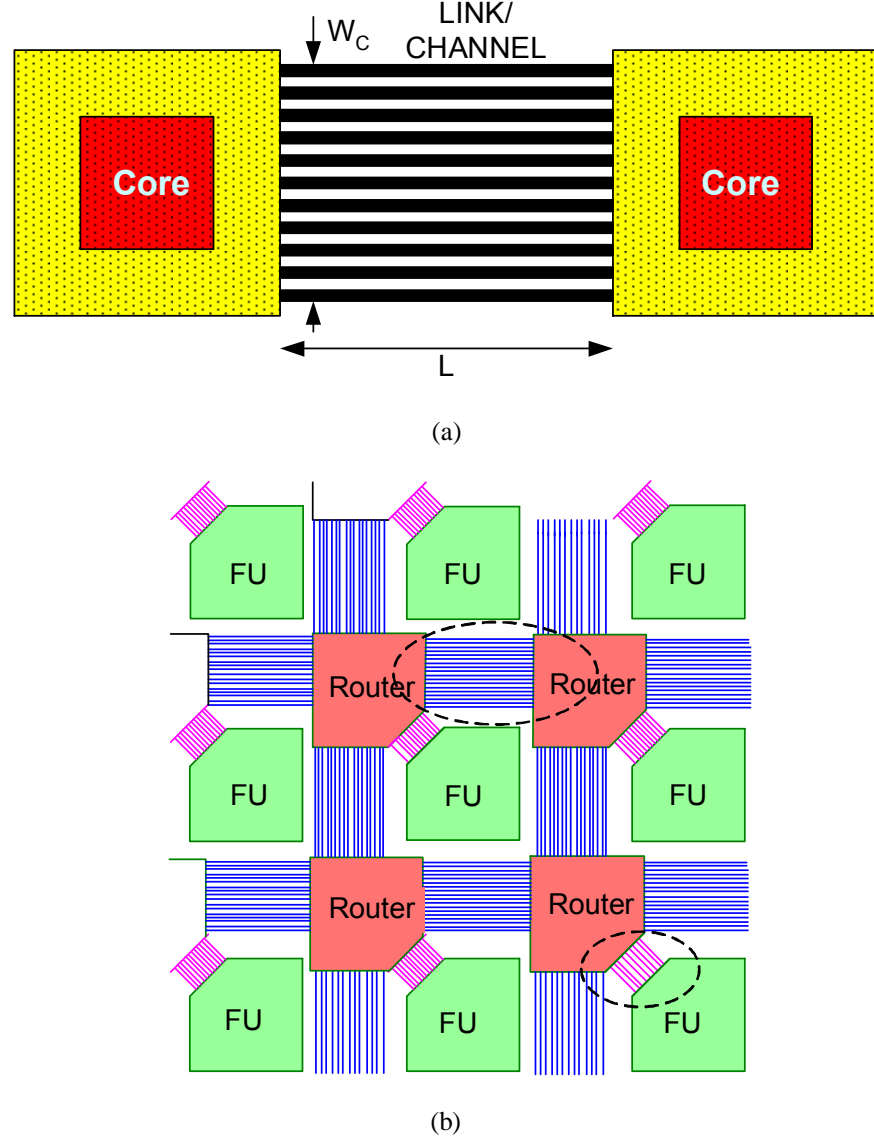
Figure 6.1: Simple Core-Core link consisting of multiple interconnects (a), Functional unit-Router and Router-Router links in a Network-on-Chip (b).

As the process dimensions are shrinking to the nanometer region, the impact of variability has become extremely critical to the performance of the communication channels. The variability is affecting both the device (front-end of the line) and interconnect (back-end of the line) [130] resulting in the performance degradation of the whole channel. Moreover, under device scaling, leakage power is becoming an important source of power dissipation

107

alongside the switching power and therefore channel designers should also consider these aspects during optimization for a certain parameter. Although some recent work has been done on the modelling and analysis of the global interconnects with the consideration of variability [131]-[133], but no comprehensive work on the optimization of the data channels under different trade-offs for future technologies, where these effects are quite prominent, has been published.

## 6.2 Channel Configuration and Modelling



(a)



(b)
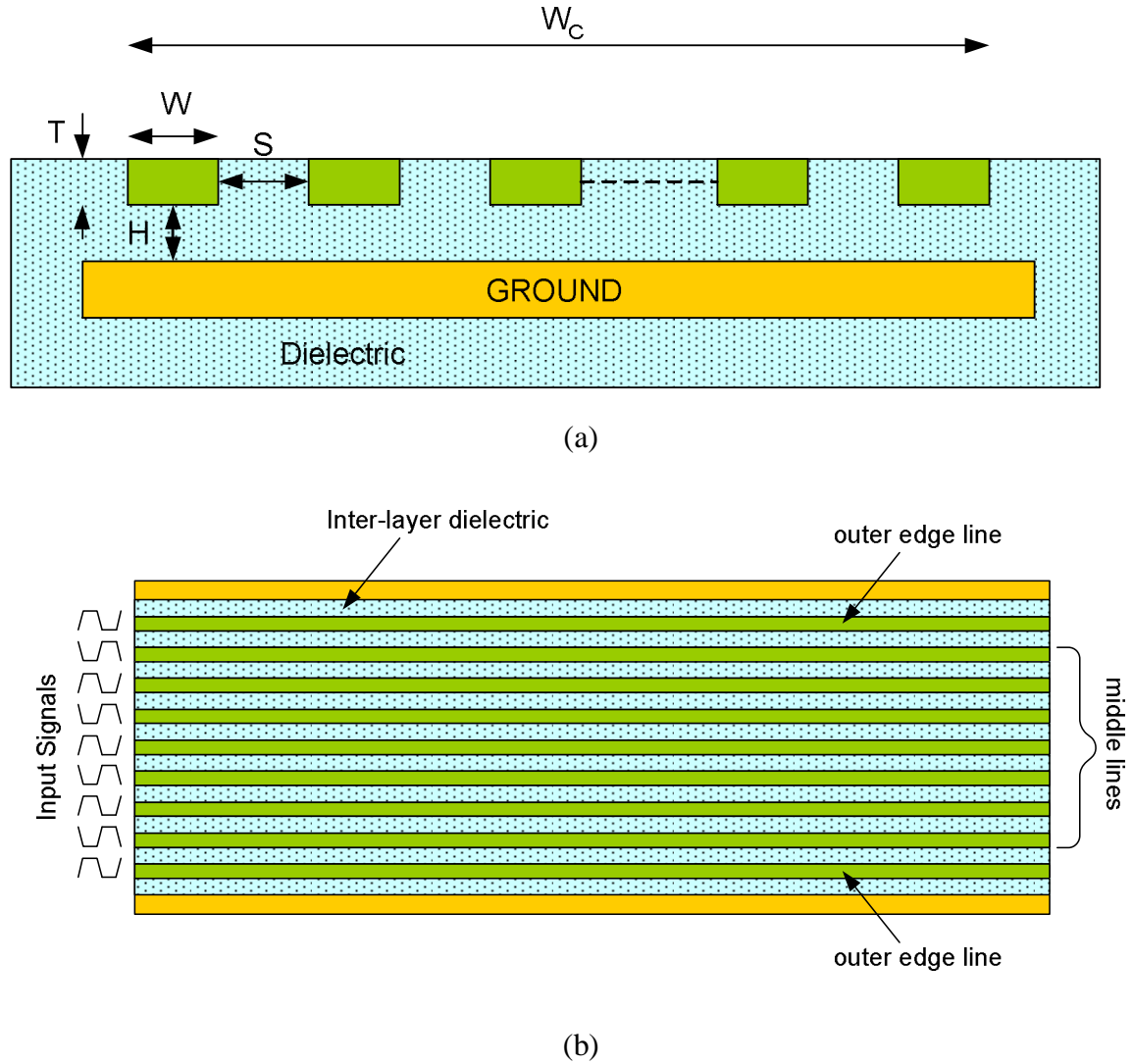
Figure 6.2: Structure of a multi-bit bus, where the number of interconnects in a fixed channel width $W_C$ depends on the interconnect width and spacing. (a) the cross-sectional view showing different dimensions and (b) the top view of the bus indicating outer and middle lines. The input signals on any two adjacent lines are opposite in phase, thus simulating the worst case of crosstalk. Each line in the bus can be considered as an aggressor or victim, as they can affect the performance of each other.

The performance of a data channel strongly depends on its geometry. There are several possible configurations of a channel corresponding to different values of interconnect

width (W), spacing (S), thickness (T) and dielectric thickness (H), as shown in Figure 6.2. The variation of these parameters affects the capacitance, resistance and inductance of interconnects, which in turn changes the delay and other metrics. Inductance is less of an issue for interconnects under consideration due to the reasons mentioned in section 2.4.3. Amongst these geometrical parameters, T and H are technology dependent and so the designers have only the choice of varying W and S to design a channel for the required performance. While designing such channels, these parameters are set at the designed values. However, these parameters are also affected due to process variations, thus affecting the geometrical dimensions of interconnects. These changes are process dependent and controllable only to some extent.

## 6.2.1 Interconnect Resistance

In a given technology generation, only interconnect width (W) affects the resistance (T and H are assumed to be fixed). The interconnect resistance for a given geometry can be calculated using equation (2.1).

## 6.2.2 Interconnect Capacitance

The capacitance of an interconnect in the channel comprises of the fringe capacitance, the coupling or mutual capacitance and parallel plate capacitance. The fringe capacitance and parallel plate capacitance add up to form the self or ground capacitance. In order to investigate the characteristics of the interconnect capacitance, we will use the electrical model of [134] as it closely matches the actual situation for interconnects in a bus.

The capacitance of a global interconnect for 18 nm technology with minimum width has been plotted as a function of the spacing between the neighbouring interconnects in Figure 6.3. The technology parameters have been taken from the ITRS 2007 [50]. The curves show that the coupling capacitance quickly drops with the increase of the spacing. Similarly, the ground capacitance increases with the increase of the spacing. The reason for the increase of ground capacitance with spacing is not very obvious. Actually the parallel plate capacitance is not affected with the increase or decrease of the spacing; however the fringe capacitance of interconnects (except at outer edges of the bus) increases with the increase of the interconnect spacing. This results in the increase of the ground capacitance with spacing. The effect of spacing on the coupling capacitance is more dominant than the ground capacitance and therefore the total capacitance decreases with the increase of the spacing. Consequently, the signal delay through widely spaced interconnects is less than the closer interconnects.
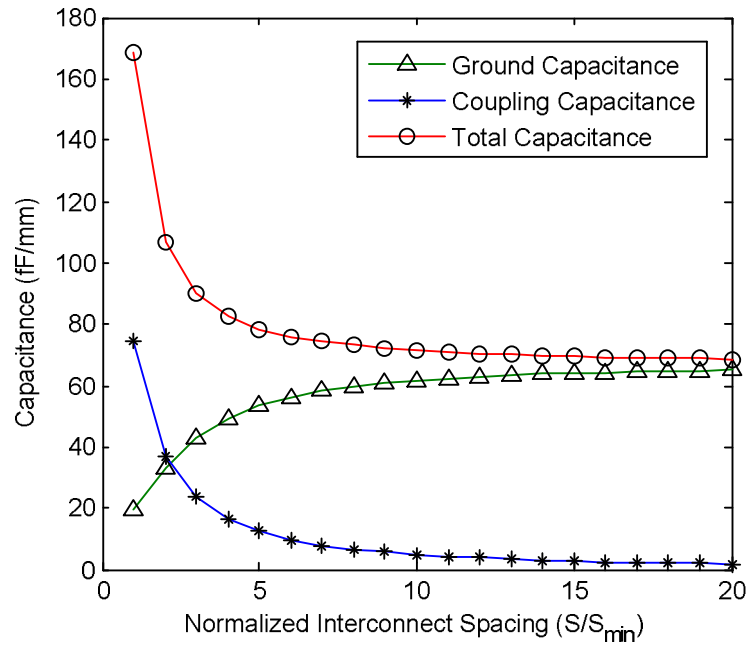
Figure 6.3: Capacitance curves for minimum width global interconnects of 18nm plotted as a function of interconnect spacing.

The impact of line width variation on the capacitance is shown in Figure 6.4. The total capacitance increases linearly with the increase of the interconnect width. The main contributor of this increased capacitance is the parallel plate capacitance, whereas the coupling capacitance remains almost constant due to the obvious reason of constant spacing.
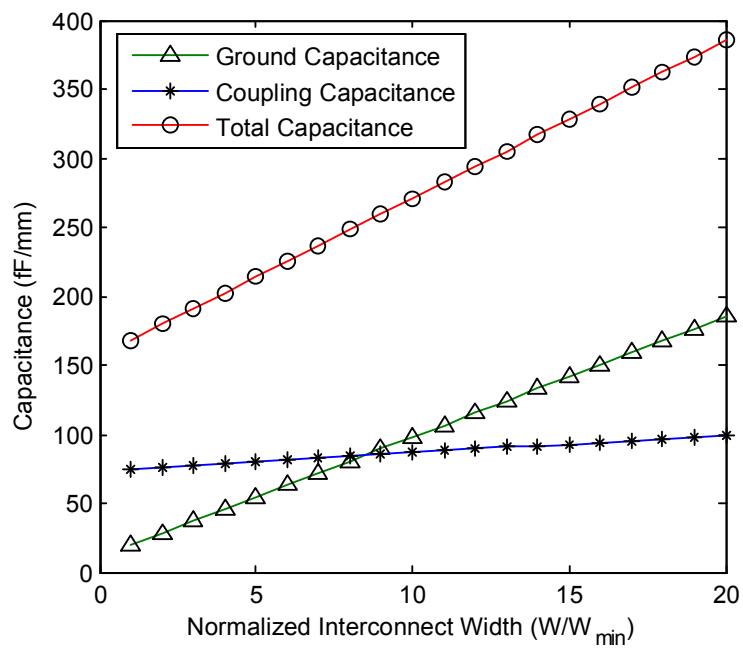


Figure 6.4: Capacitance curves for 18nm global interconnects plotted as a function of width at minimum interconnect spacing.
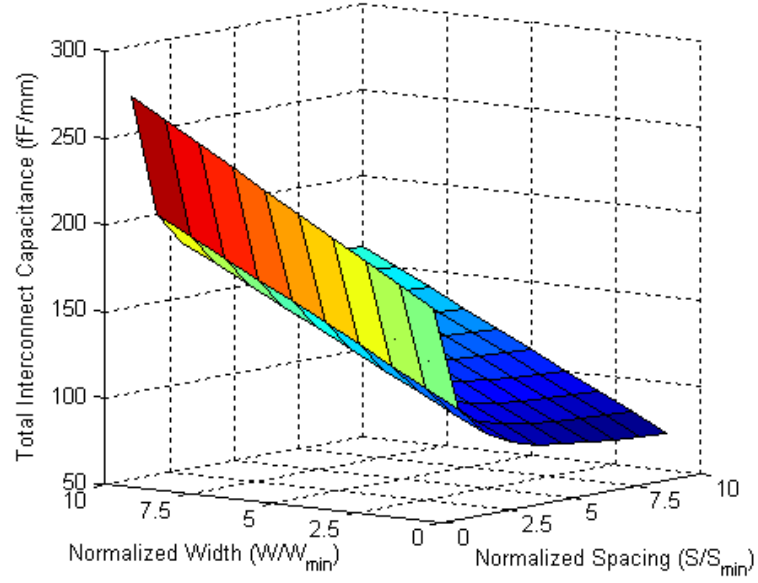
Figure 6.5: The total capacitance of an interconnect (not at the outer edge) of a bus in 18 nm technology plotted as a function of the interconnect spacing and width.

A 3D surface plot of the total capacitance of a bus interconnect as a function of the width and spacing is shown in Figure 6.5. The surface plot shows that the interconnect capacitance is largest for wider interconnects running parallel to each other at shorter inter-spacing. Both resistance and capacitance affect the delay.

### 6.2.3 Interconnect Delay

We assume that all lines in the channel bus are uniformly coupled with two neighbouring aggressor lines. The lines at the extreme-edges are, however, coupled with only one line. We also assume that the length of the bus is $L$ and all lines in the bus have the same designed geometrical dimensions. Let $R$, $C_s$, and $C_c$ be the total interconnect resistance, self capacitance and coupling capacitance of each line, respectively. Now for a step input, the delay corresponding to 50% transition level for the middle and outer edge conductors in the bus has been approximated by a simple linear model in [135] as

$$T_{mid} = 0.4RC_s + \lambda_i RC_c \tag{6.1}$$

$$T_{outer} = 0.4RC_s + \lambda_i R\left(\frac{C_c}{2}\right) \tag{6.2}$$

In equation (6.1) and (6.2), the coefficient $\lambda_i$ is selected according to the type of the switching activity in the neighbouring aggressor lines. [135] gives six possible cases corresponding to which the values of $\lambda$ is given in Table 6.1.

Case 1: Both the neighbouring aggressors switch from state 1 to state 0.

Case 2: One aggressor is quiet and the other switches from state 1 to sate 0.

Case 3: Both the aggressors are quiet.

Case 4: One aggressor switches from 0 to 1 and the other switches from 1 to zero.

Case 5: One of the aggressors switches from 0 to 1 and the other remains quiet.

Case 6: Both the aggressors switch from 0 to 1.

Table 6.1: Coefficients of the delay model for different switching patterns [135].

| Case i | Switching pattern | $\lambda_i$ | $\mu_i$ |
|--------|-------------------|-------------|---------|
| 1 | (a) | 1.51 | 2.20 |
| 2 | (b) | 1.13 | 1.50 |
| 3 | (c) | 0.57 | 0.65 |
| 4 | (d) | 0.57 | 0.65 |
| 5 | (e) | N/A | N/A |
| 6 | (f) | 0 | 0 |

If the victim line switches from zero to one then Case 1&2 will slow down the victim line and Case 5&6 will speed up it. For the time being, we consider Case 3 only to find the reference delay. In this case, equation (6.1) and (6.2) will reduce to

$$T_{mid} = 0.4RC_s + 0.57RC_c \tag{6.3}$$

$$T_{outer} = 0.4RC_s + 0.285RC_c \tag{6.4}$$
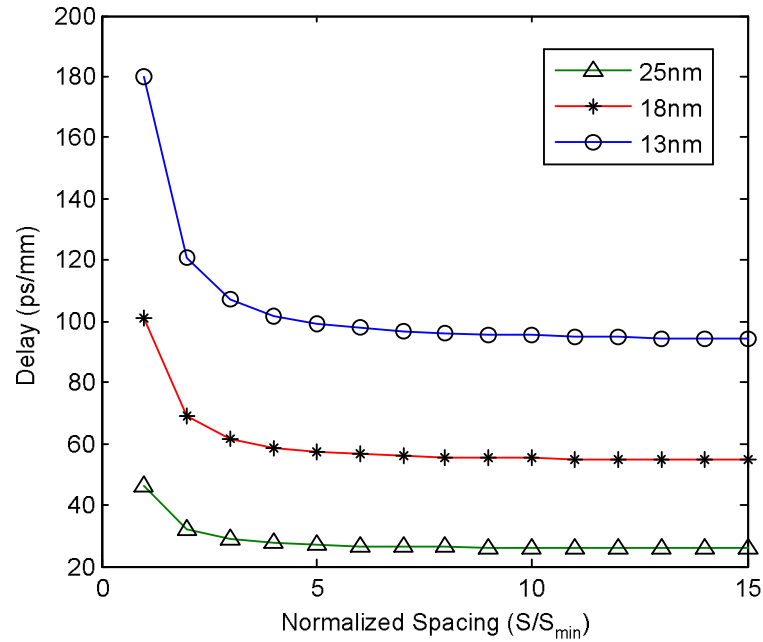


Figure 6.6: Propagation delay of the middle interconnect of minimum width of a bus for the given three technologies plotted as a function of the spacing between the conductors.

112

Using these equations, the delay of the bus interconnects has been estimated for the three technology generations. Also the dependence of the delay on interconnect spacing and width has been studied and results are shown in Figures 6.6 & 6.7. The curves show that the interconnect delay can be reduced by increasing the interconnect width and/or by increasing the spacing between the neighbouring conductors. It is, however, important to note that increasing the spacing beyond certain value is not very beneficial in terms of the delay because coupling capacitance effects are minimal after some interconnect spacing. Increasing spacing beyond this point will simply waste chip area.
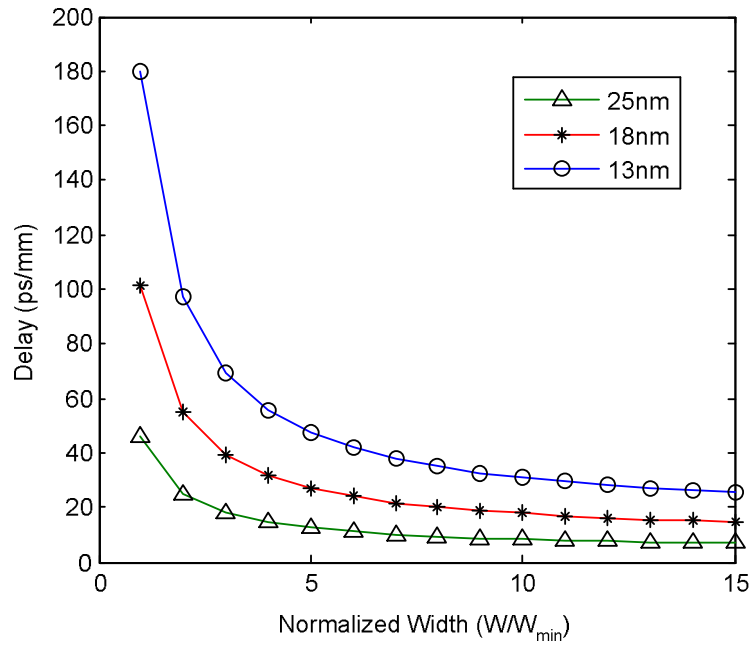


Figure 6.7: Propagation delay of the middle interconnect of a bus with neighbouring interconnects at minimum spacing for the given three technologies plotted as a function of the width of the conductors.

On the other hand, increasing width may improve delay performance over some large range of width as compared to the spacing. The decrease in the delay is due to the decrease of the interconnect resistance but at the same time the ground capacitance also increases with the increase of the width. The increase of the width has a negative effect as the switching power increases with the increase of the capacitance. Therefore, there will be some optimum value of the spacing and width that will give the best delay performance under some area and/or power constraints.

## 6.3 Repeater Insertion

The delay of the long interconnect can be reduced by inserting repeaters at appropriate locations along its length, thus dividing it into small sections. For such a system, the delay of each section can be approximated by [135]

$$t_{sec} = 0.7R_{drv}(C_s + C_{drv} + \mu_i \times 2C_c) + R(0.4C_s + \lambda_i \times C_c + 0.7C_{drv}) \tag{6.5}$$

where the coefficients $\mu_i$ and $\lambda_i$ are given in Table 6.1. $R_{drv}$ and $C_{drv}$ are driver output resistance and capacitance respectively.

The total delay of an interconnect of length $L$ is given by

$$t_L = k\left\{0.7\frac{R_{drv_m}}{h}\left(\frac{C_s}{k} + hC_{drv_m} + \mu_i\frac{2C_c}{k}\right) + \frac{R}{k}\left(0.4\frac{C_s}{k} + \lambda_i\frac{C_c}{k} + 0.7hC_{drv_m}\right)\right\} + \frac{t_r}{2} \tag{6.6}$$

where $R_{drv_m}$ and $C_{drv_m}$ are the output resistance and capacitance of a minimum sized repeater, $h$ is the size of the repeaters and $k$ is the number of repeaters inserted in the interconnect. $t_r$ refers to the rise time of the signal. The optimal values of $h$ and $k$ are obtained by taking the partial derivative of equation (6.6) with respect to $k$ and $h$ and equating it to zero

$$\frac{\partial t_L}{\partial k} = 0 \quad \Rightarrow \quad k_{opt} = \sqrt{\frac{0.4RC_s + \lambda_i RC_c}{0.7R_{drv_m}C_{drv_m}}} \tag{6.7}$$

$$\frac{\partial t_L}{\partial h} = 0 \quad \Rightarrow \quad h_{opt} = \sqrt{\frac{0.7R_{drv_m}C_s + 1.4\mu_i R_{drv_m}C_c}{0.7RC_{drv_m}}} \tag{6.8}$$
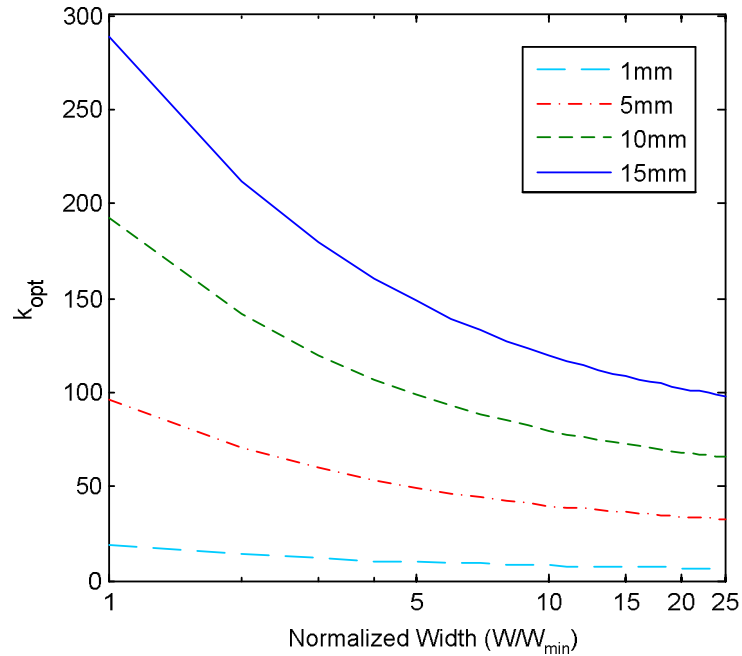


Figure 6.8: Optimum number of repeaters for minimum interconnect delay for different lengths of the global interconnect plotted as a function of the interconnect width. The interconnect is of 13 nm technology and the spacing between interconnects is $S_{min}$.

The optimal value of the delay can be obtained by using the value of $h_{opt}$ and $k_{opt}$ in equation (6.6). For different interconnect lengths, the optimum number of required repeaters are plotted in Figure 6.8 as a function of the line width. It is shown that the number of repeaters which minimizes the propagation delay of the signals decreases with the increase of the line width for all lengths of the interconnect. The results also show that the maximum line length for an interconnect of width=25$W_{min}$, which requires no repeater or only one driver is 0.152 mm. Therefore for typical interconnect lengths, large number of repeaters are required for optimum signalling (particularly as chip sizes are increasing).

As we increase the interconnect width for faster signalling, the line capacitance per unit length increases. Although fewer repeaters are required to drive wider lines, each repeater will have to drive a larger section of the interconnect. Therefore, in order to drive large interconnect sections of greater width, the repeaters will have to drive large capacitances. So the repeaters will be of large size to reduce the overall delay. Figure 6.9 clearly shows that the repeater size for optimum delay is an increasing function of the interconnect width.
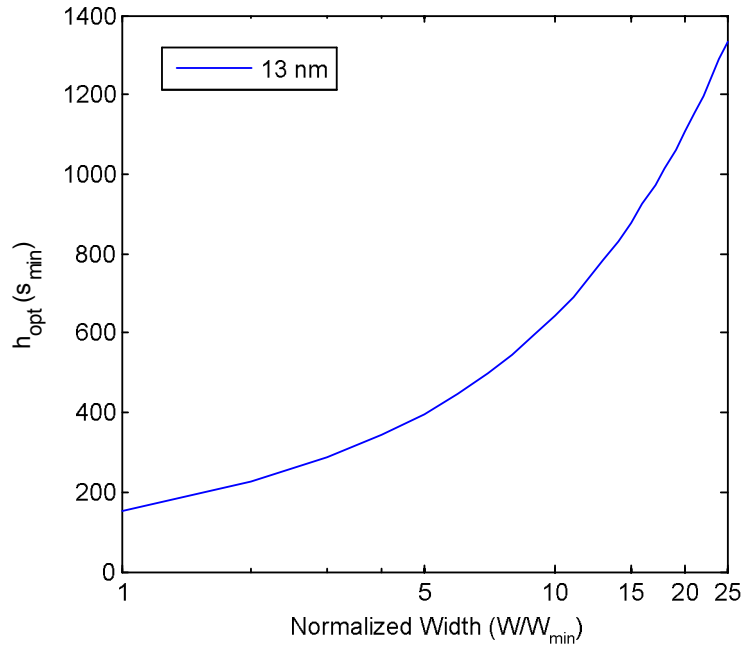


Figure 6.9: Optimum repeater size for minimum interconnect delay for different interconnect widths (global interconnect) for 13 nm technology. The spacing between interconnects is $S_{min}$.

## 6.4 Bandwidth Estimation

If $T$ is the minimum pulse width that can be transmitted through the channel interconnects and correctly registered at the receiving register, then the bandwidth of a single interconnect is given by

$$BW_{wire} = \frac{1}{T} \qquad (6.9)$$

If $t_r$ is the rise time of the signal from 10% to 90%, then the duration of a good signal is at least $3t_r$ [136]. The rise time of the signal can be approximated from the RC time constant $\tau$ as $t_r = 2.2\tau$ [6]. Since 0-50% time $t_{0.5} = 0.69\tau$, therefore $t_r = 3.188t_{0.5}$. and $T \approx 9t_{0.5}$. The pulse width of the signals in the bus interconnects will then be

$$T_{p,mid} = 9T_{mid} \qquad (6.10)$$

$$T_{p,outer} = 9T_{outer} \qquad (6.11)$$

For $N$ conductors in the channel bus, the total bandwidth is given by

$$BW_{total} = \frac{N-2}{T_{p,mid}} + \frac{2}{T_{p,outer}} \qquad (6.12)$$

Equation (6.4) shows that the outer edge wires will offer less delay as compared to the middle wires and thus can give larger bandwidth. However, when a complete data word is transmitted over all the lines, the early arrival of the data bits travelling on the outer edge lines may not be very beneficial until the complete word is registered at the receiver (or complex receivers will be required). Therefore, we will estimate the worst case bandwidth due the middle wires.

$$BW_{total} = \frac{N}{\max \left[T_{p,mid}, T_{p,outer}\right]} = \frac{N}{T_{p,mid}}$$
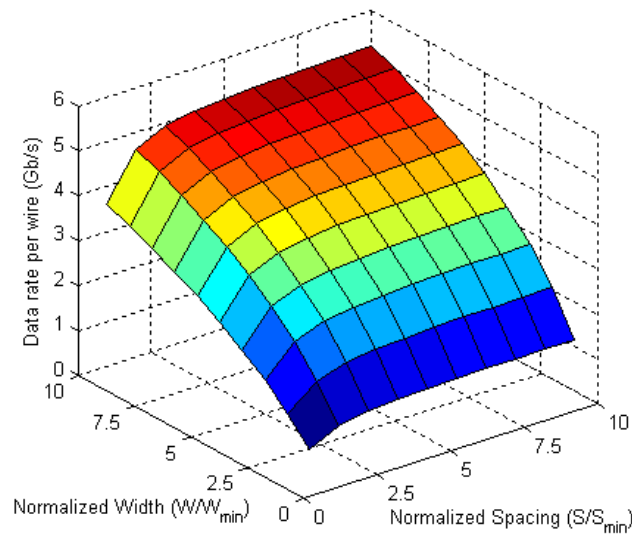


Figure 6.10: Data rate per wire of a channel bus in 13nm technology plotted as a function of spacing and width.

Figure 6.10 shows the possible data rate per wire for a 13nm technology bus plotted as a function of the interconnect spacing and width without using repeaters. The plot shows that the bandwidth per wire can be increased by increasing wire width and/or spacing.

### 6.4.1 Bandwidth as a Function of Length

It is obvious that the interconnect delay increases with length (with and without the use of repeaters). This will directly impact the bandwidth. Repeater inserted interconnects provide more bandwidth as compared to interconnects without repeaters, as shown in Figure 6.11.

The maximum allowed interconnect length corresponding to some desired bandwidth, with and without the use of repeaters, is plotted in Figure 6.11. The use of repeaters is more beneficial for the bandwidth at larger interconnect lengths. The curves also show that the interconnect become slower with technology scaling and provides reduced bandwidth for the same length.
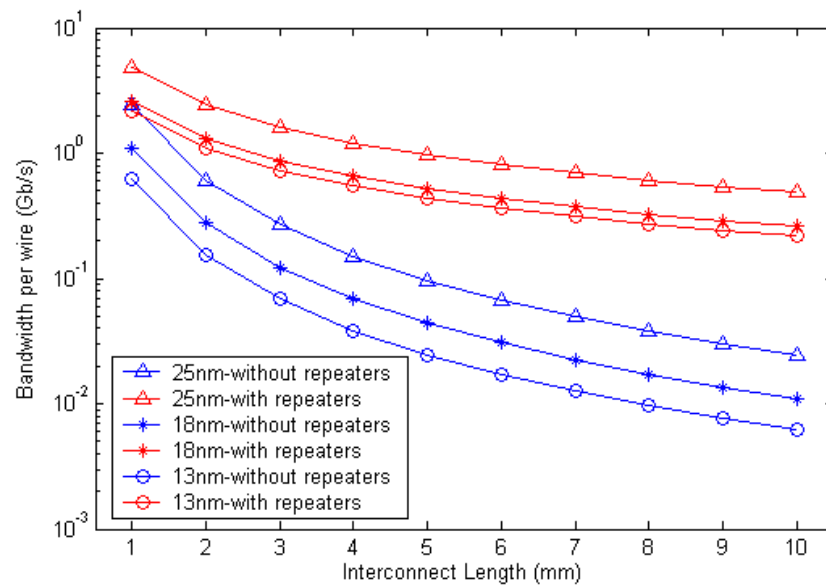


Figure 6.11: Maximum allowed interconnect length for a particular bandwidth with and without the use of repeaters for the given three technologies. These curves have been plotted for minimum interconnect width and spacing.

## 6.5 Channel Performance under Variability

In practical circuits, the performance of the communication links is always affected by the device and interconnect variability. Similarly due to the capacitive coupling, the switching activity in the neighbouring interconnects affects the delay characteristics of an interconnect (crosstalk effects). Therefore, in order to make a realistic estimate of the channel performance, both these effects should be considered in the analysis.

In order to study the worst case due to the crosstalk effect on the victim line, we consider Case 1 in section 6.2.3 where both the neighbouring aggressor lines switch simultaneously in opposite direction with respect to the victim line. This will slow down the victim line and thus will reduce its bandwidth. The delay equation (6.6) will then be modified accordingly using the appropriate coefficients from Table 6.1 corresponding to Case 1.

### 6.5.1 Sensitivity Analysis of the Delay under Variability

The uncertainties in the communication structures (drivers, interconnects, repeaters FFs) introduce uncertainty in the delay characteristics of the interconnect-buffer system. We will study the impact of process variations in the interconnect and statistical device variations on the delay performance of the link. The variation in the width, spacing, thickness and ILD thickness are taken into consideration. It is assumed that every part of bus wires is uniformly fluctuated. The primary interconnect parameters have been extracted from the ITRS2007 [50] and are given in Table 6.2 along with some device parameters. Since the actual levels of interconnect variability are not available from the manufacturing industry for the future technology generations, we assume three cases of the interconnect variability in which the $3\sigma$ percentage variation for the given dimensions of the interconnect are kept at 5%, 10% and 15% of their mean value corresponding to case 1, 2 and 3 respectively. We also assume that the variation in these parameters follow Gaussian distribution.

Table 6.2: Primary interconnect and device parameters based on the ITRS and the device model cards [76], [77]. The device parameters are for the uniformly doped devices.

| Technology Generation/ Parameters | 25nm | 18nm | 13nm |
|---|---|---|---|
| $w_{min}$ $(nm)$ | 105 | 67.5 | 48 |
| $P_{min}$ $(nm)$ | 210 | 135 | 96 |
| $A/R$ | 2.3 | 2.4 | 2.5 |
| $T$ $(nm)$ | 241.5 | 162 | 120 |
| $H(nm)$ | 241.5 | 162 | 120 |
| $\varepsilon_r$ | 2.5 | 2.3 | 2.1 |
| $\rho(10^{-8}\mu\Omega.cm)$ | 2.2 | 2.2 | 2.2 |
| $r_s$ $(\Omega)$ | 18487 | 21166 | 23936 |
| $c_0(fF)$ | 0.1436 | 0.086592 | 0.046315 |
| $c_p(fF)$ | 0.0425 | 0.083741 | 0.029071 |
| $Chip\ size\ at\ production\ (mm^2)$ | 310 | 310 | 310 |
| $V_{dd}(V)$ | 1.1 | 1.0 | 0.9 |

The interconnect capacitance and resistance are not statistically independent. Figure 7.12 shows the relation between interconnect resistance and capacitance for 5% thickness variation in the global interconnect of minimum width. Similarly, Figure 7.13 shows the similar graph for a variation of 5% in the width and thickness. Both these plots show that

with the increase of width and thickness, interconnect resistance decreases but capacitance increases.
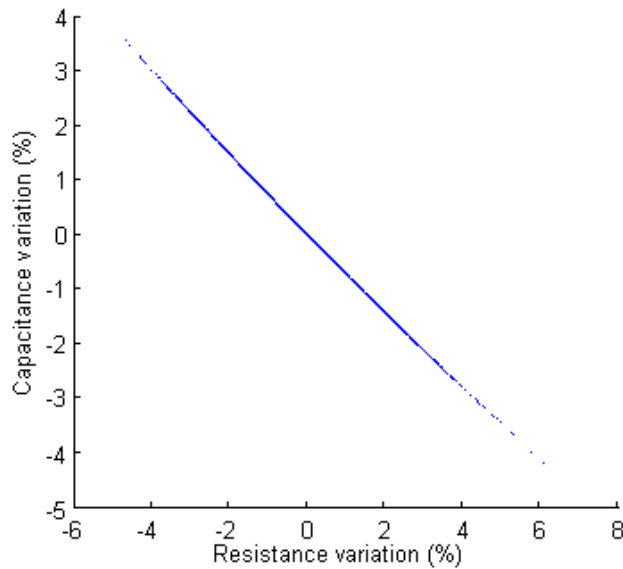


Figure 6.12: Scatter plot of interconnect resistance and capacitance with thickness variation of 3σ=5% in a 13nm technology interconnect of 1mm length.
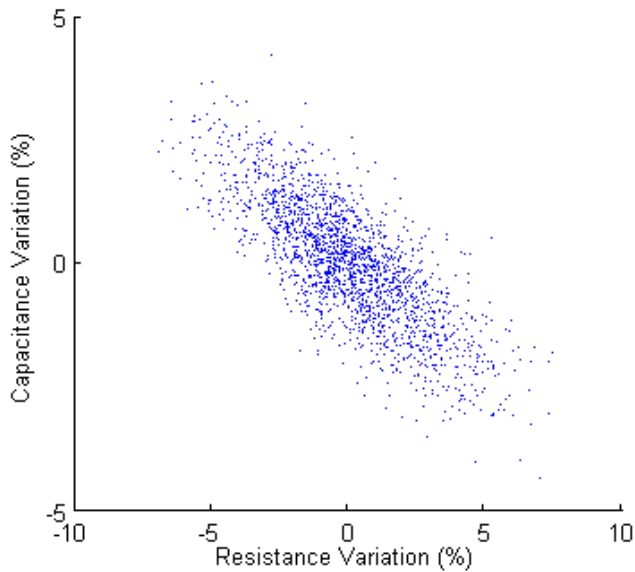


Figure 6.13: Scatter plot of interconnect resistance and capacitance with width and thickness variation of 3σ=5% in a 13nm technology interconnect of length 1mm.

The variability in the geometrical dimensions of the interconnect and repeaters affect the delay in different proportions and a comparison is shown in Figure 6.14. In the plot, the impact of variation for $3\sigma=5\%$ in W, S, T and H (separately and all variations together) in the interconnect and due to RDF in the repeaters, on the delay of an interconnect of minimum dimensions has been shown in the form of a bar chart. The interconnect with and

without the use of repeaters have been considered. The results have been obtained by first transforming the interconnect geometrical variations into the electrical variations (using the analytical models) and then modelling and simulating the interconnect in HSPICE using MC simulations. From the results, it can be clearly inferred that the interconnect delay is more sensitive to width and thickness variation. The effect of RDF is least as compared to other sources of variation due to large size of the delay optimal repeaters. It may also be noted that interconnects without the use of repeaters are more vulnerable to delay variability. Moreover, a small variation in all interconnect parameters together can introduce significant variability in the delay.
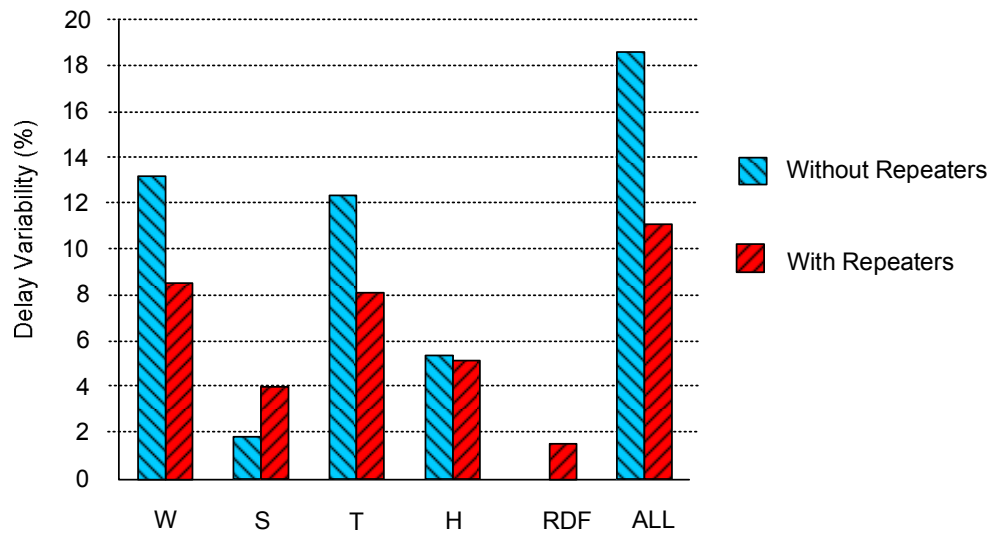


Figure 6.14: Contribution of different parametric variations on the delay of a bus line of length 1mm of minimum width and spacing in 13nm technology.

## 6.6 Area Constrained Channel Bandwidth

On chip area is a precious resource and is not freely available. Therefore, on-chip communication channels are also designed with optimum use of area. During floor-planning, a fixed area is allocated to each link and a particular number of lines are fitted into this area. In order to minimize the effects of capacitive coupling, shielding wires are also used along the signal wires. The shielding wires are normally used with minimum width as permitted by the technology generation, independent of the size of the signal wires. In this way, an effective shielding against RC coupling can be achieved with minimum area consumption.

Let $W_c$ be the channel width and $N$ be the number of lines, each having width $W$ and interspacing $S$. Then the constraints relating these quantities are approximated by [137] for the shielded and unshielded wires respectively.

120

$$W_c = NW + (N - 1)S \tag{6.13}$$

$$W_c = NW_{signal} + (N - 1)(2S + W_{shield}) \tag{6.14}$$

In the following sections we will explore the impact of variability on channel performance under fixed channel width $W_c$ for the channel without shielded wires.

### 6.6.1 Experimental Setup and Simulation Results

We consider a channel bus consisting of 128 lines connecting two cores or NoC routers. The physical width of the channel is assumed to be $W_c = 128 \times P_{min}$, where $P_{min}$ is the minimum allowable pitch in the given technology generation. The wires have been considered as parallel global copper traces placed over a ground plane. Interconnect geometrical and material parameters have been extracted from the ITRS2007 and given in Table 6.2 along with the device parameters. The interconnects have been designed with and without the use of repeaters. The variability in the devices due to RDF and due to variations in the width, spacing, thickness and ILD thickness of interconnects has been considered. Again we consider the following three cases of interconnect variability:

Case 1: $3\sigma_w = 5\%$, $3\sigma_s = 5\%$, $3\sigma_T = 2\%$, $3\sigma_H = 5\%$, $3\sigma_{Dev} = As\ actual\ in\ devices$

Case 2: $3\sigma_w = 10\%$, $3\sigma_s = 10\%$, $3\sigma_T = 2\%$, $3\sigma_H = 10\%$, $3\sigma_{Dev} = As\ actual\ in\ devices$

Case 3: $3\sigma_w = 15\%$, $3\sigma_s = 15\%$, $3\sigma_T = 2\%$, $3\sigma_H = 15\%$, $3\sigma_{Dev} = As\ actual\ in\ devices$

These values are with respect to the minimum interconnect dimensions in the corresponding technology. It is also assumed that variability follows Gaussian distribution. The repeaters have been constructed using the model card libraries with RDF effects. The bus length is taken to be 1mm in this study and worst case crosstalk effects (aggressor lines switch in opposite direction with reference to the victim line) are considered.

The objective of this study is to explore the channel configuration which gives optimum performance under the impact of variability and its relation with the power and area. For this purpose several experiments were designed and extensive Monte Carlo simulations performed to get the results. The circuit netlists were generated and HSPICE simulations were performed until convergence (~6000 simulations in each case). In order to simulate the distributed nature of interconnects, each wire has been made up of 250 ladder segments.

### 6.6.2 Results

Here we present results for Case 1 of variability for 13nm technology, as the results for the other cases are similar.

**6.6.2.1 Delay**

The mean delay, the standard deviation and delay variability of the channel bus at different values of the interconnect width and spacing are shown in Figure 6.15, 6.16 and 6.17 respectively. The actual data is given in Tables A.1, A.2 and A.3 respectively and placed in the Appendix-A. As expected, the delay decreases both with the increase of the interconnect spacing and width. However, increasing interconnect width is more beneficial as compared to spacing in order to improve delay performance under the same channel width. In the same way, the standard deviation and delay variability decreases more rapidly with the increase of the interconnect width than the spacing.
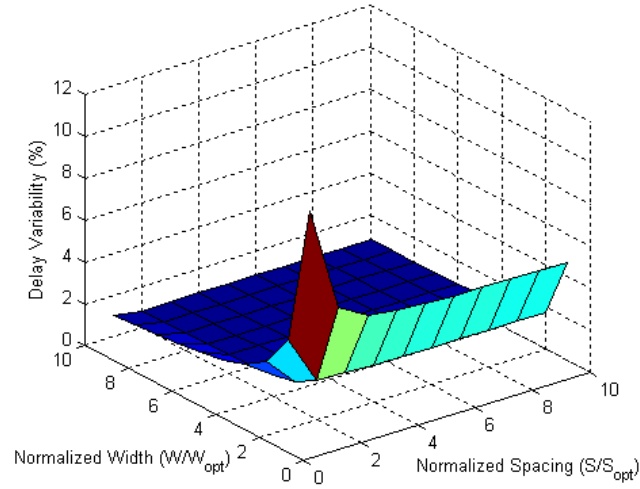


Figure 6.15: Mean delay (in picoseconds) of interconnects (without repeaters) in the channel bus of 13 nm for different geometrical configurations under variability Case 1.
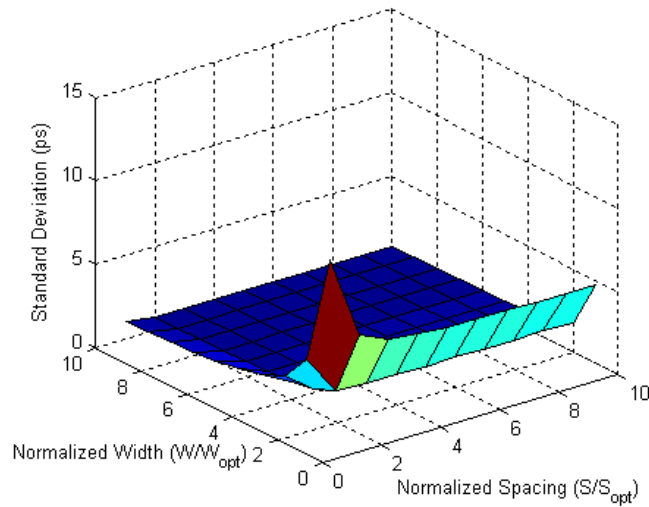


Figure 6.16: The standard deviation (in picoseconds) of the delay of interconnects (without repeaters) in the channel bus of 13nm for different geometrical configurations under variability Case 1.
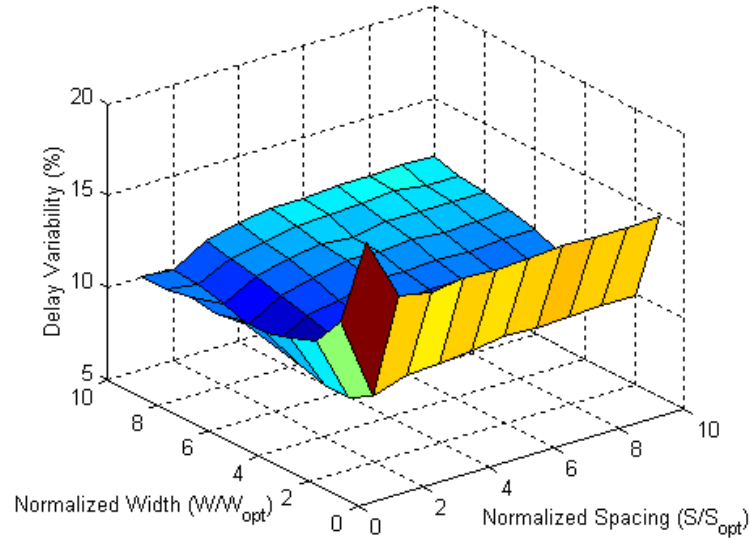
Figure 6.17: Delay variability (%) of interconnects (without repeaters) in the channel bus of 13nm for different geometrical configurations under variability Case 1.

The simulations were also performed to find the performance of the channel inserted with optimal repeaters. The size and number of repeaters depends on the geometrical dimensions of the interconnect (width, spacing, etc) and the parameters of minimum sized repeater in a given technology. For 13 nm technology, the number and size of the repeaters per unit length of the interconnect is shown in Figure 6.18 and 6.19, respectively. The corresponding data is given in Tables A.4 and A.5 respectively.
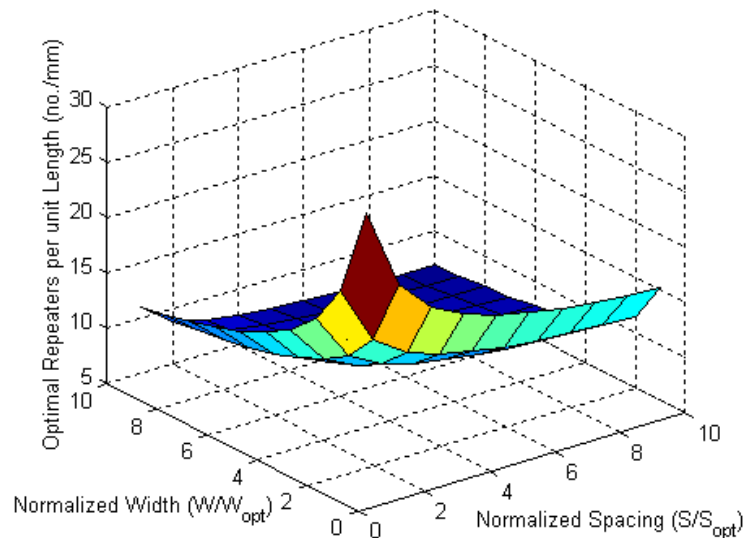


Figure 6.18: The number of repeaters per unit length required for different interconnect dimensions (width and spacing) for a 13 nm bus under worst crosstalk. The numbers have been rounded-off.

The mean delay, the standard deviation and delay variability have been measured for different configurations of the bus inserted with repeaters and the results are shown in Figure 6.20, 6.21 and 6.22 respectively. The corresponding data is given in Table A.6, A.7 and A.8 respectively. The results show that the delay of interconnects improves with the insertion of the repeaters, as expected. More importantly, the delay variability also decreases as compared to the case when repeaters are not used.
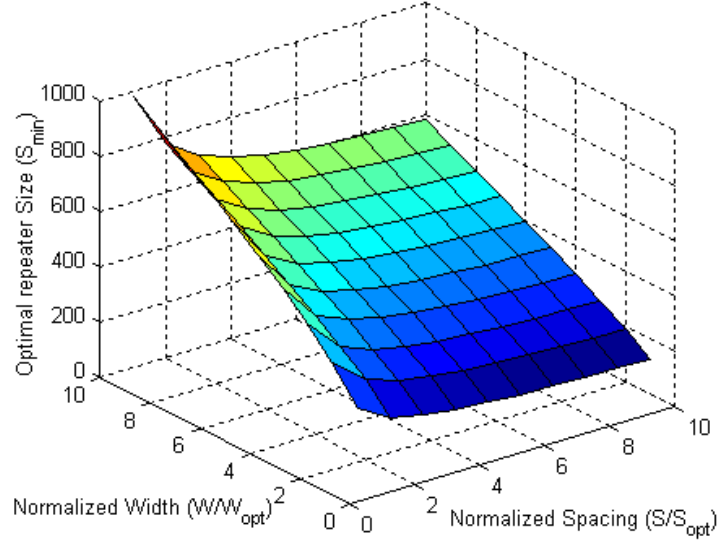


Figure 6.19: The size of the repeaters for different interconnect dimensions (width and spacing) for a 13 nm bus under worst crosstalk. The repeater sizes have been rounded-off.
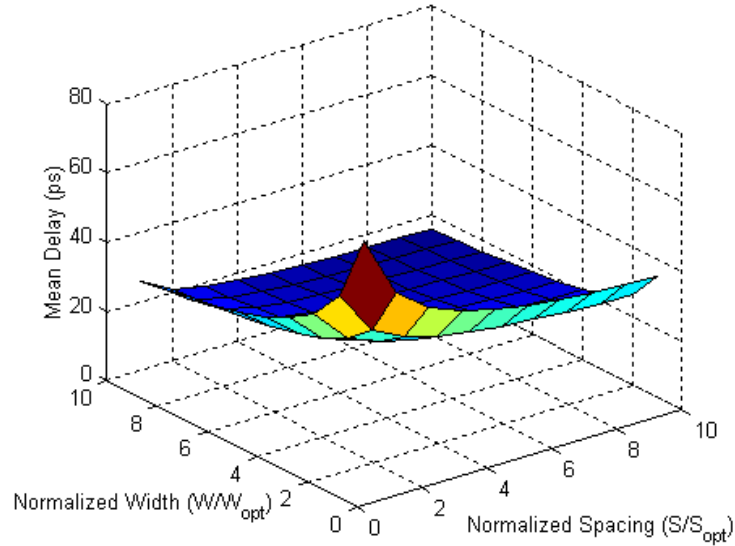


Figure 6.20: Mean delay (in picoseconds) of interconnects (with repeaters) in the channel bus of 13nm for different geometrical configurations under variability Case 1.
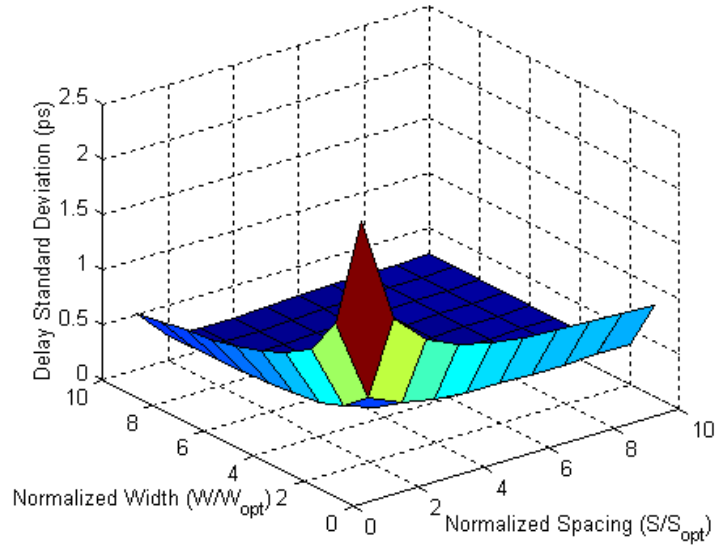
Figure 6.21: The standard deviation (in picoseconds) of the delay of interconnects (with repeaters) in the channel bus.
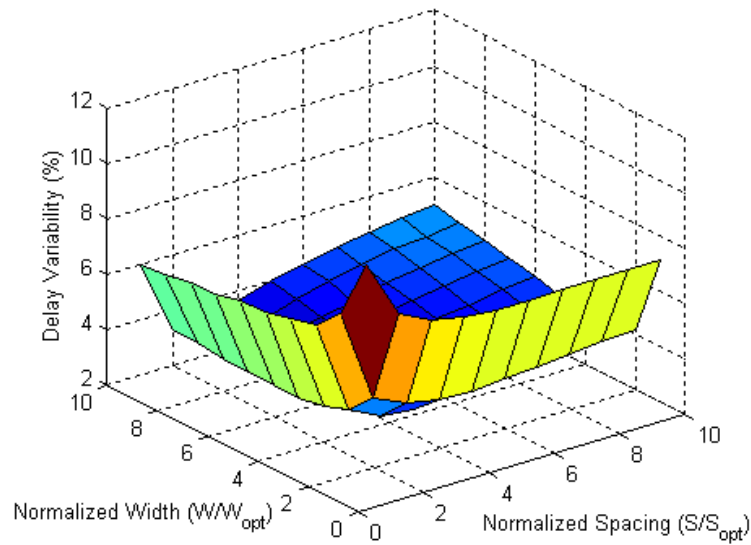


Figure 6.22: Delay variability (%) of interconnects (with repeaters) in the channel bus of 13nm for different geometrical configurations under variability Case 1.

### 6.6.2.2 Bandwidth

Using the data of Table A.1 and A.6, the bandwidth of the individual lines of the bus has been calculated with and without repeaters and results are shown in Figure 6.23 and 6.24 respectively. The corresponding data is given in Table A.9 and A.10 respectively. The results clearly show that the bandwidth can be increased by increasing the width of the interconnect and/or by increasing the spacing between interconnects. Moreover, the insertion of repeaters further increases the bandwidth.
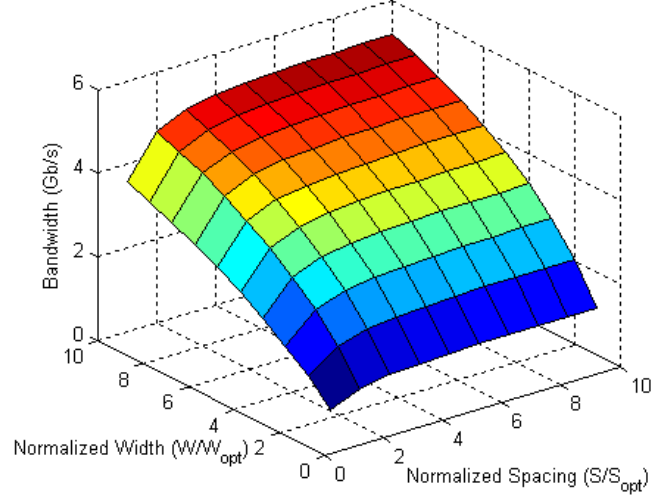
Figure 6.23: Bandwidth of the individual interconnect lines (without repeaters) in Gb/s given as a function of the interconnect width and spacing for 13 nm.
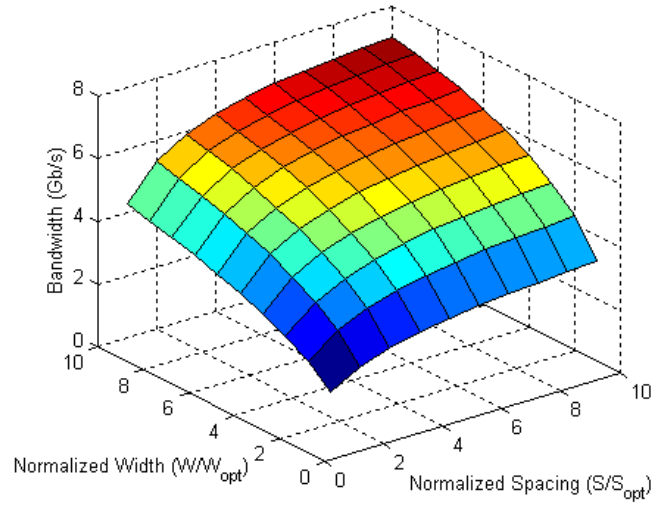


Figure 6.24: Bandwidth of the individual interconnect lines (with repeaters) in Gb/s given as a function of the interconnect width and spacing for 13 nm.

For a channel link, it is important to determine the total bandwidth which it can support. In order to meet high bandwidth requirements under un-constrained area, the configuration of the bus interconnects which gives maximum bandwidth of the individual lines (large value of W and S) is used to get the maximum total bandwidth through a particular channel width (no. of lines). But this may occupy sufficiently large chip area. However in the actual designs, only a limited area budget is allocated for the channel links. Therefore, in this situation the bandwidth will be less than the unconstrained area case. Hence some sort of optimization is required to obtain the best possible bandwidth within the available area budget. During this optimization process, the delay variability as well as the power

dissipation is required to be considered, because these quantities may become worse while looking for a configuration which gives best bandwidth.

In this study, we have explored the geometrical space of interconnects which gives optimum total bandwidth under a channel area constraint. The total bandwidth has been calculated using equation (6.12), where the value of $N$ has been computed from equation (6.13) for different values of $W$ and $S$. The results are shown in Figure 6.25 (without repeaters case) and Figure 6.26 (with repeaters case) and corresponding data is given in Table A.11 and Table A.12.
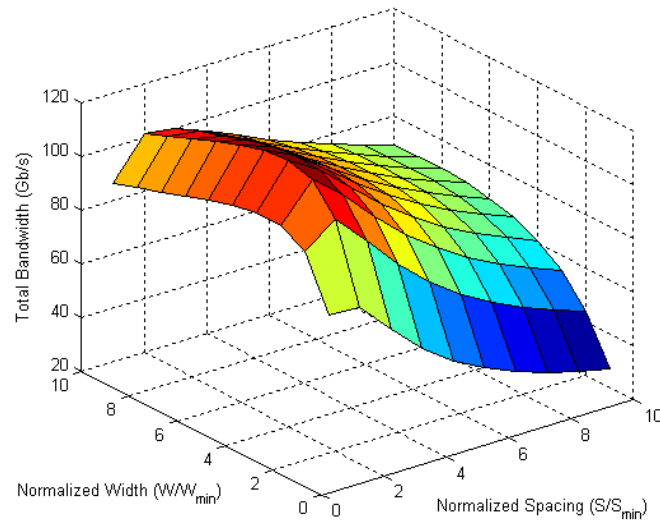


Figure 6.25: Total bandwidth (Gb/s), without repeaters, plotted as a function of interconnect width and spacing.
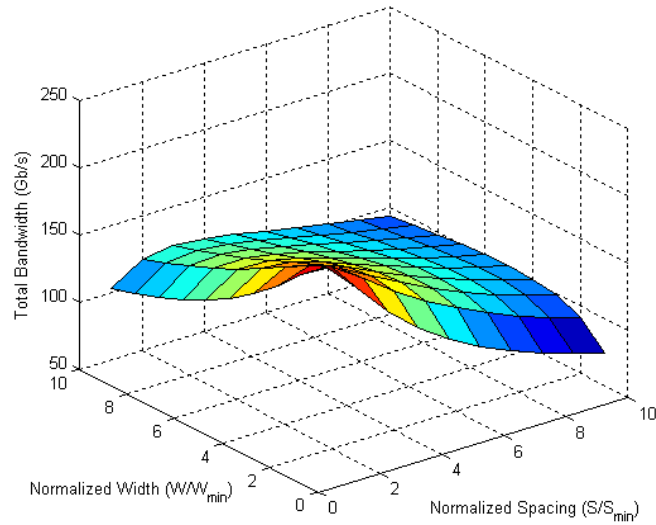


Figure 6.26: Total bandwidth (Gb/s), with repeaters, plotted as a function of interconnect width and spacing.

From the results, it can be seen that there is a clear optimum point which gives the maximum total bandwidth. For the channel bus with no repeaters used, this point corresponds to $W = 4W_{min}$ and $S = 2S_{min}$. Similarly, for the channel bus when repeaters are used, the optimum bandwidth is achieved at $S = S_{min}$ and $W = W_{min}$.

### 6.6.2.3 Power Dissipation

Total power dissipation (switching) in the channel bus for maximum throughput in each of the bus configuration is given in Table A.13 (for the bus without repeaters) and in Table A.14 for the bus with repeaters. The results are shown in Figure 6.27 and 6.28. The power dissipation increases with the increase of the interconnect width due to increased wire capacitance. From the results, the additional power dissipation in the repeaters may also be observed. It is important to mention that this power dissipation is corresponding to the maximum bandwidth of the channel.
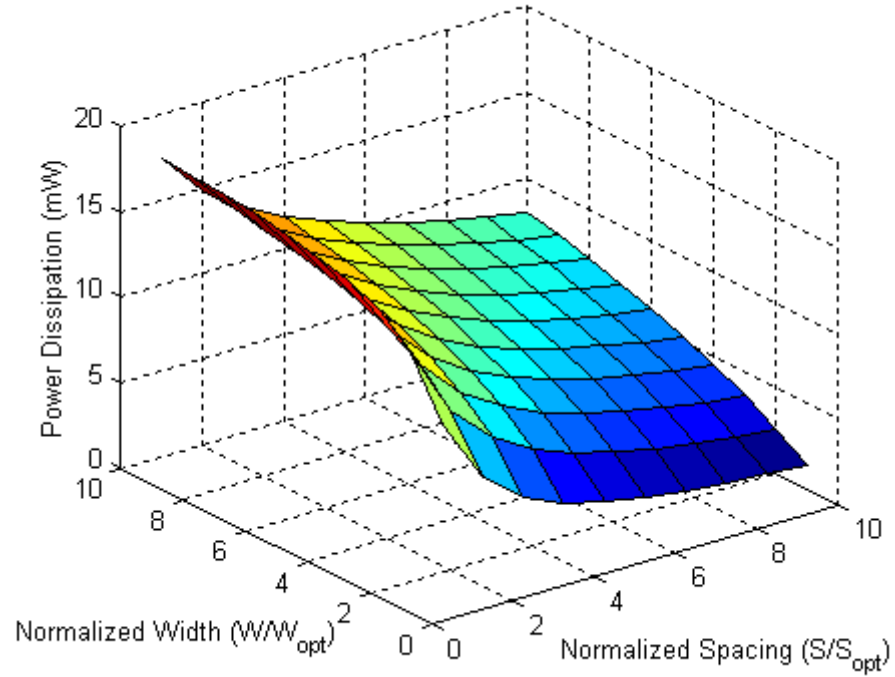


Figure 6.27: Power dissipation (mW) at maximum bandwidth for the interconnect of 13 nm technology without repeaters.

The cost of data transfer in terms of power consumption is measured as the total bandwidth per unit power and is shown in Figure 6.29 (see Table A.15) for the repeater inserted case. It can be inferred from the results that transferring data from one point to the other through widely spaced interconnects is cheaper in terms of power consumption. This cost is different for different channel configurations.
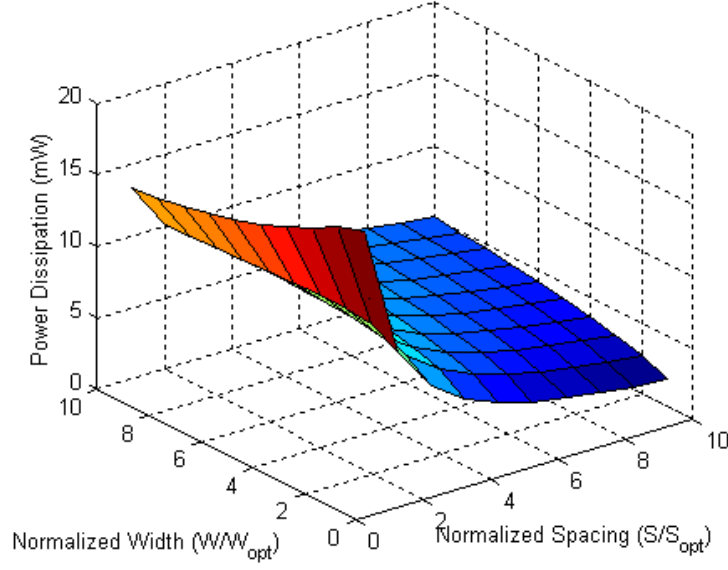
Figure 6.28: Power dissipation (mW) at maximum bandwidth for the interconnect of 13 nm technology with repeaters.
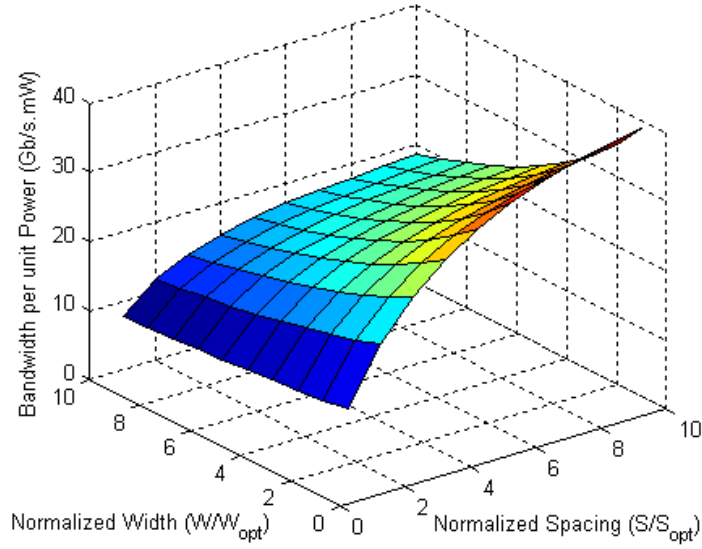


Figure 6.29: Total bandwidth per unit power (Gb/s.mW) consumption for interconnects with repeaters.

**6.6.2.4 Area**

The area consumed by interconnects and repeaters in the channel bus is given by

$$Area_{WR} = W_{wire} L N_{lines} \tag{6.15}$$

$$Area_R = W_{wire} L N_{lines} + N_{opt}(S_{opt} L_{eff} S_{min}) N_{lines} \tag{6.16}$$

where

$Area_{WR}$ = Total area when repeaters are not used,

129

$Area_R$= Total area when repeaters are used,

$W_{wire}$ = Wire width,

$L$= Bus length,

$N_{lines}$= No. of interconnect lines in the channel,

$N_{opt}$=No. of optimal repeaters per unit interconnect length,

$S_{opt}$= Size of the optimal repeaters,

$L_{eff}$= Effective gate length,

$s_{min}$= Width of a minimum sized repeater.
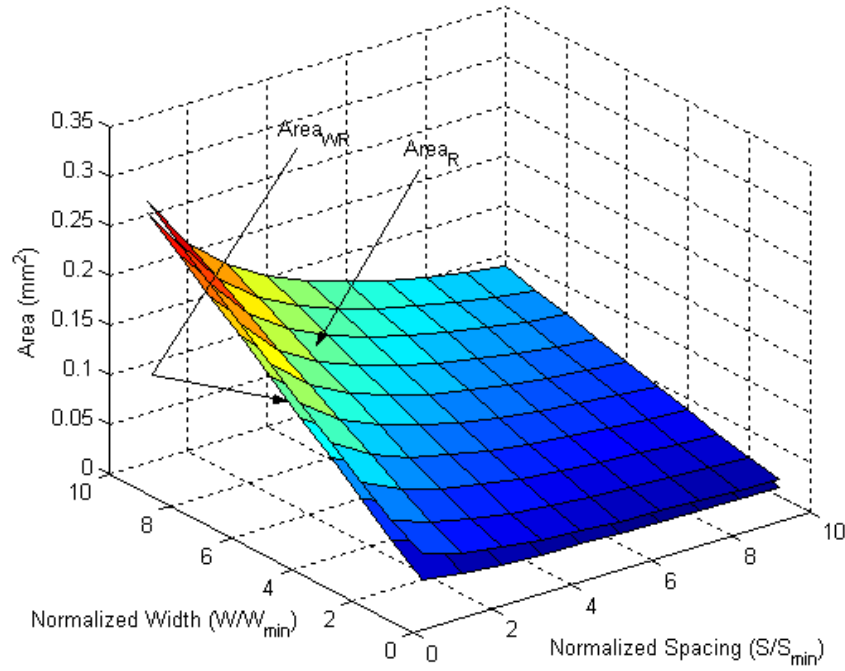


Figure 6.30: Surface plot of the area consumed by the channel bus interconnects, with and without repeaters.

Figure 6.30 shows that maximum area is required when we use wider wires at minimum spacing. The area required with repeater insertion is larger than the case when no repeaters are used. However, the major portion of the area is consumed by the wires. Figure 6.30 may be compared with Figures 6.15 and 6.20 to see the relation between performance and area cost.

## 6.7 Optimization under Different Trade-offs

An ideal data channel is expected to give the maximum bandwidth, small latency per unit length and minimum uncertainty in the arrival times of the signals at the receiver with minimum area and power costs. However, there are trade-offs between delay performance,

bandwidth, area and power. Therefore the aim of an optimization study can be the maximization of one or more parameters.

We define a figure of merit $F$ to achieve the most desired objectives

$$F = \frac{B_{TOT}}{D \times P \times A \times V} \tag{6.17}$$

Where $D$ is the delay, $V$ is the delay variability, $P$ is the power dissipation and $A$ is the area. For the repeater inserted interconnect, the figure of merit $F$ is shown in figure 6.31. Again one can find an optimum interconnect configuration for maximum figure of merit. For instance, for the channel configuration under consideration, the optimum value of $F$ is corresponding to $S = 4S_{min}$ and $W = 5W_{min}$.
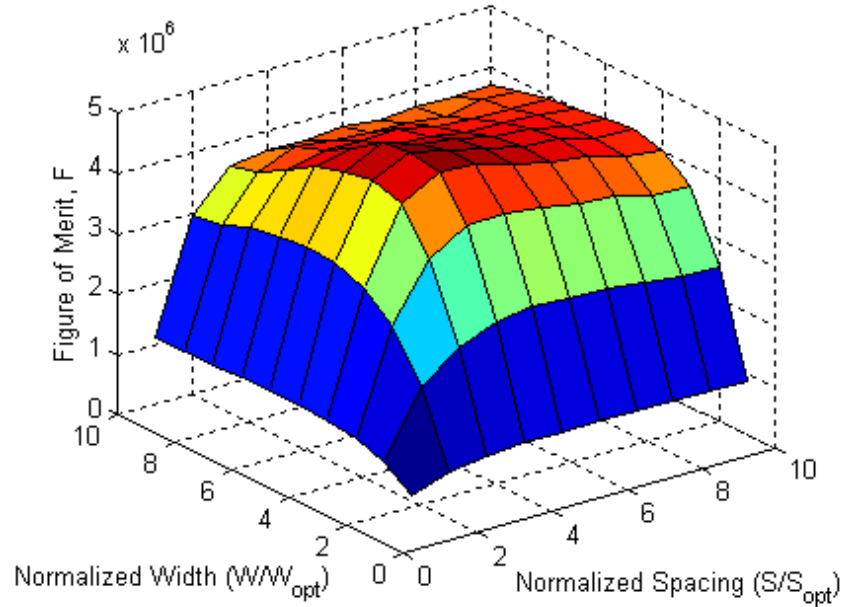


Figure 6.31: The figure of merit $F$ plotted as a function of spacing and width for the repeater inserted interconnect.

## 6.8 Failure of Channels under Variability

During the optimization of the channel, the magnitude of the delay variability should also be considered in conjunction with other parameters like delay, power and area. In a sequential channel link, the data from the transmitter moves through the interconnect lines to the receiver simultaneously with a common synchronous clock, as shown in Figure 6.32. As we have seen, variability in the devices and interconnects introduces delay variability; this will produce data skew at the receiving end of the channel. The skew beyond a certain

acceptable limit can result in data loss. This may also result in timing failures, as the data may not be properly latched at the receiving register.

Let $T_{setup^i}$ be the setup time of the $i-th$ flip-flop, $T_{wire^i}$ be the delay of the $i-th$ interconnect line, the clock frequency $f_{CLK}$ and $T_{CLK}$ be the clock period.
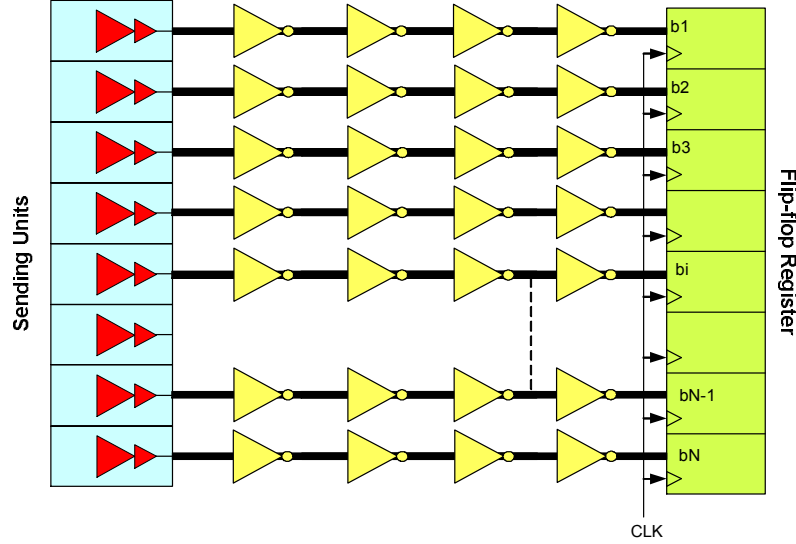


Figure 6.32: A multi-bit communication link. Tapered buffers have been used on the transmission side, whereas flip-flop registers have been used at the receiving end.

For proper latching of the data bit, the following delay constraint must be satisfied

$$0 \leq T_{wire^i} \leq T_{CLK} - T_{setup^i} \tag{6.18}$$

The probability of correct data transmission can, therefore, be expressed as follows

$$q = \Pr\left(0 \leq T_{wire^i} \leq T_{CLK} - T_{setup^i}\right) \tag{6.19}$$

Since $T_{wire^i}$, $T_{CLK}$ and $T_{setup^i}$ are random variables, therefore $\delta = T_{wire^i} + T_{setup^i} + (-T_{CLK})$ will also be a random variable with a $p.d.f$ $P(\delta) = P(T_{wire^i}) * P(T_{setup^i}) * P(-T_{CLK})$, where (*) is the convolution operator. If the flip-flops used in the receiving register are of large size, the timing distribution of the setup time will be Normal. Similarly, due to sufficiently large size of the optimal repeaters (see Table A.4), the delay distribution of the repeaters will also be normal. Also the delay distribution of interconnects under variability is assumed to be Normal. Then

$$\mu_\delta = \mu_{wire} + \mu_{setup} - \mu_{CLK} \tag{6.20}$$

$$\sigma_\delta^2 = \sigma_{wire}^2 + \sigma_{setup}^2 + \sigma_{CLK}^2 \tag{6.21}$$

and the probability of correct data transmission is given by the error function [20]

132

$$q = \frac{1}{2} + \text{erf}\left(\frac{\mu_\delta}{\sigma_\delta}\right) \qquad (6.22)$$

where

$$\text{erf}(x) = \frac{1}{\sqrt{2\pi}} \int_0^x \exp\left(-\frac{t^2}{2}\right) dt \qquad (6.23)$$

The probability of failure for one data bit transmitted through the interconnect is given by

$$PoF_{single} = 1 - q \qquad (6.24)$$

In a multi-bit link consisting of $N$ channel lines, if the signal timing does not meet the target value in one or more lines, the communication link fails. So the probability of failure in such a link is given by

$$PoF_{multiple} = 1 - q^N \qquad (6.25)$$

As we have seen that the magnitude of the delay variability also depends upon the channel configuration (width, spacing), this will directly impact the link failure probability; otherwise the operating frequency of the link will have to be reduced. The maximum frequency at which a link can operate depends upon the delay of interconnects. Tables A.6 gives the delay and A.7 gives the standard deviation of the associated delay variability as a function of the interconnect width and spacing. At the receiving end of the channel, flip-flop registers have been used having setup time $\mu_{setup} = 12.1ps$ and $\sigma_{setup} = 0.15ps$. The probability of failure (PoF) has been calculated using equation (6.24) at 5% below the maximum possible frequency of the link with a particular geometrical configuration and results are given in Table A.16. The results show that $PoF$ is highest for S=1X and W=1X due to large variability in this configuration and decreases with the increase of width and/or spacing. The operating frequency of the link and $PoF$ depends on the delay and delay variability as shown in Figure 6.33.

As the channel width increases, the $PoF$ increases and is governed by equation (6.25). In an area constrained channel, the $PoF$ is given in Table A.17 using equation (6.25) while considering the possible number of lines in the given area. The results show that $PoF$ is extremely large for the wider links. Therefore, while optimizing a channel for any of the parameters, the $PoF$ should also be considered in the figure of merit. Otherwise, the channel speed and hence performance frequency will not be met. This is obviously undesirable for high performance designs.
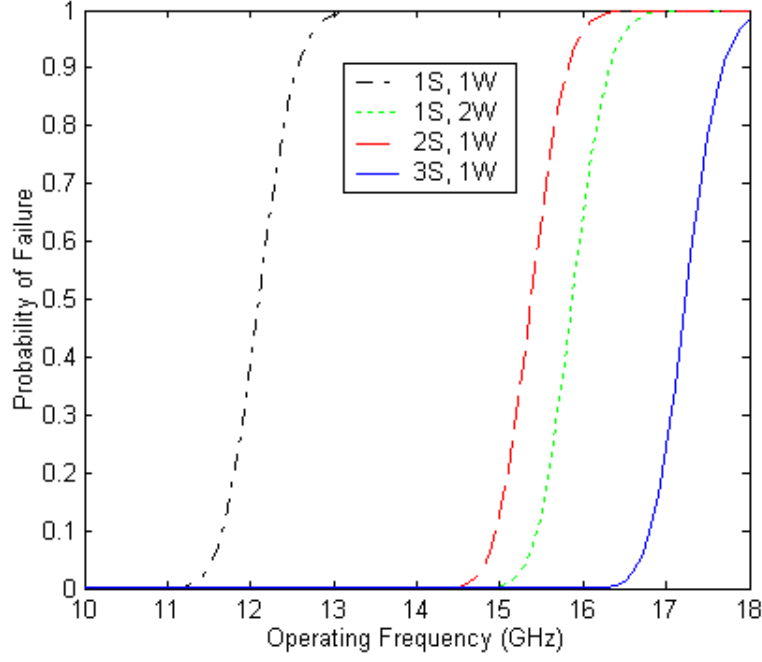
Figure 6.33: Probability of link failure as a function of operating frequency.

## 6.9. Channel Serialization

The channel width (bit-width) determines the size of the *physical transfer unit* (phit) or vice versa. The data packet is accordingly divided into smaller units and transmitted through the on-chip communication network. If the bit-width of a processing unit (PU) is larger than the phit size of the channel, some sort of serialization will be required by the factor of:

$$Degree \; of \; Serialization = \frac{I/O \; bitwidth}{phit \; size}$$

The throughput is the average rate of successful data transmission over a communication channel. The throughput is usually less than the bandwidth; which is the maximum capacity of a channel. In a throughput centric design, the channel can be designed in such a way that the desired throughput requirements can be achieved at optimum power and area consumption. In this section, we will investigate the effect of channel serialization on throughput, area and power consumption.

### 6.9.1 Concept

The power dissipation in a repeater-interconnect system is given by

$$P_{Rep-Int} = P_{switching} + P_{short-circuit} + P_{leakage} \qquad (6.26)$$

The switching power is the most dominant component of power dissipation and strongly depends on the interconnect capacitance (along with the size and input/output capacitances of the driver) and is governed by the following expressions

$$P_{switching-wr} = L(c_s + 2c_c)V_{dd}^2 f_{clk} \times N_{lines} \tag{6.27}$$

$$P_{switching-rep} = \left(\alpha\left(s(c_p + c_o) + l(c_s + 2c_c)\right)V_{dd}^2 f_{clk}\right) \times k_{opt} \times N_{lines} \tag{6.28}$$

where

$P_{switching-wr}$= switching power of the bus without repeaters,

$P_{switching-rep}$= switching power of the bus with repeaters,

$c_o$= input capacitance of the repeater,

$c_p$ = output parasitic capacitance of the repeater,

$c_s$= self capacitance per unit length of the interconnect,

$c_c$= coupling capacitance per unit length of the interconnect,

$l$= interconnect length between repeaters,

$L$= total interconnect length,

$k_{opt}$=number of optimal repeaters per unit length,

$\alpha$=switching activity,

$f_{clk}$=clock frequency,

$N_{lines}$= number of lines in the bus.

Equations (6.27) & (6.28) dictate that in order to reduce bus power, the coupling capacitance (principal component of the bus capacitance) should be reduced. This is possible by increasing the spacing between interconnects and so the bit-width will have to reduce in area-constrained design. This motivates to use Serial links.

## 6.9.2 Channel Structure

The conceptual diagram of a serial data channel is given in Figure 6.34. Multi-bit parallel data (having U-bits) from the computational unit (or a router in NoC) is transformed into the serial data (having V-bits) using a special unit called the Serializer. The degree of serialization is defined as $\lambda = U/V$. The serial data moves through interconnects which are widely spaced as compared to the parallel case. The serial data before entering the receiver is converted back into U-bits of parallel data through a special unit called De-serializer. In this way, the serializer and de-serializer provide an interface between the computational units and the link. The serializer is based on a chain of multiplexers in conjunction with

flip-flops as shown in Figure 6.35. A more intelligent serializer and deserializer (SerDes) is shown in Figure 6.36.
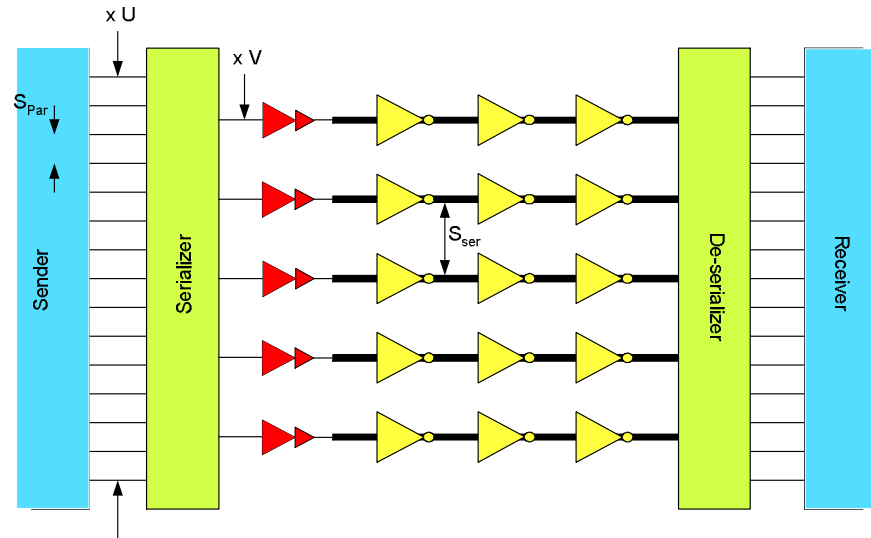


Figure 6.34: Structure of a semi-serial communication channel.



SERIALIZER
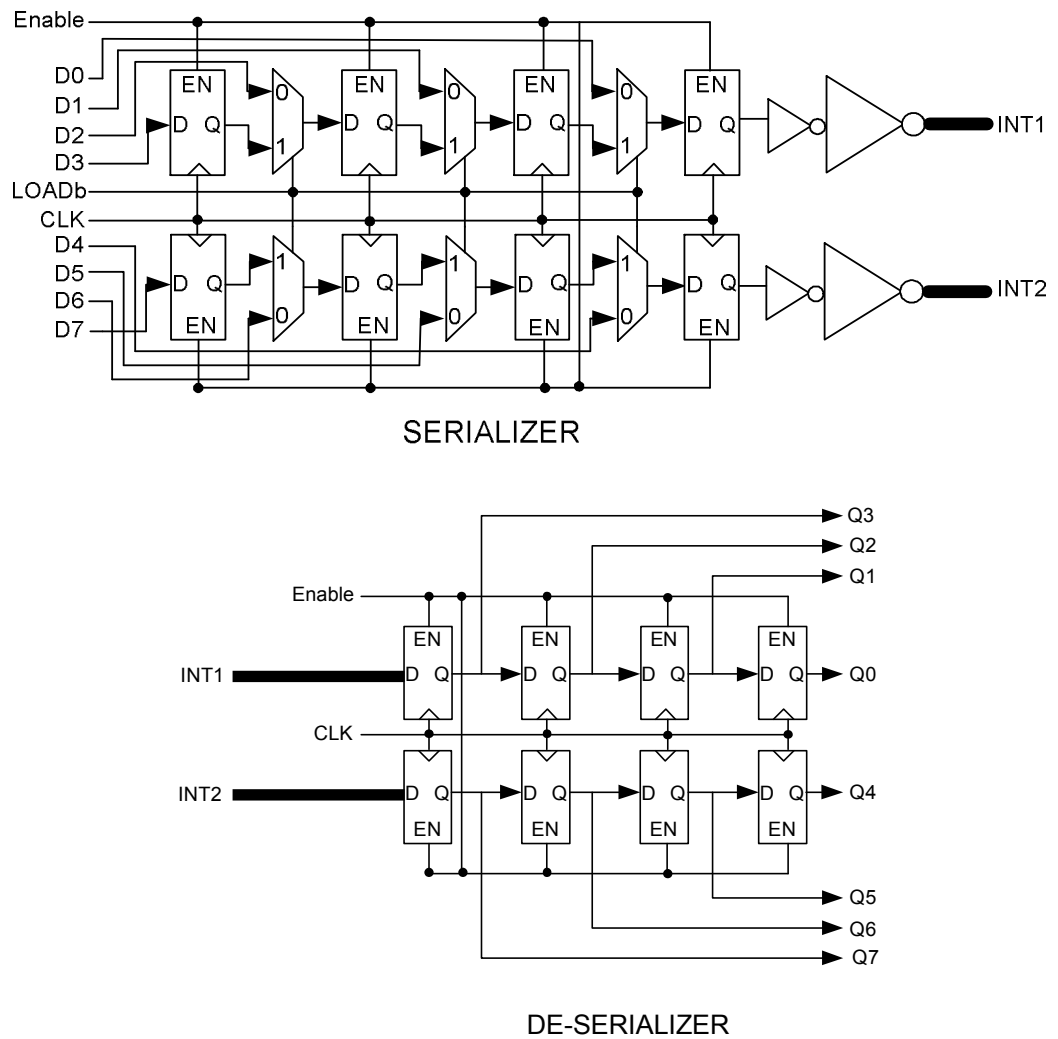


DE-SERIALIZER

Figure 6.35: Conventional shift-register type SerDes.

136
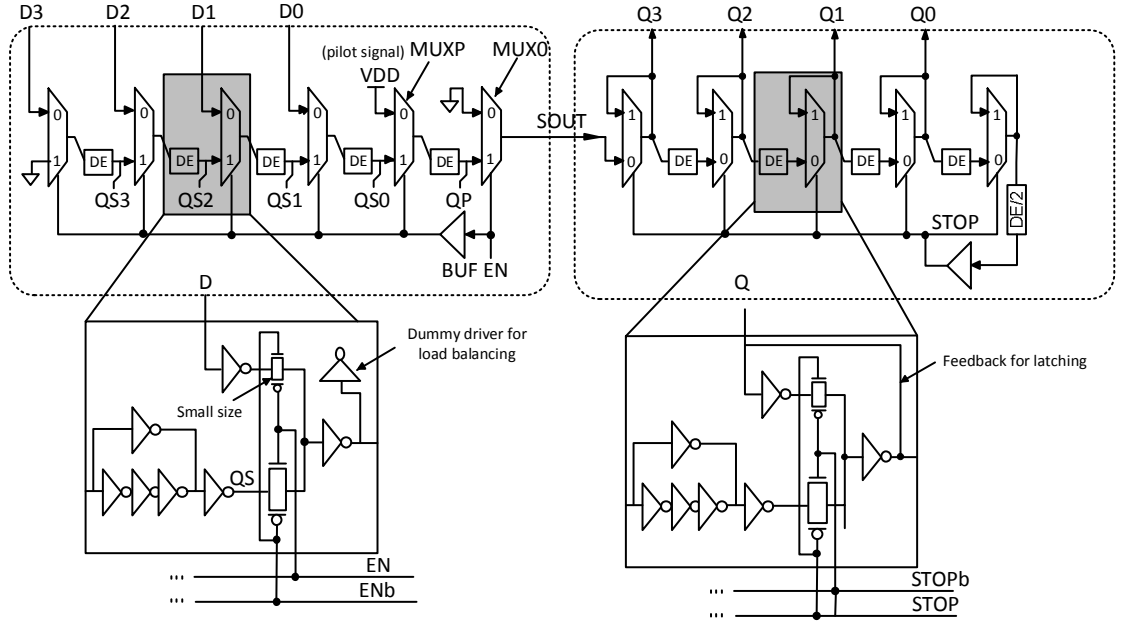
Figure 6.36: Wave front train Serializer and Deserializer [138].

The throughput of the parallel link $(T_{par})$ and serial link $(T_{ser})$ can be calculated as follows

$$T_{par} = f_{par} \times \lambda V \tag{6.29}$$

$$T_{ser} = f_{ser} \times V \tag{6.30}$$

To obtain the same throughput from the serial link as that of the parallel link

$$f_{ser} = \lambda f_{par} \tag{6.31}$$

Therefore the serial bus will have to operate $\lambda$ times faster than the parallel bus.

The total power dissipation in a parallel and serial link is given by

$$P_{par-link} = P_{drivers} + P_{rep} \tag{6.32}$$

$$P_{ser-link} = P_{drivers} + P_{rep} + P_{SerDes} \tag{6.32}$$

Note that the power dissipation in parallel links does not include the power dissipation in the SerDes (Serializer-Deserializer). The power dissipation in the repeaters, drivers and SerDes is mainly due to the switching and leakage power. The short-circuit power has a relatively less contribution in the total power during bus operation and therefore can be neglected.

Using equation (6.28), the switching power dissipation in a repeater inserted parallel link is given by

$$P_{switching-par} = \left( \alpha \left( s(c_p + c_o) + l(c_{s-par} + 2c_{c-par}) \right) V_{dd}^2 f_{par} \right) \times k_{opt} \times U \tag{6.33}$$

$$P_{switching-ser} = \left( \alpha \left( s(c_p + c_o) + l(c_{s-ser} + 2c_{c-ser}) \right) V_{dd}^2 f_{ser} \right) \times k_{opt} \times V \qquad (6.34)$$

Equation (6.33) and (6.34) show that the switching power of a serial bus is less than the parallel bus by a factor $(c_{c-par}/c_{c-ser})$.

### 6.9.3 Experimental Results

The performance of the parallel and serial buses constrained in width $W_c$ for the same throughput has been calculated and results are given in Table 6.3. The results show that for $\lambda = 2$, (W=W$_{min}$, S=3S$_{min}$) the power dissipation decreases by 55.21% and 47.05% for the bus with and without repeaters respectively. Excluding the area of SerDes, the area of the serial bus is 34.57% and 33.21% less than the area of the corresponding parallel buses. Although interconnect spacing is a weak function of delay variability, the serial bus has less variability effects as compared to the parallel bus. Similarly, a serial bus will also be less vulnerable to the crosstalk effects due to increased interconnect spacing. Additional advantages of serial links are the minimization of skew between different lines of the link due to the reduced number of wires. The operational duty of a parallel link is less than a serial link and therefore leakage power becomes a significant portion of the total power in parallel links. Again, a serial bus reduces leakage power.

Table 6.3: Performance of a parallel and a serial bus of degree 2 for the same throughput

| Parameters | Parallel Bus | | Serial bus of degree 2 | |
|---|---|---|---|---|
| | Without Repeaters | With Repeaters | Without Repeaters | With Repeaters |
| Interconnect Width | $1S_{min}$ | $1S_{min}$ | $1S_{min}$ | $1S_{min}$ |
| Interconnect Spacing $(\mu m)$ | $1S_{min}$ | $1S_{min}$ | $3S_{min}$ | $3S_{min}$ |
| Number of Interconnects | 128 | 128 | 64 | 64 |
| Throughput (Gb/s) | 66.23 | 154.8 | 66.23 | 154.8 |
| Frequency (GHz) | 0.5174 | 1.2093 | 1.0349 | 2.4194 |
| Power Dissipation (Watt) | 0.008499 | 0.014289 | 0.0045 | 0.0064 |
| Area (mm$^2$) | 0.02511 | 0.05229 | 0.01677 | 0.03421 |
| Delay Variability (%) | 18.16 | 14.35 | 10.13 | 7.39 |

By considering all possible geometrical configurations of the bus (space spanned by W and S), we can explore different possibilities which can give best performance for a particular parameter and accordingly the serialization degree may be ascertained. The extreme case of serialization is the conversion of a multi-bit link to a single wire link. For instance, a serialization degree of 1, 1.5, 2.0, …,4.5 can be obtained either by increasing interconnect

spacing from $1S_{min}$ to $8S_{min}$ (keeping width constant at $W_{min}$) or by increasing the width from $1W_{min}$ to $8W_{min}$ (keeping spacing constant at $S_{min}$). Now if we want to operate the link at a bandwidth of 87.9 Gb/s, the channel performance in the two cases will be different as shown in Figure 6. 37. The results show that the serial bus using wide interconnects is efficient in terms of signal speed and delay variability and inefficient in terms of power and area, as compared to the bus with widely spaced interconnects. Also observe the reduction in bandwidth capacity in the two cases. Therefore, depending upon the metrics of interest and constraints, the channel configuration for serialization can be selected.



(a)



(b)
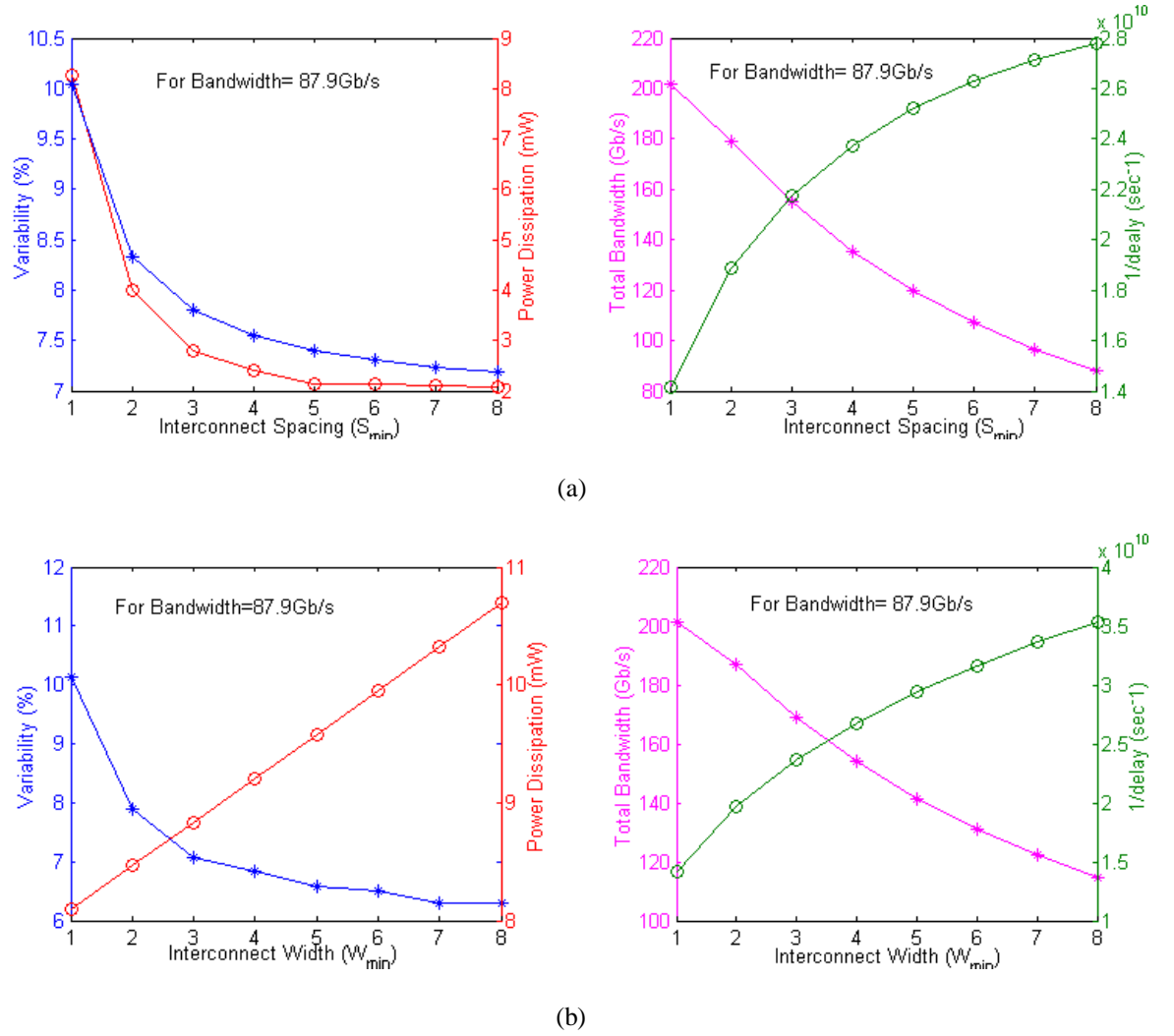
Figure 6.37: Different performance metrics for a bus with different serialization ratios (1, 1.5, 2.0…, 4.5 corresponding to S= $1S_{min}$ to $8S_{min}$ or W= $1W_{min}$ to $8W_{min}$), (a) by increasing spacing and keeping width constant, (b) by increasing width and keeping spacing constant.

## 6.10 Link Utilization and Power Dissipation

As we have already seen that leakage power is increasing significantly with technology scaling, especially in the circuits where the activity level is low. In a SoC and NoC,

different link types with various utilization rates are used which can be as low as few percent [121]. It has been reported that average activity level of microprocessor nets is 4.5% [123], however some links may operate at higher utilization rates approaching 100%.

In order to investigate the impact of link utilization on the total power consumption, we have considered two types of links (S=Smin, W=Wmin and S=Smin, W=5Wmin) and contribution of leakage power in the total power dissipation has been measured corresponding to different link utilization rates. The results are shown in Figure 6.38. It can be seen that contribution of the leakage power in the total power dissipation increases as the link utilization rates reduce. The leakage power becomes the dominant source of power dissipation at very low link utilization rates.
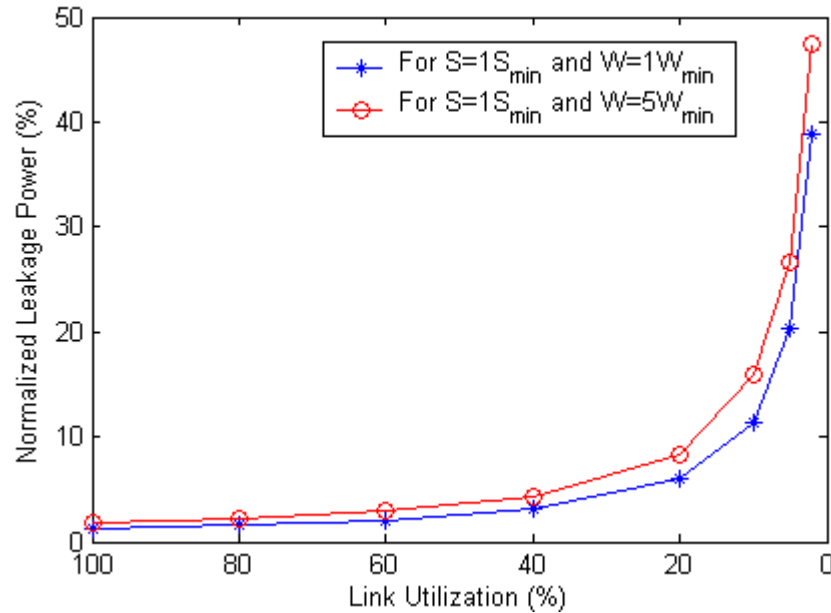


Figure 6.38: Leakage power normalized with the total power for different link utilization rates.

NoC links are designed to operate at low utilization rates in order to meet the stringent requirements for latency. Moreover the links with higher bandwidth capacity are used to reduce packet collisions [146]. For such designs, leakage power may become a critical design parameter and therefore, a careful consideration of all the performance parameters will help to achieve better optimization.

## 6.11 Summary

In this chapter we have discussed the performance of multibit links under the impact of variability. We started with the modelling of interconnects in DSM region and then simulation results for the delay and power measurement have been presented. From these

results several plots for the delay, delay variability, bandwidth and power dissipation have been presented. A figure of merit has been introduced for the optimization of channel performance under delay, power, area, and variability constraints. Then the failure of channels under variability has been discussed. In the end, it has been shown that channel serialization is an attractive approach for power, area and variability efficient designs for throughput centric systems. Moreover, it has been demonstrated that leakage power becomes an important component of power dissipation for the links operating at low activity levels. Therefore, this consideration may also be very beneficial for power-efficient link designs.

# Chapter 7

# Crosstalk in Coupled Interconnects

## 7.1 Introduction

Coupling capacitances have increased due to reduced interspacing and larger aspect ratios of wires in progressive DSM technologies. The technology scaling results in the increased dominance of coupling capacitance and it can be as high as 80% of the total wire capacitance [139].

The technology scaling has also pushed the signal frequencies to the gigahertz region and at such high speeds the transmission line effects such as crosstalk, distortion and reflection are becoming evident. Crosstalk represents the situation when a neighbouring wire unintentionally affects the performance of another wire through electromagnetic field interaction. It occurs due to coupling between the neighbouring wires and can be classified into *functional noise and delay noise*. Functional noise refers to a fluctuation in the signal state of a quiet wire (non-switching) due to switching in the neighbouring wire. This noise produces a glitch that may propagate through the interconnect to the dynamic node or a latch and may tend to change the signal state. Excessive noise will change the signal state and will result in circuit malfunction depending on the noise margin available. Crosstalk can also cause variation in the delay of signals depending on the phases of the aggressor and victim line signals. On a chip, an interconnect may have multiple couplings with

neighbouring wires and simultaneous switching on these wires will effect propagation delays, thereby resulting in delay variations [55], referred to as delay noise. The delay noise (variations) may result in timing failures. The delay noise is contributing a significant fraction of the circuit delay [140]. Therefore, crosstalk effects need serious considerations during the design process, otherwise, the system will suffer from performance degradation or even system failure.

In actual circuits there are equal chances that the signal transitions on the victim and aggressor lines appear simultaneously or with some skew. Similarly, process variations in the circuits are translated into delay variations resulting in the introduction of skew at the input of aggressor and victim drivers. It has been observed that the amount of the delay noise on the victim line depends on the victim-aggressor skew [140]. This will cause delay variability at the receiver. Under these situations, signal delay noise and crosstalk are seriously affecting the performance of high performance designs. Accurate estimation of these effects is necessary for the design of high performance systems otherwise the designers will have to go through the extra design iterations which are computationally and time wise expensive [28].

In the past, many researchers have published crosstalk analysis models and algorithms [28]-[30], [141] but all of them either require numerical techniques to solve them or do not give sufficient insight into the underlying crosstalk effects on signal responses. Therefore, we present closed form expressions that give accurate voltages for the aggressor and victim lines in time domain, as a function of wire length, due to switching transitions on them. Extension to this work is continued to derive analytical expressions in order to determine the conditions that gives maximum crosstalk effects under the impact of variability.

## 7.2 Coupled RC Transmission Lines

Consider a coupled RC transmission line consisting of two signal conductors and a ground line with distributed RC parameters amongst them. A lumped element representation is shown in Figure 7.1, where the capacitance ($c_s, c_c$) are the self and coupling capacitance (per unit length), and the resistance R is the series resistance per unit length for each line. We are interested in determining the transient behavior of the system when the lines are driven by a unit step input at the source (x=0), corresponding to a high/low or low/high transition in any combination. In real digital systems, transition of the line drivers do not occur concurrently, but rather the transitions are mutually delayed by a short time $\delta$, called the skew of the lines. The skew is not maintained constant throughout the line, but rather it

is increased or decreased depending on specific conditions. The aim of this study is to determine those conditions and to quantify the amount of passive skew amplification or reduction in such a system (defined as the ratio between the input and output skew). As a first step towards this objective, an accurate crosstalk model has been developed that can be used to determine those conditions. Here we will skip the derivation and present only the final results of this model developed by F. Rodriguez [142].
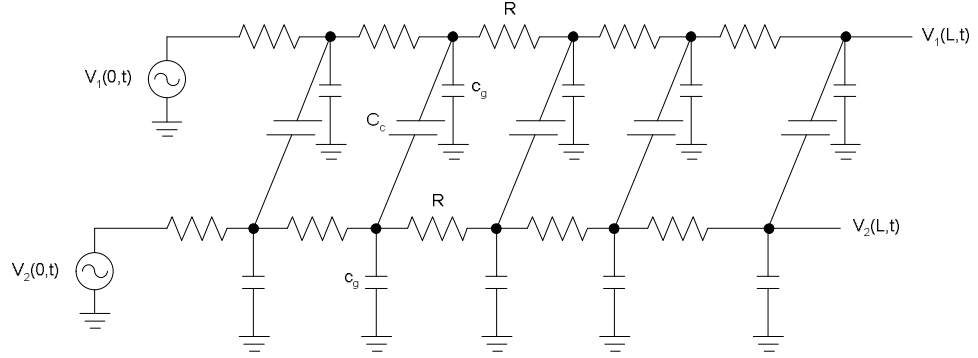


Figure 7.1: Coupled RC transmission line model with distributed RC parameters.

## 7.2.1 Voltage Representation

The voltage on the victim line as a function of the interconnect length and time is given below for up-up and up-down transitions

$$\mathbf{v}_{uu}(x,t) = \frac{1}{2}\mu(t)\begin{bmatrix} w_1(x,t) + w_2(x,t) \\ w_1(x,t) - w_2(x,t) \end{bmatrix} + \frac{1}{2}\mu(t-\delta)\begin{bmatrix} w_1(x,t-\delta) - w_2(x,t-\delta) \\ w_1(x,t-\delta) + w_2(x,t-\delta) \end{bmatrix} \quad (7.1)$$

$$\mathbf{v}_{ud}(x,t) = \frac{1}{2}\mu(t)\begin{bmatrix} w_1(x,t) + w_2(x,t) \\ 2 + w_1(x,t) - w_2(x,t) \end{bmatrix}$$
$$- \frac{1}{2}\mu(t-\delta)\begin{bmatrix} w_1(x,t-\delta) - w_2(x,t-\delta) \\ w_1(x,t-\delta) + w_2(x,t-\delta) \end{bmatrix} \quad (7.2)$$

and describe the signals in the wires due to a skewed input. Notice the response is formed by two functions which act at different times. When the input to the aggressor line is turned on at $t = 0$, a transitory waveform, $w_1(x,t) - w_2(x,t)$ is induced in the victim line. Similarly, the switching in the victim line induces a transient response in the aggressor line whose magnitude is $|w_1(x,t) - w_2(x,t)|$, when it is switched at $t = \delta$. In both cases, the steady state solution is started in each line when its corresponding input switches.

$w_1$ and $w_2$ used in expression (7.1) and (7.2) can be calculated for the following two cases:

### 7.2.1.1 Finite Line with Open end

For the finite line with open end, the vector $\mathbf{w}$ is given by

$$\mathbf{w_o} = \mu(t)\left(1 - \frac{4}{\pi}\sum_{i=1}^{\infty} a_i\, e^{-\frac{\alpha_i^2 t}{\lambda}}\sin \alpha_i x\right) \tag{7.3}$$

where $a_i = (2i-1)^{-1}$ and $\alpha_i = \pi(2i-1)/2L$.

The eigenvalues $\boldsymbol{\lambda}$ (used in (7.3)) are given below in the form of a column vector

$$\boldsymbol{\lambda} = \begin{bmatrix} RC_s \\ R(C_s + 2C_c) \end{bmatrix} \tag{7.4}$$

### 7.2.1.2 Finite Line with Capacitive Load

Similarly, the vector $\mathbf{w}$ for finite lines with capacitive loads connected at their output is given by

$$\mathbf{w_C} = 1 - \sum_{i=1}^{\infty} \mathbf{A}_i\, e^{-\frac{\alpha_i^2 t}{\lambda}}\sin \boldsymbol{\alpha}_i x \tag{7.5}$$

The coefficients of the series are given below

$$A_i = \frac{2(\alpha_i^2 + \xi^2)}{\alpha_i[L(\alpha_i^2 + \xi^2) + \xi]} \tag{7.6}$$

where the parameter $\xi \equiv \lambda/C_L$ and is related to $\propto$ through the following equation

$$\propto \tan(\propto L) = \xi \tag{7.7}$$

There are an infinite number of such roots from which we only need to choose the positive ones as the proposed solution is an even function. The periodicity of the tangent function implies that the i-th root is within $\frac{\pi(i-1)}{L} < \alpha_i < \frac{\pi(2i-1)}{2L}$ for $i \geq 1$ and so numerical solutions can be easily found by the bisection method.

### 7.2.2 Model Validation

For the validation of the proposed model, we consider victim and aggressor line configuration of Figure 7.1. The interconnects of length 1mm from 25 nm technology generation have been used having $R = 867.6\Omega, C_g = 22.3\, pF, C_c = 88.8\, pF$. The victim and aggressor lines are excited by the step inputs and the signal on the victim line appears 0.1 nsec later than the signal on the aggressor line. The response of the system using our model for the finite line with open end is shown in Figure 7.2 and 7.3 for the up / up and up / down transitions respectively. HSPICE simulation results are also shown in the same figures. The curves clearly show that the model accurately matches with the simulation results and confirms its validity.
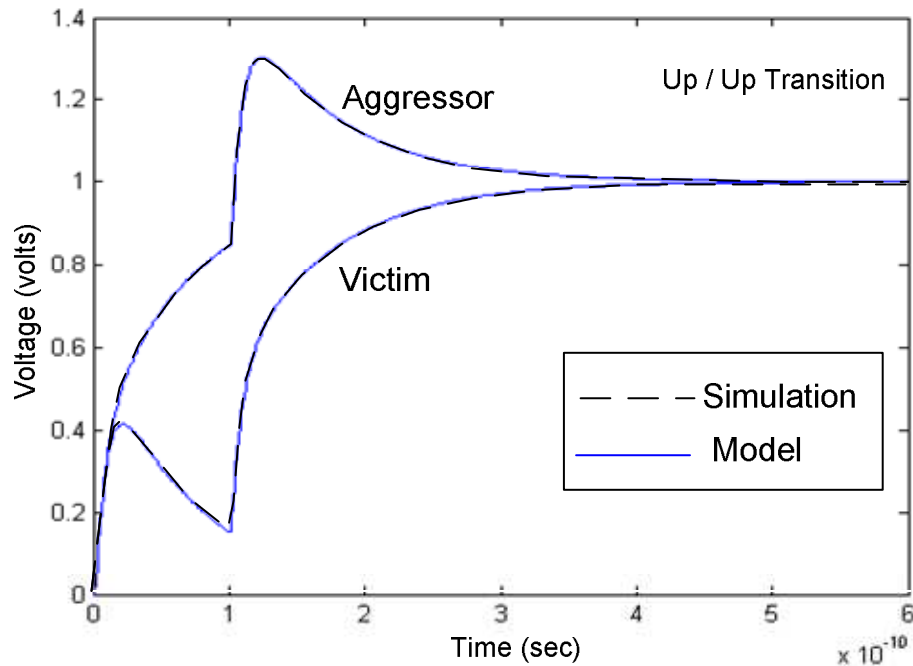
Figure 7.2: Typical responses of aggressor and victim lines during up/up transitions for finite lines with open ends.
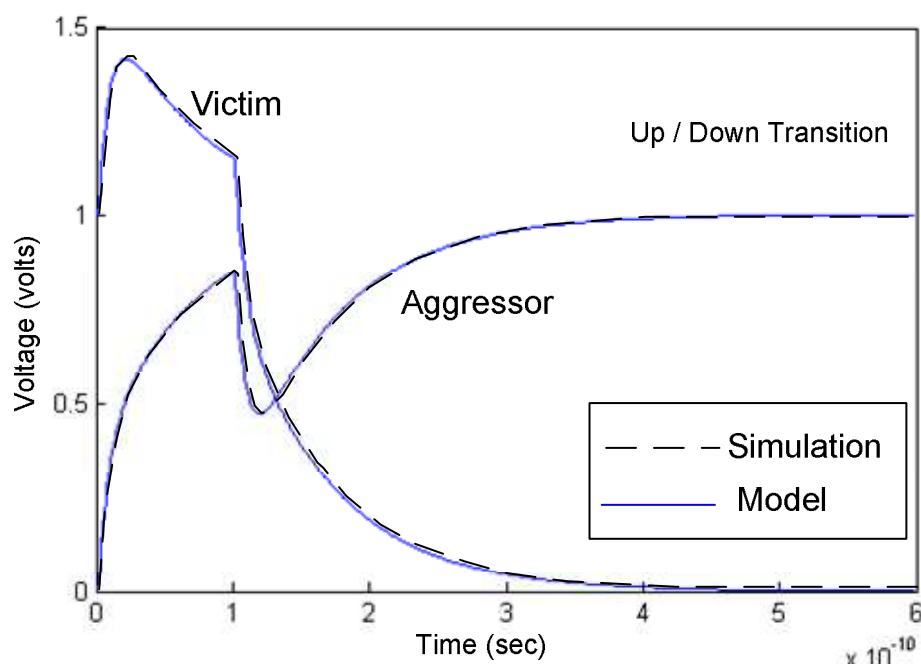


Figure 7.3: Typical responses of aggressor and victim lines during up/down transitions for finite lines with open ends.

Similarly, the response of the model for finite lines with capacitive loads is plotted in Figure 7.4 and 7.5 for the up / up and up / down transitions respectively. Again the responses accurately match the simulation results shown along with the model curves.

146
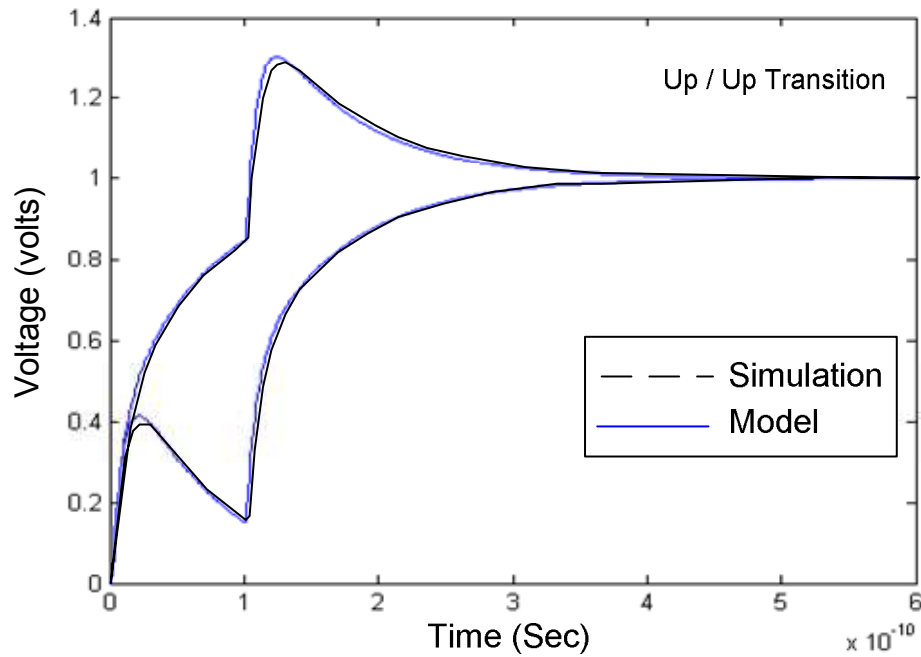
Figure 7.4: Typical responses of aggressor and victim lines during up/up transitions for finite lines with capacitive loads.
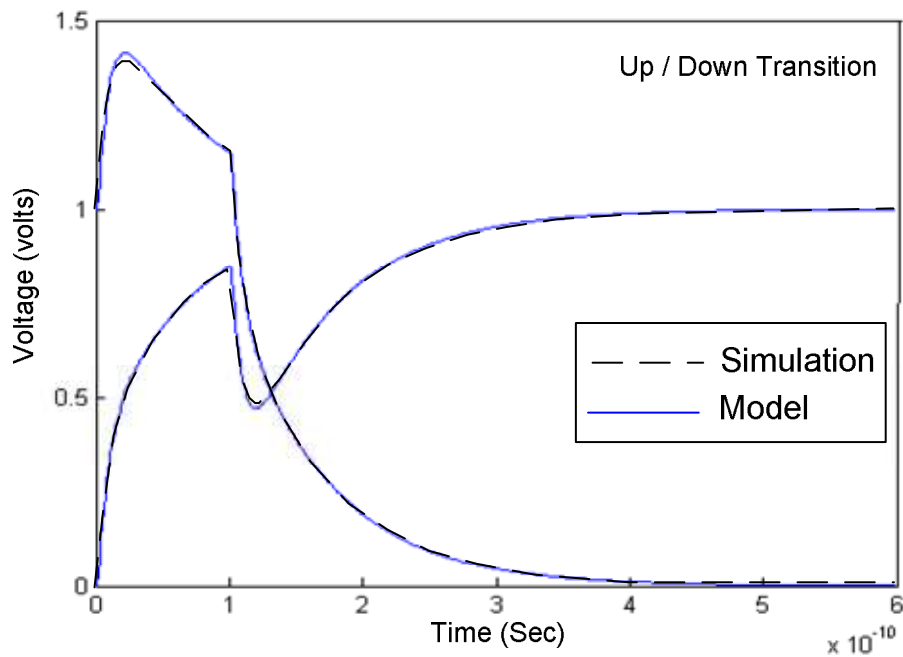


Figure 7.5: Typical responses of aggressor and victim lines during up/down transitions for finite lines with capacitive loads.

## 7.3 Skew Amplification under Variability

As mentioned before, the skew amplification is defined as the ratio between the input and output skew. The analytical model and the plots show that the arrival time of the signals at

147

the output of the victim line depends on the input skew. The arrival time will be maximized (or minimized) when the skew in its driver occurs at the same time at which the aggressor line has managed to couple the maximum amount of energy into the victim. Under this condition, the input skew is amplified at the far end of the interconnect. Now, in a particular circuit configuration, if the signal transitions in the aggressor and victim lines always occur such that this condition is satisfied then a constant skew will be observed at the output of the channel. However, in the presence of variability, the output skew (and hence the skew amplification) will be in the form of a probability distribution. Therefore, under this condition, the uncertainty in the arrival time will also be amplified. As stated before, analytical expressions are being developed to determine the conditions and also to quantify the effects. In order to emphasise its significance, a case study is given below.

We consider three coupled interconnects such that the victim line is surrounded by two aggressor lines. The resistance, self capacitance and coupling capacitance of the interconnect lines are taken to be 92.22 ohms/mm, 126.99 fF/mm and 39.26 fF/mm respectively. The supply voltage is taken to be 1.15V. The system response can either be measured using our proposed model or using simulations. Here we used Monte Carlo simulation method to incorporate the variability effects. We assume that due to variability the arrival time of the signals at the input of the victim line driver follows a normal distribution with standard deviation equal to 3ps. The system response has been measured corresponding to different values of input skew (taken as the time between the aggressor switching and mean of the arrival time distribution for the victim line). The delay measurements have been taken between the input and output of the victim line corresponding to 95% of the voltage levels. The results are shown in Table 7.1.

The victim delay has been measured in the absence of X-talk for reference and is about 81.34ps. Then an input signal is applied on the victim line with input skew=0 and standard deviation of the input delay=3ps. In order to simulate the in-phase X-talk situation, both aggressors were allowed to switch simultaneously in-phase with the victim line. It has been observed that the mean delay reduces to 72.25ps due to in-phase crosstalk. However, variability of 3ps in the input signal is amplified by 20.83% as the variability in the output signal increases to 3.625ps. However, the amplification in the delay variability reduces as the input skew is either increased or decreased from the zero value.

Similar experiments were repeated to measure the effect on delay variability due to out-of-phase crosstalk. It may be noted that the input delay variability is amplified as the input

skew increases from negative values. The negative values of offset shows the situation when the aggressor switches prior to the victim switching. An amplification of input delay variability up to 43.46% has been observed with input skew of 60ps.

Table 7.1: Monte Carlo simulation results for studying the effect of input signal variability on skew amplification.

| No X-talk | | In-Phase X-Talk | | | Out of phase X-talk. | | |
|---|---|---|---|---|---|---|---|
| Mean delay (ps) | Input Skew (ps) | Mean delay (ps) | Increased stdev(ps) | % age increase | Mean delay (ps) | Increased stdev(ps) | % age increase |
| 81.34 | 60 | | | | 105.9 | 1.304 | 43.46 |
| 81.34 | 50 | 63.78 | 0.863 | 28.76 | 101.48 | 1.216 | 40.53 |
| 81.34 | 40 | 65.513 | 0.844 | 28.13 | 98.21 | 1.019 | 33.96 |
| 81.34 | 30 | 68.17 | 0.470 | 15.66 | 95.4 | 0.696 | 23.20 |
| 81.34 | 20 | 69.07 | 0.227 | 7.56 | 93.15 | 0.572 | 19.06 |
| 81.34 | 10 | 70.26 | 0.483 | 16.10 | 91.14 | 0.606 | 20.20 |
| 81.34 | 0 | 72.24 | 0.625 | 20.83 | 89.09 | 0.543 | 18.10 |
| 81.34 | -10 | 70.26 | 0.480 | 16.00 | 87.27 | 0.44 | 14.66 |
| 81.34 | -20 | 76.32 | 0.460 | 15.33 | 85.82 | 0.375 | 12.50 |
| 81.34 | -30 | 77.722 | 0.316 | 10.53 | 84.71 | 0.284 | 9.46 |
| 81.34 | -40 | 78.744 | 0.254 | 8.466 | 83.82 | 0.217 | 7.23 |
| 81.34 | -50 | 79.46 | 0.184 | 6.133 | 83.07 | 0.173 | 5.70 |

## 7.4 Summary

In this chapter we have presented a crosstalk model that can be used to accurately describe the signals in the aggressor and victim lines under crosstalk effects due to RC coupling. Then we have shown that under crosstalk conditions, the delay variability in the arrival times of the signals is also amplified and can result in increased failure rates.

# Chapter 8

# Conclusions and Future Work

## 8.1 Conclusions

Since variability is a major constraint in the design of state of the art systems, especially in deep sub-micron technologies, and technology scaling has caused communication to slow relative to computation. Future designs will require to enhance the on-chip communications while tolerating the inherent variability present in the system. Regardless of the communication architecture employed, this study has shown that variability in the communication infrastructures can compromise the ability to meet the designed targets, unless due attention to it is given during the design phase. In particular, we have critically examined the effect of device variability due to RDF on the performance of the basic elements of on-chip communication structures, such as tapered buffer drivers with different tapering factor, repeaters of different sizes, and data storage registers (FFs). FO4 delay measurements have also been taken, as representative of the logic circuitry and results can be used as a performance benchmark. The study revealed that RDF has significant impact on the performance of communication structures and their performance deteriorates very significantly with technology scaling from 25 to 13 nm.

A simple design methodology, scaling up of circuits in the critical paths can be employed to minimize the effects of device variability, in particular, since we have shown that this

trade-off is not linear and a small increase in the repeater size can give substantial benefits towards performance. In a real system, however, the power and area penalties due to this passive technique of circuit scaling should be compared with any active countermeasure techniques which can be used to mitigate the delay variability.

Although NoC is more robust against on-chip communication failure than simpler designs, we note that such occurrences have increased hyper-linearly (and will continue to do so) due to device variability. In order to evaluate the performance of a typical point-to-point link, we have derived analytical models to predict link failure probability (LFP) using the characterization data of the individual on-chip communication elements. The results show that link failure probability increases significantly with the increase of device variability and is a limiting factor in the maximum operating frequency of a synchronous link.

It has also been observed that the timing distributions of different communication circuits are non-Gaussian, especially for smaller geometries. We have extended the study of these distributions on flip-flops and flip-flop based pipelined circuits. The simulation data shows that the timing distributions of FFs are positively skewed (except for the hold time, which is negatively skewed) and present nonzero higher moments, such as Kurtosis, which increase as the technology scales. The accurate estimation of the shape of the distributions, especially in the tail sections, is of great importance for large circuit designs, to improve performance and reliability in the presence of variability. The use of Gaussian approximation is common in SSTA (mainly because the necessary SSTA operations are known and easy to compute). However, as this work shows, the real distributions of the timing parameters deviate significantly from normality in the region of interest (the tail of the distribution) and hence will ultimately produce inaccurate results. The use of the skew-normal distribution is an interesting alternative; however, it lacks enough degrees of freedom to fit the fourth moment of the distribution. Furthermore, it has been argued that the skewed distributions of arrival times are not represented accurately by it. Pearson and Johnson systems have enough degrees of freedom and can provide a very good fit to the timing distributions of FFs as shown in this thesis, and therefore their use during SSTA will provide improved results and significantly reduce the probability of yield loss. However, for this approach to be fully successful, it is required that different SSTA operations (e.g., SUM, MIN, or MAX) be analytically formulated for Pearson and Johnson systems, to allow efficient analysis.

The implications of skewed timing distributions on SSTA of pipelined circuits have also been discussed in this thesis. Due to skew in the timing distributions of FFs, the pipeline segment delay distributions are positively skewed about the mean and the degree of skewness increases with technology scaling. Therefore, in this situation determining the slowest pipeline segment (which determines the operating frequency of the pipeline) during SSTA using Clark's approximation is not a good choice and will give wrong results, which will result in yield loss. Again, the skew-normal distribution is not a very ideal choice for approximating the timing distributions in highly scaled device, especially where the device count on a chip has jumped to several billions of devices. This is because a small deviation of the approximation from the actual results will produce significant yield loss.

Power dissipation is an important design metric which plays a critical role in the design of on-chip communication architectures. The impact of technology scaling on power dissipation of buffers has been investigated in this thesis. The results show that the relative proportion of different components of power dissipation is changing and leakage power is emerging as a serious problem in the design of high performance and power optimal chips. Therefore, design methodologies should consider individual components of power dissipation along with the total power. Wider point-to-point links which are preferred for better latency, will consume more power due to higher leakage currents at low activity levels.

The variability in the devices which is affecting the delay characteristics is also effecting the distribution of power dissipation. Since there is an inverse correlation between delay performance and leakage power, a significant asymmetry has also been observed in the distribution of leakage power. This in turn, will badly affect the yield in addition to delay variability. Therefore, it will be more advantageous to consider power variability along with delay variability while making different circuit optimizations. Active countermeasures, such as the use of sleep transistors, could be a possible solution against leakage power.

In this thesis we emphasize that due to variability, power and area optimal repeater insertion methodologies should also consider variability in their optimization methodology. Analytical models for area, power, performance and probability of link failure have been presented in terms of the size of the repeaters and inter-repeater segment length. It has been found that beyond a certain reduction in the size of the repeaters, the delay variability may exceed acceptable limits while still satisfying other constraints. For instance, with only 4%

of performance loss due to the use of smaller repeaters, almost 30% of power and 40% of area savings can be achieved; however timing certainty is reduced by 24%. Therefore, while optimizing area, power and performance of on-chip communication links, delay (and power) variability should also be included in the figure of merit; performance and area alone are no longer a suitable metric.

The performance of multi-bit parallel links under the impact of variability has also been discussed in this thesis. Based on the simulation data, optimum channel configuration for maximum bandwidth has been determined under area and power constraints. It has been found that delay variability also depends on the channel configuration (interconnect width and spacing) and so it determines the link operating frequency and the link failure probability. Moreover, the link failure probability also increases under variability as the number of lines in the channel increases. We have also compared the performance of parallel and semi-serial (serial) links for a particular throughput under some area constraint. This thesis proposes the use of semi-serial links for power efficient and fault tolerant links; these also have the additional benefit of less vulnerability to crosstalk effects due to larger interconnect spacing. Moreover, it has also been shown that leakage power becomes an important component of power dissipation for the links operating at low activity level and therefore this aspect needs to be considered in the link optimization methodology.

In DSM technologies, the effects of crosstalk cannot be avoided and crosstalk severely affects the performance of data links. Analytical models have been presented in this thesis that can be used for accurate analysis of crosstalk effects in RC coupled interconnects. The simulation results confirm their validity for different channel configurations. The models are computationally efficient, more accurate and give direct outputs in the time domain. These models can be very effective for the design of variability tolerant links. This work also shows that crosstalk increases the input skew as well as skew variability.

## 8.2 Future Work

Although the research work that was undertaken in the beginning is extensive for this thesis, there are still several dimensions in which this research can be extended. The suggested areas for future work are as follows:

- The variability effects due to other sources can also be considered to evaluate the performance of on-chip communication architectures in DSM region.

- Using the characterization data of communication structures and applying methods proposed in this thesis, variability tolerant network-on-chip can be designed along with its performance evaluation with different network topologies.

- Complete set of statistical analysis tools can be developed that could work with skewed distributions of Pearson and Johnson systems for the accurate statistical static timing analysis (SSTA) in deep submicron technologies.

- It would be an interesting area of research to devise active fault tolerant techniques that could effectively minimize the communication errors against increased level of variability in DSM circuits. Similarly, there is a need to develop circuit level techniques which could reduce leakage power, being a significant component of power dissipation in future technologies.

# Appendix A

The following tables are related to Chapter 6

Table A.1: Mean delay (in picoseconds) of interconnects (without repeaters) in the channel bus of 13nm for different geometrical configurations under variability Case 1. The columns of the table show the interconnect spacing and the rows show the width.

| S/W | 1X | 2X | 3X | 4X | 5X | 6X | 7X | 8X | 9X | 10X |
|-----|-----|-----|-----|-----|-----|-----|-----|-----|-----|-----|
| 1X | 180.7 | 121.4 | 107.4 | 102.1 | 99.53 | 97.95 | 97.01 | 96.46 | 95.98 | 95.59 |
| 2X | 97.51 | 67.25 | 60.27 | 57.6 | 56.29 | 55.52 | 55.08 | 54.66 | 54.49 | 54.24 |
| 3X | 69.81 | 49.32 | 44.57 | 42.79 | 41.93 | 41.41 | 41.08 | 40.86 | 40.7 | 40.53 |
| 4X | 55.92 | 40.36 | 36.75 | 35.38 | 34.72 | 34.33 | 34.08 | 33.93 | 33.79 | 33.69 |
| 5X | 47.59 | 34.95 | 32.05 | 30.96 | 30.4 | 30.09 | 29.89 | 29.73 | 29.67 | 29.58 |
| 6X | 42.08 | 31.39 | 28.95 | 28.00 | 27.53 | 27.27 | 27.09 | 26.97 | 26.9 | 26.84 |
| 7X | 38.11 | 28.84 | 26.66 | 25.87 | 25.47 | 25.24 | 25.13 | 25.03 | 24.93 | 24.87 |
| 8X | 35.15 | 26.92 | 25.02 | 24.31 | 23.96 | 23.72 | 23.6 | 23.55 | 23.45 | 23.4 |
| 9X | 32.82 | 25.41 | 23.71 | 23.05 | 22.75 | 22.58 | 22.48 | 22.39 | 22.33 | 22.26 |
| 10X | 30.97 | 24.23 | 22.68 | 22.08 | 21.79 | 21.63 | 21.51 | 21.46 | 21.4 | 21.36 |

Table A.2: The standard deviation (in picoseconds) of the delay of interconnects (without repeaters) in the channel bus of 13nm for different geometrical configurations under variability Case 1.

| S/W | 1X | 2X | 3X | 4X | 5X | 6X | 7X | 8X | 9X | 10X |
|-----|-----|-----|-----|-----|-----|-----|-----|-----|-----|-----|
| 1X | 10.94 | 5.95 | 5.14 | 4.98 | 4.84 | 4.79 | 4.78 | 4.74 | 4.72 | 4.72 |
| 2X | 4.27 | 1.93 | 1.85 | 1.79 | 1.78 | 1.79 | 1.78 | 1.77 | 1.79 | 1.77 |
| 3X | 2.65 | 1.28 | 1.27 | 1.28 | 1.29 | 1.28 | 1.28 | 1.25 | 1.28 | 1.24 |
| 4X | 2.03 | 1.05 | 1.08 | 1.08 | 1.09 | 1.11 | 1.10 | 1.08 | 1.10 | 1.09 |
| 5X | 1.67 | 0.96 | 1.00 | 1.00 | 1.02 | 1.03 | 1.02 | 1.00 | 1.02 | 1.00 |
| 6X | 1.47 | 0.90 | 0.93 | 0.93 | 0.96 | 0.95 | 0.95 | 0.94 | 0.96 | 0.95 |
| 7X | 1.29 | 0.87 | 0.89 | 0.91 | 0.93 | 0.92 | 0.92 | 0.91 | 0.91 | 0.91 |
| 8X | 1.22 | 0.85 | 0.87 | 0.88 | 0.89 | 0.87 | 0.89 | 0.89 | 0.88 | 0.88 |
| 9X | 1.11 | 0.83 | 0.84 | 0.85 | 0.87 | 0.87 | 0.87 | 0.88 | 0.85 | 0.86 |
| 10X | 1.05 | 0.81 | 0.83 | 0.84 | 0.85 | 0.84 | 0.85 | 0.85 | 0.85 | 0.85 |

Table A.3: Delay variability (%) of interconnects (without repeaters) in the channel bus of 13nm for different geometrical configurations under variability Case 1.

| S/W | 1X | 2X | 3X | 4X | 5X | 6X | 7X | 8X | 9X | 10X |
|-----|-----|-----|-----|-----|-----|-----|-----|-----|-----|-----|
| 1X | 18.16 | 14.7 | 14.35 | 14.65 | 14.59 | 14.67 | 14.78 | 14.74 | 14.75 | 14.81 |
| 2X | 13.12 | 8.632 | 9.219 | 9.322 | 9.5 | 9.686 | 9.68 | 9.718 | 9.837 | 9.776 |
| 3X | 11.4 | 7.81 | 8.554 | 8.955 | 9.199 | 9.276 | 9.328 | 9.211 | 9.42 | 9.202 |
| 4X | 10.89 | 7.793 | 8.826 | 9.154 | 9.436 | 9.671 | 9.657 | 9.536 | 9.747 | 9.717 |
| 5X | 10.51 | 8.241 | 9.317 | 9.736 | 10.08 | 10.22 | 10.26 | 10.1 | 10.27 | 10.17 |
| 6X | 10.46 | 8.587 | 9.671 | 9.989 | 10.47 | 10.49 | 10.56 | 10.47 | 10.67 | 10.64 |
| 7X | 10.19 | 9.024 | 10.05 | 10.54 | 10.95 | 10.89 | 11.03 | 10.88 | 10.94 | 11.02 |
| 8X | 10.38 | 9.453 | 10.45 | 10.85 | 11.13 | 10.98 | 11.3 | 11.31 | 11.29 | 11.33 |
| 9X | 10.14 | 9.847 | 10.68 | 11.08 | 11.46 | 11.5 | 11.58 | 11.76 | 11.48 | 11.54 |
| 10X | 10.13 | 9.974 | 11.01 | 11.47 | 11.71 | 11.7 | 11.91 | 11.84 | 11.93 | 11.87 |

Table A.4: The size of the repeaters for different interconnect dimensions (width and spacing) for a 13 nm bus under worst crosstalk. The repeater sizes have been rounded-off.

| S/W | 1X | 2X | 3X | 4X | 5X | 6X | 7X | 8X | 9X | 10X |
|-----|-----|-----|-----|-----|-----|-----|-----|-----|-----|-----|
| 1X | 266 | 199 | 172 | 157 | 148 | 141 | 136 | 133 | 130 | 128 |
| 2X | 384 | 289 | 252 | 231 | 218 | 209 | 203 | 198 | 194 | 192 |
| 3X | 479 | 364 | 319 | 294 | 278 | 267 | 260 | 254 | 250 | 247 |
| 4X | 563 | 431 | 379 | 351 | 333 | 321 | 313 | 306 | 302 | 298 |
| 5X | 640 | 494 | 436 | 405 | 386 | 373 | 363 | 356 | 351 | 347 |
| 6X | 713 | 553 | 491 | 458 | 436 | 422 | 412 | 405 | 399 | 395 |
| 7X | 783 | 611 | 545 | 508 | 486 | 471 | 460 | 452 | 446 | 442 |
| 8X | 850 | 667 | 597 | 558 | 535 | 519 | 508 | 499 | 493 | 488 |
| 9X | 916 | 722 | 648 | 608 | 583 | 566 | 554 | 546 | 539 | 534 |
| 10X | 980 | 776 | 698 | 656 | 630 | 613 | 601 | 592 | 585 | 579 |

Table A.5: The number repeaters per unit length required for different interconnect dimensions (width and spacing) for a 13 nm bus under worst crosstalk. The numbers have been rounded-off.

| S/W | 1X | 2X | 3X | 4X | 5X | 6X | 7X | 8X | 9X | 10X |
|-----|-----|-----|-----|-----|-----|-----|-----|-----|-----|-----|
| 1X | 30 | 23 | 20 | 18 | 17 | 17 | 16 | 16 | 15 | 15 |
| 2X | 22 | 16 | 14 | 13 | 13 | 12 | 12 | 12 | 12 | 11 |
| 3X | 18 | 14 | 12 | 11 | 11 | 10 | 10 | 10 | 10 | 9 |
| 4X | 16 | 12 | 11 | 10 | 10 | 9 | 9 | 9 | 9 | 9 |
| 5X | 15 | 11 | 10 | 9 | 9 | 9 | 9 | 8 | 8 | 8 |
| 6X | 13 | 11 | 10 | 9 | 9 | 8 | 8 | 8 | 8 | 8 |
| 7X | 13 | 10 | 9 | 9 | 8 | 8 | 8 | 8 | 8 | 8 |
| 8X | 12 | 10 | 9 | 8 | 8 | 8 | 8 | 7 | 7 | 7 |
| 9X | 12 | 9 | 8 | 8 | 8 | 7 | 7 | 7 | 7 | 7 |
| 10X | 11 | 9 | 8 | 8 | 7 | 7 | 7 | 7 | 7 | 7 |

Table A.6: Mean delay (in picoseconds) of interconnects (with repeaters) in the channel bus of 13nm for different geometrical configurations under variability Case 1.

| S/W | 1X | 2X | 3X | 4X | 5X | 6X | 7X | 8X | 9X | 10X |
|-----|-----|-----|-----|-----|-----|-----|-----|-----|-----|-----|
| 1X | 70.57 | 52.95 | 45.93 | 42.08 | 39.65 | 37.99 | 36.83 | 35.97 | 35.3 | 34.77 |
| 2X | 50.91 | 38.49 | 33.65 | 30.99 | 29.31 | 28.18 | 27.39 | 26.77 | 26.33 | 25.97 |
| 3X | 42.37 | 32.31 | 28.4 | 26.27 | 24.94 | 24.05 | 23.41 | 22.93 | 22.58 | 22.28 |
| 4X | 37.38 | 28.73 | 25.39 | 23.57 | 22.44 | 21.68 | 21.14 | 20.74 | 20.44 | 20.2 |
| 5X | 34.03 | 26.34 | 23.39 | 21.79 | 20.79 | 20.13 | 19.65 | 19.3 | 19.04 | 18.83 |
| 6X | 31.62 | 24.63 | 21.96 | 20.52 | 19.62 | 19.02 | 18.6 | 18.29 | 18.05 | 17.87 |
| 7X | 29.76 | 23.32 | 20.87 | 19.55 | 18.74 | 18.19 | 17.81 | 17.53 | 17.31 | 17.14 |
| 8X | 28.31 | 22.3 | 20.02 | 18.81 | 18.05 | 17.54 | 17.19 | 16.94 | 16.73 | 16.58 |
| 9X | 27.09 | 21.46 | 19.34 | 18.19 | 17.5 | 17.03 | 16.71 | 16.46 | 16.28 | 16.12 |
| 10X | 26.1 | 20.77 | 18.77 | 17.7 | 17.04 | 16.6 | 16.29 | 16.07 | 15.89 | 15.76 |

Table A.7: The standard deviation (in picoseconds) of the delay of interconnects (with repeaters) in the channel bus.

| S/W | 1X | 2X | 3X | 4X | 5X | 6X | 7X | 8X | 9X | 10X |
|-----|------|------|------|------|------|------|------|------|------|------|
| 1X | 2.384 | 1.412 | 1.133 | 1.011 | 0.935 | 0.894 | 0.874 | 0.854 | 0.837 | 0.829 |
| 2X | 1.338 | 0.581 | 0.445 | 0.387 | 0.363 | 0.36 | 0.353 | 0.354 | 0.359 | 0.358 |
| 3X | 0.998 | 0.39 | 0.289 | 0.258 | 0.254 | 0.256 | 0.26 | 0.261 | 0.272 | 0.27 |
| 4X | 0.851 | 0.317 | 0.233 | 0.217 | 0.22 | 0.229 | 0.237 | 0.242 | 0.25 | 0.256 |
| 5X | 0.747 | 0.278 | 0.213 | 0.205 | 0.216 | 0.225 | 0.234 | 0.238 | 0.248 | 0.251 |
| 6X | 0.687 | 0.256 | 0.207 | 0.201 | 0.214 | 0.222 | 0.233 | 0.238 | 0.249 | 0.253 |
| 7X | 0.624 | 0.244 | 0.201 | 0.205 | 0.22 | 0.226 | 0.237 | 0.242 | 0.248 | 0.256 |
| 8X | 0.594 | 0.234 | 0.205 | 0.208 | 0.219 | 0.225 | 0.239 | 0.246 | 0.251 | 0.257 |
| 9X | 0.552 | 0.235 | 0.208 | 0.208 | 0.223 | 0.233 | 0.242 | 0.252 | 0.251 | 0.258 |
| 10X | 0.523 | 0.228 | 0.206 | 0.215 | 0.227 | 0.234 | 0.247 | 0.251 | 0.258 | 0.262 |

Table A.8: Delay variability (%) of interconnects (with repeaters) in the channel bus of 13nm for different geometrical configurations under variability Case 1.

| S/W | 1X | 2X | 3X | 4X | 5X | 6X | 7X | 8X | 9X | 10X |
|-----|------|------|------|------|------|------|------|------|------|------|
| 1X | 10.13 | 8.003 | 7.398 | 7.208 | 7.074 | 7.062 | 7.12 | 7.12 | 7.112 | 7.15 |
| 2X | 7.881 | 4.527 | 3.964 | 3.745 | 3.717 | 3.828 | 3.866 | 3.962 | 4.084 | 4.133 |
| 3X | 7.067 | 3.619 | 3.049 | 2.943 | 3.051 | 3.194 | 3.334 | 3.408 | 3.612 | 3.631 |
| 4X | 6.829 | 3.31 | 2.75 | 2.763 | 2.939 | 3.172 | 3.36 | 3.496 | 3.672 | 3.805 |
| 5X | 6.585 | 3.163 | 2.726 | 2.826 | 3.117 | 3.349 | 3.577 | 3.705 | 3.913 | 3.993 |
| 6X | 6.514 | 3.117 | 2.821 | 2.931 | 3.276 | 3.506 | 3.763 | 3.91 | 4.134 | 4.255 |
| 7X | 6.295 | 3.134 | 2.894 | 3.145 | 3.517 | 3.723 | 3.989 | 4.135 | 4.299 | 4.472 |
| 8X | 6.297 | 3.148 | 3.07 | 3.319 | 3.633 | 3.839 | 4.172 | 4.361 | 4.506 | 4.652 |
| 9X | 6.11 | 3.279 | 3.23 | 3.436 | 3.817 | 4.11 | 4.344 | 4.595 | 4.632 | 4.798 |
| 10X | 6.009 | 3.294 | 3.285 | 3.636 | 3.997 | 4.222 | 4.54 | 4.692 | 4.877 | 4.987 |

Table A.9: Bandwidth of the individual interconnect lines (without repeaters) in Gb/s given as a function of the interconnect width and spacing for 13 nm.

| S/W | 1X | 2X | 3X | 4X | 5X | 6X | 7X | 8X | 9X | 10X |
|-----|------|------|------|------|------|------|------|------|------|------|
| 1X | 0.615 | 0.915 | 1.035 | 1.088 | 1.116 | 1.134 | 1.145 | 1.152 | 1.158 | 1.162 |
| 2X | 1.14 | 1.652 | 1.844 | 1.929 | 1.974 | 2.001 | 2.017 | 2.033 | 2.039 | 2.048 |
| 3X | 1.592 | 2.253 | 2.493 | 2.597 | 2.65 | 2.683 | 2.705 | 2.72 | 2.73 | 2.742 |
| 4X | 1.987 | 2.753 | 3.024 | 3.141 | 3.2 | 3.236 | 3.26 | 3.275 | 3.288 | 3.298 |
| 5X | 2.335 | 3.179 | 3.467 | 3.589 | 3.655 | 3.692 | 3.718 | 3.737 | 3.746 | 3.757 |
| 6X | 2.641 | 3.54 | 3.838 | 3.968 | 4.036 | 4.074 | 4.102 | 4.12 | 4.13 | 4.14 |
| 7X | 2.916 | 3.853 | 4.168 | 4.295 | 4.362 | 4.402 | 4.422 | 4.439 | 4.458 | 4.468 |
| 8X | 3.161 | 4.127 | 4.44 | 4.571 | 4.638 | 4.683 | 4.707 | 4.718 | 4.738 | 4.748 |
| 9X | 3.385 | 4.374 | 4.687 | 4.82 | 4.884 | 4.921 | 4.943 | 4.963 | 4.975 | 4.991 |
| 10X | 3.588 | 4.585 | 4.9 | 5.032 | 5.1 | 5.138 | 5.165 | 5.178 | 5.193 | 5.202 |

Table A.10: Bandwidth of the individual interconnect lines (with repeaters) in Gb/s given as a function of the interconnect width and spacing for 13 nm.

| S/W | 1X | 2X | 3X | 4X | 5X | 6X | 7X | 8X | 9X | 10X |
|---|---|---|---|---|---|---|---|---|---|---|
| **1X** | 1.574 | 2.099 | 2.419 | 2.641 | 2.802 | 2.925 | 3.017 | 3.089 | 3.147 | 3.195 |
| **2X** | 2.183 | 2.887 | 3.302 | 3.586 | 3.79 | 3.943 | 4.057 | 4.15 | 4.219 | 4.279 |
| **3X** | 2.622 | 3.439 | 3.912 | 4.229 | 4.454 | 4.621 | 4.747 | 4.845 | 4.922 | 4.986 |
| **4X** | 2.972 | 3.867 | 4.377 | 4.714 | 4.951 | 5.125 | 5.256 | 5.356 | 5.437 | 5.501 |
| **5X** | 3.265 | 4.218 | 4.751 | 5.099 | 5.343 | 5.521 | 5.654 | 5.756 | 5.835 | 5.9 |
| **6X** | 3.514 | 4.511 | 5.059 | 5.415 | 5.663 | 5.841 | 5.975 | 6.076 | 6.155 | 6.219 |
| **7X** | 3.734 | 4.764 | 5.324 | 5.682 | 5.93 | 6.108 | 6.238 | 6.337 | 6.419 | 6.482 |
| **8X** | 3.925 | 4.983 | 5.549 | 5.908 | 6.155 | 6.334 | 6.464 | 6.56 | 6.641 | 6.703 |
| **9X** | 4.101 | 5.179 | 5.746 | 6.107 | 6.351 | 6.524 | 6.651 | 6.75 | 6.826 | 6.891 |
| **10X** | 4.257 | 5.349 | 5.919 | 6.278 | 6.521 | 6.694 | 6.822 | 6.916 | 6.992 | 7.052 |

Table A.11: Total bandwidth (Gb/s) through the bus constrained in channel width $W_c$, without repeaters in 13nm.

| S/W | 1X | 2X | 3X | 4X | 5X | 6X | 7X | 8X | 9X | 10X |
|---|---|---|---|---|---|---|---|---|---|---|
| **1X** | 78.70 | 78.10 | 66.23 | 55.72 | 47.63 | 41.49 | 36.65 | 32.77 | 29.64 | 27.05 |
| **2X** | 97.62 | 106.16 | 94.77 | 82.62 | 72.47 | 64.29 | 57.60 | 52.24 | 47.64 | 43.87 |
| **3X** | 102.66 | 116.26 | 107.21 | 95.70 | 85.46 | 76.92 | 69.78 | 63.78 | 58.69 | 54.41 |
| **4X** | 102.93 | 118.83 | 111.88 | 101.69 | 92.10 | 83.82 | 76.76 | 70.68 | 65.51 | 61.01 |
| **5X** | 101.18 | 118.09 | 112.66 | 103.69 | 95.03 | 87.27 | 80.55 | 74.75 | 69.56 | 65.12 |
| **6X** | 98.46 | 115.49 | 111.31 | 103.56 | 95.76 | 88.60 | 82.35 | 76.80 | 71.86 | 67.53 |
| **7X** | 95.49 | 112.17 | 109.20 | 102.31 | 95.24 | 88.72 | 82.76 | 77.53 | 72.99 | 68.86 |
| **8X** | 92.37 | 108.54 | 106.17 | 100.17 | 93.84 | 87.98 | 82.54 | 77.55 | 73.30 | 69.38 |
| **9X** | 89.38 | 104.96 | 103.12 | 97.89 | 92.10 | 86.61 | 81.56 | 77.07 | 72.97 | 69.35 |
| **10X** | 86.43 | 101.25 | 99.88 | 95.24 | 90.09 | 85.10 | 80.51 | 76.24 | 72.43 | 68.93 |

Table A.12: Total bandwidth (Gb/s) through the bus constrained in channel width $W_c$, with repeaters in 13nm.

| S/W | 1X | 2X | 3X | 4X | 5X | 6X | 7X | 8X | 9X | 10X |
|---|---|---|---|---|---|---|---|---|---|---|
| **1X** | 201.5 | 179.1 | 154.8 | 135.2 | 119.6 | 107.0 | 96.6 | 87.9 | 80.6 | 74.4 |
| **2X** | 187.0 | 185.5 | 169.7 | 153.6 | 139.2 | 126.7 | 115.9 | 106.7 | 98.6 | 91.6 |
| **3X** | 169.1 | 177.5 | 168.2 | 155.9 | 143.7 | 132.5 | 122.5 | 113.6 | 105.8 | 99.0 |
| **4X** | 154.0 | 166.9 | 162.0 | 152.6 | 142.5 | 132.7 | 123.8 | 115.6 | 108.3 | 101.8 |
| **5X** | 141.5 | 156.7 | 154.4 | 147.3 | 138.9 | 130.5 | 122.5 | 115.1 | 108.4 | 102.3 |
| **6X** | 131.0 | 147.2 | 146.7 | 141.3 | 134.4 | 127.0 | 119.9 | 113.3 | 107.1 | 101.4 |
| **7X** | 122.3 | 138.7 | 139.5 | 135.3 | 129.5 | 123.1 | 116.7 | 110.7 | 105.1 | 99.9 |
| **8X** | 114.7 | 131.0 | 132.7 | 129.5 | 124.5 | 119.0 | 113.3 | 107.8 | 102.7 | 97.9 |
| **9X** | 108.3 | 124.3 | 126.4 | 124.0 | 119.8 | 114.8 | 109.7 | 104.8 | 100.1 | 95.7 |
| **10X** | 102.5 | 118.1 | 120.7 | 118.8 | 115.2 | 110.9 | 106.3 | 101.8 | 97.5 | 93.4 |

Table A.13: Power dissipation (mW) at maximum bandwidth for the interconnect of 13 nm technology without repeaters.

| S/W | 1X | 2X | 3X | 4X | 5X | 6X | 7X | 8X | 9X | 10X |
|-----|------|------|------|------|------|------|------|------|------|------|
| 1X | 10.13 | 6.29 | 4.46 | 3.43 | 2.78 | 2.34 | 2.01 | 1.77 | 1.58 | 1.43 |
| 2X | 13.38 | 9.33 | 7.06 | 5.67 | 4.74 | 4.07 | 3.57 | 3.19 | 2.87 | 2.62 |
| 3X | 14.90 | 11.08 | 8.77 | 7.25 | 6.19 | 5.42 | 4.82 | 4.34 | 3.95 | 3.63 |
| 4X | 15.78 | 12.21 | 9.95 | 8.43 | 7.32 | 6.49 | 5.84 | 5.30 | 4.87 | 4.50 |
| 5X | 16.33 | 13.01 | 10.84 | 9.34 | 8.23 | 7.38 | 6.69 | 6.13 | 5.66 | 5.26 |
| 6X | 16.71 | 13.58 | 11.52 | 10.06 | 8.97 | 8.12 | 7.42 | 6.84 | 6.35 | 5.93 |
| 7X | 16.99 | 14.03 | 12.07 | 10.66 | 9.60 | 8.75 | 8.04 | 7.46 | 6.95 | 6.52 |
| 8X | 17.20 | 14.38 | 12.52 | 11.17 | 10.13 | 9.29 | 8.59 | 8.00 | 7.50 | 7.06 |
| 9X | 17.35 | 14.68 | 12.90 | 11.61 | 10.59 | 9.76 | 9.08 | 8.49 | 7.98 | 7.54 |
| 10X | 17.49 | 14.92 | 13.23 | 11.97 | 10.99 | 10.19 | 9.52 | 8.93 | 8.42 | 7.98 |

Table A.14: Power dissipation (mW) at maximum bandwidth for the interconnect of 13 nm technology with repeaters.

| S/W | 1X | 2X | 3X | 4X | 5X | 6X | 7X | 8X | 9X | 10X |
|-----|------|------|------|------|------|------|------|------|------|------|
| 1X | 18.55 | 9.50 | 6.35 | 4.76 | 3.81 | 3.18 | 2.72 | 2.39 | 2.12 | 1.91 |
| 2X | 18.01 | 10.51 | 7.54 | 5.92 | 4.89 | 4.17 | 3.64 | 3.23 | 2.91 | 2.65 |
| 3X | 17.00 | 10.70 | 8.05 | 6.52 | 5.51 | 4.79 | 4.24 | 3.81 | 3.46 | 3.17 |
| 4X | 16.13 | 10.67 | 8.30 | 6.89 | 5.93 | 5.22 | 4.68 | 4.24 | 3.88 | 3.58 |
| 5X | 15.42 | 10.58 | 8.44 | 7.14 | 6.23 | 5.55 | 5.02 | 4.58 | 4.22 | 3.92 |
| 6X | 14.83 | 10.47 | 8.52 | 7.32 | 6.47 | 5.82 | 5.30 | 4.87 | 4.51 | 4.21 |
| 7X | 14.36 | 10.36 | 8.58 | 7.46 | 6.65 | 6.03 | 5.53 | 5.11 | 4.76 | 4.46 |
| 8X | 13.96 | 10.26 | 8.61 | 7.56 | 6.80 | 6.21 | 5.73 | 5.32 | 4.98 | 4.68 |
| 9X | 13.63 | 10.18 | 8.64 | 7.65 | 6.93 | 6.36 | 5.90 | 5.50 | 5.17 | 4.87 |
| 10X | 13.35 | 10.10 | 8.66 | 7.73 | 7.04 | 6.50 | 6.05 | 5.67 | 5.34 | 5.05 |

Table A.15: Total bandwidth per unit power (Gb/s.mW) consumption for interconnects with repeaters.

| S/W | 1X | 2X | 3X | 4X | 5X | 6X | 7X | 8X | 9X | 10X |
|-----|------|------|------|------|------|------|------|------|------|------|
| 1X | 10.86 | 18.84 | 24.37 | 28.38 | 31.38 | 33.66 | 35.43 | 36.83 | 37.95 | 38.85 |
| 2X | 10.38 | 17.64 | 22.5 | 25.95 | 28.47 | 30.37 | 31.83 | 32.98 | 33.89 | 34.63 |
| 3X | 9.947 | 16.59 | 20.89 | 23.89 | 26.06 | 27.67 | 28.9 | 29.85 | 30.61 | 31.23 |
| 4X | 9.545 | 15.65 | 19.51 | 22.14 | 24.03 | 25.42 | 26.46 | 27.27 | 27.91 | 28.43 |
| 5X | 9.176 | 14.81 | 18.29 | 20.63 | 22.29 | 23.49 | 24.4 | 25.11 | 25.65 | 26.1 |
| 6X | 8.831 | 14.06 | 17.21 | 19.31 | 20.78 | 21.84 | 22.64 | 23.26 | 23.73 | 24.11 |
| 7X | 8.513 | 13.38 | 16.27 | 18.15 | 19.46 | 20.41 | 21.11 | 21.65 | 22.08 | 22.42 |
| 8X | 8.216 | 12.77 | 15.41 | 17.12 | 18.3 | 19.16 | 19.79 | 20.26 | 20.64 | 20.94 |
| 9X | 7.942 | 12.21 | 14.64 | 16.2 | 17.28 | 18.04 | 18.61 | 19.04 | 19.38 | 19.65 |
| 10X | 7.684 | 11.69 | 13.94 | 15.38 | 16.36 | 17.05 | 17.57 | 17.96 | 18.26 | 18.5 |

Table A.16: Probability of link failure (in parts per thousand) of the individual lines of the channel under variability.

| S/W | 1X | 2X | 3X | 4X | 5X | 6X | 7X | 8X | 9X | 10X |
|---|---|---|---|---|---|---|---|---|---|---|
| 1X | 34.29 | 8.02 | 3.81 | 2.69 | 2.06 | 1.88 | 1.89 | 1.81 | 1.72 | 1.75 |
| 2X | 6.92 | 0.06 | 0.05 | 0.05 | 0.05 | 0.05 | 0.05 | 0.05 | 0.05 | 0.05 |
| 3X | 2.31 | 0.05 | 0.05 | 0.05 | 0.05 | 0.05 | 0.05 | 0.05 | 0.05 | 0.05 |
| 4X | 1.34 | 0.05 | 0.05 | 0.05 | 0.05 | 0.05 | 0.05 | 0.05 | 0.05 | 0.05 |
| 5X | 0.77 | 0.05 | 0.05 | 0.05 | 0.05 | 0.05 | 0.05 | 0.05 | 0.05 | 0.05 |
| 6X | 0.58 | 0.05 | 0.05 | 0.05 | 0.05 | 0.05 | 0.05 | 0.05 | 0.05 | 0.05 |
| 7X | 0.35 | 0.05 | 0.05 | 0.05 | 0.05 | 0.05 | 0.05 | 0.05 | 0.05 | 0.05 |
| 8X | 0.31 | 0.05 | 0.05 | 0.05 | 0.05 | 0.05 | 0.05 | 0.05 | 0.05 | 0.05 |
| 9X | 0.21 | 0.05 | 0.05 | 0.05 | 0.05 | 0.05 | 0.05 | 0.05 | 0.05 | 0.05 |
| 10X | 0.16 | 0.05 | 0.05 | 0.05 | 0.05 | 0.05 | 0.05 | 0.05 | 0.05 | 0.05 |

Table A.17: Probability of link failure (in parts per thousand) for the channel under area constraint.

| S/W | 1X | 2X | 3X | 4X | 5X | 6X | 7X | 8X | 9X | 10X |
|---|---|---|---|---|---|---|---|---|---|---|
| 1X | 988.51 | 496.90 | 216.64 | 128.74 | 84.38 | 66.34 | 58.87 | 50.19 | 43.21 | 40.02 |
| 2X | 448.43 | 3.69 | 2.73 | 2.27 | 1.94 | 1.70 | 1.51 | 1.36 | 1.24 | 1.14 |
| 3X | 138.36 | 2.73 | 2.28 | 1.95 | 1.71 | 1.52 | 1.37 | 1.24 | 1.14 | 1.05 |
| 4X | 67.18 | 2.28 | 1.96 | 1.71 | 1.52 | 1.37 | 1.25 | 1.14 | 1.06 | 0.98 |
| 5X | 32.93 | 1.97 | 1.72 | 1.53 | 1.38 | 1.25 | 1.15 | 1.06 | 0.98 | 0.92 |
| 6X | 21.48 | 1.73 | 1.54 | 1.38 | 1.26 | 1.15 | 1.06 | 0.99 | 0.92 | 0.86 |
| 7X | 11.53 | 1.54 | 1.39 | 1.26 | 1.16 | 1.07 | 0.99 | 0.93 | 0.87 | 0.82 |
| 8X | 9.11 | 1.39 | 1.27 | 1.16 | 1.07 | 1.00 | 0.93 | 0.87 | 0.82 | 0.78 |
| 9X | 5.47 | 1.27 | 1.17 | 1.08 | 1.00 | 0.93 | 0.87 | 0.82 | 0.78 | 0.74 |
| 10X | 3.90 | 1.17 | 1.08 | 1.00 | 0.94 | 0.88 | 0.83 | 0.78 | 0.74 | 0.71 |

# References

[1] Gordon E. Moore, "Cramming More Components onto Integrated Circuits", *Electronics*, Volume 38, Number 8, April 19, 1965.

[2] Ethiopia Enideg Nigussie, "Exploration and Design of High Performance Variation Tolerant On-Chip Interconnects," *Ph.D Thesis Turun Yliopisto University of Turku*, 2010.

[3] Marvell 88F6282 SoC data sheet. *Marvell ®*. Available online at:

http://www.datasheets.org.uk/88F6282-datasheet.html

[4] *International Technology Roadmap for Se*miconductor, Semiconductor Industry Association, 2003, http://www.itrs.net/

[5] J. W. McPherson, "Reliability challenges for 45nm and beyond," in *Proceedings of the 43rd Design Automation Conference*, pages 176– 181, July 2006.

[6] R. Ho, K. Mai, and M. Horowitz, "The future of wires," in *Proceedings of the IEEE*, 89(4):490–504, April 2001.

[7] S. Borkar, "Design challenges of technology scaling," *Micro, IEEE*, 19(4):23–29, 1999.

[8] Simon Ogg, "Serialization and Asynchronous Techniques for Reliable Network-on-Chip communication," *PhD. Thesis, Southampton University*, May 2009.

[9] H. Ron, M. Ken and M. Horowitz, "Managing wire scaling: a circuit perspective," in *Proc. of Interconnect Technology Conference*, 2003.

[10] N. Magen, A. Kolodny, U. Weiser, and N. Shamir, "Interconnect power dissipation in a microprocessor," in *IEEE/ACM International Workshop on System Level Interconnect Prediction*, pp. 7-13, Feb. 2004.

[11] T. Mudge, "Power: A first-class architectural design constraint," *IEEE Computer*, 34(4):52–58, April 2001.

[12] D. Blaauw, A. Devgan, F. Najm, "Leakage power: trends, analysis and avoidance," *Embedded Tutorial II, ASP-DAC* 2005.

[13] Y. Chen and S. Y. Kung, "Trend and Challenge on System-on-a-Chip designs," *Journal of Signal Processing systems*, vol. 53, issue 1-2, Nov. 2008.

[14] S. R. Nassif, "Model to Hardware Matching; For nanometer Scale Technologies," *International Conference on Simulation of Semiconductor Processes and Devices 2006*, pp. 5-8, Sept. 2006.

[15] Dennis Sylvestera, Kanak Agarwalb and Saumil Shaha, "Variability in nanometer CMOS: Impact, analysis, and minimization," *Integration, the VLSI Journal*, Vol. 41, No. 3, pp. 319-339, May 2008.

[16] S. Borkar, T. Karnik, S. Narendra, J. Tschanz, A. Keshavarzi, and V. De, "Parameter variations and impact on circuits and microarchitectures," in *Proc. of the Design Automation Conf.*, 2003, pp. 338–342.

[17] Asen Asenov, "Statistical device variability and its impact on yield and performance," *13th IEEE International On-Line Testing Symposium (IOLTS 2007).*

[18] H. Mahmoodi, S. Mukhopadhyay, and K. Roy, "Estimation of delay variations due to random-dopant fluctuations in nanoscale CMOS circuits," *IEEE J. Solid-State Circuits*, vol. 40, no. 9, pp. 1787–1796, Sep. 2005.

[19] Y. Li and C.-H. Hwang, "High-frequency characteristic fluctuations of nano-MOSFET circuit induced by random dopants," *IEEE Trans.Microw. Theory Tech.*, vol. 56, no. 12, pp. 2726–2733, Dec. 2008.

[20] Y. Li, C.-H. Hwang, T.-C. Yeh, H.-M. Huang, T.-Y. Li, and H.-W. Cheng, "Reduction of discrete-dopant-induced /high-frequency characteristic fluctuations in nanoscale CMOS circuit," in *Int. Conf. Simul. Semicond. Process. Devices*, Sep. 2008, pp. 209–212.

[21] K. Kuhn *et al*, "Managing process variation in Intel's 45nm CMOS technology," *Intel Technology Journal*, vol. 12, issue 02, June 17, 2008.

[22] Paul P. Sotiriadis and Anantha Chandrakasan, "Low Power Bus Coding Techniques Considering Inter-wire Capacitances," *IEEE Custom Integrated Circuits Conference*, 2000.

[23] P. Subrahmanya, R. Manimegalai, V. Kamakoti, Madhu Mutyam, "A Bus Encoding Technique for Power and Cross-talk Minimization," *Proceedings of the 17th International Conference on VLSI Design (VLSID'04),* 2004.

[24] K. Banerjee and A. Mehrotra, "A power-optimal repeater insertion methodology for global interconnects in nanometer designs," IEEE Trans. on Elec. Dev., vol. 49, pp. 2001-2007, Nov. 2002.

[25] Man Lung Mui, K. Banerjee and Amit Mehrotra, "A global interconnect optimization scheme for nanometer scale VLSI with implications for latency, bandwidth, and power dissipation," *IEEE transactions on Electron Devices*, vol. 51, no. 2, February 2004.

[26] Anastasia Barger and David Goren, Avinoam Kolodny, "Simple Design Criterion for Maximizing Data Rate in NoC Links," IEEE Workshop on signal propagation on interconnects, pp. 149-152, 2006.

[27] Magdy A. El-Moursy, Eby G. Friedman, "Optimum wire sizing of RLC interconnect with repeaters," Integration, the VLSI Journal, 38 (2004) 205–225.

[28] [5] B. K. Kaushik, S. Sarkar, R. P. Agarwal and R. C. Joshi, "Crosstalk analysis of simultaneously switching coupled interconnects driven by unipolar inputs through heterogeneous resistive drivers," ICET 2007.

[29] L. M. Coulibaly, H. J. Kadim, "Analytical crosstalk noise and its induced delay estimation for distributed RLC interconnects under ramp excitation," ISCAS 2005.

[30] Xiaopeng Ji, Long Ge, X. Han, Z. Wang, "Crosstalk noise analysis for distributed parameter high-speed interconnect lines based on the transfer function," CCDC 2008.

[31] Sudeep Pasricha and Nikil Dutt, "On-Chip Communication Architectures-System on Chip Interconnect," Morgan Kaufmann Publishers, 2008.

[32] C. Sangik, and K. Shinwook, "Implementation of an on-chip bus bridge between heterogeneous buses with different clock frequencies," in Proceedings of 5th System-on-Chip for Real-Time Applications, 2005, pp. 530-534.

[33] AMBA system architecture,

http://www.arm.com/products/solutions/AMBA/HomePage.html

[34] Giovanni De Micheli and Luca Benini, "Networks on Chips," Morgan Kaufmann, Elsevier Inc. 2006.

[35] L. Benini and G. D. Micheli, "Networks on chips: A new SoC paradigm," *IEEE Computer*, 35(1):70–78, January 2002.

[36] W. J. Dally and B. Towles, "Route packets, not wires: On-chip interconnection networks," In *Proceedings of the 38th Design Automation Conference*, 2001.

[37] T. Bjerregaard and S. Mahadevan, "A survey of research and practices of network on-chip", *ACM Computing Survey*, 38(1):1–54, 2006.

[38] Zhonghai Lu, "Design and Analysis of On-Chip Communication for Network- on-Chip Plateforms", *PhD thesis, submitted in Royal Institute of Technology (KTH),* 2007.

[39] S. Murali and G. De Micheli, "SUNMAP: a tool for automatic topology selection and generation for NoCs," San Diego, CA, USA, 2004, pp. 914-919.

[40] Edmund Lee, "Interconnect driver design for long wires in field-programmable gate arrays," M.S.c Thesis, The University of British Columbia, June 2006.

[41] J. Nurmi, H. Tenhunen, J. Isoaho, A. Jantsch, "Interconnect-Centric Design for Advanced SOC and NOC," 2004, ISBN: 978-1-4020-7835-4.

[42] "Design of VLSI Systems" Online Available at:
http://lsmwww.epfl.ch/Education/former/2002-2003/VLSIDesign/ch04/ch04.html.

[43] Raphael User's Guide, Technology Modeling Associates, 1997.

[44] K. Nabors and J. White, "Fastcap: A Multipole Accelerated 3-D Capacitance Extraction Program," *IEEE Trans. on Computer-Aided Design of Integrated Circuits and Systems*, Vol. 10, No. 11, pp. 1447-1459, Nov. 1991.

[45] Jue-Hsien Chern, Jean Huang, Lawrence Arledge, Ping-Chung Li, and Ping Yang, "Multilevel Metal Capacitance Models For CAD Design Synthesis Systems," *IEEE Electron Device Letters*, vol. 13, no. 1, Jan. 1992.

[46] Shyh-Chyi Wong, Trent Gwo-Yann Lee, Dye-Jyun Ma, and Chuan-Jane Chao, "An Empirical Three-Dimensional Crossover Capacitance Model for Multilevel Interconnect VLSI Circuits," *IEEE Trans. on Semiconductor Manufacturing*, vol. 13, no. 2, May 2000.

[47] T. Sakurai, "Closed-Form Expressions for Interconnection Delay, Coupling, and Crosstalk in VLSI's", *IEEE Trans. on Electron Devices*, Vol. 40, No. 1, pp. 118-124, Jan. 1993.

[48] S. Simon Wong *et al* "On-Chip Interconnect Inductance –Friend or Foe," *Proceedings of the Fourth International Symposium on Quality Electronic Design* (ISQED'03).

[49] K. Banerjee and A. Mehrotra, "Analysis of On-Chip Inductance Effects for Distributed RLC Interconnects," *IEEE Transactions on Computer-Aided Design of Integrated Circuits and Systems*, vol. 21, pp. 904-915, 2002.

[50] International technology roadmap for semiconductors 2007. Online available at: http://www.itrs.net/Links/2007ITRS/2007_Chapters/2007_Interconnect.pdf

[51] H. Bakoglu, "Circuits, Interconnections, and Packaging for VLSI," Addison-Wesley, 1990.

[52] W. C. Elmore, "The Transient Response of Damped Linear Networks with Particular Regard to Wideband Amplifiers," *Applied Physics*, pp. 55-63, 1948.

[53] M. J. Mills, "Variation Aware Design of Data Receiver Circuits for On-Chip Optical Interconnect," *Master of Engineering Thesis*, MIT EECS, 2002.

[54] R. Gandikota, D. Blaauw, Dennis Sylvester, "Modeling crosstalk in statistical static timing analysis," *DAC 2008*, June 8-13 2008.

[55] T. Xiao and M. Marek-Sadowska, "Gate sizing to eliminate crosstalk induced timing violation," *in Proc. Intl. Conf. on Computer Design*, 2001, pp. 186–191.

[56] K. Agarwal, D. Sylvester, and D. Blaauw, "Modeling and analysis of crosstalk noise in coupled RLC interconnects," *IEEE trans. on Comp. Aided Design of Int. Cir. and Sys.*, vol. 25, no. 5, May 2006.

[57] J. V. R. Ravindra, M. B. Srinivas, "Modelling and Analysis of Crosstalk for Distributed RLC interconnects using difference model approach," SBCCI'07.

[58] O. S. Nakagawa, D. Sylvester, J. McBride, and S.-Y. Oh, "On-Chip Cross Talk Noise Model for Deep-Submicrometer ULSI Interconnect," *The Hewlett-Packard Journal*, pp. 39-45, May 1998.

[59] J. Cong and L. He, "An efficient technique for device and interconnect optimization in deep submicron designs," *in Proc. Int. Symp. Physical Design*, 1998, pp. 45-51.

[60] D. Sylvester, and K. Keutzer, "Getting to the bottom of deep submicron II : a global paradigm," Proceedings of International Symposium on *Physical Design*, pages 193-200, 1999.

[61] G. Chen and E. Friedman, "Low power repeaters driving RC interconnects with delay and bandwidth constarints," *in Proc. Of ASIC/SOC*, pp. 335-339, 2004.

[62] Patrick P. Gelsinger, 41$^{st}$ DAC keynote, DAC 2004, (www.dac.com).

[63] Anantha P. Chandrakasan and Robert W. Brodersen, "Minimizing Power Consumption in CMOS Circuits," *Dept. of EECS, University of California at Burkeley*.

[64] Ndubuisi Ekekwe, "Power dissipation and interconnect noise challenges in nanometer CMOS technologies," *IEEE potentials*, 2010.

[65] S. Markov, "Gate Leakage Variability in Nano-CMOS Transistors," *PhD thesis, Glasgow University*, 2009.

[66] S. Saxena, C. Hess, H. Karbasi, A. Rossoni, S. Tonello, P. McNamara, S. Lucherini, S. Minehane, C. Dolainsky, and M. Quarantelli, "Variation in transistor performance and leakage in nanometer-scale technologies," *IEEE Transactions on Electron Devices*, vol. 55, p. 131, 2008.

[67] H. Tuinhout, "Impact of parametric mismatch and fluctuations on performance and yield of deep-submicron CMOS technologies," *ESSDERC 2002 - Proceedings of the 28$^{th}$ European Solid-State Device Research Conference*, vol. Florence, Italy, pp. 95 101, 2002.

[68] R. H. J. M. Otten and G. S. Garcea, "Are wires plannable?," *in Proc. Int. Workshop on System-Level Interconnect Prediction*, pp. 59-66, 2001.

[69] K. A. Bowman, S. G. Duvall, and J. D. Meindl, "Impact of die-to-die and within-die parameter fluctuations on the maximum clock frequency distribution for gigascale integration," *IEEE J. Solid-State Circuits*, vol. 37, no. 2, pp. 183–190, Feb. 2002.

[70] K. Agarwal, R. Rao, D. Sylvester and R. Brown, "Parametric yield analysis and optimization in leakage dominated technologies," *IEEE trans. on very large scale integration (VLSI) systems*, vol.15, no. 6, June 2007.

[71] G. Roy, F. Adamu-Lema, A. R. Brown, S. Roy, A. Asenov, "Intrinsic parameter fluctuations in conventional MOSFETs until the end of the ITRS: A statistical simulation study," in *Journal of Physics: Conference Series 38 (2006)*, p. 188191.

[72] M. F. Bukhori, Scott Roy and Asen Asenov, "Statistical Simulation of RTS Amplitude Distribution in Realistic Bulk MOSFETs Subject to Random Discreet Dopants," ULIS 2008, pp. 171-174, 2008.

[73] H. Mahmoodi, S. Mukhopadhyay and Kaushik Roy, "Estimation of DelayVariations due to Random-Dopant Fluctuations in Nanoscale CMOS Circuits," *IEEE Journal of Solid-State Circuits*, vol. 40, N0. 9, September, 2005.

[74] B. Cheng, S. Roy, A.R. Brown, C. Millar, A. Asenov, "Evaluation of statistical variability in 32 and 22 nm technology generation LSTP MOSFETs," *Solid-State Electronics* 53 (2009) 767–772.

[75] Yiming Li, Chih-Hong Hwang, and Tien-Yeh Li, "Discrete-dopant-induced timing fluctuation and suppression in nanoscale CMOS circuit," *IEEE Trans. on Circuits and Systems-II, Express Briefs*, vol. 56, no. 5, May 2009.

[76] B.J. Cheng, S. Roy, A. Asenov, "Impact of random dopant fluctuation on bulk CMOS 6-T SRAM scaling", *ESSDERC,* Montreux, Switzerland, Sept. 2006.

[77] B. Cheng, S. Roy, G. Roy, F. Adamu-Lema and A. Asenov, "Impact of intrinsic parameter fluctuations in decanano MOSFETs on yield and functionality of SRAM cells," *Solid-State Electronics*, Vol. 49, No. 5, pp. 740–746, 2005.

[78] International Technology Roadmap for Semiconductors, 2005.

[79] J. Liu, L. R. Zheng and H. Tenhunen, "Interconnect intellectual property for Network-on-Chip (NoC)" *Journal of Systems Architecture, 50*(2-3), 65-79, 2004.

[80] M. Bhushan, M. B. Ketchen, S. Polonksy and A.Gattiker, "Ring Oscillator BasedTechnique for Measuring Variability Statistics," *Proceedings of the International Conference on Microelectronic Test Structures*, pp. 87-92, 2006.

[81] B. J. Cheng, S. Roy, G. Roy, A. Asenov, "Integrating 'atomistic', intrinsic parameter fluctuations into compact model circuit analysis," In, *ESSDERC '03 : 33rd Conference on European Solid-State Device Research, 16-18 September 2003*, pages pp. 437-440, Estoril, Portugal.

[82] B. S. Cherkauer and E. G. Friedman, "Design of tapered buffers with local interconnect capacitance," *IEEE Journal of Solid State Circuits, 30*(2), 151-155, 1995.

[83] M. Nemes, "Driving large capacitances in MOS LSI systems," *IEEE J. Solid-State Circuits, 19*(1), 159-161, 1984.

[84] TSMC 0.18µm process 1.8 volt in SAGE-X$^{TM}$ standard cell library, *databook, Artisan components, Inc., Release 3.1,* 2001.

[85] N. Lotze, M. Ortmanns, Y. Manoli, "Variability of flip-flop timing at sub-threshold voltages," *Proceedings of the 13$^{th}$ International Symposium on Low Power Electronics and Design, ISLPED* 2008.

[86] D. Pamunuwa, H. Tenhunen, "Repeater insertion to minimise delay in coupled interconnects," *14$^{th}$ International Conference on VLSI Design*, 2001.

[87] P. Borjesson and C.-E. Sundberg, "Simple approximations of the error function Q(x) for communications applications," *IEEE transanctions on communications, 27*(3), 639-643, 1979.

[88] Cristiano Forzan, Davide Pandini, "Statistical static timing analysis: A survey," *Integration, The VLSI Journal*, 42 (2009) 409–435.

[89] Izumi Nitta, T. Shibuya, K. Homma, "Statistical static timing analysis technology," *Fujitsu Science and Technology journal*, 43(4), pp. 516-523, October 2007.

[90] E. Salman, A. Dasdan, F. Taraporevala, K. Kucukcakar, and E.G. Friedman, "Pessimism reduction in static timing analysis using interdependent setup and hold times,". *Proceedings of the 7th ISQED'06*, page 6, March 2006.

[91] S. Srivastava and J. Roychowdhury, "Interdependent latch setup/hold time characterization via Euler-Newton curve tracing on state-transition equations," *DAC*, pp. 136-141, June 2007.

[92] Saibal Mukhopadhyay, "A generic method for variability analysis of nanoscale circuits," *ICICDT 2008*, pp. 285-288, 2008.

[93] Sani Nassif et al. "High performance CMOS variability in the 65nm regime and beyond," *IEDM Digest of Technical Papers*, pp. 569-571, 10-12 Dec. 2007.

[94] Urban Kovac et al, "Statistical simulation of random dopant induced threshold voltage fluctuations for 35 nm channel length MOSFET," Microelectronics Reliability 48 (2008) 1572-1575.

[95] MathWorks. Online available at:

http://www.mathworks.com/help/toolbox/stats/br5k833-1.html#br5k833-2

[96] J. Heinrich, "A guide to the Pearson type IV distribution," CDF/MEMO/STATISTICS/PUBLIC/6820. 1, 2.

[97] Y. Nagahara, "The PDF and CF of Pearson type IV distributions and the ML estimation of the parameters," *Statistics and Probability Letters* 43 (1999) 251-264.

[98] Michel, N. and M. Stoitsov, "Fast computation of the Gauss hypergeometric function with all its parameters complex with application to the Poschl-Teller –Ginocchio potential wave functions," *Computer Physics Communications*, 178, 535-551, 2008.

[99] M. Abramowitz and I.A. Stegun, editors, "Handbook of mathematical functions with formulas, graphs, and mathematical table," *Courier Dover Publications*, 1965.
Available online at:
http://knovel.com/web/portal/browse/display?_EXT_KNOVEL_DISPLAY_bookid=528&VerticalID=0

[100] David J. DeBrota, J. J. Swain, S. D. Roberts, S. Venkatraman, "Input modeling with the Johnson system of distributions," *Proceedings of the 1988 Winter Simulation Conference*, 1988.

[101] Manish Garg, "High performance pipelining method for static circuits using hetrogeneous pipelining elements," *Proceedings of ESSCIRC'03*, pp. 185-188.

[102] J. L. Hennessy et al., "Computer Architecture: A Quantitative Approach," *Morgan Kaufmann, 3$^{rd}$ edition*, May 2002.

[103] Datta, A.; Bhunia, S.; Mukhopadhyay, S.; Roy, K.; , "Delay modeling and statistical design of pipelined circuit under process variation," *IEEE Transactions on CAD of Integrated Circuits and Systems,* , vol.25, no.11, pp.2427-2436, Nov. 2006.

[104] Min Pan, C.C.N Chu and H. Zhou, "Timing yield estimation using statistical static timing analysis," ISCAS 2005.

[105] C. E. Clark, "The greatest of a finite set of random variables", Operations Research 9(2), March-April, 1961, pp. 145-162.

[106] D. Blaauw, K. Chopra, A. Srivastava and L. Scheffer, "Statistical timing analysis: From basic principles to state of the art," *IEEE Transanctions on Computer Aided Design of Integrated Circuits and Systems,* vol. 27, no. 4, April, 2008.

[107] Faiz-ul-Hassan, Binjie Cheng, Wim Vanderbauwhede, Fernando-Rodriguez, "Impact of device variability in the communication structures for future synchronous SoC designs," *SoC 2009*, Finland.

[108] L. Zhang, W. Chen, Y. Hu, J. A. Gubner and C.C-P. Chen, "Correlation-preserved non-gaussian statistical timing analysis with quadratic timing model," *DAC '05*, pp. 83-88.

[109] L. Xie and A. Davoodi, "Fast and accuare statistical static timing analysis with skewed process parameter variation," *ISQED, 2008*.

[110] Chun-Yu Chuang, Wai-Kei Mak, "Accurate closed form parametrized block-based statistical timing analysis applying skew-normal distribution," *ISQED'09*, 2009.

[111] K. Chopra, B. Zhai, D. Blaauw, D. Sylvester, "A new statistical max operation in propagating skewness in statistical timing analysis," *ICCAD'06, November 5-9, 2006*.

[112] A. M. Ross, "Useful bounds on the expected maximum of correlated normal variables," *ISE Working Paper 03W-004,* Aug 2003.

[113] H. Chang, et al, "Statistical timing analysis under spatial correlations," *IEEE TCAD* 24(9), 2005.

[114] K. Banerjee , S. J. Souri, P. Kapur , and K. C. Saraswat, "3-D ICs: A novel chip design for improving deep-submicrometer interconnect performance and systems-on-chip integration," *Proc. IEEE*, vol. 89, pp. 602-633, May 2001.

[115] J. Cong, "Challenges and Opportunities for Design Innovations in Nanometer Technologies," *In SRC Design Sci. Concept Paper*, 1997.

[116] Giuseppe S. Garcea, Nick P. van der Meijs, Ralph H. J. M. Otten, "Simultaneous analytic area and power optimization for repeater insertion," *Proceedings of ICCAD '03*.

[117] Y. Cao, P. Gupta, A. B. Kahng, D. Sylvester and J. Yang, "Design sensitivities to variability: extrapolations and assessments in nanometer VLSI," *in Proc. of the 15th Annual IEEE International ASIC/ SOC conf.*, pp. 411-415, Sept. 2002.

[118] S. R. Nassif, "Modeling and forecasting of manufacturing variations," *in Proc. of the ASP-DAC*, pp. 145-149, Feb. 2001.

[119] A.P. Chandrakasan and R. W. Brodersen, "Sources of power consumption" in low power digital CMOS design, Norwell, MA: Kluwer, 1995.

[120] Rajeev Rao et al, "Parametric yield estimation considering leakage variability," *IEEE DAC 2004*, 442-447.

[121] E. Bolotin, I. Cidon, R. Ginosar, A. kolodny, "QNoC: QoS architecture and design process for Network on Chip," vol. 50, pp. 105-128, 2004.

[122] L. Zhang, Y. Hu, "Statistical timing analysis in sequential circuit for on chip global interconnect pipelining," *Proceedings of Design Automation Conference*, 2004, pp. 904-907.

[123] N. Magen, A. Kolodny, U. Weiser, N. Shamir, "Interconnect-power dissipation in a microprocessor", *SLIP Conf.*, Feb., 2004.

[124] R. H. Havemann and J. A. Hutchby, "High-performance interconnects: an integration overview," *Proc. IEEE*, vol. 89, no. 5, pp. 586-601, May 2001.

[125] S. Takahashi, M. Edahiro, and Y. Hayashi, "Interconnect design strategy: Structures, repeaters and materials with strategic system performance analysis (S2PAL) model," *IEEE Trans. Electron Devices*, vol. 48, no. 2, pp. 239-251, Feb. 2001.

[126] H. Shah, P. Shiu, B. Bell, M. Aldredge, N. Sopory, and J. Davis, "Repeater insertion and wire sizing optimization for throughput-centric VLSI global interconnects," in *Proc. IEEE/ACM Int. l Conf. Computer –Aided Design*, 2002, pp. 280-284.

[127] A. B. Kahng, S. Muddu, and E. Sarto, "Interconnect optimization strategies for high-performance VLSI designs," in *Proc. IEEE Int. Conf. VLSI Design*, 1999, pp. 464–469.

[128] D. Pamunuwa, L.-R. Zheng, and H. Tenhunen, "Optimising bandwidth over deep sub-micron interconnect," in *Proc. IEEE Int. Symp. Circuits Syst.*, 2002, pp. IV/193–IV/196.

[129] A. Naeemi, R. Venkatesan, and J. D. Meindl, "System-on-a-chip global interconnect optimization," in *Proc. ASIC/SoC Conf.*, Sep. 2002, pp. 399–403.

[130] Z. Lin. C. Spanos, L. Milor and Y. Lin, "Circuit sensitivity to interconnect variation," *IEEE Transactions on Semiconductor Manufacturing*, vol. 11, pp. 557-568, Nov. 1998.

[131] T. Fukuoka, A. Tsuchiya, H. Onodera, "Worst-case delay analysis considering the variability of transistors and interconnects," *ISPD'07*, March, 2007.

[132] V. Wason and K. Banerjee, "A probabilistic framework for power-optimal repeater insertion in global interconnects under parameter variations," *ISLPED'05*, August 2005.

[133] K. Agarwal, M. Agarwal, D. Sylvester and D. Blaauw, "Statistical interconnect metrics for physical design optimization," *IEEE Trans. On comp. Aided design of Integrated Circuits and Systems*, vol. 25, no. 7, July 2006.

[134] Li-Rong Zheng, Dinesh Pamunuwa, Hannu Tenhunen, "Accurate a priori signal integrity estimation using a multilevel dynamic interconnect model for deep submicron VLSI design," in *Proc. ESSCIRC*, Sep. 2000, pp. 324-327.

[135] D. Pamunuwa and H. Tenhunen, "On dynamic delay and repeater insertion in distributed capacitively coupled interconnects," *Proc. of ISQED'02*.

[136] J. Liu, L-R Zheng, D. Pamunuwa, H. Tenhunen, "A global wire planning scheme for network-on-chip," *Proc. of the ISCAS'03*.

[137] D. Pamunuwa, Li-Rong Zheng, and Hannu Tenhunen, "Maximizing throughput over parallel wire structures in the deep submicron regime," *IEEE Trans. on VLSI Systems*, vol. 11, no. 2, April 2003.

[138] S.J. Lee, et al, "Adaptive Network-on-Chip with wave-front train serialization scheme," Proc. Of VLSI circuits, 104-107, 2005.

[139] R. Arunachalam, K. Rajagopal, L. T. Pileggi, TACO: Timing analysis with coupling, *Proc. of Design Automation Conf.*, pp. 266-269, June 2000.

[140] R. Gandikota, D. Blaauw, D. Sylvester, "Modeling crosstalk in statistical static timing analysis," *DAC* 2008.

[141] L. Dou, Z. Wang, "One high-efficiency analysis method for high-speed circuit network containing distributed parameter elements," *J. of Control Theory and Applications*, vol. 3, no. 2, 117-120, 2005.

[142] F. Rodriguez, Faiz-ul-Hassan, Wim Vanderbauwhede, "Passive skew amplification in coupled RC transmission lines," TO BE SUBMITTED IN *IEEE Trans.*, 2011.

[143] Y. I. Ismail and E. G. Friedman, "Effects of inductance on the propagation delay and repeater insertion in VLSI circuits," IEEE Transactions on Very Large Scale Integration (VLSI) Systems, Vol. 8, No. 2, pp. 195-206, April 2000.

[144] James R. Thompson, Richard A. Tapia, "Nonparametric Function Estimation, Modelling and Simulation," Society for Industrial Mathematics, Siam, 1990.

[145] Kamsani, N.A., Cheng, B., Roy, S. and Asenov, A. "Statistical circuit simulation with the effect of random discrete dopants in nanometer MOSFET devices," In: Design *Automation and Test in Europe: Workshop W2, Impact of Process Variability on Design and Test*, 10-14 March 2008, Munich, Germany.

[146] Arkadiy Morgenshtein, Israel Cidon, Avinoam Kolodny, Ran Ginosar, "Low leakage repeaters for NoC Interconnects," 2005.